



Terms and Conditions of Use of Digitised Theses from Trinity College Library Dublin

Copyright statement

All material supplied by Trinity College Library is protected by copyright (under the Copyright and Related Rights Act, 2000 as amended) and other relevant Intellectual Property Rights. By accessing and using a Digitised Thesis from Trinity College Library you acknowledge that all Intellectual Property Rights in any Works supplied are the sole and exclusive property of the copyright and/or other IPR holder. Specific copyright holders may not be explicitly identified. Use of materials from other sources within a thesis should not be construed as a claim over them.

A non-exclusive, non-transferable licence is hereby granted to those using or reproducing, in whole or in part, the material for valid purposes, providing the copyright owners are acknowledged using the normal conventions. Where specific permission to use material is required, this is identified and such permission must be sought from the copyright holder or agency cited.

Liability statement

By using a Digitised Thesis, I accept that Trinity College Dublin bears no legal responsibility for the accuracy, legality or comprehensiveness of materials contained within the thesis, and that Trinity College Dublin accepts no liability for indirect, consequential, or incidental, damages or losses arising from use of the thesis for whatever reason. Information located in a thesis may be subject to specific use constraints, details of which may not be explicitly described. It is the responsibility of potential and actual users to be aware of such constraints and to abide by them. By making use of material from a digitised thesis, you accept these copyright and disclaimer provisions. Where it is brought to the attention of Trinity College Library that there may be a breach of copyright or other restraint, it is the policy to withdraw or take down access to a thesis while the issue is being resolved.

Access Agreement

By using a Digitised Thesis from Trinity College Library you are bound by the following Terms & Conditions. Please read them carefully.

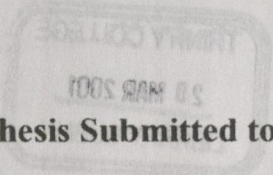
I have read and I understand the following statement: All material supplied via a Digitised Thesis from Trinity College Library is protected by copyright and other intellectual property rights, and duplication or sale of all or part of any of a thesis is not permitted, except that material may be duplicated by you for your research use or for educational purposes in electronic or print form providing the copyright owners are acknowledged using the normal conventions. You must obtain permission for any other use. Electronic or print copies may not be offered, whether for sale or otherwise to anyone. This copy has been supplied on the understanding that it is copyright material and that no quotation from the thesis may be published without proper acknowledgement.

Declaration

**Molecular Simulations of Poly(3-alkylthiophene)s:
Thermochromism and Transport Behaviour of Dopants**

BY

Hongwei Xie



**A Thesis Submitted to
The University of Dublin
for the Degree of
Doctor of Philosophy**

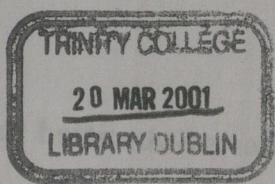
September 2000

Department of Chemistry
Trinity College
University of Dublin

Molecular Simulations of Poly(α -alkylphosphine)s:
Thermodynamics and Transport Behaviour of Gopants

BY

Hoangwei Ma



THESIS
6326

Department of Chemistry

September 2000

Department of Chemistry

Trinity College

University of Dublin

Declaration

This thesis has not been submitted as an exercise for a degree at any other University. Except where otherwise stated, the work described herein has been carried out by the author alone. This thesis may be borrowed or copied upon request with the permission of the Library, Trinity College, University of Dublin. The copyright belongs jointly to the University of Dublin and Hongwei Xie.

Signature of Author:

Hongwei Xie

Hongwei Xie

September 2000

Acknowledgements

It is my prime duty to thank both of my supervisors without whom this thesis would not have been possible. I would like to thank Dr. D. A. Morton-Blake for providing me with guidance and discussion at every step of the thesis. He spent a lot of precious time to supervise my research. I wish to thank Prof. John Corish for his insights into my research and for his support and encouragement during the three years of my study.

I wish to thank Dr. Dónall A MacDónaill for his help both in private staff and in research.

I would especially like to thank Mrs. Corinne Harrison for her help and encouragement during the three years of my study. I would also like to thank Ms. Helen O'Halloran and Ms. Teresa Lalor for their long-time help. It was their help made my study here easy to undertake.

I also wish to thank Ms. Teresa McDonnell for the equipment support.

I gratefully acknowledge the award of a High Performance Computing Fellowship which has made the work reported in this thesis possible. This Fellowship was funded by a gift to the Trinity Foundation from a private donor.

Summary

The solubility, processability, environmental stability and thermochromism of poly(3-alkylthiophenes) (P3ATs) in comparison with other π -conjugated conducting polymers make these materials attractive choices for both theoretical and experimental investigations of polymers with electrical and optical activity. In the work reported here the thermochromic phenomena and dopant transport behavior in these materials are studied on an atomic level by using molecular mechanics (MM) and molecular dynamics (MD) simulations.

The energy minimization methods of MM simulations were first used to optimize the lattice structure of poly(3-butylthiophene) (P3BT), the simplest P3AT that exhibits the properties of interest. The lattice parameters obtained (a and b) show good agreement with those from X-ray diffraction measurements, which indicated that the force field developed for this system is reasonable and can be used with confidence for further investigations.

The first special property of P3ATs investigated was its thermochromism which can be used for thermochromic displays and light emitting devices. It is commonly accepted that the thermochromism is the result of the increase of energy gap between the valence and conduction bands resulting from the conformational changes caused by thermal effects. Until now the mechanism has not been determined.

The MM simulation investigations show that stable thermally assessed higher energy conformations with some higher torsional angles (*ca.* 50°) in the P3BT main chains exist. The torsions were investigated in three different periodicities ($[+\varphi, 0, -\varphi, 0]$, $[+\varphi, -\varphi, 0, +\varphi, -\varphi, 0]$ and $[+\varphi, 0, 0, -\varphi, 0, +\varphi, 0, 0, -\varphi, 0]$). The energy difference is approximately 0.3 eV if the polymer shifts from the lower to the higher energy conformations with torsional angle about 50° . The band gap calculated by Extended Hückel Theory (EHT) was enhanced by 0.4-0.7 eV. These results are consistent with experimental measurements. Electronic energy spectra and UV spectra showed that the energy change for thermochromism is *ca.* 0.5 eV, while *ab-initio* calculations showed it to be of the order of 0.7 eV.

MD simulations were applied to monitor the conformation changes both in the side and main chains of P3BT from 10 to 450 K. The simulations showed that

although the carbon links in the side chains largely retain a *trans* conformation, *gauche* and other conformations with higher energies appeared on heating and that the probability of these conformations increased with temperature. For the main chain, a step-like increase in the mean value of the torsional angle between the thiophene rings appeared at $T=340$ K perhaps as a result of the dissipation of torsional energy stored in the alkyl side-chains. This suggests the occurrence of an abrupt reduction in the π -conjugation in the polymer main chain at this temperature and this should lead to an increased bandwidth resulting in the onset of a thermochromic change. A mechanism for the thermochromism is proposed based on the MD and MM simulations.

The second property of P3ATs investigated was dopant transport in the lattice. The purpose was to understand the high conductivity of regioregular HT-P3ATs.

MM and MD simulations with the polymer chains frozen were first used to optimize the structural models and the positions of dopants in the lattice: little information on the latter is available from experiments. Two structural models, the Kawai and interplanar, have been proposed and both were investigated here.

Then, MD simulations were used to investigate the diffusion of dopants Cl^- and BF_4^- in P3BT lattice with the above proposed structural models and different charge models on the temperature range 10 - 450 K. The diffusion coefficients of dopants calculated from mean square displacement (MSD) plots are of the order of one to several hundred $10^{-12} \text{ m}^2\text{s}^{-1}$, which are much higher than those measured from diffusion of dopants in other π -conjugated conducting polymers. This suggests that doped P3ATs could be excellent potential materials for battery applications, where the rates of charge and discharge are determined by diffusion and the best values should be around $10^{-12} \text{ m}^2\text{s}^{-1}$.

The migration of dopants in P3BT lattice studied by MM simulations suggests that the dopants are more mobile in the proposed interplanar structural model than in the Kawai structural model.

The study of diffusion from MD and the migration from MM contribute an understanding of the transport behavior of dopants in P3AT lattice. Both of them suggest that the dopants in P3AT lattices possess high mobility, which is the requirement for the high ionic conductivity of regioregular HT-P3AT materials.

Contents

I INTRODUCTION AND THEORY	1
1 Introduction to Conducting Polymers and Soluble Poly(3-alkylthiophene)s	2
1.1 Conducting Polymers	2
1.1.1 Doping	6
1.1.2 Transport of Charge in Conducting Polymers	11
1.1.3 Stability and Processibility	13
1.1.4 Applications	15
1.2 Soluble Conducting Polymers—Poly(3-alkylthiophene)s	16
1.2.1 Synthesis	18
1.2.2 Regioregularity	19
1.2.3 Self-assembly and High Electrical Conductivity in Regioregular HT-P3ATs	21
1.2.4 Stability	22
1.2.5 Solubility and Processibility	23
1.2.6 Crystalline and Lattice Structure	23
1.2.6.1 Kawai Structure Model	24
1.2.6.2 Winokur Structure Model	25
1.2.6.3 One-Chain Models	25
1.2.6.3 Conformational Structure	25
1.2.7 Thermochromism	26
1.2.8 Applications	27
1.3 Aims of the Present Work	28
Bibliography	30
2 Computational Theory and Methodology	36
2.1 Interatomic Potentials	37
2.1.1 Bonded Potentials	37
2.1.1.1 Bond Potentials	38
2.1.1.2 Valence Angle Potentials	39

2.1.1.3 Dihedral Angle Potentials	40
2.1.1.4 Cross Terms	42
2.1.2 Non-bonded Potentials	43
2.1.2.1 The van der Waals Potentials	43
2.1.2.2 Electrostatic Potential	46
2.1.3 External Fields	49
2.1.4 Parameterization	49
2.1.4.1 Empirical Methods	50
2.1.4.2 Theoretical Calculation Methods	51
2.2 Energy Minimization	52
2.2.1 Newton-Raphson Methods	52
2.2.2 Steepest Descent Method	54
2.2.3 Conjugate Gradient Methods	55
2.3 Computational Methods	56
2.3.1 Molecular Mechanics Simulations	56
2.3.1.1 Perfect Lattice Simulations	57
2.3.1.2 Point Defect Simulations	58
2.3.2 Molecular Dynamics	59
2.3.2.1 Radial Distribution Function $g(r)$	60
2.3.2.2 Diffusion Coefficient	61
2.3.3 Monte Carlo Method	61
2.4 Simulation Codes	62
2.4.1 GULP	62
2.4.2 DL_POLY	63
Bibliography	65
3. The Force Field	67
3.1 Bond Potential (U_b)	69
3.2 Valence Angle Potential (U_a)	71
3.3 Dihedral Angle Potential (U_t)	72
3.4 Van der Waals Potential (U_{vdw})	72
3.5 Coloumbic Potential (U_q)	74
Bibliography	75

II MOLECULAR SIMULATION OF THERMOCHROMIC PHENOMENA IN POLY(3-ALKYLTHIOPHENE)S	77
4 MM Simulation of Thermochromic Phenomena in Poly(3-alkylthiophene)s	78
4.1 Introduction	78
4.2 Lattice Structure and Parameters	80
4.3 Literature Review of MM Investigations on Poly(3-alkylthiophene)s	83
4.4 Discussion of the Main Chain Torsional Periodicity	86
4.5 Method of Calculation	87
4.6 Results and Discussion	88
4.6.1 Lattice Parameters	88
4.6.2 Lattice Energy Profile of Two-chain Staggered Structure	93
4.6.3 Lattice Energy Profile for the One-chain Eclipsed Structure	95
4.6.4 Information for the Thermochromic Distortion	99
4.6.5 Electronic Bandgap Change with Torsional Angle ϕ_5 in Different Torsional Sequences	100
4.7 Conclusion	102
Bibliography	104
5 MD Simulation of Thermally Induced Conformation Changes and Thermochromic Mechanism of Poly(3-alkylthiophene)s	107
5.1 Introduction	107
5.2 Computational Structure	108
5.3 Method of Calculations	110
5.4 Results and Discussion	111
5.4.1 Energy change with Simulation Time	111
5.4.2 Energy Change with Temperature	114
5.4.3 Conformation at Low Temperature	114
5.4.4 Conformation Change with Temperature	117
5.4.5 Thermochromic Changes	131
5.4.6 Effect of Conformations in Alkyl Side Chains on the Shift in $\langle\phi_5\rangle$	134

5.4.7 Effect of Pressure on the Shift of $\langle\varphi_5\rangle$	138
5.4.8 Mechanism of Thermo-chromic Distortion	140
5.5 Conclusions	141
Bibliography	145

III MOLECULAR SIMULATION OF TRANSPORT

BEHAVIOUR OF DOPANTS (Cl^- AND BF_4^-) IN POLY(3- ALKYLTHIOPHENE) LATTICES 147

6 MD Simulation of Diffusion of Dopants (Cl^- and BF_4^-) in P3AT Lattices	148
6.1 Introduction	149
6.2 The Charge Model for the Main Chain in Doped P3ATs	150
6.3 Dopant Position and Lattice Structure	152
6.4 MD Simulation of P3BT Lattice with Dopant Cl^- and BF_4^-	156
6.4.1 Cl^- doped P3BT Lattice	158
6.4.1.1 P3BT Doped at 25% Level with Cl^-	158
6.4.1.2 P3BT Doped at 50% Level with Cl^-	166
6.4.1.3 Discussion	171
6.4.2 BF_4^- Doped P3BT	178
6.4.2.1 P3BT Doped at 25% Level with BF_4^-	178
6.4.2.2 P3BT Doped at 50% Level with BF_4^-	183
6.4.2.3 Discussion	188
6.5 Conclusion	192
Bibliography	194
7 MM Simulation of Migration of Dopants (Cl^- and BF_4^-) in P3BT Lattices	195
7.1 Introduction	196
7.2 Calculation Methods	197
7.3 Results and Discussion	198
7.3.1 Migration Route of Dopant Cl^- in P3BT Lattice	198
7.3.2 Migration of Dopant Cl^- in P3BT Lattice	200
7.3.3 Migration of Dopant BF_4^- in P3BT Lattice	205

7.4 Conclusion	208
Bibliography	210
8 Conclusions and Future Work	211
Bibliography	216

1.2 The McCallough method for the regioregular synthesis of P3ATs with 100% monomer incorporation	19
1.3 The Rieke method of preparing regioregular HT-P3ATs	19
1.4 Possible regiochemical coupling in P3ATs	20
1.5 The lattice structure of P3ATs proposed by Kawai <i>et al.</i> (a) viewed along c axis, (b) viewed along b axis	24
2.1 The intermolecular bond vector	38
2.2 The torsion angle and associated vectors	40
2.3 The dihedral angle and associated vectors	40
2.4 Comparison of U_{eff} functionals for the H_2 -He potential	46
2.5 The model of the Ewald sum method	48
2.6 The illustration of radial distribution function $g(r)$	61
3.1 The carbon types in poly(butyl-1,4-phenylene)	69
4.1 The Chain structure of regioregular HT-P3BT	81
4.2 The lattice structure for the two-chain cell showing the staggered relationship of the thiophene rings stacked along b axis. The two chains are distinguished by shading. One in $b=0$ and the other in $b=1/2b$. In the one-chain reduced structure one chain is displaced by $1/2c$ along the c axis and the two chains are in different cells	82
4.3 Energy profile as obtained by lattice energy minimization of QM/P, when a torsion ϕ is applied to one butyl chain along links 2, 3 and 4, allowing the lattice to relax	84
4.4 Energy profile as obtained by a Monte Carlo calculation, when a torsion ϕ is applied to one butyl chain along links 1, 2, 3 and 4, allowing the other links in the butyl chains to relax	85

List of Figures

1.1 The oxidation processes of π -conjugated conducting polymers and the creation of polaron, bipolaron and soliton states. (a) Nondegenerate P3AT, (b) Degenerate polyacetylene. Where $R = H$ or alkyl group; $X^- = ClO_4^-, PF_6^-, I_3^-$, etc.....	9
1.2 The McCullough method for the regioregular synthesis of P3ATs with 100% head-to-tail couplings.....	19
1.3 The Rieke method of preparing regioregular HT-P3ATs.....	19
1.4 Possible regiochemical coupling in P3ATs.....	20
1.5 The lattice structure of P3ATs proposed by Kawai <i>et al.</i> (a) viewed along c axis, (b) viewed along b axis.....	24
2.1 The interatomic bond vector.....	38
2.2 The valence angle and associated vectors.....	40
2.3 The dihedral angle and associated vectors.....	40
2.4 Comparison of U_{vdw} functionals for the H_2 -He potential.....	46
2.5 The model of the Ewald sum method.....	48
2.6 The illustration of radial distribution function $g(r)$	61
3.1 The carbon types in poly(butylthiophene).....	69
4.1 The Chain structure of regioregular HT-P3BT.....	81
4.2 The lattice structure for the two-chain cell showing the staggered relationship of the thiophene rings stacked along b axis. The two chains are distinguished by shading. One in $b=0$ and the other in $b= \frac{1}{2}b$. In the one-chain eclipsed structure one chain is displaced by $\frac{1}{2}c$ along the c axis and the two chains are in different cells.....	82
4.3 Energy profile, as obtained by lattice energy minimization of GULP, when a torsion ϕ is applied to one butyl chain along links 2, 3 and 4, allowing the lattice to relax.....	84
4.4 Energy profile, as obtained by a Monte Carlo calculation, when a torsion ϕ is applied to one butyl chain along links 1, 2, 3 and 4, allowing the other links in the butyl chains to relax.....	85

- 4.5 The effect of the torsion schemes A, B and C on the cell parameters a (open symbols \square , Δ and \circ refer to schemes A, B, C, respectively) and b (closed symbols). (a) two-chain structure, (b) one-chain structure.....89
- 4.6 The lattice density after relaxation as a function of torsional angle φ_5 (in units of degree) at three different torsional schemes in the two-chain and one-chain structures. d_1 represents the density in the one-chain structure, d_2 – the density in the two-chain structure; A – torsional scheme A $(+\varphi, 0, -\varphi, 0)$, B – torsional scheme B $(+\varphi, -\varphi, 0, +\varphi, -\varphi, 0)$, C – torsional scheme C $(+\varphi, 0, 0, -\varphi, 0, +\varphi, 0, 0, 0, -\varphi, 0)$90
- 4.7 The interdigitation exists between alkyl side chains of two neighboring polymers in the same ac plane.....91
- 4.8 The lattice energy per thiophene unit for the two-chain staggered structure in which the chains have been subjected to torsion schemes A (\square), B (\times) and C(Δ).....94
- 4.9 Effect of torsional periodicity on the polymer main chain structure. (a) Torsional scheme A applied, (b) Torsional scheme B applied, (c) Torsional scheme C applied. An adjacent chain is included in (c). In the torsional schemes A and B each chain can change its direction by up to 10°96
- 4.10 A comparison of the lattice energy profile of the one-chain eclipsed structure (\bullet) with that of the two-chain staggered structure (\square) for torsional schemes A, B and C.....97
- 4.11 The bandgap of P3BT as a function of torsional angle φ_5 (in units of degree) at three different torsional schemes. A represents torsional scheme A $(+\varphi, 0, -\varphi, 0)$, B – torsional scheme B $(+\varphi, -\varphi, 0, +\varphi, -\varphi, 0)$, C – torsional scheme C $(+\varphi, 0, 0, -\varphi, 0, +\varphi, 0, 0, 0, -\varphi, 0)$ 101
- 5.1 The $2 \times 2 \times 2$ supercell structure of P3BT with $a=27 \text{ \AA}$, $b=14.6 \text{ \AA}$ and $c=15.52 \text{ \AA}$. (a) viewed along c axis; (b) viewed along b axis. The atoms in P3BT are represented by different colors in the diagram, red – S atom, gray – C atom and blue – H atom.....109
- 5.2 The plots of energies of P3BT system as the calculation proceeds in NVT ensemble at a selection of temperatures as illustrated in the diagrams. (a) Total energy, (b) Configurational energy, (c) Torsional energy..... 112

5.3	The energies of P3BT system after 100 ps relaxation in NVT ensemble as a function of temperature. (a) Total and configurational energies, (b) Torsional energy.....	113
5.4	Time-evolution of torsional angles in a thiophene monomer unit at 10 K simulated in NVT ensemble.....	115
5.5	Time evolution of terminal CH ₃ motions at 340 K in randomly selected butyl side chains simulated in NVT ensemble. The torsional angles are in units of degree. Note the “jump” from 0°-centered positions to the equivalent 120°-centered positions.....	116
5.6	Time evolution of torsional angle φ_3 at 340 K in randomly selected butyl side chains simulated in NVT ensemble. The torsional angles are in units of degree. Note that φ_3 can jump from <i>trans</i> to <i>gauche</i> at this temperature.....	116
5.7	DTA of φ_1 (Link 1) at different temperatures calculated in NVT ensemble. The torsional angles are in units of degree.....	118
5.8	DTA of φ_2 (Link 2) at different temperatures calculated in NVT ensemble. The torsional angles are in units of degree.....	119
5.9	DTA of φ_3 (Link 3) at different temperatures calculated in NVT ensemble. The torsional angles are in units of degree.....	120
5.10	DTA of φ_4 (methyl group) at different temperatures calculated in NVT ensemble. The torsional angles are in units of degree.....	121
5.11	DTA of φ_5 (torsional angle between thiophene rings in units of degree) at different temperatures calculated in NVT ensemble.	122
5.12	RDF of C-C in the alkyl side chains at different temperatures. When all the links in the alkyl side chain are in <i>trans</i> (0°), the distance (r) (in units of Å) between alkyl carbon number 1 and 4 is 3.916 Å. The appearance of <i>gauche</i> in the alkyl chain will reduce the distance.....	126
5.13	RDF of C-C in the P3BT main-chain thiophene rings at different temperatures. The peak A corresponds to the distance (in units of Å) between carbon number 2 and 5, or 4 and 7; B (1 – 5, or 4 – 8, or 3 – 6); C (1 – 6, or 3 – 8); D (2 – 6, or 3 – 7); E (4 – 9); F (2 – 7, or 3 – 9, or 4 – 10); G (1 – 8)	127
5.14	RDF of H-H in P3BT at different temperatures. The peak A corresponds to the distance (in units of Å) between hydrogen number 1 and 3, or 2 and 4, or 3 and 5, or 4 and 5; B (2 – 3, or 1 – 4).....	128

5.15	A comparison of conformations of P3BT after 100 ps relaxation at 10, 300 and 400 K. (a) 10 K, (b) 300 K and (c) 400 K. The atoms in P3BT are represented by different colors, red – S atom, gray – C atom and blue – H atom.....	129
5.16	The average torsional angle $\langle \varphi_5 \rangle$ (in units of degree) as a function of temperature.....	132
5.17	A comparison of DTA of φ_5 (in units of degree) at 300 K and 340 K.....	132
5.18	A comparison of DTA at 330 and 340 K for the torsional angles (in units of degree) in the P3BT alkyl side chains. (a) φ_1 , (b) φ_2 , (c) φ_3 , (d) φ_4	135
5.19	The average torsional angles φ_5 , φ_1 and φ_2 (in units of degree) as a function of temperature.....	136
5.20	Average torsional angle $\langle \varphi_5 \rangle$ (in units of degree) as a function of temperature when one of the links in the alkyl side chains was clamped.....	136
5.21	DTA of φ_5 (in units of degree) at various temperatures as one of the links in the side chains was clamped. (a) Clamped link 1, (b) Clamped link 2, (c) Clamped link 3.....	137
5.22	Average torsional angle $\langle \varphi_5 \rangle$ (in units of degree) as a function of temperature at three different values of the lattice parameter b in NVT ensemble. (a) $b=14.1$ Å, (b) $b=14.6$ Å, (c) $b=15.1$ Å.....	139
5.23	Average torsional angle $\langle \varphi_5 \rangle$ (in units of degree) as a function of pressure at 360 K calculated in NPT ensemble, $\langle \varphi_1 \rangle$ and $\langle \varphi_2 \rangle$ are also included.....	139
5.24	An illustration of the proposed mechanism for thermochromism in P3BT.....	140
6.1	The charge distribution associated with (a) a polaron (b) a bipolaron on a P3BT chain, which extends over four thiophene rings.....	151
6.2	The Kawai structural Model for Cl^- doped P3BT. (a) viewed along \mathbf{c} axis, (b) viewed along \mathbf{b} axis. The atoms in the system are represented by different colors: green—S, gray—C, blue—H, and red—dopant ion Cl^-	153
6.3	The interplanar structural model for Cl^- doped P3BT. (a) viewed along \mathbf{c} axis, (b) viewed along \mathbf{b} axis. The atoms in the system are represented by different colors: green—S, gray—C, blue—H, and red—dopant ion Cl^-	154

6.4 MSD of Cl ⁻ in 25% Cl ⁻ doped P3BT lattice at 10, 300 and 450 K (Kawai structural model and the charges evenly distributed in the polymer main chains).....	159
6.5 MSD of Cl ⁻ in 25% Cl ⁻ doped P3BT lattice at 10, 300 and 450 K (Kawai structural model and polaron charge model in the polymer main chains).....	160
6.6 MSD of Cl ⁻ in 25% Cl ⁻ doped P3BT lattice at 10, 300 and 450 K (the interplanar structural model and the charges evenly distributed in the polymer main chains).....	161
6.7 MSD of Cl ⁻ in 25% Cl ⁻ doped P3BT lattice at 10, 300 and 450 K (the interplanar structural model and polaron charge model in the polymer main chains).....	162
6.8 RDF of C-Cl in 25% Cl ⁻ doped P3BT lattices with different models.....	164
6.9 RDF of S-Cl in 25% Cl ⁻ doped P3BT lattices with different models.....	165
6.10 MSD of Cl ⁻ in 50% Cl ⁻ doped P3BT lattice at 10, 300, 450 K (the Kawai structural model and the charges evenly distributed in the polymer main chains).....	167
6.11 MSD of Cl ⁻ in 50% Cl ⁻ doped P3BT lattice at 10, 300, 450 K (the Kawai structural model and bipolaron charge model in the polymer main chains).....	168
6.12 MSD of Cl ⁻ in 50% Cl ⁻ doped P3BT lattice at 10, 300 and 450 K (the interplanar structural model and the charges evenly distributed in the polymer main chains).....	169
6.13 MSD of Cl ⁻ in 50% Cl ⁻ doped P3BT lattice at 10, 300 and 450K (the interplanar structural model and bipolaron charge model in the polymer main chains).....	170

6.14 LogD of Cl ⁻ as a function of reciprocal Kelvin temperature at 50% doping level in the Kawai structural model with even charge distribution.....	174
6.15 A comparison of P3BT relaxed conformation before and after Cl ⁻ doping at 50% doping level at 300K. (a) Pristine, (b) Cl ⁻ doped, the Kawai structure, (c) Cl ⁻ doped, the interplanar structure. The atoms in the system are represented by different colors: green – S, gray – C, blue – H and red – dopant ion Cl ⁻	176
6.16 A comparison of P3BT relaxed conformation before and after Cl ⁻ doping at 50% doping level at 400K. (a) Pristine, (b) Cl ⁻ doped, the Kawai structure, (c) Cl ⁻ doped, the interplanar structure. The atoms in the system are represented by different colors: green – S, gray – C, blue – H and red – dopant ion Cl ⁻	177
6.17 MSD of B and F in 25% BF ₄ ⁻ doped P3BT lattice at 10, 300 and 450 K (the Kawai structural model and the charges evenly distributed in the polymer main chains).....	179
6.18 MSD of B and F in 25% BF ₄ ⁻ doped P3BT lattice at 10, 300 and 450 K (the Kawai structural model and polaron charge model in the polymer main chains).....	180
6.19 MSD of B and F in 25% BF ₄ ⁻ doped P3BT lattice at 10, 300 and 450 K (the interplanar structural model and the charges distributed in the polymer main chains).....	181
6.20 MSD of B and F in 25% BF ₄ ⁻ doped P3BT lattice at 10, 300 and 450 K (the interplanar structural model and polaron charge model in the polymer main chains).....	182

6.21 MSD of B and F in 50% BF_4^- doped P3BT lattice at 10, 300 and 450 K (the Kawai structural model and the charges distributed in the polymer main chains).....	184
6.22 MSD of B and F in 50% BF_4^- doped P3BT lattice at 10, 300 and 450 K (the Kawai structural model and bipolaron charge model in the polymer main chains).....	185
6.23 MSD of B and F in 50% BF_4^- doped P3BT lattice at 10 300 and 450 K (the interplanar structural model and the charges distributed in the polymer main chains).....	186
6.24 MSD of B and F in 50% BF_4^- doped P3BT lattice at 10, 300 and 450 K (the interplanar structural model and bipolaron charge model in the polymer main chains).....	187
7.1 The most likely migration path of dopant in interplanar structural Model. The dopants are located in half way between the two planes that are shown in black and blue colours.....	199
7.2. The most likely migration path of dopant in Kawai structural model. The two ploymer chains and the dopants are in the same plane.....	199
7.3 Lattice energy after relaxation when dopant Cl^- at the doping levels indicated in the diagram migrates in P3BT lattice with the interplanar structural model along the path as proposed in Figure 7.1. dc is the distance that dopants migrated along the c axis.....	201
7.4 Lattice energy after relaxation when dopant Cl^- at the doping levels indicated in the diagram migrates in P3BT lattice with the Kawai structural model along the path as proposed in Figure 7.2. Twenty points in the path were selected as the	

6.21 MSD of B and F in 50% BF_4^- doped P3BT lattice at 10, 300 and 450 K (the Kawai structural model and the charges distributed in the polymer main chains).....	184
6.22 MSD of B and F in 50% BF_4^- doped P3BT lattice at 10, 300 and 450 K (the Kawai structural model and bipolaron charge model in the polymer main chains).....	185
6.23 MSD of B and F in 50% BF_4^- doped P3BT lattice at 10 300 and 450 K (the interplanar structural model and the charges distributed in the polymer main chains).....	186
6.24 MSD of B and F in 50% BF_4^- doped P3BT lattice at 10, 300 and 450 K (the interplanar structural model and bipolaron charge model in the polymer main chains).....	187
7.1 The most likely migration path of dopant in interplanar structural Model. The dopants are located in half way between the two planes that are shown in black and blue colours.....	199
7.2. The most likely migration path of dopant in Kawai structural model. The two ploymer chains and the dopants are in the same plane.....	199
7.3 Lattice energy after relaxation when dopant Cl^- at the doping levels indicated in the diagram migrates in P3BT lattice with the interplanar structural model along the path as proposed in Figure 7.1. dc is the distance that dopants migrated along the c axis.....	201
7.4 Lattice energy after relaxation when dopant Cl^- at the doping levels indicated in the diagram migrates in P3BT lattice with the Kawai structural model along the path as proposed in Figure 7.2. Twenty points in the path were selected as the	

dopant position with the distance between two nearest two points is the same.....	202
7.5 Change in the lattice parameter b when dopant Cl^- at the doping levels indicated in the diagram migrates in P3BT lattice with the interplanar structural model along the path as proposed in Figure 7.1. \mathbf{dc} is the distance that dopants migrated along the \mathbf{c} axis	203
7.6 Change in the lattice density when dopant Cl^- at the doping levels indicated in the diagram migrates in P3BT lattice with the interplanar structural model along the path as proposed in Figure 7.1. \mathbf{dc} is the distance that dopants migrated along the \mathbf{c} axis	204
7.7 Change in the lattice parameter b when dopant Cl^- at the doping levels indicated in the diagram migrates in P3BT lattice with Kawai structural model along the path as proposed in Figure 7.2. Twenty points in the path were selected as the dopant position with the distance between two nearest two points is the same	206
7.8 Change in the lattice density when dopant Cl^- at the doping levels indicated in the diagram migrates in P3BT lattice with the Kawai structural model along the path as proposed in Figure 7.2. Twenty points in the path were selected as the dopant position with the distance between two nearest two points is the same	207

List of Tables

1.1	Stability and processing status of representative conducting polymers.....	13
3.1	The bond types in P3AT and relative parameters for Morse potential function $U(r)=E_0\{1-\exp[-(k/2E_0)^{1/2}(r_{ij}-r_0)]\}-E_0$	70
3.2	The bond angle types and relative parameters for harmonic potential function $U(r)=\frac{1}{2}k(\theta-\theta_0)^2$	71
3.3	The parameters for non-bonded potentials.....	73
4.1	The calculated electronic bandgap differences in eV when some torsional angles are imposed on the polymer main chain in the three different torsional schemes	100
6.1	Lattice parameters a and b of pristine and doped P3BT obtained by optimization.	155
6.2	Diffusion coefficients of Cl^- ion (in units of $10^{-12} m^2/s$) at three temperatures in 25% Cl^- doped P3BT lattice with different structural models. KM represents Kawai model; IM -- Interplanar model; E -- Equal Charge distribution; P -- Polaron charge model.	163
6.3	Diffusion coefficient of Cl^- ion (in units of $10^{-12} m^2/s$) at three temperatures in 50% Cl^- doped P3BT lattice with different structural models. KM represents Kawai model; IM -- Interplanar model; E -- Equal Charge distribution; BP -- Bipolaron charge model.....	171
6.4	Diffusion coefficients (in units of $10^{-12} m^2s^{-1}$) of B and F atoms at three temperatures in 25% BF_4^- doped P3BT lattice in different structural models. KM represents Kawai model; IM -- Interplanar model; E -- Equal Charge	

distribution; P -- The charge distribution in the polymer corresponds to that of a polaron.....	183
6.5 Calculated diffusion coefficients (in units of 10^{-12} m ² /s) of B and F atoms at three temperatures in 50% BF ₄ ⁻ doped P3BT lattice with different structural models. KM represents Kawai model; IM -- Interplanar model; E -- Equal Charge distribution; BP -- The charge distribution in the polymer corresponds to that of a bipolaron.....	188
7.1 The energy barriers in eV for migration of dopant Cl ⁻ in P3BT lattice.....	200

Part I

INTRODUCTION AND THEORY

Chapter 1

INTRODUCTION TO CONDUCTING POLYMERS AND SOLUBLE POLY(S-ALKYLTHIOPHENE)S

1.1 Conducting Polymers

Part I

INTRODUCTION AND THEORY

In the past 30 years, conducting polymer systems have increasingly been used as alternatives for structural materials such as wood, ceramics, and metals because of their high strength, light weight, ease of chemical modification, and easy processability in large quantities.

In the late of 1970s, many researchers directed their interests to organic conductive polymers with hope that these materials could be processed using conventional technology for plastics. The search for new materials combining the processability, low density, and flexibility of plastics with the electrical conductivity of metals was a driving force in the development of conducting polymers.

In general, there are two kinds of conducting polymers. The first type consists of intrinsically conducting polymers in which the ionic doping species can conduct electricity owing to their fast random charge the matrix. The major practical function of the polymer is to serve as a matrix to hold the conductive elements together as a solid entity. These systems such as polyaniline oxide (PAO) and polypyrrole oxide (PPO) were first reported in 1973 and were considered as solid electrolytes [1]. The dopant atoms (M) in the polymer backbone are with the same size as the O, S or N atoms. The

Chapter 1

INTRODUCTION TO CONDUCTING POLYMERS AND SOLUBLE POLY(3-ALKYLTHIOPHENE)S

1.1 Conducting Polymers

In the past 50 years, conventional insulating polymer systems have increasingly been used as substitutes for structural materials such as wood, ceramics, and metals because of their high strength, light weight, ease of chemical modification, and easy processibility at low temperatures.

In the late of 1970s, many researchers directed their interests to organic conductive polymers with hope that these materials could be processed using conventional technology for plastics. The search for new materials combining the processibility, low density and durability of plastics with the electrical conductivity of metals was a driving force in the development of conducting polymers.

In general, there are two kinds of conducting polymers. The first type consists of ionically conducting polymers in which the ionic doping species can conduct electricity owing to their fast motion through the matrix. The major practical function of the polymer is to serve as a matrix to hold the conductive elements together in a solid entity. These systems such as polyethylene oxide (PEO) and polypropylene oxide (PPO) with alkali halides or alkali perchlorates were proposed as solid electrolytes [1]. The dopant cation M^+ is thought to be associated with the chain via the O, S or N atoms. The

polymers are not intrinsic electrical conductors. This thesis will not be concerned with this kind of polymers.

The second type is comprised of π -conjugated polymers in which the polymer backbones are responsible for the generation and propagation of charge carriers. In 1977, Shirakawa et al. [2] discovered that partial oxidation with iodine or other reagents made polyacetylene films 10^9 times more conductive than they were originally. In 1979, Ivory et al. [3] made a further significant advance. They found that polyparaphenylene could also be doped to give a high conductivity. Following these fundamental observations, a number of π -conjugated polymers were subsequently shown to also possess the same characteristic behavior when similarly doped. The family of these conducting and semiconducting polymers includes doped *trans*- and *cis*- polyacetylene $[(CH)_x]$, polythiophene (PT), polypyrrole (PPy), polyaniline (PAn), poly(p-phenylene) (PPP), poly(p-pyridine) (PPyr), poly(p-phenylene vinylene) (PPV), poly(p-pyridyl vinylene) (PPyV), and poly(1,6-heptadiyne).

The electrical conductivity of the intrinsically conducting polymer systems now ranges from those typical of insulators ($<10^{-10}$ S/cm) to those typical of semiconductors such as silicon ($\sim 10^{-5}$ S/cm) to those greater than 10^{+4} S/cm (nearly that of a good metal such as copper, $5 \times 10^{+5}$ S/cm) [4,5].

A key feature of these polymers is a backbone consisting of alternating single and double bonds resulting in a π -conjugated network, which is formed by overlap of p_z orbitals of atoms such as C, N, S in the polymer backbone and alternating bond lengths [6]. This in turn leads to a relatively small energy gap, enabling the appearance of both semiconducting and metallic properties. The maximum extent of delocalization is in the range of about 15-20 multiple bonds linked together [7,8]. All neutral conjugated

polymers are large band gap semiconductors with band gaps generally in excess of about 1.5 eV [9-12].

An extended π -conjugation is necessary but not sufficient for this type of polymer to be conductive. Doping a large number of free carriers into the polymer with the extended π -electron systems is essential to make the polymer conductive. In the doped form, the polymer backbone is either positively or negatively charged according to the charge on the small counter ions, dopants, such as I_3^- or Li^+ which are the products of the oxidizing or reducing agents such as I_2 or Li , respectively. An important criterion in selecting potentially conducting polymers is therefore the ease with which the system can be oxidized or reduced. This accounts in part for the choice of π -conjugated unsaturated polymers in which electrons of π character can be relatively easily removed or added to produce a charge in the polymer backbone without much disruption of the σ bonds which are primarily responsible for holding the polymer together.

In some cases oxidation or reduction of the polymer can be achieved electrochemically by subjecting the neutral polymer to the appropriate oxidizing or reducing voltage in an electrochemical cell. The charge appearing on the polymer chain is then balanced by a counter ion from the electrolyte solution. Electrochemical doping of polyacetylene was demonstrated in 1979 [13]. An important subgroup of intrinsically conducting polymers consists of those prepared by the electrochemical oxidation of some monomers which polymerize at the anode of an electrochemical cell. This class includes PT, PPy and their derivatives.

Initially these polymers were unstable in air, insoluble and not readily processed. Over the past decade, major advances have been made in the synthesis of new forms of conducting and semiconducting polymers that enable processing under a broad range of conditions including organic solvents, inorganic solvents, and aqueous media. There are

even melt-processible versions of some of the electronic polymers such as poly(3-alkylthiophene)s (P3ATs) [38-41].

A prime focus of the field has been the determination of the mechanisms for charge conduction and intrinsic conductivity of these fascinating materials, especially doped polymers. However, in the past decade, interest has increased in the semiconducting (generally undoped) forms of these polymers, including photophysical behaviour and their use in a wide variety of devices [50,54]. The reports of light-emitting devices fabricated from molecular and oligomeric constituents in the mid-1980s and from polymeric constituents in 1990 stimulated interest in this area of research. In addition to the fundamental science of the semiconducting and highly conducting states there has been increased emphasis in the potential uses of these materials for a broad range of applications.

The use of conducting polymers to dissipate static electricity has been under commercial development for some time [5]. Some of these polymers are of interest in the areas of electromagnetic-interference shielding and electron beam resists. The semiconducting forms of polymers have been of interest in the areas ranging from light-emitting devices to uses as second-order and third-order nonlinear optical materials.

Numerous other applications are dependent upon the change in the optical or charge-transport properties of polymers upon exposure to various environments. These include uses [5,9,14,15] for electrochromic displays, drug-delivery systems, volatile organic-compound sensors, photovoltaics, batteries, pH control, electron-beam resists, and anticorrosion coatings for ferrous materials.

1.1.1 Doping

π -conjugated polymers can be rendered electrically conductive by chemical or electrochemical oxidation and reduction. Upon exposure to suitable electron acceptors (oxidizing agents) or electron donors (reducing agents), a transformation from an insulator to a conductor takes place in these polymers. This process is called doping.

Typical oxidizing agents include I_2 , AsF_5 , $FeCl_3$, and $NOPF_6$, whereas chemical reduction, when possible, is best accomplished with reducing agents such as sodium naphthalide [14,15]. Upon exposure to these charge transfer agents, the conductivity of the polymer rises rapidly and eventually levels off at some maximum conductivity characteristic of the particular polymer and the type of chemical agent used to dope it. The doping agents influence the level of conductivity in a number of ways including how homogeneously they are distributed throughout the polymer and whether or not they are capable of initiating side reactions that inhibit the polymer's ability to achieve high conductivity. Note that charge transfer agents are frequently referred to as dopants by analogy with the doping process used to raise the conductivity of inorganic semiconductors such as silicon. Although, this analogy may not be completely appropriate, its pervasive use in the literature cannot be ignored and in this thesis we shall also refer to these charge-transfer agents as "dopants".

The influences of the processes of oxidation (p-type doping) and reduction (n-type doping) on the band gap are through the addition of electrons to the conduction band (n-type doping) or removal of electrons from the valence band (p-type doping).

However, unlike the doping of inorganic semiconductors, the concentration of free spins in most conducting polymers is simply too low to account for the level of conductivity observed in these materials. In particular, it has been found that at low dopant levels the concentration of free spins increases with the conductivity, but as the

doping is continued, it saturates and eventually decreases to become undetectable at higher doping levels [16]. This is due to the special way that the charges are stored on the polymer backbone and their influence on the electronic band structure of the polymer.

Essentially two main types of conjugated polymer backbones can be identified: those with nondegenerate ground state structures such as polypyrrole, polythiophene and their derivatives [17] and those with degenerate ground state structures such as polyacetylene [18].

During the doping process of nondegenerate ground state structures [19-25], first, an electron is removed (oxidation) from the π system of the backbone creating a free radical with spin $\frac{1}{2}$ and a spinless cation. The radical and cation are coupled to each other via a local bond rearrangement, which in this case takes the form of a sequence of quinoid-like rings as illustrated in Fig. 1.1(a) by an example of P3AT. The quinoid-like lattice distortion is of higher energy than the remaining portion of the chain which still retains a benzoid-like bonding configuration. Thus, separation of these defects along the chain and the concomitant creation of additional high energy quinoid-like structure costs a considerable amount of energy. This limits the number of quinoid-like rings that can link these two bond species together. In the cases of polypyrrole and polythiophene, the lattice distortion is believed to extend over about four pyrrole or thiophene rings [12,26]. This combination of a charged site coupled to a free radical via a local lattice distortion is called a polaron as shown in Fig. 1.1(a). A polaron can take the form of a radical cation (chemical oxidation) or a radical anion (chemical reduction). Polaron formation creates new localized electronic states in the gap, with the lower energy states being occupied by single unpaired electrons. So a polaron has spin. Theoretical studies indicate that the polaron states of polypyrrole are symmetrically located about 0.5 eV from the band edges [11]. Upon further oxidation, an electron can be removed from either the polaron or the

remaining neutral portion of the chain. In the former case, the free radical of the polaron is removed and a dication is created comprised of two positive charges coupled through the lattice distortion. This new spinless defect is called a bipolaron (shown in Fig. 1.1(a)). Removal of a second electron from a neutral portion of the chain, on the other hand, would create two polarons. Since the formation of a bipolaron produces a larger decrease in ionization energy compared to the formation of two polarons [9], the former process is thermodynamically more favorable than the latter. At higher doping levels, it also becomes energetically possible for two polarons on the same chain to combine to produce a bipolaron. Thus, additional oxidation is accompanied by the elimination of polarons and the emergence of new localized bipolaron states. These new empty bipolaron states are also located symmetrically within the band gap about 0.75 eV away from the band edges in the case of polypyrrole [11]. Continued doping of the polymers creates additional localized bipolaron states which, at high enough doping levels, can overlap to form continuous bipolaron bands. The band gap of the polymer is also increasing during this process as the newly formed bipolaron states are created at the expense of the band edges. For conjugated polymers that can be heavily doped, it is theoretically possible that the upper and lower bipolaron bands will eventually merge with the conduction and valence bands respectively to produce partially filled bands and metallic-like conductivity.

For the conjugated polymer with degenerate ground state structures, the situation shows some difference [18]. The initial oxidation of the conjugated polymer, trans-polyacetylene, also creates polarons as illustrated in Fig. 1.1(b). Further oxidation of the polymer, however, since the ground state structure of polyacetylene is twofold degenerate, the charged cations are not bound to each other by a higher energy bonding configuration and can freely separate along the chain. In other words, the bonding

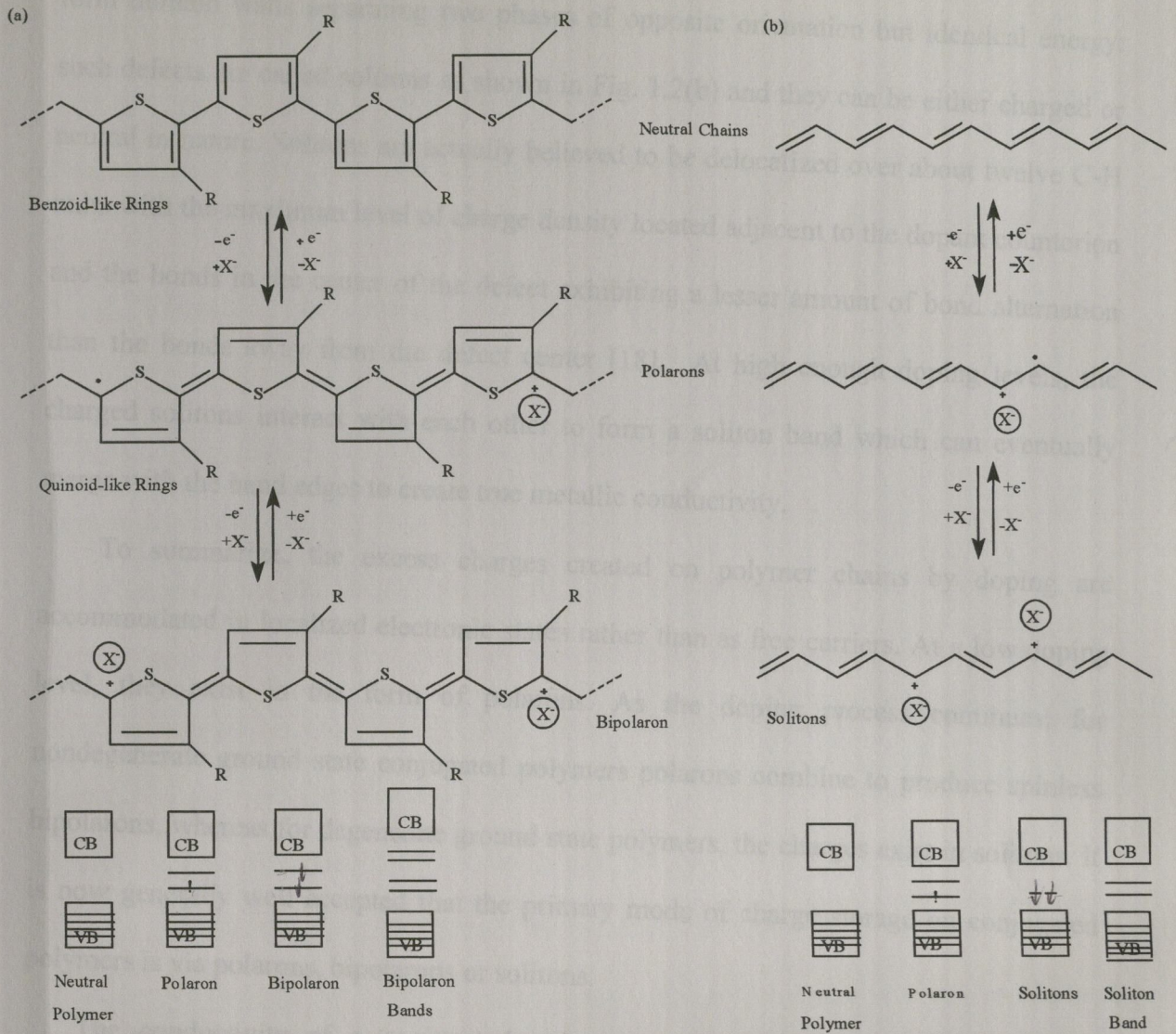


Fig.1.1 The oxidation processes of π -conjugated conducting polymers and the creation of polaron, bipolaron and soliton states. (a) Nondegenerate P3AT, (b) Degenerate polyactylene. Where R = H or alkyl group; $X^- = ClO_4^-, PF_6^-, I_3^-,$ etc

configurations on either side of the charged defects are resulted by a shift of the single and double bonds along the conjugated chain and are therefore energetically equivalent resonance forms. In essence, we now have isolated noninteracting charged defects that form domain walls separating two phases of opposite orientation but identical energy: such defects are called solitons as shown in Fig. 1.2(b) and they can be either charged or neutral in nature. Solitons are actually believed to be delocalized over about twelve C-H units with the maximum level of charge density located adjacent to the dopant counterion and the bonds in the center of the defect exhibiting a lesser amount of bond alternation than the bonds away from the defect center [18]. At high enough doping levels, the charged solitons interact with each other to form a soliton band which can eventually merge with the band edges to create true metallic conductivity.

To summarize, the excess charges created on polymer chains by doping are accommodated in localized electronic states rather than as free carriers. At a low doping level, they exist in the form of polarons. As the doping process continues, for nondegenerate ground state conjugated polymers polarons combine to produce spinless bipolarons, whereas for degenerate ground state polymers, the charges exist in solitons. It is now generally well accepted that the primary mode of charge storage on conjugated polymers is via polarons, bipolarons or solitons.

The conductivity of a conjugated polymer varies with the amount of dopant incorporated in the polymer. It should be noted that electron transfer through chemical oxidation (or reduction) involves the creation of a charged polymeric backbone and the introduction of a counterion that ensures that the charge neutrality is preserved. Thus, the amount of dopant incorporated in the polymer is usually expressed as the mole fraction of counterion per repeat unit. At low doping level, the conductivities of the polymers increase with the amount of dopants. As the concentration of dopants increases to a

particular level, the conductivity reaches the highest value and a plateau region appears. For most conducting polymers, the plateau region represents a level of conductivity between 1.0 and 1000 S/cm with the highest being 10^5 S/cm for polyacetylene [27]. In contrast to traditional semiconductor doping where doping levels in the parts per million range are typically used to enhance conductivity, most conducting polymers become highly conducting only when the doping exceeds about 1 mole % dopant/monomer.

1.1.2 Transport of Charge in Conducting Polymers

Although solitons and bipolarons are believed to be the primary source of charge carriers in conducting polymers, the exact mechanisms by which charge is transported in these materials are still largely unknown. The problem arises because, unlike the well ordered state of a crystalline metal or semiconductor lattice, most polymers are highly disordered materials comprised of both crystalline and amorphous regions. Substantial disorder is also introduced into the polymer by the diffusion of counterions during the doping process thus essentially ensuring that the electronically conductive form of a conjugated polymer will be dominated by the effects of disorder. This state of affairs is further complicated by the fact that many doping processes do not produce a homogeneously doped material but rather create a polymer comprised of regions of both highly doped material and undoped or lightly doped material [28]. It therefore becomes necessary to consider not only the transport of charges along and between chains, but also across the complex domain boundaries established by the multitude of phases that can be present in the material. The amazing fact that many conducting polymers exhibit high levels of conductivity in spite of their high degree of structural disorder continues to fuel the search for better ways to control the microstructure of these materials.

As a result of the large variation in ordering possible in conducting polymers and the diverse microstructures present in these materials, many different possible conduction mechanisms have been proposed following experiments [29]. The large change in electrical conductivity that occurs with doping also suggests that a number of different conduction mechanisms may be needed to explain the observed transport behavior. The common way to explore the mechanism of conduction in materials is to examine the temperature and frequency dependence of the conductivity over a range of many decades. These measurements provide valuable information about the nature of the charge carriers, their mobility, and the activation energies associated with the charge transport.

At low doping levels the charged defects on the conjugated polymer chains do not exist within extended states but rather are confined to localized states. As the doping level increases, these states can overlap to form soliton or bipolaron bands; however, they will be either completely filled (n-type doping) or completely empty (p-type doping). Only at very high doping levels will these latter bands merge with the conduction and valence bands to produce true metallic-like conductivity and this final state is known to occur in only a select number of conducting polymers. Thus, over much of the conducting regime of these materials, transport occurs by the movement of charge carriers either between localized states or between soliton, polaron, or bipolaron states. Alternatively, in those cases where inhomogeneous doping produces metallic islands dispersed throughout an insulating matrix, conduction occurs by movement of carriers between these highly conducting domains. The net result is that transport in conducting polymers is dominated by thermally activated hopping or tunneling processes in which carriers hop across, or tunnel through, barriers created by the presence of isolated states or domains. By its very nature, charge transport of this type dictates that the conductivity will decrease with decreasing temperature.

Although several models for charge transport have been proposed by theoretical calculations over the past decades [30-34]. The study of charge transport in doped conducting polymers is very difficult especially by direct experimental measurements. In the real materials it is usual to study the transport behavior of dopants (or counterions) instead of making a direct investigation of the charge transport behaviour.

1.1.3 Stability and Processibility

Good environmental stability and processibility are very important for all the conjugated polymers to be successful commercial materials. Table 1.1 [9] lists the

Table 1.1. Stability and processing status of representative conducting polymers*.

Polymer	Conductivity (S/cm)	Stability (doped state)	Processing Possibilities
Polyacetylene	$10^3 - 10^5$	poor**	limited***
Polyphenylene	1000	poor	limited
PPS	100	poor	excellent
PPV	1000	poor	limited
Polypyrroles	100	good	good
Polythiophenes	100	good	excellent
Polyanilines	10	good	good

* cited from Rubner M F. "Molecular Electronics, Chapter 2 Conjugated Polymeric Conductors", p89, Ed. Ashwell G J., Research Studies Press LTD, England, 1992.

** "poor" means essentially unstable in its doped state under normal atmospheric conditions.

*** "limited" means that the polymer can only be processed into usable forms by specialized techniques whereas "excellent" indicates that processibility can be achieved by a number of different conventional processing techniques.

stability and processibility of a number of conjugated polymers along with the typical levels of conductivity reached after doping with suitable oxidizing agents. In general, the conducting polymers based on heterocyclic repeat units (thiophenes and pyrroles) exhibit the best overall environmental stability [35]. The environmental stability of these heterocyclic conducting polymers can be further enhanced by introducing an electron donating substituent onto the three or four position of the heterocyclic ring which has the effect of lowering the oxidation potential of the polymer and stabilizing its positively charged bipolaron states [36]. The poly(3-alkylthiophene)s (P3ATs) provide an excellent example of these kind of polymers [37]. A great deal of progress has been made towards the development of stable conducting polymers; however, this issue continues to be of paramount importance to the successful utilization of these materials in commercial applications.

The very structural attributes that give rise to the interesting electrical and optical properties of these materials, namely their rigid, planar conjugated backbones, severely limit the ways in which the polymer can be processed. Many of the initially prepared conducting polymers were formed as intractable, insoluble films or powders that, once synthesized, could not be further manipulated into forms with more ordered, controllable structures. To overcome these limitations, many techniques have been developed to improve their processibility or allow the state of the final product to be more controllable. They include the preparation of soluble precursor polymers or soluble conducting polymer derivatives and copolymers, the in-situ polymerization of conducting polymers in insulating matrix polymers, and the manipulation of conducting polymers via a Langmuir Blodgett technique.

One of the attractive ways to improve the derivatives of heterocyclic conducting polymers is by simply substituting the hydrogen atom attached to the three position of

thiophene ring with an alkyl group containing at least four carbons. It is possible to obtain conjugated polythiophenes that are both soluble and melt processible [38-41] in this way. The conductivities of the doped derivatives are also comparable to that of the doped parent polymer and generally range from 1-200 S/cm and even as high as 1000 S/cm for regioregular head-to-tail P3ATs (HT-P3ATs) [42-45]. Thus the substitution dramatically modifies the processibility of the polythiophenes without severely compromising their electrical properties. Regioregular HT-P3ATs are the materials in which our interest lies in this thesis and we will discuss them in greater detail in section 2 and in the following chapters. Water soluble derivatives of polythiophene [46,47] and polypyrrole [48] can also be prepared by placing carboxylic acid or sulfonic acid groups within the alkyl chains. These materials are fitted with built-in ionizable groups that can be utilized to maintain charge neutrality in the oxidized state; hence they are sometimes referred to as "self-doped" polymers. LB films have also been fabricated directly from P3ATs [49]. A continued effort along this path will no doubt produce a wide variety of electrically conductive polymers with excellent processing attributes and good environmental stability.

1.1.4 Applications

Full reviews on applications of electrically conducting polymers can be found in references [5, 55-58]. The first section of applications of these polymers takes advantage of their reversible redox properties. The second section, on the other hand, focuses on the fact that these materials can be made electrically conductive. In the former case, each application exploits the fact that the electrical and optical properties of conducting polymers depend, in a controllable manner, on their level of oxidation or reduction. By

reversibly switching between two redox states, for example, it is possible to construct molecular electronic devices [50], electrochromic displays [51], polymer based rechargeable batteries [52]. Controlled drug release systems [53] can also be made by systematically releasing dopant counterions that contain active drug components by electrochemically reversing the doping process. Chemical and biochemical sensors based on conducting polymers also rely on reversible changes in the optical and electrical properties of these materials that occur in the presence of redox active chemical agents. The second section of applications includes uses as electrostatic materials, conducting adhesives and electromagnetic shielding materials.

Finally, it should be noted that the neutral forms of these conjugated polymers exhibit extremely large and fast optical nonlinearities that could prove useful in optoelectronic and all optically signal processing applications [54]. The operating frequency of the molecular electronic device is affected by diffusion rates of ions into and out of the polymer films. The transport of charge carriers affects the optical properties of devices.

1.2 Soluble Conducting Polymers--- Poly(3-alkylthiophene)s

Due to the problems of solubility, processibility and stability, it has only recently become possible for companies to bring products of π -conjugated conducting polymers to the market. The development of highly conductive polymers with good environmental stability and more acceptable processing attributes has been a focus since the basic structural features required to obtain highly conductive materials were identified. This is

because most of the conjugated polymers of interest were essentially unstable in air and not capable of being processed into scientifically or technologically usefully forms.

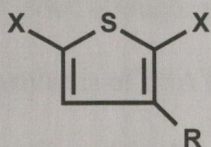
Of the many interesting conducting polymers that have been developed over the past 25 years, those based on polyanilines, polypyrroles, polythiophenes, polyphenylenes and poly(p-phenylene vinylene)s have attracted the most attention. Although the polyaniline family stands out for its ability to form processible conductive forms at relatively low cost and in bulk amounts [59], unfortunately the possible presence of benzidine moieties in the polymer backbone might yield toxic (carcinogenic) products upon degradation [60]. The hetero aromatic polypyrrole and polythiophene, as well as poly(p-phenylene vinylene), are possibly more environmentally "friendly" systems. In order to overcome the disadvantage that these polymers are insoluble and infusible, numerous substituted derivatives have been developed that carry alkyl, alkoxy, and other substituents along their backbones. Although these side chains provide a level of control of both the physical and electronic properties, they often result in a degradation of the ultimate accessible electronic properties relative to the parent [61-64].

Soluble P3ATs have been intensively investigated because of their interesting physical properties in both neutral and oxidized states and their great synthetic flexibility [64,65]. Moreover, the presence of alkyl substituents on the polythiophene backbone not only modify the processibility but can also modulate the electrical, electrochemical, and optical properties of the resulting polymers. The presence of substituents can even lead to physical phenomena such as thermochromism that are not found in the parent unsubstituted polymer [66-69]. The nonoxidized forms of these conjugated polymers have exceptionally large nonlinear optical susceptibilities [54] that could prove useful in the development of new materials for the emerging area of nonlinear optics (photonics).

Doped regioregular HT-P3ATs possess excellent conductivity with high degrees of crystallinity and self-assembled structure [70,71].

1.2.1 Synthesis

The first chemical synthesis of environmentally stable and soluble P3ATs was reported by Elsenbaumer and co-workers [41,66,72] in 1985 by coupling 3-alkylthiophene or



where X = I, Br or Cl, and R is alkyl group.

Very shortly after these reports, other groups [39-40,73] also reported both chemical and electrochemical preparation of P3ATs.

In general, P3ATs can be prepared by FeCl_3 methods, Grignard coupling methods and electrochemical methods. The ^1H NMR of P3AT showed that the polymer contains only a 2,5 linkage with random regiospecificity.

It is important to point out that these methods produce irregular P3ATs with only 60-80% head to tail (HT) couplings and different conjugation lengths. Regioregular HT coupled P3ATs can be synthesized by the McCullough method [42,43,74-81] and Rieke method [44-45,82-84] as illustrated in Figures 1.2 and 1.3, respectively.

The McCullough and Rieke methods of synthesis of regioregular HT-coupled P3ATs produce comparable materials that are not spectroscopically distinct. Both methods appear to be generally applicable to thiophenes that are tolerant to organolithium, Grignard reagents, or zinc reagents.

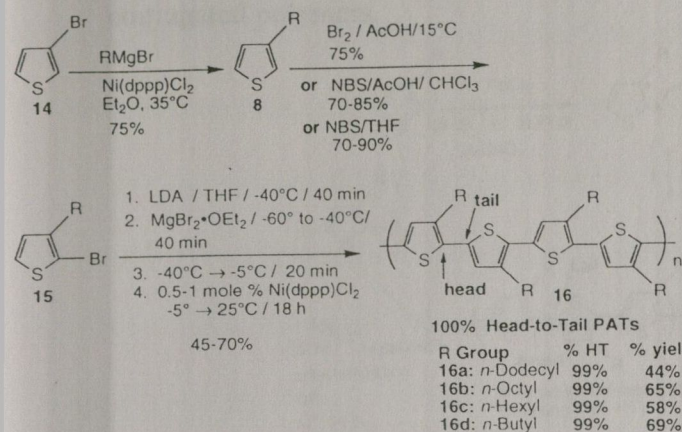


Fig. 1.2. The McCullough method for the regioregular synthesis of P3ATs with 100% head-to-tail couplings (cited from ref.70).

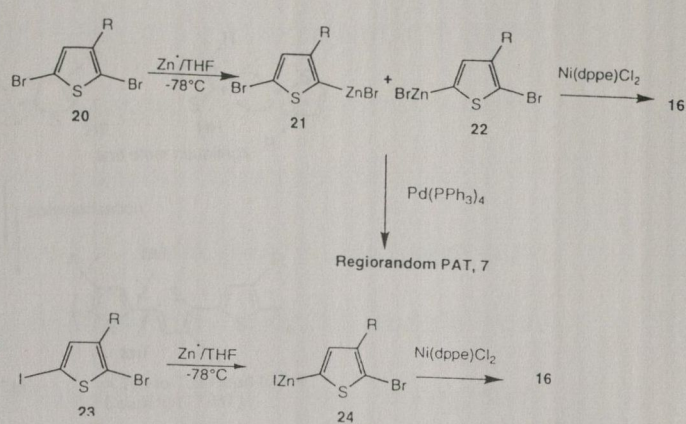


Fig. 1.3. The Rieke method of Preparing regioregular HT-P3ATs (cited from ref. 70)

1.2.2 Regioregularity

Since 3-alkylthiophene is not a symmetrical molecule, there are three relative orientations available as shown in Figure 1.4 when two thiophene rings are coupled between the 2- and 5-positions. The first of these is 2,5 or head-to-tail coupling (referred to hereafter as HT), the second is 2,2 or head-to-head coupling (HH), the third is 5,5 or tail-to-tail coupling (TT). FeCl₃ methods, Grignard coupling methods and electrochemical methods afford products with three possible regiochemical couplings: HH, TT, and HT. This leads to a mixture of four chemically distinct triad regioisomers when 3-substituted thiophene monomers are employed. These structurally irregular polymers will be denoted as irregular or non-HT. Irregularly substituted polythiophenes have structures where unfavorable HH couplings cause a sterically driven twist of thiophene rings, resulting in a loss of conjugation. On the other hand, regioregular HT P3ATs (McCullough and Rieke

methods) can easily access a low energy planar conformation, leading to highly conjugated polymers.

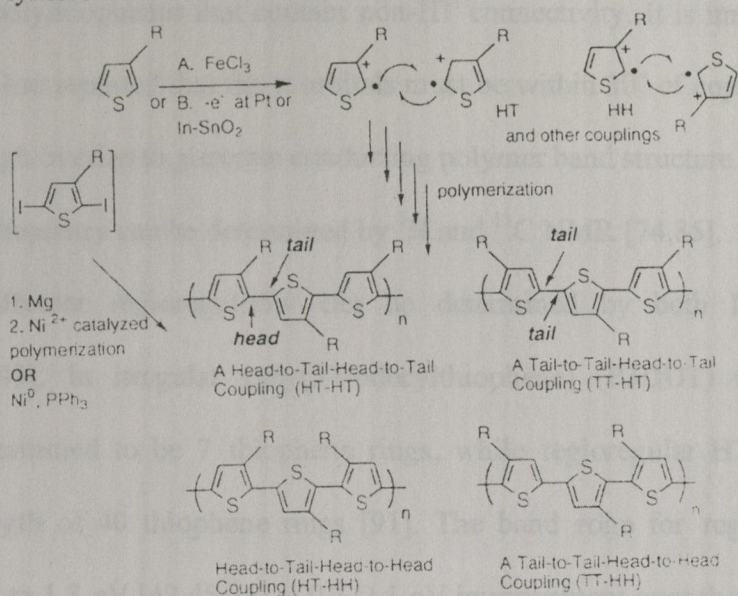


Fig.1.4. Possible regiochemical coupling in P3ATs (cited from ref. 70).

An increase of the torsion between thiophene rings leads to greater bandgaps, with consequent destruction of high conductivity and other desirable properties. Therefore increases in HT coupling lead to a more highly conductive P3AT.

Molecular mechanics and *ab-initio* methods [85-86] show that for HT P3ATs the thiophene rings prefer an *anti* coplanar orientation. Structures with the rings twisted by up to 20° (molecular mechanics) or up to 50° (*ab-initio*-STO-3G) from co-planarity all lie within less than 1 kcal of each other on a very flat potential energy surface and accordingly are easily accessible [87]. The advantage of HT coupling is supported by crystalline evidence from HT-HT oligomers of 3-methylthiophene [88]. HT trimers of 3-methylthiophene are calculated to have a torsional angle of $7-8^\circ$ between conjoined rings [85]. This compares favorably with $6-9^\circ$ observed in X-ray structure of unsubstituted α -terthienylene [88].

The quantum mechanical calculations indicate that HH and TT couplings destroy conjugation, inhibit intrachain charge mobility [89], and can result in poor electrical conduction in polythiophenes that contain non-HT connectivity. It is important to point out that Brédas has reported that the π orbitals must be within 30° of coplanarity in order to achieve enough overlap to generate conducting polymer band structure [90].

The regiochemistry can be determined by ^1H and ^{13}C NMR [74,85]. The conjugation length with different regioregularity can be determined by both IR and UV-vis spectroscopy [45]. In irregular poly(3-dodecylthiophene) (P3DDT) the conjugation length was determined to be 7 thiophene rings, while regioregular HT-P3DDT has a conjugation length of 40 thiophene rings [91]. The band edge for regioregular P3AT ranges from 1.7 to 1.8 eV [42,45,75], a 0.3-0.4 eV improvement over the 2.1 eV reported for a regiorandom sample [12].

In this thesis, we deal only with HT-coupling regioregular P3ATs. These materials are highly crystalline and have the longest planar conjugation structure and highest conductivity in both their neutral and other oxidation states.

1.2.3 Self-assembly and High Electrical Conductivity in Regioregular

HT-P3ATs

One of the most fascinating physical properties of HT-P3ATs is their supermolecular ordering. Self-assembly in regioregular HT-P3ATs was first discovered by McCullough [42-43]. Solution light scattering studies [92-96] by Berry and co-workers [97] coupled with X-ray studies by McCullough et al. [42] and Winokur et al. [98] on thin films show

that macromolecular self-assembly occurs in these conducting polymers and presents in ordered planar superstructures.

The self-assembled structures lead to a large increase in electrical conductivity in HT-P3ATs relative to irregular P3ATs. While the measured conductivity of HT-P3AT films cast from the same sample can differ markedly as a result of varying morphology from film to film, for the conductivities of HT-P3ATs the maximum reported value is 1000-2000 S/cm [42,44,45] and the lowest is about 100-200 S/cm [42,74,85]. This is still much higher than that of irregular P3ATs synthesized by FeCl_3 methods the value for which is typically 0.1-1 S/cm.

1.2.4 Stability

Despite the fact that polythiophenes are one of the most environmentally and thermally stable materials that can be used as polymeric electrical conductors, the stability of the oxidized (conducting) state of P3ATs is limited in air at high temperatures ($>100^\circ\text{C}$) [99]. This is partly due to the relatively high oxidation potential (ca. 0.8-1.0 eV).

Initial studies [100] on alkyl-substituted polythiophenes have suggested that thermally induced steric interactions between the side chain and the counterions (which maintain the electroneutrality of the polymer upon oxidation) could be responsible for the dedoping reaction observed at high temperatures. Indeed, it has been found that a regular empty space along the backbone, created by decreasing the number of flexible side chains, gives better stability in the doped state.

It seems that the introduction of flexible side chains induces limited thermal stability in the conducting state. However, it is clear that, for a given polymer, the nature of the

counterions may also have a strong influence on the stability of the conducting state [101-103].

1.2.5 Solubility and Processibility

P3ATs with alkyl groups with a number of carbon atoms equal to or greater than four are soluble in common organic solvents such as chloroform, THF, xylene, toluene, methylene chloride, anisole, nitrobenzene, benzonitrile, and nitropropane [104-107]. Casting from any of the aforementioned solvents affords thin films of P3ATs. So P3ATs can be easily processed in solution and even in the melt [38-41].

1.2.6 Crystalline and Lattice Structure

Regiorandom P3ATs are partially crystalline or amorphous, whereas regioregular HT-P3ATs are self-assembled crystalline materials [45, 70-71]. In contrast to regiorandom P3ATs where the microcrystallization and orientation of polymers are induced by mechanical stretching, regioregular HT-P3ATs are polycrystalline and self-orienting polymers with three-dimensional ordering [108-110]. The X-ray diffraction patterns of regioregular HT-P3ATs cast from chloroform solution by air evaporation showed strong first-, second- and third-order reflections. For example, regioregular HT-P3HT presents peaks at 2θ angles of 5.4, 10.8 and 16.3° [45]. Polarized microscopy also showed their self-assembled crystalline texture with self-organized lamellar morphology which was obviously caused by the “alternating inverse comb” structure of polymers induced by the head-to-tail regiospecificity [45].

From their unit cell dimensions determined by X-ray diffraction (XRD) patterns, several models for the crystalline structure have been proposed. Basically they can be divided into two groups: two-chain models and one-chain models. Two chain-models are more favorable for regioregular HT-P3ATs.

1.2.6.1 Kawai Structure Model

In the structure proposed from the X-ray diffraction studies of Kawai et al [111-114], two chains are aligned along the **c** axis of an orthorhombic unit cell. The second chain, while parallel with the first, is separated from it by $\frac{1}{2} b$ along the **b** axis. It is also shifted by $\frac{1}{2} c$ along the **c** axis so that viewed along **b**, alternate rings are staggered as shown in Fig. 1.5. The interplanar layers are formed by the stacking of coplanar sub-

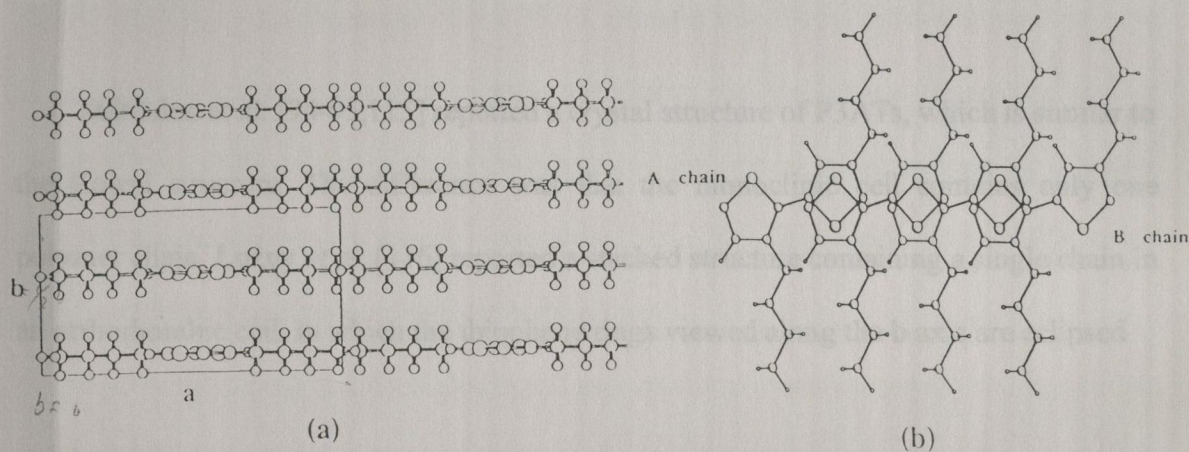


Fig. 1.5 The lattice structure of P3ATs proposed by Kawai *et al.* [111-114],

(a) viewed along **c** axis, (b) viewed along **b** axis.

chains, while the side chains with nearly planar alternating zigzag (or nearly all-trans) conformation are filled between two neighboring layers with partial interdigitation.

1.2.6.2 Winokur Structure Model

In the structure proposed by Winokur and coworkers, resulting from X-ray diffraction measurements [92,93, 98,110], the thiophene rings constituting the main chain are coplanar in the orthorhombic unit cell which contains two polymer chains. Each alkyl side chain, although in a planar (*all-trans*) conformation, is uniformly twisted along the C-C bond attaching it to the thiophene ring, resulting in a nonplanarity of the polymer backbone with its side chains. In this arrangement of the alkyl chains interdigitation is precluded and correlated torsional motion in the side chains of neighboring coplanar polymers should be absent.

1.2.6.3 One-chain Models

Mårdalen et al. [94-95,115] reported a crystal structure of P3ATs, which is similar to the Kawai structure. The difference was that the monoclinic cell contains only one polymer chain. Łuźny *et al.* [116] reported a stacked structure containing a single chain in an orthorhombic cell, in which the thiophene rings viewed along the **b** axis are eclipsed.

1.2.6.4 Conformational Structure

From an analysis of XRD patterns and IR absorption spectra of P3ATs [92-96,111-114,117], it has been inferred, respectively, that a planar *anti* conformation of the main chain is preferred and that major fractions with *trans* conformations appear in the alkyl side chains at low temperatures. But the main chain is not perfectly *anti* as it has small

distortions from complete planarity, and the alkyl chains have limited *gauche* or other conformations. The sulfur atoms of two neighboring stacking thiophene rings are more likely to lie in opposite directions, so that the steric repulsion between the H atoms of the alkyl side chains of the two stacking main chains can be relieved.

1.2.7 Thermochromism

Thermally induced disordering of the side chains in poly(3-alkylthiophene)s may lead to twisting of the conjugated backbone, associated with a strong blue shift in the absorption maximum in the visible region. These thermochromic effects can be observed with P3ATs [68,112,118-123] and poly(3-alkoxyl-4-methylthiophene)s [124] both in solution and in solid state. An example is poly(3-octylthiophene) (P3OT), which below 303 K is red, but when heated to above 353 K changes to yellow. Upon cooling, it returns to red. During the process the maximum absorption peak in UV-vis absorption spectra shows a blue shift and the peak in the electronic absorption spectra moves to a higher energy area as the temperature is increased [71,117]. This kind of reversible color change with temperature is called thermochromism.

Structural studies have revealed that these optical phenomena result from a delicate balance between repulsive side-chain steric interactions and attractive interchain interactions [125]. At low temperatures, P3ATs can form planar or nearly planar highly conjugated assemblies. Upon heating the regularity of the chains is disrupted due to disordering of the side groups, the twisting of the backbone being associated with this disruption. It was also revealed that cooperative twisting of the backbone (indicated by the presence of an isosbestic point in the temperature-dependent optical measurements) takes place in regioregular HT P3ATs, whereas in non-regioregular P3ATs, only

localized conformational defects can be created along the backbone, leading to a monotonic blue shift in the absorption maximum upon heating [126]. However, the mechanism of the thermochromic phenomenon is still not clear.

The thermochromic properties can be useful not only as optical temperature indicators but also as materials for thermal recording [127]. Moreover, by being able to control the absorption properties of these conjugated polymers, their luminescence properties can be modified, leading to the development of light-emitting diodes with tunable colors [128].

1.2.8 Applications

Because of their excellent stability, processibility and special properties such as thermochromism, self-assembly, and high crystallinity of regioregular HT-P3ATs, P3ATs have after about 10 years of investigation now reached the stage of being used for various electrical and optical devices. Their great potential relies not only on their ability to compete with other materials in existing devices but also on their use as field responsive materials for completely new applications. They should find applications in the development of light-emitting diodes, display devices, and other applications of π -conjugated conducting polymers described in Subsection 1.1.4.

1.3 Aims of the Present Work

As discussed before, P3ATs are partially crystalline and regioregular HT-P3ATs are highly crystalline. It is therefore possible and valuable to use atomistic simulation methods to model the important properties and potentials of these new materials.

There are many applications of computer simulation that can usefully investigate various aspects of π -conjugated conducting polymers such as lattice and conformational structure, electronic structure and bandgaps, doping processes, and the mobility of charge carriers. However, this thesis will mainly concentrate on using molecular mechanics (MM) and molecular dynamics (MD) to simulate the following two important phenomena of P3ATs:

- (i) Thermally induced conformational changes and their relation to thermochromism;
- (ii) The doping and transport behavior of dopants Cl^- and BF_4^- .

Thermochromism is a special behavior of P3ATs and its mechanism is still not clear. It is believed that thermochromic behavior is associated with conformational changes induced upon heating. MM and MD are good methods to predict the properties of polymer chains that depend on their structures and conformations. In particular, MD provides an efficient way to simulate thermal agitation. These simulations will be helpful to understand and explain the thermochromic behavior.

Higher conductivity needs higher mobility or increased numbers of the charge carriers. To understand the high conductivity of regioregular HT-P3ATs, it would be useful to investigate the effects of nature of the dopants (charge carriers or counterions) by using different species such as Cl^- and BF_4^- and of the concentration of dopants on the conduction process. The transport behavior of dopants also affects the optical properties of these polymers because the operating frequency of molecular electronic devices is

affected by diffusion rates of dopant ions into and out of the polymer films. The investigation of dopant transport is of great importance in the application of these materials to molecular electronics. The diffusion rates of the dopants are also vital for the battery applications of these materials. MD can directly investigate diffusion behavior of dopants in the polymer lattices because it can calculate the diffusion coefficients of dopants under different conditions from the mean square displacement of the dopant ions, while MM is useful in the determination of the migration path and the energy barrier.

Simulations will also be useful to evaluate the thermal stability and temperature effects on conductivity of these soluble conducting polymers by analyzing the change of conformation of the polymer and diffusion of dopants with temperature.

[7] Prinsloo, A.J. and Chance R.R. *J. Polym. Sci. Polym. Phys. Ed.*, 1976, 14:2837

[8] Schwaner, K.C. *J. Chem. Phys.*, 1986, 85:4181

[9] Kubota, M. K. in "Conjugated Polymeric Conductors", Edited by Ashwell G. J., Research Studies Press Ltd, England, 1992

[10] Heeger, C.R., Peebles, D.L., Heeger, A.J., Dray, M.A., Matsumura, S., MacDiarmid, A.G., Shirakawa, H., and Ikeda, S. *Solid State Commun.*, 1978, 27:869

[11] Bradley, J.J. and Street, G.B. *Acc. Chem. Res.*, 1985, 18:309

[12] Bradley, H., Thomas, B., Fright, J.G., and Andre, J.M. *Phys. Rev. B Cond. Mat.*, 1984, 29:6281

[13] Nigry, P., MacDiarmid, A.G. and Heeger, A.J. *J. Chem. Soc. Chem. Commun.*, 1979, 13:594

[14] Skotheim, T.A. Ed. "Handbook of Conducting Polymers" Vol. 1 & 2, Marcel Dekker, New York, 1986

[15] Sereno, J. and Williams, J. "Introduction to Synthetic Electrical Conductors", Academic Press, Inc., Orlando, Florida, 1982

[16] Sereno, P. in "Handbook of Conducting Polymers", Vol. 2, p.1099, Skotheim T. A. Ed., Marcel Dekker, New York, 1986

[17] Bradley, H., Thomas, B., Fright, J.G., and Andre, J.M., and Chance R.R. *Synth. Met.*, 1984, 9:143

Bibliography

- [1] Armand M B, Chabagnon J M and Duclot M J. in "**Fast Ion Transport in Solids**", Edited by Vashita P. North Holland, New York, 1979, p665
- [2] Shirakawa H, Louis E J, MacDiarmid A G, Chiang C K and Heeger A J. *J. Chem. Soc. Chem. Commun.*, 1977, **16**:578
- [3] Ivory D M, Miller G G, Sowa J M, Shacklette L W, Chance R R and Baughman R H. *J. Chem. Phys.*, 1979, **71**:1506
- [4] Kohlman R S, Joo J, and Epstein A J. in "**Physical Properties of polymers Handbook**", edited by Mark J E, AIP Press, Woodbury, NY, 1996
- [5] Epstein A J. *MRS Bulletin*, 1997, 16
- [6] Heeger A J, Kivelson S A, Schrieffer J R, and Su W P. *Rev. Mod. Phys.*, 1988, **60**:781
- [7] Baughman R H and Chance R R. *J. Polym. Sci, Polym. Phys. Ed.*, 1976, **14**:2037
- [8] Schweizer K C. *J Chem. Phys.*, 1986, **85**:4181
- [9] Rubner M F. in "**Conjugated Polymeric Conductors**", Edited by Ashwell G J, Research Studies Press Ltd, England, 1992
- [10] Fincher C R, Peebles D L, Heeger A J, Druy M A, Matsumura Y, MacDiarmid A G, Shirakawa H, and Ikeda S. *Solid State Commun.*, 1978, **27**:849
- [11] Brédas J L and Street G B. *Acc Chem Res.*, 1985, **18**:309
- [12] Brédas J L, Themans B, Fripiat J G, and André J M. *Phy. Rev. B. Conds. Mat.*, 1984, **29**:6761
- [13] Nigrey P J, MacDiarmid A G and Heeger A J. *J. Chem. Soc. Chem. Commun.*, 1979, **13**:594
- [14] Skotheim T A, Ed. "**Handbook of Conducting Polymers**" Vol. 1 & 2, Marcel Dekker, New York, 1986
- [15] Ferraro J and Williams J. "**Introduction to Synthetic Electrical Conductors**", Academic Press, Inc., Orlando, Florida, 1987
- [16] Bernier P, in "**Handbook of Conducting Polymers**", Vol. 2, p.1099, Skotheim T A, Ed., Marcel Dekker, New York, 1986
- [17] Brédas J L, Themans B, Fripiat J G, and André J M, and Chance R R. *Synth. Met.*, 1984, **9**:265

- [18] Heeger A J, in "*Handbook of Conducting Polymers*", Vol. 2, p729, Skotheim T A, Ed., Marcel Dekker, New York, 1986
- [19] Su W P, Schrieffer J R, and Heeger A J. *Phys. Rev. B*, 1980, **22**:2209
- [20] Bishop A R, Campbell D K, and Fesser K. *Mol. Cryst. Liq. Cryst.*, 1981, **77**:253
- [21] Scott J C, Brédas J L, Yakushi K, Pflüger P, and Street G B. *Synth. Met.*, 1984, **9**:165
- [22] Brédas J L, Scott J C, Yakushi K, and Street G B. *Phys. Rev. B. Conds. Mat.*, 1984, **30**:1024
- [23] Scott J C, Brédas J L, Kaufman J H, Pflüger P, Street G B, and Yakushi K. *Mol. Cryst. Liq. Cryst.*, 1985, **118**:163
- [24] Scott J C, Krounbi M, Pflüger P, Street G B. *Phys. Rev. B. Conds. Mat.*, 1983, **28**:2140
- [25] Chung T C, Kaufman J H, Heeger A J, and Wudl F. *Phys. Rev. B. Conds. Mat.*, 1984, **30**:702
- [26] Salmon M, Diaz A F, Logan A J, Krounbi M, and Bargon J. *Mol. Cryst. Liq. Cryst.*, 1983, **83**:1297
- [27] Naarmann H, Theophilou N. *Synth. Met.*, 1987, **22**:1
- [28] Sichel E K, Rubner M F, Tripathy S K. *Phys. Rev. B*, 1982, **26**:6719
- [29] Epstein A, In "*Handbook of Conducting Polymers*", Vol.2, p.1041, Skotheim T A, Ed., Marcel Dekker, New York, 1986
- [30] Kivelson S. *Phys. Rev. B.*, 1982, **25**:3789
- [31] Emin D. in "*Handbook of Conducting Polymers*", Vol.2, p.915, Skotheim T A, Ed., Marcel Dekker, New York, 1986
- [32] Chance R R, Brédas J L, Silbey R. *Phys. Rev. B.*, 1984, **29**:4491
- [33] Mott N F and Davis E A. "*Electronic Processes in Non-Crystalline Materials*", 2nd Ed., Clarendon, Oxford, 1979
- [34] Sheng P, Abeles B, Arie Y. *Phys. Rev. Lett.*, 1973, **31**:44
- [35] Druy M A, Rubner M F, Walsh S P. *Synth. Met.*, 1986, **13**:207
- [36] Elsenbaumer R L, Jen K.-Y., Eckhardt H, Schacklette L, Jow R. in "*Electronic Properties of Conjugated Polymers*", pp400, Kuzmany H, Mehring M, Roth S, Ed., Springer-Verlag, Berlin, 1987
- [37] Gustafsson G, Inganas O, Nilsson J O, Liedberg B. *Synth. Met.*, 1988, **26**:297

- [38] Yatsumi K, Nakajima S, Fujii M, Sugimoto R. *Polym. Commun.*, 1987, **28**:309
- [39] Sato M, Tanaka S, Kaeriyama K. *J. Chem. Soc., Chem. Commun.*, 1986, 873
- [40] Hotta S, Rughooputh S D D V, Heeger A J, Wudl F. *Macromolecules*, 1987, **20**:212
- [41] Elsenbaumer R L, Jen K Y, Oboodi R. *Synth. Met.*, 1986, **15**:169
- [42] McCullough R D, Tristram-Nagle S., Williams S P, Lowe R D, Jayaraman M. *J. Am. Chem. Soc.*, 1993, **55**:1198
- [43] McCullough R D, Williams S P, Tristram-Nagle S., Jayaraman M, Ewbank P C, Miller L. *Synth. Met.*, 1995, **69**:279
- [44] Chen T.-A., Rieke R D. *Synth. Met.*, 1993, **60**:175
- [45] Chen T.-A., Wu X., Rieke R D. *J. Am. Chem. Soc.*, 1995, **117**:233
- [46] Patil A O, Ikenoue Y, Basescu N, Colaneri N, Chen J, Wudl F, Heeger A J. *Synth. Met.*, 1987, **20**:151
- [47] Patil A O, Ikenoue Y, Wudl F, Heeger A J. *J. Am. Chem. Soc.*, 1987, **109**:1858
- [48] Sundaresan N S, Basak S, Pomerants M, Reynolds J R. *J. Chem. Soc., Chem. Commun.*, 1987, 621
- [49] Logsdon P B, Pflieger J, Prasad P. *Synth. Met.*, 1988, **26**:369
- [50] Potember R S, Hoffman R C, Hu S U, Cocchiario J E, Viands C V, Murphy R A, Poehler T O. *Polymer*, 1987, **28**:574
- [51] Gazard M, in "**Handbook of Conducting Polymers**", Vol.1 p673, Skotheim T A, Ed., Marcel Dekker, New York, 1986
- [52] MacDiarmid A G, Kaner R B, in "**Handbook of Conducting Polymers**", Vol.1 pp689, Skotheim T A, Ed., Marcel Dekker, New York, 1986
- [53] Blankespoor R L, and Miller L L. *J. Chem. Soc., Chem. Commun.*, 1985, 90
- [54] Heeger A J, Moses D, Sinclair M. *Synth. Met.*, 1986, **15**:95
- [55] Yang Y. *MRS Bulletin*, 1997, 31
- [56] MacDiarmid A G and Zheng W. *MRS Bulletin*, 1997, 24
- [57] Tsutsui T. *MRS Bulletin*, 1997, 39
- [58] Salaneck W R and Brédas J L. *MRS Bulletin*, 1997, 46
- [59] Trivedi D C. in "**Handbook of Organic Conductive Molecules and Polymers**", Vol.2, pp505, Nalwa H S, Ed., Wiley, Chichester, UK, 1997
- [60] Lux F. *Farbe & Lack*, 1998, **104**:32
- [61] Koßmehl G, Schopf G. *Adv. Polym. Sci.*, 1996, **129**:1

- [62] Heeger A J. *Synth. Met.*, 1993, **55-57**:3471
- [63] Roncali J. *J. Mater. Chem.*, 1999, **9**:1875
- [64] Roncali J. *Chem. Rev.*, 1997, **97**:173
- [65] Schopf G, Koßmehl G. *Adv. Polym. Sci.*, 1997, **129**:1
- [66] Jen K Y, Miller GG and Elsenbaumer. *J. Chem. Soc., Chem. Commun.*, 1986, 1346
- [67] Rughooputh S D D V, Nowak S, Hotta S, Heeger A J and Wudl F. *Synth. Met.*, 1987, **21**:41
- [68] Rughooputh S D D V, Hotta S, Heeger A J and Wudl F. *J. Polym. Sci., Polym. Phys. Ed.*, 1987, **25**:1071
- [69] Inganäs O. in “*Handbook of Organic Conductive Molecules and Polymers*”, Vol.3, pp785, Nalwa H S, Ed., Wiley, Chichester, UK, 1997
- [70] McCullough R D. *Adv. Mater.*, 1998, **10**:93
- [71] Leclerc M and Faïd K. *Adv. Mater.*, 1997, **9**:1087
- [72] Jen K Y, Oboodi R, Elsenbaumer R L. *Polym. Mater. Sci. Eng.*, 1985, **53**:79
- [73] Sugimoto R, Takeda S, Gu H B, Yoshino K. *Chem. Express*, 1986, **1**:635
- [74] McCullough R D, Lowe R D. *J. Chem. Soc., Chem. Commun.*, 1992,70
- [75] Van Pham C, Mark H B, Zimmer H Jr., *Synth. Commun.*, 1986, **16**:689
- [76] Cunningham D D, Laguren-Davidson L, Mark H B, Van Pham C, Zimmer H Jr. *J. Chem. Soc., Chem. Commun.*, 1987, 1021
- [77] Consiglio G, Gronowitz S, Honfeldt A.-B., Maltesson B, Noto R, Spinelli D. *Chem. Sci.*, 1977, **11**:175
- [78] Tamao K, Sumitani K, Kiso Y, Zembayashi M, Fujioka A, Kodama S, Nakajima I, Minato A, Kumada M. *Bull Chem. Soc. Jpn.*, 1976, **49**:1958
- [79] Kodama S, Naajima I, Kumada M, Minato A, Suzuki K. *Tetrahedron*, 1982, **38**:3347
- [80] McCullough R D, Lowe R D. *Polym. Prepr.*, 1992, **33**:195
- [81] McCullough R D, Lowe R D, Jayaraman M, Ewbank P C, Anderson D L, Tristram-Nagle S. *Synth. Met.*, 1993, **55**:1198
- [82] Chen T.-A., O'Brien R A, Rieke R D. *Macromolecules*, 1993, **26**:3462
- [83] Chen T.-A., Rieke R D. *J. Am. Chem. Soc.*, 1992, **114**:10087
- [84] Wu X, Chen T.-A., O'Brien R A, Rieke R D. *Macromolecules*, 1995, **28**:2101

- [85] McCullough R D, Lowe R D, Jayaraman M, Anderson D L. *J. Org. Chem.*, 1993, **58**:904
- [86] Barbarella G, Bongini A, Zambianchi M. *Macromolecules*, 1994, **27**:3039
- [87] Zagorska M, Kulszewicz-Bajer I, Pron A, Firlcj L, Berier P, Galtier M. *Synth. Met.*, 1991, **45**:385
- [88] Barbarella G, Zambianchi M, Bongini A, Antolini L. *Adv. Mater.*, 1994, **6**:561
- [89] Baughman R H, Chance R R. *J. Appl. Phys.*, 1976, **47**:4295
- [90] Brédas J L. *J. Chem. Phys.*, 1985, **82**:3809
- [91] Bjørnholm T, Greve D R, Geisler T, Petersen J C, Jayaraman M, McMullough R D. *Adv. Mater.*, 1996, **8**:920
- [92] Prosa T J, Winokur M J, Moulton J, Smith P, Heeger A J. *Synth. Met.*, 1993, **55**:370
- [93] Winokur M J, Wamsley P, Moulton J, Smith P, Heeger A J. *Macromolecules*, 1991, **24**:3812
- [94] Mårdalen J, Samuelsen E J, Gautun O R, Carlsen P H. *Solid State Commun.*, 1991, **80**:687
- [95] Mårdalen J, Samuelsen E J, Gautun O R, Carlsen P H. *Synth. Met.*, 1992, **48**:263
- [96] Chen S.-A., Ni J.-M., *Macromolecules*, 1992, **25**:6081
- [97] Yue S, Berry C, McMullough R D. *Macromolecules*, 1996, **29**:933
- [98] Prosa T, Winokur M J, McMullough R D. *Macromolecules*, 1996, **29**:3654
- [99] Leclerc M, Diaz F M, Wegner G. *Makromol. Chem.*, 1989, **190**:3105
- [100] Inganäs O. *Trends Polym. Sci.*, 1994, **2**:189
- [101] Wang Y, Rubner M F, *Synth. Met.*, 1990, **39**:153
- [102] Abdou M S A, Holdcroft S *Synth. Met.*, 1993, **60**:93
- [103] Djellab H, Armand A, Delabouglise D. *Synth. Met.*, 1995, **74**:223
- [104] Nguyen M T, Leclerc M, Diaz A F. *Trends Polym. Sci.*, 1995, **3**:186
- [105] Faïd K, Leclerc M. *Chem. Commun.*, 1996, 2761
- [106] Chen S A, Hua M Y. *Macromolecules*, 1993, **26**:7108
- [107] Zinger B, Mann K R, Hill m G, Miller L L. *Chem. Mater.*, 1992, **4**:1113
- [108] Garnier F, Yassar A, Hajlaoui R, Orowitz G, Deloffre F, Servet B, Ries S, Alnot P. *J. Am. Chem. Soc.*, 1993, **115**:8716
- [109] McCullough R D, Tristram-Nagle S, Williams S P, Lowe R D, Jayarman M. *J. Am. Chem. Soc.*, 1993, **115**:4910

- [110] Winokur M J, Prosa T J, Moulton J, Smith P, Heeger A J. *Macromolecules*, 1992, **25**:4364
- [111] Kawai T, Nakazono M, Sugimoto R, Yoshino K. *Jpn. J. Appl. Phys.*, 1992, **61**:3400
- [112] Tashiro K, Ono K, Minagawa Y, Kobayashi M, Kawai T, Yoshino K. *J. Polym. Sci., Part B: Polym. Phys.*, 1991, **29**:1223
- [113] Kawai T, Nakazono M, Yoshino K. *J. Mater. Chem.*, 1992, **2**:903
- [114] Tashiro K, Kobayashi M, Morita S, Kawai T, Yoshino K. *Synth. Met.*, 1995, **69**:397
- [115] Samuelsen E J, Mardalen J, Carlsen P H, Leguennec P, Travers J.-P., Ressouche E.. *Synth Met.*, 1993, **55-57**:365
- [116] Kaniowski T, Łużny W, Nizioł S, Sanetra J, Trznadel M. *Synth. Met.*, 1998, **92**:7
- [117] Iwasaki K.-I., Fujimoto H, Matsuzaki S. *Synth. Met.*, 1994, **63**:101
- [118] Inganäs O, Salaneck W R, Osterholm J E, Laakso J. *Synth. Met.*, 1988, **22**:395
- [119] Yoshino K, Nakajima S, Onoda M, Sugimoto R, *Synth. Met.*, 1989, **28**:C349
- [120]] Inganäs O, Gustafsson G, Salaneck W R. *Synth. Met.*, 1989, **28**:C377
- [121] Winokur M J, Spiegel D, Kim Y, Hotta S, Heeger A J. *Synth. Met.*, 1989, **28**:C419
- [122] Zerbi G, Chierichetti B,] Inganäs O. *J. Chem. Phys.*, 1991, **94**:4646
- [123] Eklebad P O,] Inganäs O. *Polym. Commun.*, 1992, **32**:436
- [124] Roux C, Leclerc M. *Macromolecules*, 1992, **25**:2141
- [125] Roux C, Bergeron J Y, Leclerc M. *Makromol. Chem.*, 1993, **194**:869
- [126] Leclerc M, Fréchette M, Bergeron J Y, Ranger M, Lévesque I, Faïd K. *Macromol. Chem. Phys.*, 1996, **197**:2077
- [127] Hirota N, Hisamatsu N, Maeda S, Tsukahara H, Hyodo K. *Synth. Met.*, 1996, **80**:67
- [128] Berggren M, Gustafsson G, Inganäs O, Andersson M R, Wennerstrom O, Hjertberg T. *Appl. Phys. Lett.*, 1994, **65**:1489

Chapter 2

COMPUTATIONAL THEORY AND METHODOLOGY

Progress in computer technology together with the resultant advances in computer simulation has provided solutions to many chemical problems such as molecular structure, the design of properties, and the predication of reaction processes. This has brought beneficial effects in molecular design, the prediction and explanation of structures and properties, especially for macromolecules.

Electronic structure calculations and force field methods are two principal techniques in computational chemistry [1-3]. Electronic structure methods, such as density functional theory, use first principles in which the electrons are treated at varying levels of approximation. They are more suited to the treatment of small assemblies. Force field methods are based on using interatomic potentials including both short and long-range terms to represent the interactions between the species. In the force field methods, the calculation of electronic energy E_e for a given nuclear configuration is bypassed by writing E_e as a parametric function of the nuclear coordinates. The parameters are fitted either to experimental or to higher level computational data. QM calculations are often used to derive the potentials. Force field methods include molecular mechanics (MM), molecular dynamics (MD) and Monte Carlo (MC) techniques. They are suitable for both small and large molecule systems. As described in Chapter 1 the interest in this thesis lies in the structures and properties of poly(3-alkyl thiophene)s. Both MD (program DL_POLY) and MM

(program GULP) techniques have been used to investigate P3ATs. Extended Hückel theory was also used to calculate the effect of different torsional angles between thiophene rings on the π - π^* bandgap of poly(3-butylthiophene). In this Chapter the force field methods and related computational theory are described.

2.1 Interatomic Potentials

The core of atomistic simulation methods is the force field. A force field is the set of energy functions needed to define the interactions in a molecular system. The functions may have a wide variety of analytical forms, with some basis in chemical physics, which must be parameterized to give the correct energy and forces. These mathematical functions used to represent the interactions (potential energy) of the system as a function of particle coordinates are called interatomic potentials. The total configuration energy of a molecular system is decided by bonded potentials, non-bonded potentials and external field potentials. The choosing of good potentials and related parameters is critical for successful and accurate atomistic simulations.

2.1.1 Bonded Potentials

Bonded potentials are interactions between atoms in the same molecule connected through bonds. They include bond potentials, valence angle potentials and dihedral angle potentials (or torsion potentials).

2.1.1.1 Bond Potentials

The bond potentials describe explicit bonds between specified atoms as shown in Fig. 2.1. It is the energy function for stretching or compressing a bond between two

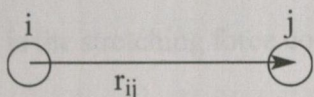


Fig. 2.1 The interatomic bond vector.

atoms i and j . In its simplest form, it is written as a Taylor expansion around a “natural”, or “equilibrium” bond length, r_0 . Terminating the expansion at second order gives the expression as:

$$U(r_{ij}) = U(0) + k_1(r_{ij}-r_0) + \frac{1}{2} k_2(r_{ij}-r_0)^2$$

The $U(0)$ term is normally set to zero. This is just the zero point for the energy scale. The second term is zero as the expansion is around the equilibrium values of energy and bond length. In its simplest form the bond potential can thus be written as harmonic form:

$$U(r_{ij}) = \frac{1}{2} k(r_{ij}-r_0)^2 \quad 2.1$$

where k is the stretching force constant for the i - j bond.

The harmonic form is the simplest possible atom-pair potential. It is in fact sufficient for the determination of most equilibrium geometries. However, for strained and crowded molecular systems, the results from a harmonic approximation are significantly different from experimental values. If the force field should reproduce features such as vibrational frequencies, the function form must be improved. The straightforward approach is to include more terms in the Taylor expansion. This results in more parameters to be assigned. Another drawback of these polynomial

expansions is that the stretch energy does not have the correct limiting behavior at large internuclear values of r .

The correct limiting behavior for a bond stretching to infinity is that the energy converges towards the bond dissociation energy, E_0 . A simple function which satisfies this criterion is the Morse potential [4]:

$$U(r_{ij}) = E_0 \{ [1 - \exp(-k'(r_{ij} - r_0))]^2 - 1 \} \quad 2.2$$

where $k' = (k/2E_0)^{1/2}$, k is the stretching force constant; r_0 the equilibrium bond length.

The Morse function reproduces the actual energy variation of a bond quite accurately over a wide range of distances. But it is not perfect for application to bonds with long bond lengths or for distorted structures. In these cases, it displays a slow convergence towards the equilibrium bond length due to an excessively small restoring force.

The harmonic function is mathematically simple. However, the Morse potential can be best used to represent the bonded interactions and its parameters, bond dissociation energy, stretching force constant and minimum energy separation are all experimentally measurable quantities that reflect the strength of the bond.

Atom-pair bond potentials can also be represented by Lennard-Jones (12-6), restrained harmonic and other potentials. As detailed in Chapter 3 we use Morse potentials in our simulations.

2.1.1.2 Valence Angle Potentials

The valence angle potentials describe the bond bending terms between the specified atoms as shown in Fig. 2.2. It is the energy required for bending an angle formed by three atoms j - i - k , where there is a bond between j and i , and between i and

k. Just as for an atom-pair bond potential, it is usually expanded as a Taylor series around a "natural" bond angle, θ_0 , and terminated at second order, giving a harmonic function as:

$$U(\theta_{jik}) = \frac{1}{2} k(\theta_{jik} - \theta_0)^2 \quad 2.3$$

where k is the bending force constant.

For more accuracy, the improvement of the function should include higher order terms such as a third term. But the simple harmonic expansion is quite adequate for most applications. The energy cost for bending is so large that most molecules only deviate a few degrees from their natural bond angle. This is in the range of accuracy of harmonic functions, normally confined to about $\pm 20^\circ$ [5].

The bond bending force constant can be calculated from the experimental studies of the infrared and/or Raman spectra of various molecules. The ability to determine these force constants depends upon being able to assign a particular band in a spectrum to a specific deformation.

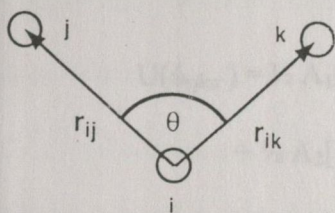


Fig. 2.2 The valence angle and associated vectors.

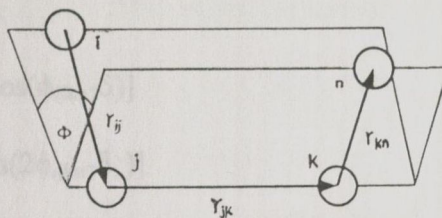


Fig. 2.3 The dihedral angle and associated vectors.

2.1.1.3 Dihedral Angle Potentials

The dihedral angle potentials describe the interactions arising from torsional forces in molecules. They are sometimes referred to as torsional potentials. It is the

energy associated with rotation around a j-k bond in a four-atom sequence i-j-k-n, where i-j, j-k and k-n are bonded as shown in Fig. 2.3. Looking down the j-k bond, the torsional angle, ϕ_{ijkn} , is defined as the angle formed by the i-j and k-n bonds. The angle ϕ_{ijkn} may be taken to be in the range $[0^\circ, 360^\circ]$ or $[-180^\circ, 180^\circ]$.

Because of its periodicity and the possibility of large deviation from the minimum energy structure, a Taylor expansion of torsional energy is not a good idea. To encompass the periodicity, it is better to write it as a Fourier series:

$$U(\phi_{ijkn}) = \sum A_m \cos(m\phi_{ijkn} - \delta)$$

Where δ is the equilibrium angle and A_m are constants that determine the size of the barrier for rotation around the j-k bond. The $m=1$ term describes a rotation which is periodic by 360° , the $m=2$ term is periodic by 180° , the $m=3$ term is periodic by 120° and so on.

It is customary to shift the zero point of the potential by adding a factor of 1 to each term. A popular expression for the torsional energy is therefore:

$$\begin{aligned} U(\phi_{ijkn}) = & \frac{1}{2} A_1 [1 + \cos(\phi_{ijkn} - \delta)] \\ & + \frac{1}{2} A_2 [1 - \cos(2\phi_{ijkn} - \delta)] \\ & + \frac{1}{2} A_3 [1 + \cos(3\phi_{ijkn} - \delta)] \\ & + \dots \end{aligned}$$

The + and - signs are chosen so that the onefold rotational term has a minimum for an angle of 180° , the twofold rotation has minima for angles of 0° and 180° , and the threefold rotational term for angles of 60° , 180° , and 300° (-60°). The factor $\frac{1}{2}$ is included so that the parameter A_m directly gives the height of the torsional energy barrier if only one term is presented.

Depending on the situation, some A_m constants are zero. For our P3AT system, the polymer main chain is π -conjugated. The π component of the chain must be periodic by 180° similar to the rotation around C=C bond, and thus only the $m=2$ term will be not zero. So, for our system, the expression for the torsional energy can be written as:

$$U(\phi_{ijkn}) = \frac{1}{2} A [1 - \cos(2\phi_{ijkn} - \delta)] \quad 2.4$$

In this work the torsion potential is only considered on the torsion existing in the bonds on the thiophene rings and between the thiophene rings in the polymer main chains.

2.1.4 Cross Terms

The cross terms cover the coupling between above bonded fundamental potentials. They include diagonal terms between bond and bond, bond and valence angle, bond and dihedral angle, and etc. The most important of these is the bond/valence-angle term which for an i-j-k sequence may be written as:

$$U_{\text{bond/valence-angle}} = k_{ijk} (\theta_{ijk} - \theta_0) [(r_{ij} - r_0) + (r_{jk} - r_0)]$$

The constants involved in the cross terms are dependent on all the atom types involved. For example the constants for above equation in principle depend on all three atoms, i, j and k. So the determination of constants in cross terms is a difficult task. However, for the k_{ijk} , it is usually taken to depend only on the central atom, i.e., $k_{ijk} = k_j$, or chosen as a universal constant which is taken to be independent of atom type.

It is usually necessary to include cross terms only if the simulations are aimed to fit precise experimental data such as vibrational frequencies.

2.1.2 Non-bonded Potentials

Non-bonded potentials include short-range van der Waals potentials and long-range electrostatic (Coulombic) potentials.

2.1.2.1 The van der Waals Potentials

Van der Waals potentials describe the repulsion and attraction between atoms that are not directly bonded. At large interatomic distances they are zero, and for small distances the potential becomes very repulsive. At intermediate distances, two atoms show slight attraction.

The attraction between two non-bonded atoms is due to induced dipole-dipole moments. Even if the molecule (or part of molecule) has no permanent dipole moment, the motion of electrons may create a slightly uneven distribution at a given time. This dipole moment will induce a charge polarization in the neighboring molecule (or another part of the same molecule) and create an attraction. It can be shown theoretically that this attraction varies as the inverse sixth power of the distance between the two fragments so that:

$$U(r_{ij}) = -\frac{3}{2} \alpha_i \alpha_j r^{-6} \frac{I_i I_j}{I_i + I_j}$$

where α_i and α_j are the atomic polarizability volumes and I_i and I_j the first ionization potentials of the individual atoms i and j .

Actually there are also contributions to the attraction from induced quadrupole-dipole, quadrupole-quadrupole etc. interactions. These vary as r^{-8} , r^{-10} etc. with the r^{-6}

dependence having the asymptotic behavior at long distance. The force associated with this attraction is often referenced as a “dispersion” or “London” force [6].

Van der Waals potentials are very positive at small distance (actually due to Pauli exclusion), and have minima which is slightly negative at distances at which the two atoms just “touch” each other. They decay to zero as the distance becomes large.

To fit these features, the general functional form used is:

$$U_{\text{vdw}} = U_{\text{repulsive}}(r) - C/r^6$$

For the repulsive interaction, it is required to go to zero as r goes to infinity and should approach zero faster than r^{-6} . A good function that obeys these requirements is the Lennard-Jones potential [7]

$$U_{\text{vdw}} = C_1 r^{-12} - C_2 r^{-6} \quad 2.5$$

Here C_1 and C_2 are suitable constants. There are no theoretical arguments for choosing the exponent in the repulsive part to be 12. It is purely due to a computational convenience. In fact there is some evidence that an exponent of 9 or 10 gives better results. The Lennard-Jones potential can also be written as:

$$U_{\text{vdw}} = \varepsilon \left[\left(\frac{r_0}{r} \right)^{12} - 2 \left(\frac{r_0}{r} \right)^6 \right]$$

where r_0 is the minimum energy distance and ε the depth of the minimum. These depend on both atom types. A commonly used method is to take the van der Waals minimum distance as the sum of two van der Waals radii and the interaction parameter as the geometrical mean of atomic “softness” constants.

$$r_0^{ij} = r_0^i + r_0^j$$

$$\varepsilon^{ij} = (\varepsilon^i \varepsilon^j)^{1/2}$$

From electronic structure theory it is known that the repulsion is due to the overlap of the electronic wave functions, and furthermore that the electron density falls off approximately exponentially with the distance from the nucleus. There is therefore some justification for choosing the repulsive part as an exponential function. This is Buckingham potential [8]

$$U_{\text{vdw}} = Ae^{-\rho r} - C/r^6 \quad 2.6$$

where A, ρ and C are suitable constants. It can also be written in a little more convoluted form as

$$U_{\text{vdw}} = \varepsilon \left[\frac{6}{\alpha - 6} e^{\alpha(1-r/r_0)} - \frac{\alpha}{\alpha - 6} \left(\frac{r_0}{r} \right)^6 \right]$$

where r_0 and ε have been defined above, and α is a suitable parameter.

The Buckingham potential has a problem for very short interatomic distances where it “turns over”. That is, as r goes toward zero the potential goes to infinitely negative instead of infinitely positive as shown in Fig. 2.4.

Another functional form for the van der Waals potential is that of the Morse potential as described in equation 2.2. It does not have the r^{-6} dependence at long range. As mentioned before, the attraction could, in reality, be present in other terms. The parameters of a Morse function describing the van der Waals potential will, of course, have different meanings than those relevant for a bonded potential. Here the values of E_0 and k should be much smaller, and r_0 will be longer.

For small molecules such as H_2 -He system, the Morse function actually gives a slightly better description of the van der Waals potential than does the Buckingham function, which again performs significantly better than the Lennard-Jones potential. They are shown in Fig. 2.4 [9].

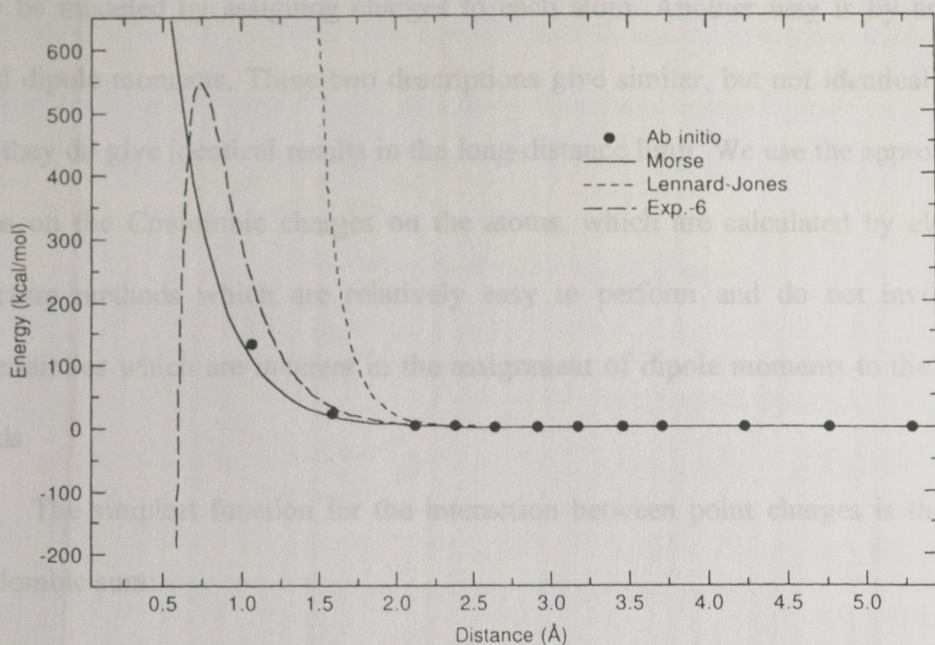


Fig. 2.4 Comparison of U_{vdw} functionals for the H_2 -He potential (cited from ref. 9).

Although the Morse and Buckingham potentials describe the van der Waals interactions better than does the Lennard-Jones potential, most force fields employ the Lennard-Jones potential because it is computationally more efficient and provides results comparable to those given by the more accurate functions. For large molecules, the calculation of the non-bonded energy in the force field energy expression is the one which takes by far the most time. The difference between the three functions considered above lies in their repulsive parts at short distance. Their behaviour in the attractive part, which is essential for intermolecular interactions, is very similar for the three functions.

2.1.2.2 Electrostatic Potential

The electrostatic potential is due to the internal distribution of the electrons, creating positive and negative parts of the molecule. At the lowest approximation this

may be modeled by assigning charges to each atom. Another way is by assigning bond dipole moments. These two descriptions give similar, but not identical results. But they do give identical results in the long-distance limit. We use the approach that relies on the Coulombic charges on the atoms, which are calculated by electronic structure methods which are relatively easy to perform and do not involve the uncertainties which are inherent in the assignment of dipole moments to the various bonds.

The simplest function for the interaction between point charges is the direct Coulombic sum:

$$U(\mathbf{r}_{ij}) = \frac{1}{4\pi\epsilon_0} \frac{q_i q_j}{r_{ij}} \quad 2.7$$

where ϵ is a dielectric constant and r_{ij} is the distance between point charges q_i and q_j . It can be used for both periodic and non-periodic systems. Sometimes it is necessary for the accurate simulation of isolated (non-periodic) systems. Since it depends on r_{ij}^{-1} , there is likely to be problem of convergence. One way to improve the convergence is to employ the truncated and shifted Coulombic sum:

$$U(\mathbf{r}_{ij}) = \frac{q_i q_j}{4\pi\epsilon_0} \left(\frac{1}{r_{ij}} - \frac{1}{r_{cut}} \right) \quad 2.7a$$

This drastically reduces the range of electrostatic interactions without giving an abrupt step in the potential energy at the cutoff (r_{cut}). Its main use is for a preliminary preparation of systems for computation and it is not recommend as a realistic model.

The best technique for calculating electrostatic interactions in a periodic (or pseudo-periodic) system is the Ewald sum [10]. The basic model of a periodic system with overall unit cell neutrality is a system of charged point ions mutually interacting

via the Coulombic potential. The Ewald method makes two amendments to this simple model as shown in Fig. 2.5 supposing the central charge is positive.

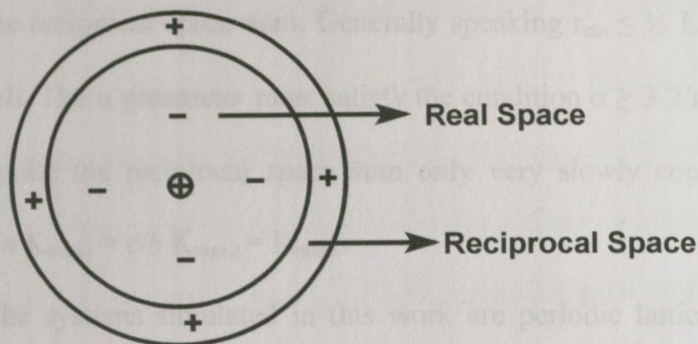


Fig. 2.5 The model of the Ewald sum method.

Firstly each ion is effectively neutralised (at long range) by the superposition of a spherical Gaussian cloud of opposite charge centered on the ion. The combined assembly of point ions and Gaussian charges becomes the real space part of the Ewald sum, which is now short-ranged and treatable by equation 2.7. The second modification is to superimpose a second set of Gaussian charges, this time with the same charges as the original point ions and again centered on the point ions (so nullifying the effect of the first set of Gaussians). The potential due to these Gaussians is obtained from Poisson's equation and is solved as a Fourier series in reciprocal space. The complete Ewald sum requires an additional correction, known as the self energy correction, which arises from a Gaussian acting on its own site, and is constant. The Ewald sum therefore replaces a potentially infinite sum in real space by two finite sums: one in real space and one in reciprocal space; these are supplemented by the self-energy correction. For molecular systems, additional modifications are necessary to correct for the excluded (intra-molecular) Coulombic interactions.

The convergence of the Ewald sum is controlled by three variables: the real space cutoff r_{cut} , the convergence parameter α , and the largest reciprocal space vector k_{max} used in the reciprocal space sum. Generally speaking $r_{\text{cut}} \leq \frac{1}{2} L$, where L is the width of the cell. The α parameter must satisfy the condition $\alpha \geq 3.2/r_{\text{cut}}$, but too large a value will make the reciprocal space sum only very slowly convergent. $K_{\text{max}} > 3.2L/r_{\text{cut}}$ and $c/a K_{\text{max}1} = c/b K_{\text{max}2} = K_{\text{max}3}$.

Since the systems simulated in this work are periodic lattices whose atoms bear partial electrostatic charges we use the Ewald sum method to deal with long-range electrostatic potentials in both the MD (DL_POLY code) and MM (GULP code) calculations.

2.1.3 External Fields

If an external field is applied in the simulating system, the force field should include such an external field. Examples of this kind of fields include:

1. Electric Field: $\mathbf{F}_i = \mathbf{F}_i + q_i \mathbf{H}$
2. Magnetic Field: $\mathbf{F}_i = \mathbf{F}_i + q_i (\mathbf{v}_i \wedge \mathbf{H})$
3. Oscillating Shear: $\mathbf{F}_x = A \cos(2n\pi z/Lz)$

Since the application of an external field may change the momenta of the particles and the temperature, a thermostat must be included in the calculation.

2.1.4 Parameterisation

Once the choice of the form of interatomic potential has been made the next task is to evaluate the potential parameters. In general there are two strategies. The first includes fitting to known properties (empirical potentials) and the second relies on electronic structure calculations.

2.1.4.1 Empirical Methods

The values of the parameters are adjusted, generally via a least squares fitting procedure, $R = \sum W_j^2 (E_j - C_j)^2$, where W_j is a weighting factor and E_j is the value of a relevant property measured from experiments. C_j is a fitting parameter obtained from calculations such as molecular mechanics simulations to give the best values for the observed experimental quantities. These include properties such as crystal energies and structure, and elastic and dielectric constants. Molecular spectra can also provide valuable information for the determination of parameters in interatomic potentials. The bond length and bond angle measured from X-ray diffraction can be used to fit the equilibrium separation in a bond potential and the equilibrium bond angle in a valence angle potential. IR and Raman spectra are useful for fitting stretching force constants and bending force constants. As will be described in detail in the next chapter, the parameters used in our force fields are mostly derived from this method through literature searching for the values of the parameters.

An important aspect of empirical potential parameterisation is the question of transferability. For example, are models derived in the simulation of binary oxides transferable to ternary oxides? Studies by Cormack, *et al.* [11] and Parker and Price [12,13] conclude that transferability works well in many cases, although systematic modifications are needed when potentials are transferred to compounds with different coordination numbers. In general such transfers require that care is taken in the process.

There are now several sets of empirical potential parameters for a range of solids, for example, the work of Williams [14] and of Kiselev [15] for non-bonded van der Waals potentials of hydrocarbon compounds.

2.1.4.2 Theoretical Calculation Methods

Empirical procedures are still extensively used in developing potential parameters. They do, however, have obvious inadequacies: (a) It is necessary to have a good range of accurate empirical data and this may not be possible when new systems are being studied; (b) There is no guarantee of the validity of the potential function when used outside the range of interatomic spacings employed in the parameterisation. One obvious example is the design and prediction of properties of new materials by simulation: there are no experimental data available for empirical methods in this situation. For this reason, there has been considerable incentive in recent years for the development of reliable theoretical procedures for calculating parameters. To date such efforts have been directed largely towards parameterisation of effective charges and of short range potentials and some three-body components of the potential.

In these methods the Schrödinger equation is solved approximately for a cluster or periodic array of atoms using methods such as the electron-gas technique for a variety of internuclear geometries; the resulting variation in the total energy is then fitted to an interatomic potential function. Explicit quantum mechanical methods such as *ab initio* Hartree-Fork methods are being increasingly used in such studies. The importance of the quality of the potential in determining the reliability of the simulation will ensure that the use of this kind of methods will be greatly extended in the future so that the most appropriate interatomic potentials can be provided.

Detailed discussions and applications of these methods can be found in references [1-3, 16].

2.2 Energy Minimization

A very important feature of atomistic simulation is the relaxation of the simulation system. The relaxation procedure is an energy minimization. Three basic kinds of energy minimization methods are generally used: these are the Newton-Raphson, the method of steepest descent, and conjugate gradient methods [1].

2.2.1 Newton-Raphson Methods

The energy about any given point in configuration space \mathbf{x} can be expanded as a Taylor series:

$$U(\mathbf{x}+\mathbf{dx}) = U(\mathbf{x}) + \mathbf{U}'(\mathbf{x})\mathbf{dx} + \frac{1}{2}\mathbf{U}''(\mathbf{x})\mathbf{dx}^2 + \dots \quad 2.8$$

If there are n atoms in the system, $\mathbf{x} \equiv (x_1, x_2, x_3, \dots, x_{3n})$, i.e., it is a $3n$ -dimensional row vector of the atomic coordinates. Then $\mathbf{U}'(\mathbf{x})$, the vector of first derivatives of the energy with respect to \mathbf{x} has length $3n$ and $\mathbf{U}''(\mathbf{x})$ is a $3n \times 3n$ square matrix containing second derivatives of the energy.

We neglect higher order terms, and write

$$\mathbf{g} = \mathbf{U}'(\mathbf{x}) \quad \text{and} \quad \mathbf{H} = \mathbf{U}''(\mathbf{x})$$

which are explicitly

$$g_i = \partial U / \partial x_i \quad \text{and} \quad H_{ij} = \partial^2 U / \partial x_i \partial x_j$$

The later quantity defines the Hessian matrix \mathbf{H} . The system is now described by a harmonic well. In order to locate the coordinate vector close to the energy minimum note that the energies $U(\mathbf{x}+\mathbf{dx})$ and $U(\mathbf{x})$ are approximately equal. Differentiation of the resulting equation

$$0 = \mathbf{g} \cdot \mathbf{dx} + \frac{1}{2} \mathbf{H} (\mathbf{dx})^2$$

with respect to \mathbf{dx} gives

$$\mathbf{dx} = -\mathbf{H}^{-1} \mathbf{g} \quad 2.9$$

which is the change in the coordinate vector \mathbf{x} that is necessary in order to bring the system to the bottom of the energy well.

Recalling the component make-ups of vector \mathbf{g} and matrix \mathbf{H} :

$$\mathbf{g} = (g_1, g_2, g_3, \dots, g_{3n})$$

and

$$\mathbf{H} = \begin{bmatrix} H_{11} & H_{12} & \dots & H_{1,3n} \\ H_{i1} & H_{i2} & \dots & H_{i,3n} \\ H_{n1} & H_{n2} & \dots & H_{n,3n} \end{bmatrix}$$

and displacement of the coordinates by \mathbf{dx} as given in Equation 2.9 will generate the energy minimum configuration. However, in fact, it will not be valid to truncate the summation at the quadratic term, except when very close to the minimum. But Equation 2.9 provides the basis of an effective iterative procedure for attaining the minimum.

The advantage of the Newton-Raphson method is that the convergence is second-order near a stationary point. If the functions only contain terms up to second-order, the step will go to the stationary point in only one iteration. In general the function contains higher-order terms, but the second-order approximation becomes progressively better as the stationary point is approached. Sufficiently close to the stationary point, the gradient is reduced quadratically. Because it is generally rapidly convergent, this method is widely used in both perfect and defect lattice energy minimization calculations.

In the Newton-Raphson method, repeated calculation of the second derivatives and inversion of the matrix is undesirable, and if the Hessian is not positive, the Newton-Raphson procedure will converge towards a maximum along imaginary modes rather than to the true minimum. Because of these problems, a large number of improved alternative methods have been evolved [17-18]. One of the first and most famous methods is that due to Fletcher and Powell (FP) [17]. This may be written as:

$$\mathbf{H}_{i+1}^{-1} = \mathbf{H}_i^{-1} + (\mathbf{x}_{i+1} - \mathbf{x}_i)(\mathbf{x}_{i+1} - \mathbf{x}_i) / (\mathbf{x}_{i+1} - \mathbf{x}_i)(\mathbf{g}_{i+1} - \mathbf{g}_i) - (\mathbf{H}_i^{-1}(\mathbf{g}_{i+1} - \mathbf{g}_i))(\mathbf{H}_i^{-1}(\mathbf{g}_{i+1} - \mathbf{g}_i)) / (\mathbf{g}_{i+1} - \mathbf{g}_i)\mathbf{H}_i^{-1}(\mathbf{g}_{i+1} - \mathbf{g}_i)$$

where i means the i th searching step. The introduction of a shift parameter λ in the total length of step ($\Delta x_i = f_i / (\epsilon_i - \lambda)$, $\Delta \mathbf{x} = \Sigma \Delta x_i$) can ensure that the step is in the direction of a minimum [19].

It is important to remember that an energy minimum attained in this way could be a local minimum and that it is not necessarily the global energy minimum. To search for the global minimum is, in general, very difficult in a system of any complexity. Several kinds of algorithms such as Monte Carlo, Molecular Dynamics, Simulated Annealing [20], Genetic [21], and Diffusion [22] and Distance Geometry [23] methods can help to find the global minimum.

2.2.2 Steepest Descent Method

In the Steepest Descent method, a series of calculations are performed in the direction of decreasing gradient, i.e. along a search direction defined as

$$\mathbf{d}_i = -\mathbf{g}_i \quad 2.10$$

where \mathbf{g}_i is the gradient in the i th searching step and \mathbf{d}_i the searching direction in that step. Once the function starts to increase, an energy minimum has been encountered.

2.2.2 By its nature the steepest descent method can only locate a local minimum. Its advantage is that the algorithm is very simple, and requires only storage of the gradient vector. It is furthermore one of the few methods guaranteed to lower the function value. Its main use is to quickly relax from a poor starting point, before some of the more advanced algorithms are allowed to take over, or as a "backup" algorithm if the more sophisticated methods are unable to lower the value of the function.

2.2.3 Conjugate Gradient Methods

In this method, the first step is equivalent to the steepest descent method, but subsequent searches are performed along a line which is a mixture of the current negative gradient and the previous search direction.

$$\mathbf{d}_i = -\mathbf{g}_i + \beta_i \mathbf{d}_{i-1} \quad 2.11$$

Where \mathbf{d}_i and \mathbf{g}_i are the same as those appearing in equation 2.10. The value of β can be chosen from one of the following methods:

- (1) Fletcher-Reeves method

$$\beta_i^{\text{FR}} = \mathbf{g}_i^t \mathbf{g}_i / \mathbf{g}_{i-1}^t \mathbf{g}_{i-1}$$

- (2) Polak-Ribiere method

$$\beta_i^{\text{PR}} = \mathbf{g}_i^t (\mathbf{g}_i - \mathbf{g}_{i-1}) / \mathbf{g}_{i-1}^t \mathbf{g}_{i-1}$$

- (3) Hestenes-Stiefel method

$$\beta_i^{\text{HS}} = \mathbf{g}_i^t (\mathbf{g}_i - \mathbf{g}_{i-1}) / \mathbf{d}_{i-1}^t (\mathbf{g}_i - \mathbf{g}_{i-1})$$

The Polak-Ribiere prescription is usually preferred in practice.

Conjugate gradient methods have much better convergence characteristics than does the method of steepest descent and need less storage than the Newton-Raphson method. Again conjugate gradient methods are only able to locate a local minimum.

2.3 Computational Methods

2.3.1 Molecular Mechanics Simulations

Molecular mechanics (MM) simulations are energy minimizations in which the positions of constituent species are adjusted systematically in the manner described in Section 2.2 above in a relaxation search for the minimum energy configuration. They yield detailed atomistic information on the geometries and energetics of the system being simulated. The calculated energy is minimized with respect to appropriate variables such as lattice parameters, usually using iterative numerical procedures to give the most stable crystal structure. They were originally developed for crystalline materials.

If there is a molecular system containing N atoms in a lattice, \mathbf{x} is a $3N$ -dimensional row vector whose elements are the coordinates of the atoms. A MM simulation calculates the numerical values of the energy appropriate to the position vector mentioned above. The structure is then relaxed by adjusting the molecular configuration so as to minimize the energy of the system. The minimization techniques used to calculate equilibrium configurations have been discussed in Section 2.2.

If more than one minimum is present in the system, as might be expected with the occurrence of polymorphism in polymer systems, the minimization procedure may not achieve the global minimum but may stop instead at the first minimum encountered. In this case, care must be taken to ensure that the global minimum is

found typically by repeating the relaxation procedure using a series of different initial configurations.

Two common basic calculation methods for MM simulations are perfect lattice simulations and point defect simulations.

2.3.1.1 Perfect Lattice Simulations

These simulations allow the lattice (unit cell or supercell) structures and energies of crystalline materials to be calculated. A trial structure is proposed and, using the specified force field, the coordinates of the atoms and the cell dimensions are adjusted to find the configuration with minimum energy. The lattice energy and other properties are then calculated. This class of simulations has several important applications. The first is used to optimize the lattice parameters a , b , c , α , β and γ . The second can be used to compare the stability of different conformations and to determine the energy barrier of the transfer between them. The third is used to investigate the defect supercell lattice [24,25]. By generating arrays of point or extended defects in a supercell lattice, the energy of defect formation could be estimated by comparing the lattice energy before and after the defects are imposed and migration energy barrier of defect could be calculated as well. In Chapter 7, we use a similar method to calculate the migration energy barrier of dopants in P3BT lattice. The energetics of transport processes are studied by fixing the position of the migrating species at a series of positions along a chosen pathway and calculating the energy at each point with all other species in the fully relaxed lattice. Another kind of application is to exploit the ability of the method to calculate the structural, elastic and

dynamic properties of a crystal in a reverse sense to the calculation of the potential parameters in the empirical fitting procedure.

2.3.1.2 Point Defect Simulations

The MM simulations of ionic crystals are well established through the study of defective solids for the calculation of defect energies which govern the concentration and mobilities of defects [26,27]. By introducing a point defect or a defect aggregate into a perfect crystal, the simulations have developed an insight into the formation of defects and the migration of dopants through the lattice by modeling a series of chosen activated steps. This enables the defect formation energy and the migration barrier to be calculated and the procedure can be used to distinguish between possible migration pathways.

The Mott-Littleton method is a widely successful method for this kind of simulation [28]. In this method, the isolated defect or defect cluster is embedded in the crystal which extends to infinity. This approach is different from the supercell methods of perfect lattice described in the previous subsection. The normal procedure in a Mott-Littleton calculation is to relax all the atoms in a region surrounding the defect, containing typically 100-300 atoms, until all these atoms are at zero force. The relaxation of the remainder of the crystal is then described by more approximate methods. In practice, an interface region must be used between the two regions described above. Short-range interactions between ions in the inner region and those in the interface are also calculated explicitly [26].

2.3.2 Molecular Dynamics

Molecular dynamics (MD) is a conceptually simple technique and for this reason it has proved to be very versatile. The atoms in the system to be simulated are represented by an ensemble of particles which are assigned an energy and then allowed to evolve with time under specified interatomic forces by numerically integrating the classical equations of motion for the system. The computations are particularly well suited to massively parallel multi-processor high performance supercomputers, as different particles can be allocated to different processors. Calculations with in excess of 10^6 particles have been reported [1].

A variety of statistical ensembles can be employed for MD including canonical (NVT), isothermal-isobaric (NPT) and microcanonical (NVE) ensembles, where N, V and T are the number of particles, the volume and temperature of the simulation system, respectively. All the particles in the simulation box are assigned positions and velocities and the specified interatomic potentials allow the forces acting on the particles to be calculated. The simulation involves solving Newton's equations of motion for the ensemble by allowing it to proceed through a series of time steps each of Δt (typically about 10^{-14} to 10^{-15} s), which must be smaller than the time characteristic of any important process in the system e.g., the periodic vibration time. The time step is repeated many times and the position (x_i) and the velocity (v_i) of the i th particle are updated. In the limit of an infinitesimal Δt the classical equations of motion give:

$$\mathbf{x}_i(t+\Delta t) = \mathbf{x}_i(t) + \mathbf{v}_i(t)\Delta t$$

$$\mathbf{v}_i(t+\Delta t) = \mathbf{v}_i(t) + (\mathbf{F}_i(t)\Delta t)/m_i$$

Where m_i is the mass of the i th particle and \mathbf{F}_i the force acting on it.

In the initial stages of simulation, the ensemble equilibrates, i.e. it achieves an equilibrium distribution of velocities and equipartition between potential and kinetic energy. After this period, which may take thousands of steps, the simulation is run for as long as is computationally feasible or until the required information has been gathered. Normally the total simulation time is of the order of 50-100 ps, but for the simulation of transport behavior, much longer e.g., 1 ns, may be required.

MD can be applied to both crystalline and amorphous materials [29-34]. An important application is the investigation of diffusion processes in materials in which the atoms or ions move extremely rapidly [29,35-39]. However, even with modern supercomputers it is rarely possible to run simulations to represent longer than 1 ns. If the probability of the events of interest (e.g. defect jump) are low in a period of this length, the simulation may be of little value. This means that diffusion can only be studied for values of the diffusion coefficient that are not much less than that 10^{-12} m²/S. MD is also difficult in the calculation of thermodynamic properties. The case of defects is especially problematic, but formation and migration energies are effectively and easily calculated by using molecular mechanics simulation techniques.

2.3.3.1 Radial Distribution Function $g(r)$

The radial distribution function, $g(r)$, is one of the most important molecular dynamics results as it can give information on molecular structure. It is given by

$$g(r) = \rho^{(2)}(r)(N/V)^{-2}$$

where $\rho^{(2)}(r) = \langle \rho(0)\rho(r) \rangle$ is called the pair distribution function. When $r \rightarrow 0$, it is 0 and when $r \rightarrow \infty$, it is ρ^2 . N is the number of particles in volume V . It yields a value

for the probability that one kind of particles α will find another kind of particles α' in $4\pi r^2 dr$ as shown in Fig. 2.6.

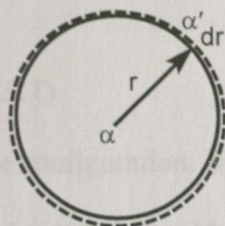


Fig. 2.6 The illustration of radial distribution function.

2.3.2.2 Diffusion Coefficient

From the mean square displacement $\langle r_\alpha^2 \rangle$ of particle α whose motion is monitored by MD as a function of time t , the diffusion coefficient D_α can be calculated from the relationship:

$$\langle r_\alpha^2 \rangle = 6 D_\alpha t + B_\alpha$$

where B_α is a parameter derived from the thermal vibration of the particle (atom), and is related to the Debye-Waller scattering factor of the atom in the environment in question at that temperature.

2.3.3 Monte Carlo Method

Monte Carlo (MC) methods involve the generation of successive configurations of an ensemble of particles representing the system studied as in MD methods. But unlike MD, there is no temporal connection between the different configurations. In MC methods [40] a sequence of configurations is generated from a initial geometry by adding a random “kick” to the coordinates of a randomly chosen particle (atom or molecule). The new configuration is accepted as a starting point for the next perturbing

step if it is lower in energy than the current. If the new configuration is higher in energy, the Boltzmann factor, W , is calculated and compared to a random number P between 0 and 1.

$$W = \exp(-E/kT)$$

where E is the energy of the configuration. If $W < P$, the new configuration is accepted, otherwise the next step is taken from the old configuration. This Metropolis procedure [41] ensures that the configurations in the ensemble obey a Boltzmann distribution, and the possibility of accepting higher energy configurations allows MC methods to climb uphill and escape from a local minimum. In order to have a reasonable acceptance ratio, however, the step size must be fairly small. This effectively means that a few million MC steps (typical computational limit) can only explore the local region around the starting configuration.

MC can be used to explore complex energy surfaces and to find low energy regions. It has been extensively used to find stable configurations and to study diffusion in alloys [42] and in superionic conductors [43].

2.4 Simulation Codes

2.4.1 GULP

The General Utility Lattice Program (GULP) code is designed to perform a variety of tasks relating to three dimensional solids by Juilian Gale [44]. It encompasses energy minimisation, phonon calculations and other useful facilities. The energy minimization methods embodied include Newton-Raphson (NR), conjugate gradient and improved NR methods. The interatomic potentials that may be

used currently include Buckingham, Lennard-Jones, Morse, Harmonic, Coulombic sum and other functions. Both unit cell and supercell perfect lattice methods are included. The embodied defect lattice methods can treat vacancies, interstitials and impurities.

GULP can be used to calculate crystal properties such as lattice energies, elastic constants, dielectric constants, phonon frequencies, etc. It can also be used to analyze structures, to treat defect formation and migration, and to fit the parameters of potential functions.

In this work GULP is used to optimize the structure and parameters of P3AT lattice, to find stable conformations and to study the migration of dopants in P3AT lattice.

2.4.2 DL_POLY

The MD program used in this work is DL_POLY_2.9b which was developed for use on a parallel computer by W. Smith, *et al.* [45]. It was designed to enable the molecular dynamics of macromolecules, polymers, ionic systems and solutions to be performed on a distributed memory parallel computer. It allows the investigation of both isolated polymer chains and lattices with cubic, orthorhombic, parallelepiped, truncated octahedral, rhombic dodecahedral and slab periodic boundary conditions.

The algorithms are all couched in the form of Verlet Leapfrog integration [39]. NVE, NVT, NPT and $N\sigma T$ ensembles are available, with a selection of thermostats (Nosé-Hoover, Berendsen, Gaussian constraints) and barostats (Hoover, Berendsen). A parallel version of the SHAKE algorithm [46] called RD-SHAKE is used for bond constraints. Rigid molecular species use Fincham's implicit quaternion (FIQA) [47] and their bonds are handled with an algorithm of the embodied QSHAKE algorithm.

Isothermal ensemble methods, mostly in NVT ensemble, were used in this simulation work with Nosé-Hoover thermostat techniques to study the thermally induced conformation changes of P3ATs and the diffusion of dopants in the polymer lattices ,

2.5 Semiempirical Molecular Orbital (MO) Methods

The semiempirical MO methods based on Extended Hückel (EH) and Complete Neglect of Differential Overlap (CNDO) are computationally economical methods to perform calculations on molecules and chains. While both methods are crude by modern standards of computational chemistry their calculations of atomic charges is fairly good [48]. The EH method applied to a 1-dimensional lattice (a chain with translational periodicity) [49] uses periodic boundary conditions to form energy bands whose important components are the 'valence' (occupied) and 'conduction' (vacant) bands and the energy gap separating them. Although the gap cannot be calculated with precision, it can reveal the effect of conformational changes.

In this thesis, the CNDO method was used to calculate partial atomic charges which could be used for the polymer chains. Despite the existence of more sophisticated computational methods, the CNDO charges were retained as they led to good results in calculations on polythiophene lattices [50]. This may be because the CNDO parameters are scaled so as to provide agreement with charges calculated from certain *ab initio* quantum chemical methods on model molecules [48].

The two methods use different recipes to approximate the elements H_{rs} of the energy matrix between the AOs r and s . Using Slater AOs to calculate the overlap integrals S_{rs} the determinantal equation $\det|H_{rs} - ES_{rs}| = 0$ is then solved to furnish the eigenvalues E (energy levels) and eigenvectors (LCAO coefficients).

Bibliography:

- [1] Jensen F. "*Introduction to Computational Chemistry*", John Wiley & Sons Ltd, Chichester, England, 1999
- [2] Catlow C R A. in "*New Trends in Materials Chemistry*", Chapter 7, Edited by Catlow C R A and Cheetham A K. Academic Publishers, Dordrecht, 1997
- [3] Corish J. in "*Mass and Charge Transport in Ceramics*", p3, Edited by Koumoto K, Sheppard L M, and Matsubara H. The American Ceramic Society, Ohio, 1996
- [4] Morse P M. *Phys. Rev.*, 1929, **34**:57
- [5] Jensen P. *J. Mol. Spectrosc.*, 1989, **133**:438
- [6] London F. *Z. Physik*, 1930, **63**:245
- [7] Lennard-Jones J E. *Proc. R. Soc. London, Ser. A*, 1924 **106**:463
- [8] Hill T L. *J. Chem. Phys.*, 1948, **16**:399
- [9] Hart J R and Rappé A K. *J. Chem. Phys.*, 1992, **97**:1109
- [10] Ewald P P. *Ann. Physik*, 1921, **64**:253
- [11] Cormack A N, Lewis G V, Parker S C, Catlow C R A. *J.P.C. Solids*, 1988, **49**:53
- [12] Parker S C, Price G D. *Phys. Chem. Miner.*, 1984, **10**:209
- [13] Price G D, Wall A, Parker S C. *Phil. Trans. Roy. Soc. Lond.*, 1989, **A328**:391
- [14] Williams D E. *J. Chem. Phys.*, 1967, **47**:4680
- [15] Kiselev A K, Lopatkin A A, Shulga A A. *Zeolites*, 1985, **5**:261
- [16] Morrison G. *Ph. D. Thesis*, The University of Kent at Canterbury, 1997
- [17] Fletcher R, Powell M J D. *Computer J.*, 1963, **6**:16
- [18] Stoneham A M, Harding J H. *Ann Rev. Phys. Chem.*, 1986, **37**:53
- [19] Banerjee A, Adams N, Simons J, Shepard R. *J. Phys. Chem.*, 1985, **89**:52
- [20] Kirkpatrick S, Gelatt Jr C D and Vecchi M P. *Science*, 1983, **220**:671
- [21] Judson R S. *Rev. Comput. Chem.*, 1997, **10**:1
- [22] Kostrowicki J and Scheraga H A. *J. Phys. Chem.*, 1992, **96**:7442
- [23] Kukui K. *Acc. Chem. Res.*, 1981, **14**:363
- [24] Cormack A N, Jones R M, Tasker P W and Catlow C R A. *J. Solid State Chem.*, 1982, **44**(2):174
- [25] Catlow C R A and James R. *Nature*, 1978, **272**:603
- [26] Catlow C R A and Mackrodt W C. "*Computer Simulation of Solids, Lecture Notes in Physics, Vol.166*", Springer, Berlin, 1982

- [27] Catlow C R A and Mackrodt W C. "*Computer Simulation of Condensed Matter: Physica, Vol.131 B*", Elsevier Science Publishers, 1985
- [28] Mott N F and Littleton M J. *Trans Faraday Soc.*, 1938, **34**:485
- [29] Armad M B, Chabagno, and Duclot M J. in "*Fast Ion Transport in Solids*", p131, ed. Vashishta P, Mundy J N, and Shenoy G K, North-Holland, 1979
- [30] Boyd R H, Gee R H, Han J, and Jin Y. *J. Chem. Phys.*, 1994, **101**:788
- [31] Gee R H, and Boyd R H. *Com. Theor. Polym. Sci.*, 1988, **8**:93
- [32] Pant P V K, Han J, Smith G D, and Boyd R H. *J. Chem. Phys.*, 1993, **99**:597
- [33] Neyertz S, Brown D, and Thomas J O. *J. Chem. Phys.*, 1994, **101**:10064
- [34] Aabloo A, and Thomas J. *Com. Theor. Polym. Sci.*, 1987, **7**:47
- [35] Van den-Begin N, Rees L V C, Caro J, Bülow M. *Zeolites*, 1989, **9**:287
- [36] Goodbody S J, Watanabe K, MacGowan D, Walton J P R B, Quirke N. *J. Chem. Soc., Faraday Trans.*, 1992, **87**:1951
- [37] Kawano M, Vessal B, Catlow C R A. *J. Chem. Soc., Chem. Commun.*, 1992, 879
- [38] Pickett S D, Nowak A K, Cheetham A K, Thomas J M. *Mol. Sim.*, 1988, **2**:353
- [39] Raham A. *Phys. Rev.*, 1964, **136**:A405
- [40] Jorgenson W L. *Adv. Chem. Phys.*, 1988, **70**:469
- [41] Metropolis N A, Rosenbluth A W, Teller A H and Teller E. *J. Chem. Phys.*, 1953, **21**:1087
- [42] Murch G E. *Phil. Mag.*, 1982, **A46**:575
- [43] Murray A D, Murch G E and Catlow C R A. *Solid State Ionics*, 1986, **18-19**:196
- [44] Gale J. "*Manual of General Utility Lattice Program (GULP)*", Version 1.1, Imperial College, London, U.K.
- [45] Forester T R and Smith W. *DL_POLY 2.9*, Daresbury, Warrington, U.K., 1997
- [46] Flyvbjerg H and Petersen H G. *J. Chem. Phys.*, 1989, **91**:461
- [47] Abramowitz M, and Stegun I A. "*Handbook of Mathematical Functions*", Dover Publications Inc, New York, 1970
- [48] Pople J A and Beveridge D L "*Approximate Molecular Orbital Theory*", McGraw-Hill 1972, p 84, Table 4.1; Chen Zh *Theor. Chim. Acta*, 1983, **62** 293
- [49] Program EHMACC_1, QCPE 1978, Bloomington, Indiana
- [50] Corish J, Morton-Blake D A, Veluri K, and Bénéière F. *J. Mol. Struct. (Theochem)*, 1993, **283**:121; *ibid* 1995, **334**:109

Chapter 3

THE FORCE FIELD

The accuracy and reliability of the results from all the force field simulation methods depend critically on the quality of the specified force field. There are several standard force fields, such as Universal FF [1-3], Dreiding II [4], AMBER [5] and MM2 [6]. AMBER was developed for the simulation of proteins and nucleic acids. MM2 is particularly suitable for small organic molecules. The Universal force field is an excellent, general-purpose force field that has been parameterized for the full periodic table. All the Universal force field parameters are generated from a set of rules based on element, hybridization and connectivity. The Universal force field has been carefully validated for many structure types: main group compounds, organic molecules, and metal complexes. The Dreiding II force field is a good all-purpose force field that can be used for structure prediction and dynamics calculations of organic, biological and inorganic molecules. The primary advantage of the Dreiding II is its robustness—the general force constants and geometry parameters are based on simple hybridizations rather than specific combinations of atoms. It allows reasonable predictions for a very larger number of structures, including those with novel combinations of elements and those for which there are few experimental data.

As mentioned in Chapter 2, we use the MD program DL_POLY_2.0 and MM program GULP to simulate the structure and properties of P3AT systems. These two programs do not contain built-in (ready-to-use) force fields. So it is necessary to choose the potentials coded in the programs and provide the relevant related

parameters suitable for our simulating systems i.e., to build a force field before starting the simulation.

A huge variety of potential forms is possible and for this reason the DL_POLY_2.0 and GULP force fields are designed to be adaptable. While these codes are not supplied with its own force field parameters, many of functional forms such as those that can be used for the Dreiding II, AMBER and GROMOS [7] force fields have been coded into these two programs, as well as additional potential forms [8]. Both also allow the possibility of user defined potentials.

The total potential energy of a molecular system is expressed as a superposition of valence (or bonded) interactions (U_{bond}) that depend on the specific connections (bonds) of the structure, nonbonded interactions (U_{nb}) that depend only the distance between the atoms and an external field potential U_{extn} if such exists:

$$U_{\text{potential}} = U_{\text{bond}} + U_{\text{nb}} + U_{\text{extn}}$$

The valence interactions consist of bond stretch (U_b , two-body), bond-angle bend (U_a , three body), dihedral angle torsion (U_t , four body), inversion terms (U_i , four body) and cross terms (U_c).

$$U_{\text{bond}} = U_b + U_a + U_t + U_i + U_c$$

The nonbonded interactions consist of van der Waals or dispersion (U_{vdw}), electrostatic (U_q) and explicit hydrogen bonds (U_{hb}) terms.

$$U_{\text{nb}} = U_{\text{vdw}} + U_q + U_{\text{hb}}$$

So to build a force field, all the potentials mentioned above have to be defined and determined.

For our P3AT systems, since there is no F, O or N atom directly bonded to a H atom, hydrogen bonds do not occur. The cross terms are also neglected and no external field is applied in this simulation work. So five types of potentials (U_b , U_a ,

U_t , U_{vdw} and U_q) are applied in our simulating systems. The following are the potentials and related parameters that were chosen for the simulations.

The functions used for the interatomic potentials were discussed in Chapter 2. The parameters involved are mainly from the literature, which were previously proved successful in the study of pure and doped polythiophene systems which are quite similar to the P3AT systems by Corish, *et al.* [9-13]. They are listed in sequence in the following sections. Other parameters are also referred to and compared as trial data. The simulation results are finally compared with experimental results such as the lattice parameters determined from X-ray diffraction measurements.

3.1 Bond Potential (U_b)

The bond potentials are represented by a Morse potential. Its function (equation 2.2) and advantages have been discussed in Chapter 2.

In order to define the potentials more precisely, we divide the C atoms in poly(3-butylthiophene) into 3 groups (C_1 , C_2 and C_3) according to their different chemical environments as illustrated for representative atoms in Fig. 3.1.

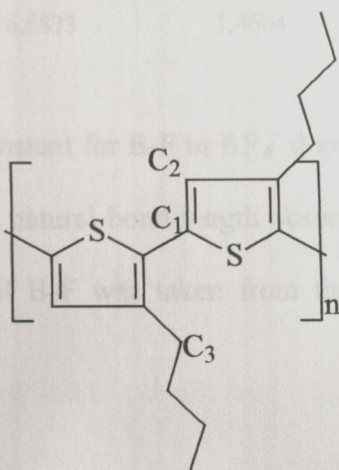


Fig. 3.1 The carbon types in poly(3-butylthiophene).

The parameters for the Morse function of our systems are listed in Table 3.1. The bond length used is the equilibrium distance r_0 . Since the basic carbon framework resembles that of polyacetylene, the double and single carbon bond force constants were obtained from a study of the Raman vibrational data and least squares fitting calculations on polyacetylene oligomers [14]. The C-S stretching force constant was obtained from a study of the combination of experimental (IR) and *ab initio* calculations on the thiophene molecule [15]. The literature values of E_0 quoted for C=C, C-C and C-H are taken from ref. [16] and those for C-S from ref. [17-18].

Table 3.1 The bond types in P3AT and relative parameters for Morse potential function $U(r) = E_0 \{1 - \exp[-(k/2E_0)^{1/2} (r_{ij} - r_0)]\}^2 - E_0$.

Bond Type	E_0 (eV)	k (\AA^{-1})	r_0 (\AA)	ref.
C ₁ -C ₁	4.5873	1.9169	1.446	[14,16]
C ₁ -C ₂	5.306	2.1353	1.384	[14,16]
C ₂ -C ₂	4.5873	1.9169	1.442	[14,16]
C ₂ -C ₃	4.5873	1.9169	1.534	[14,16]
C ₃ -C ₃	4.5873	1.9169	1.534	[14,16]
C ₂ -H	4.3051	2.1029	1.079	[14,16]
C ₃ -H	4.3051	2.1029	1.100	[14,16]
C ₁ -S	2.9963	2.0665	1.686	[15,17,18]
B-F	6.6873	1.4604	1.390	[18-20]

The stretching force constant for B-F in BF_4^- dopant is from ref. [19]. The value of r_0 was made equal to the natural bond length observed in BF_4^- (1.39 \AA) [20]. The bond dissociation energy of B-F was taken from the thermochemical calculations done on this system [18].

3.2 Valence Angle Potential (U_a)

The valence angle potentials are represented by harmonic potentials because it is simple and sufficient for our simulating systems. Its function was described in equation 2.3 in Chapter 2.

The parameters of equation 2.3 used in our systems are listed in Table 3.2. The experimentally determined bond angles are used as equilibrium bond angle θ_0 [21].

Table 3.2 The bond angle types and relative parameters

for harmonic potential function $U(r) = \frac{1}{2} k(\theta - \theta_0)^2$.

Angle Type	k (eV)	θ_0 (°)	ref.
C ₁ C ₂ C ₂	12.4	112.2	[21,22]
C ₂ C ₁ S	15.2601	110.25	[21-23]
C ₁ SC ₁	8.4883	95.1	[21,23]
C ₁ C ₂ H	5.2431	121.3	[21,22]
C ₁ C ₂ C ₃	12.42	121.3	[21,22]
HC ₂ C ₂	5.2431	126.5	[21,22]
C ₂ C ₂ C ₃	12.42	126.5	[21,22]
C ₃ C ₃ C ₃	12.42	112.2	[21,22]
C ₃ C ₃ H	5.2431	109.54	[21,22]
HC ₃ H	5.2431	106.30	[21,22]
C ₂ C ₁ C ₁	12.42	128.3	[21,22]
SC ₁ C ₁	15.2601	121.45	[21-23]
FBF	8.8032	109.50	[19]

The bond bending force constants for C-C=C, H-C-C and H-C=C are used the values for similar types in polyactylene and polyparaphenylene [22]. Since the bending force constant for the atomic triad C-C-S was not available, an average of $k(\text{C-C-C})$ and $k(\text{C-S-C})$ [23] was assumed.

The F-B-F bending force constant was taken from the IR analyses of BF_4^- [19]. The equilibrium bond angle was taken as being to the natural bond angle observed in the polyatomic ion.

3.3 Dihedral Angle Potential (U_t)

The dihedral angle potentials are represented by a cosine function as described in equation 2.4 in Chapter 2 and the reasons have been discussed there. A torsional potential was only considered on the bonds within the thiophene rings and between the thiophene rings in the polymer main chains. The equilibrium angle was 180° . Because no data are available for the energy barrier of torsion in P3AT or related systems, we chose the barriers for the intra-ring torsions by making them just high enough to ensure ring planarity. The barriers for inter-ring torsions were determined as those reproduced the X-ray experimental values of about 20° [24].

3.4 Van der Waals Potential (U_{vdw})

For the non-bonded short-range van der Waals potentials, several basic functions and their advantages were discussed in Chapter 2. In this work, a Buckingham potential (equation 2.6) was chosen to represent C...C, C...H, and H...H pair interactions. The corresponding parameters were taken from the Williams IV set [25] and are listed in Table 3.3. They were chosen because they have been widely and successfully used in calculations on hydrocarbon lattices.

The pair interactions of S...S, S...H, and S...C were represented by a Lennard-Jones (12-6) potential. The parameters of equation 2.5 of this potential are from ref. [26] and are listed in Table 3.3.

Table 3.3 The parameters for non-bond potentials

Atom Pair	Buckingham Potential $U(r)=Ae^{-r/\rho} - Cr^{-6}$			
	A (eV)	ρ (Å)	C (eVÅ ⁶)	ref.
C...C	3626.626	0.2778	24.6367	[25]
C...H	380.139	0.2725	5.4206	[25]
H...H	115.116	0.2674	1.1844	[25]
	Lennard-Jones Potential $U(r)=Ar^{-12}-Br^{-6}$			
	A (eVÅ ¹²)	B (eVÅ ⁶)		
S...H	13131.00	12.5854		[26]
S...C	116560.00	46.6608		[26]
S...S	599739.81	73.0703		[26]
Cl...C	24032.96	41.9514		[26]
Cl...H	3501.30	11.8300		[26]
Cl...S	253729.40	69.7311		[26]
Cl...Cl	87173.91	67.7363		[26]
F...C	3842.58	12.3800		[26]
F...H	405.94	4.4600		[26]
F...S	46140.50	20.5854		[26]
F...B	3842.58	12.3800		[26]
F...F	1583.70	5.8370		[26]

Non-bonded potentials among polymer-dopant atoms and dopant-dopant atoms are also represented by Lennard-Jones (12-6) functions. The parameters are listed in

Table 3.3. For the polyatomic dopant BF_4^- , the B atom is spacially surrounded by fluorine atoms the interactions involving this ion were assumed to be dominated by the F rather than B atom. Accordingly non-bonded interactions involving B atoms were neglected.

3.5 Coloumbic Potential (U_q)

As described in Section 2.1.2.2 both the DL_POLY (MD) and GULP (MM) programs use the Ewald sum method to calculate the long range electrostatic contributions to the lattice energy [28]. Partial atomic Coulombic charges were taken from the results of CNDO calculations on bithiophene molecules [27] whose use was justified in Section 2.5. After rounding off the values so as to be consistent with translational periodicity of the polymer, the resulting charges in electronic units, and those of the BF_4^- anion are as follows. The four carbon atoms of the ring bear charges of +0.025 while that on the sulphur is -0.1. The boron atom in BF_4^- was assigned a charge of +0.6 and the F atoms -0.4. Depending on the particular structure assumed for the doped polymer (Chapters 6 and 7), for a particular doping level the excess charge was distributed evenly over the number of atoms of either (a) the thiophene rings or (b) the alkyl side chains, the numbers of which were appropriate to the doping level to be considered. The same chapters will also describe modifications of these charges in accordance with the formation of phonons.

Bibliography:

- [1] Rappe A K, Casewit C J, Colwell K S, Goddard W A, Skiff W M. *J. Am. Chem. Soc.*, 1992, **114**:10024
- [2] Casewit C J, Colwell K S, Rappe A K. *J. Am. Chem. Soc.*, 1992, **114**:10046
- [3] Casewit C J, Colwell K S, Rappe A K. *J. Am. Chem. Soc.*, 1992, **114**:10035
- [4] Mayo S L, Olafson B D, Goddard W A. *J. Phys. Chem.*, 1990, **94**:8897
- [5] Weiner S J, Kollman P A, Singh U C, Ghio C, Alagona G, Profeta S, Weiner P. *J. Am. Chem. Soc.*, 1984, **106**:765
- [6] Kao J, Allinger N L. *J. Am. Chem. Soc.*, 1977, **99**:975
- [7] Linda P J D, Gillan M J. *J. Phys. Condens. Matter*, 1993, **5**:1031
- [8] Forester T R, Smith W. "**The DL_POLY_2.0 USER MANUAL**", CCLRC, Daresbury Lab., Daresbury, Warrington, England, 1997
- [9] Feeley D, Morton-Blake D A. *J. Mole. Struct. (Theochem)*, 1995, **331**:127
- [10] Corish J, Morton-Blake D A, Veluri K, and B eni ere F. *J. Mole. Struct. (Theochem)*, 1993, **283**:121
- [11] Corish J, Morton-Blake D A, Veluri K. *Molecular. Simulation*, 1995, **14**:381
- [12] Veluri K, Corish J, Morton-Blake D A, and B eni ere F. *J. Mole. Struct. (Theochem)*, 1995, **334**:109
- [13] Corish J, Morton-Blake D A, Veluri K, and B eni ere F. *Radiation Effects and Defects in Solids*, 1995, **134**:171
- [14] Takeuchi H, Furukawa Y, and Harada J. *J. Chem. Phys.*, 1986, **84**:2882
- [15] Bauer G and Mikosh H. *J. Mol. Struct.*, 1986, **142**:21
- [16] Moore W J. "**Physical Chemistry**", Longman, London, 1972
- [17] Petrucci R H and Wismar R K. "**General Chemistry with Qualitative Analysis**", 2nd Ed., Macmillan, London, 1987
- [18] Bailar J C, Moeller T, Kleinberg J, Guss C O, Castellion M E, and Metz C. "**Chemistry**", Harcourt Brace Jovanovich, San Diego, CA, 1989
- [19] Hunt R L, and Aule B S. *Spectrochim. Acta.*, 1961, **37**:63
- [20] Quist A S, Bates J B, and Boyd G E. *J. Chem. Phys.*, 1971, **54**:54
- [21] Mintmire J W, White C T, and Elert M L. *Synth. Met.*, 1988, **25**:109

- [22] Leslie M. *Physica*, 1985, **131 B**:145
- [23] Isaacs N. "***Physical Organic Chemistry***", Harlow Longman Scientific and Technical, 1987
- [24] Tashiro K, Ono K, Minagawa Y, Kobayashi M, Kawai T, and Yoshino K. *J. Polym. Sci.: Part B: Polym. Phys.*, 1991, **29**:1223
- [25] Williams D E. *J. Chem. Phys.*, 1967, **47**:4680
- [26] Hopfinger A J. "***Conformational Properties of Macromolecules***", Academic Press: New York, 1973
- [27] Veluri K. *Ph. D. Thesis*, Trinity College, University of Dublin, 1994
- [28] Allen M P, and Tildesley D J. "***Computer Simulation of Liquids***", Clarendon Press, Oxford, 1989

Chapter 4

MM SIMULATION OF THERMOCHROMIC PHENOMENA IN POLY(3-ALKYLTHIOPHENE)

4.1 Introduction

Part II

MOLECULAR SIMULATION OF THERMOCHROMIC PHENOMENA IN POLY(3-ALKYLTHIOPHENE)S

It seems likely that the blue shift is the result of a reduction in the effective conjugation length, resulting in a widening of the gap between the π and π^* orbitals. This produces a disruption of the planarity of the π conjugated system, which reduces the effective conjugation length. The disruption of planarity and the reduction in effective conjugation length are due to the presence of the alkyl side chains, which are known to be in a disordered state at room temperature.

Chapter 4

MM SIMULATION OF THERMOCHROMIC PHENOMENA IN POLY(3-ALKYLTHIOPHENE)S

4.1 Introduction

Thermochromism is a reversible color change with temperature. P3ATs are one of the several kinds of materials that exhibit this special property. When the soluble electroactive P3ATs are heated through a critical temperature the polymer materials change their color. Poly(3-dodecylthiophene), for example, changes its color from red (303 K) to yellow (353 K) and returns to red upon cooling [1-4]. If the spectrum is simultaneously monitored the thermochromic change is revealed as a distinct blue shift of the absorption band in the visible range [1-2]. Electronic absorption spectra and UV-vis spectra [1-2] showed that the energy change corresponding to the thermochromic transition was about 0.5 eV. This energy change is believed to involve a change of polymer conformations induced by temperature since the change is reversible and no chemical reaction is found to occur during the process.

It seems likely that the blue shift is the result of a twisting of the main (conjugated) chain, resulting in a widening of the gap between the π energy bands. This twisting produces a disruption of the planarity of the π conjugated system and reduces the effective conjugation length. The disruption of planarity and the reduction of conjugation length are due to the presence of the alkyl side chains, since no thermochromism is

observed in unsubstituted polythiophene. However, how the alkyl side chains affect the π -conjugated system has not been established. Although FTIR [1-2] confirmed that the number of *gauche* conformations in the alkyl side chains were enhanced after the thermochromic transition, to date, no information has been provided on the coupling between the polymer main chains and the alkyl side chains.

X-ray diffraction [2] found that the torsion between the thiophene rings was increased drastically in the transition region, and Raman spectra [1] confirmed that different conjugation lengths could be existed in P3AT π -conjugated system. But these methods can not provide information on the torsional details such as the torsional periodicity and few values of the torsional angle were given.

In our view, thermochromism is probably due to the transition between two kinds of stable conformations of P3AT with different energies. The higher energy conformations are thermally accessible. They should contain higher torsional angles in the main chains and higher energy conformations in the alkyl side chains. Molecular mechanics (MM) simulation is an excellent technique to search for stable conformations of a molecular system. Molecular dynamics (MD) simulation is a good method to investigate thermally induced conformation changes. So MM and MD simulations together should be very helpful in understanding thermochromism of P3ATs at an atomic level.

In this chapter, stable conformations with different inter-ring torsional angles in the polymer main chain were first searched, and their torsional periodicities were investigated by molecular mechanics methods. Then the bandgaps corresponding to these conformations were calculated by Extended Hückel Theory (EHT). The enhancement of energy and bandgap between possibly stable conformation changes was evaluated. The MD investigation of the conformation changes in P3AT due to the thermal agitation will

be described in the next Chapter.

4.2 Lattice Structure and Parameters

We chose to use a butyl side group as alkyl group on the polythiophene to strike a balance between, on one hand, taking chains that were sufficiently long to exhibit typical properties of P3AT such as thermochromism and, on the other, longer chains demanding excessive computing times. In the energy-minimizing method of atomistic simulations, as the alkyl chain becomes longer, the increasing conformational freedom implies a correspondingly greater risk that the structure will stabilize into local energy minima rather than into the global minimum. This problem can only be countered by allowing the lattice to relax from several initial structures with slightly different conformations, so that this approach is more difficult for longer alkyl chains.

Although P3ATs possess three different regioregularities as discussed in Chapter 1, this thesis will only deal with regioregular HT-P3ATs because they are highly crystalline and, in addition, show excellent conductivity. The chain structure of regioregular HT-poly(3-butylthiophene) (P3BT) is illustrated in Fig. 4.1. We define the torsional angles around the four carbon-carbon links of the alkyl side chains as φ_1 , φ_2 , φ_3 , and φ_4 , corresponding to link 1, link 2, link 3 and link 4, respectively. The torsional angle between two thiophene rings in the polymer main chains is defined as φ_5 . The sense here that 0° means *trans*, 120° *gauche* and 180° *cis* for φ_1 to φ_4 while 0° is *anti* and 180° *syn* for φ_5 .

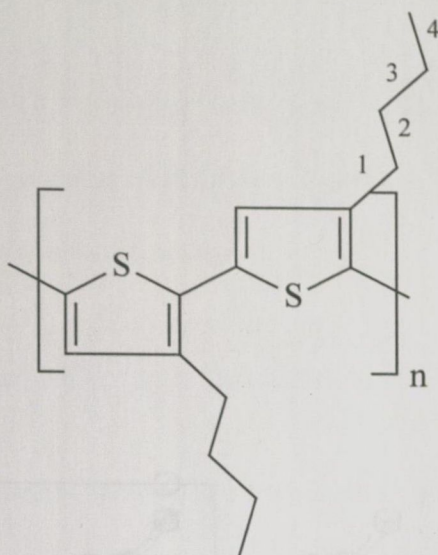


Figure 4.1 The chain structure of regioregular HT-P3BT.

The possible lattice structures of P3ATs were discussed in detail in Chapter 1. Two kinds of lattice structure are employed in the MM simulations. One is an orthorhombic lattice of stacked polymers with two chains per unit cell aligned along the **c** axis [7-10]. In this structure the setting angle of the polymer chains (that is, the angle between the plane of the backbone and the longer of the two axes **a** or **b**) is zero. The second chain in the cell, well paralleled with the first, is separated from the first by $b/2$ along the **b** axis. It is also shifted by $c/2$ along the **c** axis so that viewed along **b** the thiophene rings show a staggered relationship as shown in Figure 4.2. Because this structure was first proposed by Kawai, *et al.* and each cell has two staggered chains here we would call it as the Kawai structure or two-chain staggered structure. Another is an orthorhombic lattice stacked one chain per unit cell [11-13]. Again the setting angle is zero and the thiophene rings on the polymer chains are eclipsed when viewed along **b** as illustrated in Figure 4.2. So we will call this a one-chain eclipsed structure. In both lattice structures, all alkyl chains are in all extended *trans* conformation and the thiophene rings are in planar *anti* in the initial, or trial structure. The lattice parameters *a* and *b* are optimized by using the lattice energy

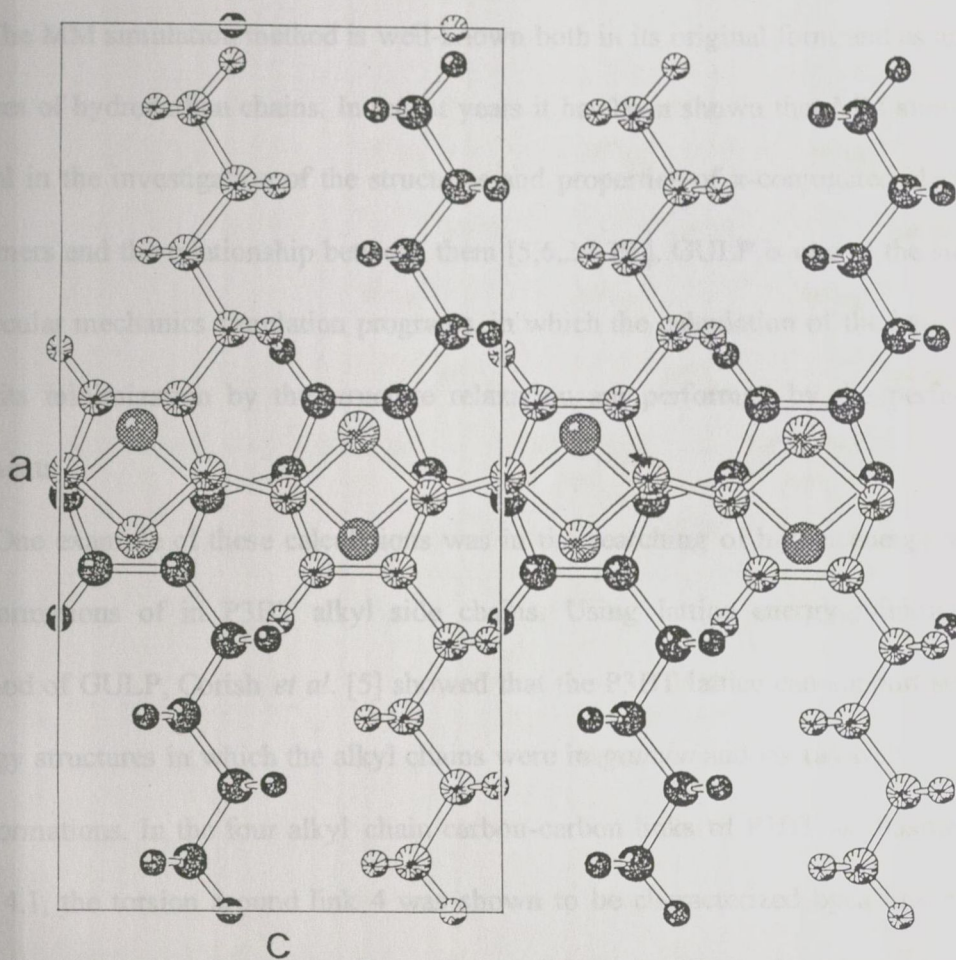


Fig.4.2 The lattice structure for the two-chain cell showing the staggered relationship of the thiophene rings stacked along **b** axis. The two chains are distinguished by shading. One in $b=0$ and the other in $b= \frac{1}{2} b$. In the one-chain eclipsed structure one chain is displaced by $\frac{1}{2} c$ along the **c** axis and the two chains are in different cells.

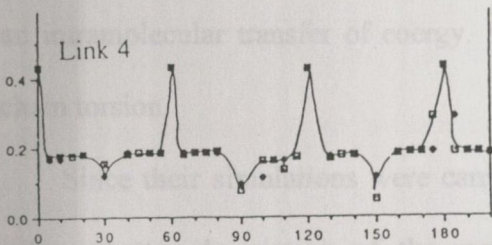
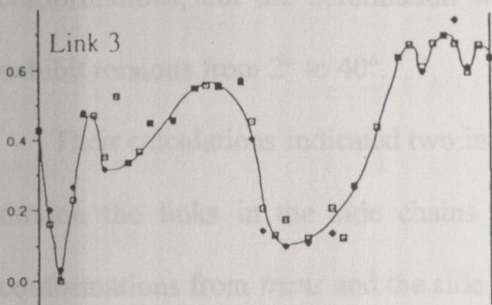
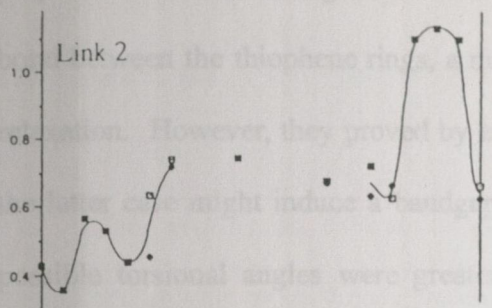
minimization method of GULP starting from many trial structures. Since the parameter c depends on the geometry of the polymer chain, it is not optimized in this way but decided by the structural model used.

4.3 Literature Review of MM Investigations of Poly(3-alkylthiophene)s

The MM simulation method is well-known both in its original form and as applied to lattices of hydrocarbon chains. In recent years it has been shown that MM simulation is useful in the investigation of the structures and properties of π -conjugated electroactive polymers and the relationship between them [5,6,24-29,]. GULP is one of the successful molecular mechanics simulation programs, in which the calculation of the lattice energy and its minimization by the structure relaxation are performed by the perfect-lattice segments.

One example of these calculations was in the searching of higher energy stable conformations of in P3BT alkyl side chains. Using lattice energy minimization method of GULP, Corish *et al.* [5] showed that the P3BT lattice can support several energy structures in which the alkyl chains were in *gauche* and *cis* (as well as *trans*) conformations. In the four alkyl chain carbon-carbon links of P3BT as illustrated in Fig. 4.1, the torsion around link 4 was shown to be characterized by a low-energy barrier (about 0.1 to 0.2 eV) as shown Fig. 4.3 [5]. Its torsion is therefore unhindered and has a periodicity of 120° . Link 3 has two barriers. It showed a well-defined minimum at about 120° , indicating the stability of the *gauche* conformation about this C-C bond. Links 1 and 2 show a near *trans*-conformation, but they were also shown to have two energy barriers in a Monte Carlo simulation (shown in Fig. 4.4 [5]) and show possible near *cis* conformations. Due to the tendency of the energy minimization

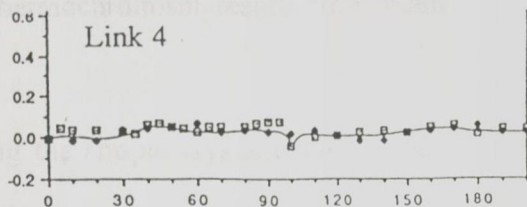
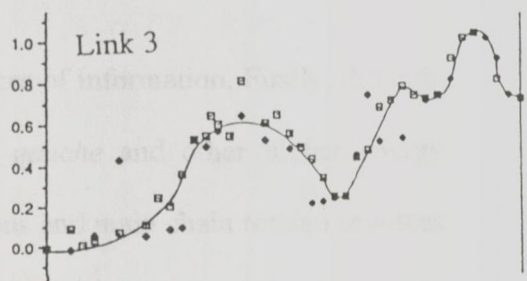
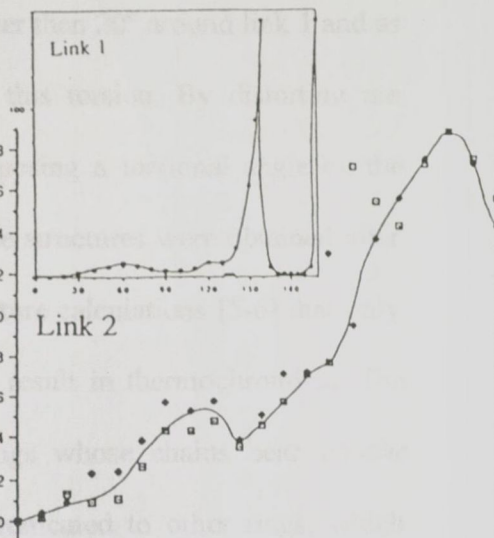
Relative lattice energy (eV)



Torsional angle ϕ (degrees)

Fig. 4.3 Energy profile, as obtained by lattice energy minimization of GULP, when a torsion ϕ is applied to one butyl chain along links 2, 3, and 4, allowing the lattice to relax (cited from reference [5]).

Relative lattice energy (eV)



Torsional angle ϕ (degrees)

Fig. 4.4 Energy Profile, as obtained by a Monte Carlo calculation, when a torsion ϕ is applied to one butyl chain along links 1, 2, 3, and 4, allowing the other links in butyl chains to relax (cited from reference [5]).

methods to show lattice instability under conditions of high steric strain, the minimization method did not tolerate torsions of greater than 20° around link 1 and as a consequence no energy profile was obtained for this torsion. By distorting the polymer main chain along the **b** direction or by imposing a torsional angle on the bond between the thiophene rings, a number of stable structures were obtained after relaxation. However, they proved by electronic structure calculations [5-6] that only the latter case might induce a bandgap increase and result in thermochromism. The possible torsional angles were greatest at those rings whose chains bear *gauche* conformations, but the deformation was also communicated to other rings, which exhibit torsions from 2° to 40° .

Their calculations indicated two important pieces of information. Firstly, through torsion the links in the side chains can access *gauche* and other higher energy conformations from *trans* and the side chain torsions and main chain torsion involves an intramolecular transfer of energy. Secondly, thermochromism results from main chain torsion.

Since their simulations were carried out using the simple crystallographic unit cell, a better description of the main chain distortion would probably require relaxation to be conducted using $n_1 \times n_2 \times n_3$ supercell. The effect of the main chain torsional periodicity was also not considered. The energy transfer between side chains and main chain is not clear. Since the calculation method used was static lattice (MM) the thermal effect was not considered although this is the most important factor for thermochromism.

In this Chapter, the MM study is extended by the use of a supercell to investigate the torsional possibility of P3BT main chain along the **c** axis in the conditions of three different torsional periodicities since it can enlarge the electronic bandgap and is

essential for thermochromism. The investigation of thermally induced conformation changes and energy transfer between side chains and main chain using MD simulations will be described in the next Chapter.

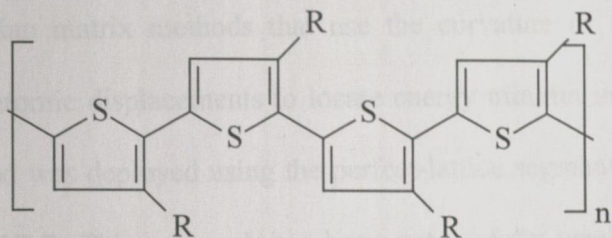
4.4 Discussion of the Main Chain Torsional Periodicity

Before starting the MM investigation, the possibilities of main chain torsional periodicity should be discussed because the pattern of torsional periodicity directly affects the bandgap of the polymers. In P3ATs, the torsional bonds on the same chain are not coaxial since successive bonds make mutual angles of 12° . As discussed in the work of Corish *et al.* [5-6], an arbitrary set of inter-ring torsions would not preserve the periodicity of the polythiophene backbones along their original direction; if the polymer chain twists around each of these bonds it must lose the direction of its original periodicity. Since the orientation of the main chain has been reported by some diffraction workers [2] to be preserved during the thermochromic transition, it is important to examine the conditions for this thermochromic torsional periodicity.

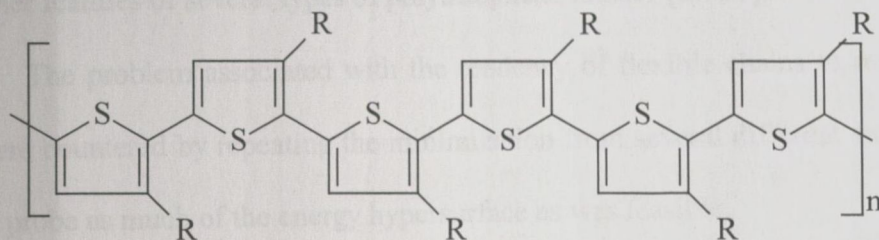
An x-ray diffraction investigation on poly(3,3'-dioctyl-2,2'-bithiophene) (PDOBT) shows that the polymer backbone is twisted even at low temperatures [30]. The 4-ring torsional scheme around the inter-thiophene C-C bonds, given by $[\varphi, 0^\circ, -\varphi, 0^\circ, \varphi, 0^\circ \dots]$, ensures that the chain is periodic for any value of φ . In PDOBT the torsional angle φ found in the diffraction investigation is about 40° . Although PDOBT (unlike P3AT) is not thermochromic and its thiophene rings are linked head-to-head rather than head-to-tail, its analogy suggests that P3AT might have the same pattern of inter-ring torsional periodicity. We also devised two other inter-ring torsional

patterns [31-33] which produce translational periodicity, and of course there are many others based on a longer repeat segment. The three trial patterns employed in our work are defined as follows:

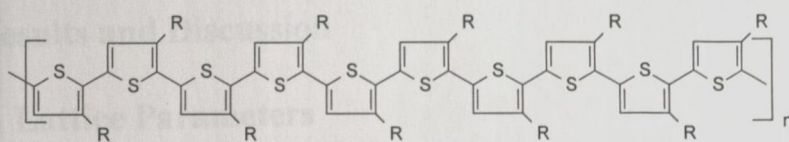
Scheme A: the 4-ring repeat segment $[\varphi, 0^\circ, -\varphi, 0^\circ]$ (found in PDOBT)



Scheme B: the 6-ring repeat segment $[+\varphi, -\varphi, 0^\circ, +\varphi, -\varphi, 0^\circ]$



Scheme C: the 10-ring segment $[+\varphi, 0^\circ, 0^\circ, -\varphi, 0^\circ, +\varphi, 0^\circ, 0^\circ, -\varphi, 0^\circ]$



For any value of φ the torsional pattern in each of these schemes leads to a non-helical, 'twisted' chain with translational periodicity.

4.5 Method of Calculation

The force field is defined by a set of 2-, 3-, and 4- atom intramolecular potential energy functions and non-bonded short and long range potentials, which allow contributions from non-bonding atom pairs, and from changes in bond lengths, bond

angles and internal torsions, to be calculated. The functions and parameters of the potentials employed have been described in Chapter 3.

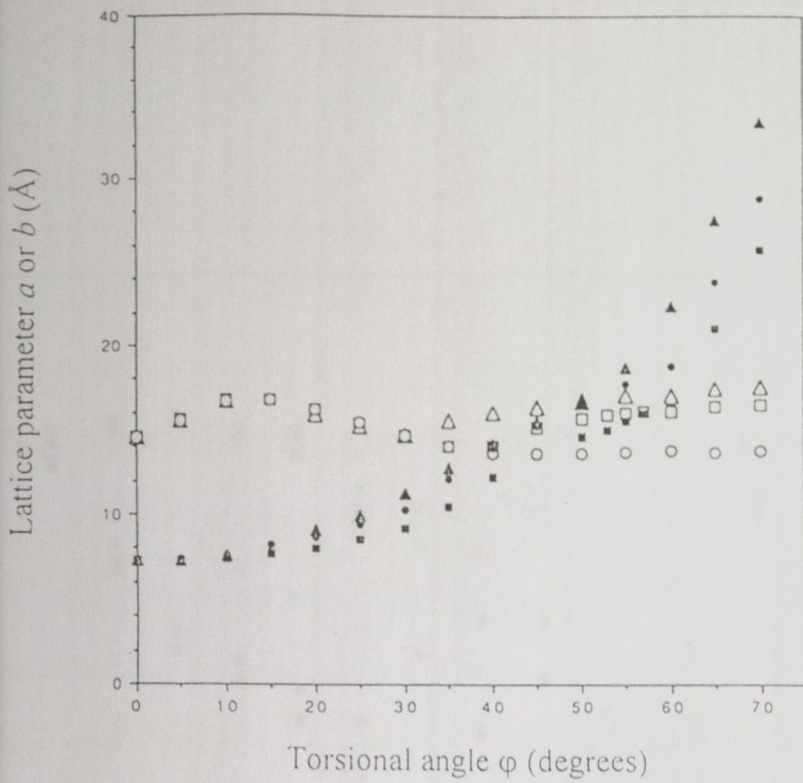
The lattice is 'relaxed' by minimizing the calculated energy with respect to the structure parameters using Newton-Raphson methods. This is commonly performed using Hessian matrix methods that use the curvature of the energy function with respect to atomic displacements to locate energy minima in the energy hypersurface. This method was deployed using the perfect-lattice segments of the lattice simulation program GULP. This approach has been successfully used to explain structural and other features of several types of polythiophene lattices [25-29].

The problem associated with the tendency of flexible chains to reach local minima were countered by repeating the minimization from several different starting points so as to probe as much of the energy hypersurface as was feasible.

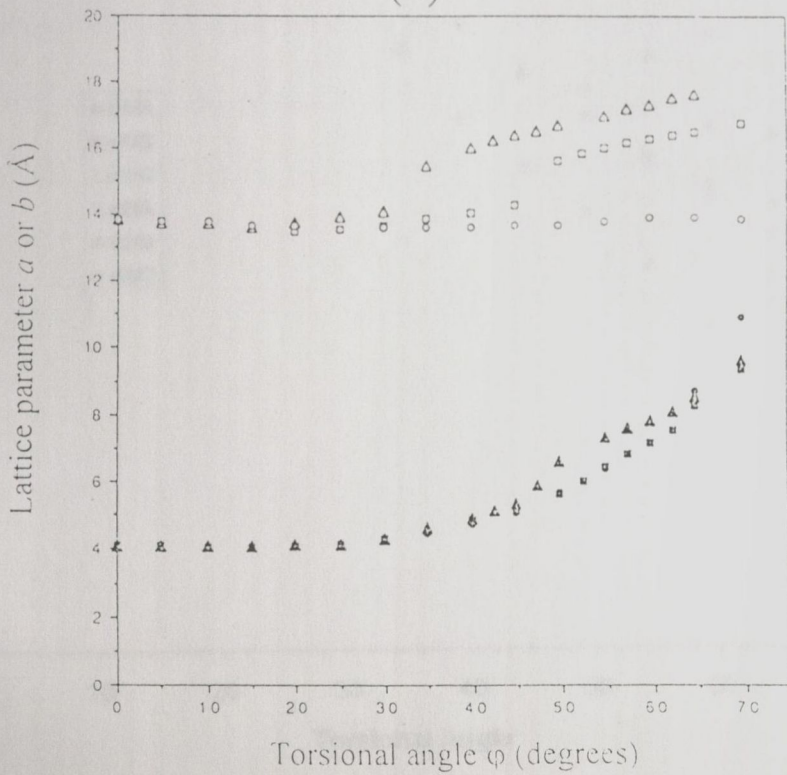
4.6 Results and Discussion

4.6.1 Lattice Parameters

The two structural models described in Section 4.2 were investigated: (1) a two-chain 'staggered' and (2) a one-chain 'eclipsed' configuration, both in an orthorhombic supercell. A number of initial lattice parameters a and b at inter-ring torsional angle $\varphi = 0^\circ$ were selected for optimization and for each combination the lattice was relaxed. The a and b with lowest relaxed lattice energy were taken as the best optimized lattice parameters for the untwisted polymer. The torsion φ was then changed by a few degrees and the same procedure followed to obtain the best values of a and b . The procedure was not applied to optimise cell vector c as this was decided by the bonding and torsion in the polymer chain.



(a)



(b)

Fig. 4.5 The effect of the torsion schemes A, B and C on the cell parameters a (the open symbols \square , Δ and \circ refer to schemes A, B and C, respectively) and b (closed symbols). (a) two-chain structure, (b) one-chain structure.

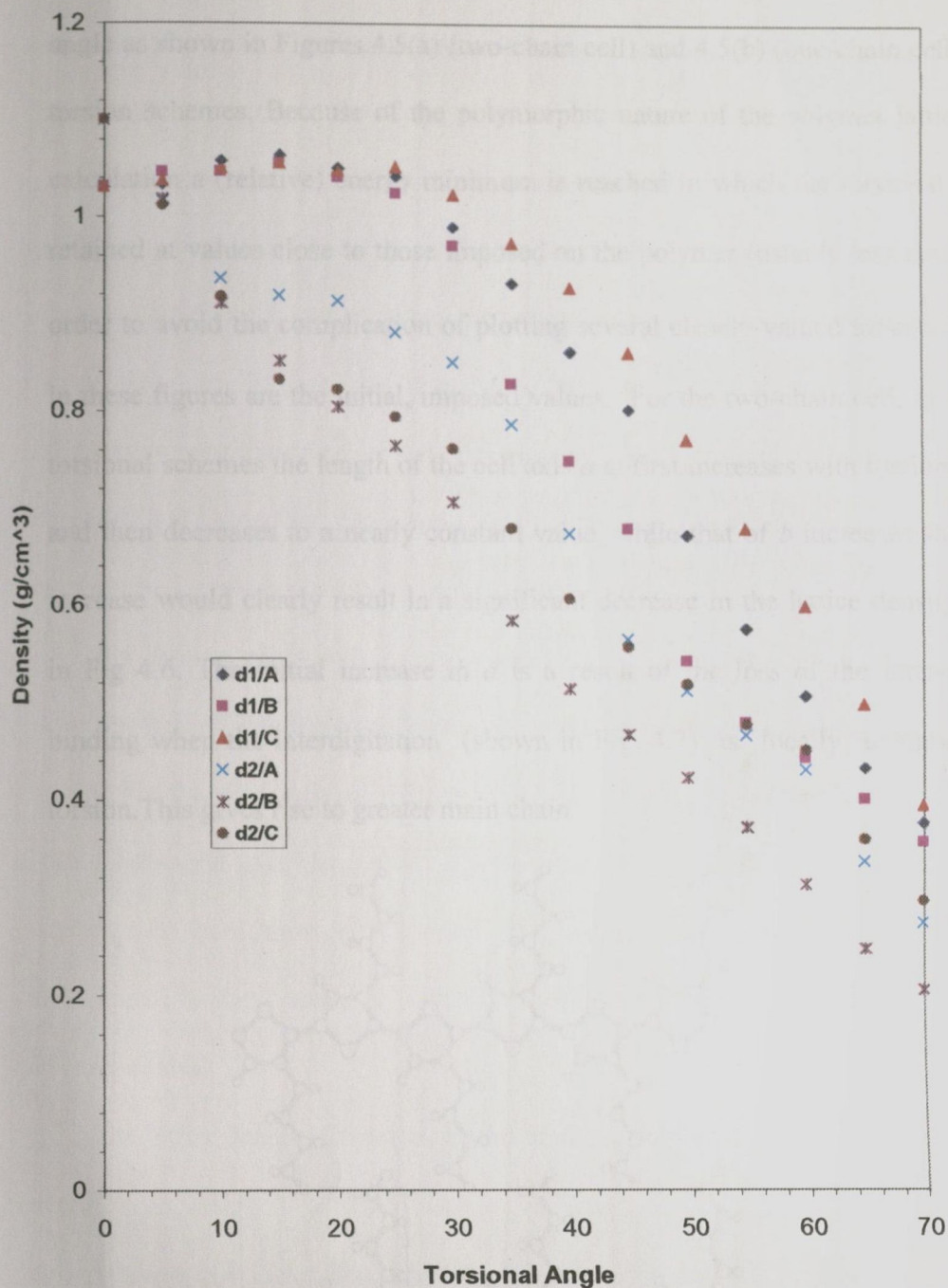


Fig. 4.6 The lattice density after relaxation as a function of torsional angle φ_5 (in units of degree) at three different torsional schemes in the two-chain and one-chain structures. d1 represents the density in the one-chain structure, d2 – the density in the two-chain structure; A – torsional scheme A $(+\varphi, 0, -\varphi, 0)$, B – torsional scheme B $(+\varphi, -\varphi, 0, +\varphi, -\varphi, 0)$, C – torsional scheme C $(+\varphi, 0, 0, -\varphi, 0, +\varphi, 0, 0, -\varphi, 0)$.

The best optimized parameters a and b after relaxation change with torsional angle as shown in Figures 4.5(a) (two-chain cell) and 4.5(b) (one-chain cell) in all the torsion schemes. Because of the polymorphic nature of the polymer lattice, in each calculation a (relative) energy minimum is reached in which the torsional angles are retained at values close to those imposed on the polymer (usually less than 10°). In order to avoid the complication of plotting several closely-valued torsional angles, φ in these figures are the initial, imposed values. For the two-chain cell, in each of the torsional schemes the length of the cell axis a at first increases with torsional angle φ_5 and then decreases to a nearly constant value, while that of b increases sharply. This increase would clearly result in a significant decrease in the lattice density as shown in Fig 4.6. The initial increase in a is a result of the loss of the inter-alkyl-chain binding when the interdigitation (shown in Fig. 4.7) is locally unzipped by the torsion. This gives rise to greater main chain

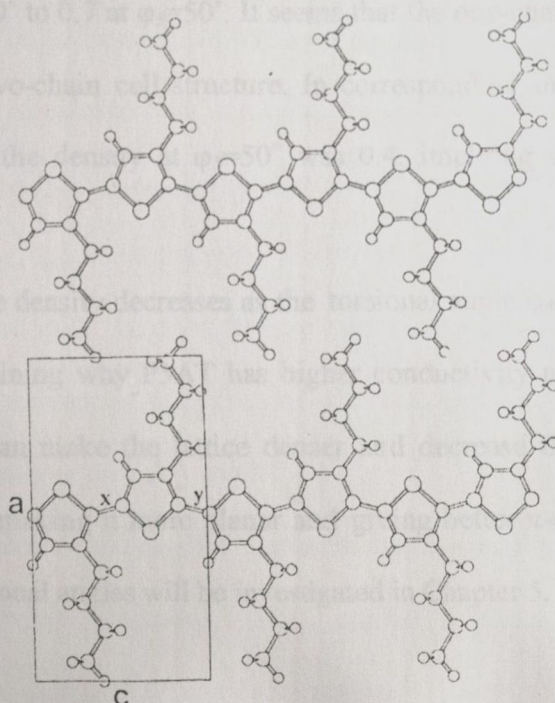


Fig. 4.7 The interdigitation exists between alkyl side chains of two neighboring polymers in the same ac plane.

separation. Greater torsions reduce the tip-to-tip extent (illustrated in Fig. 4.7) of the alkyl groups in each polymer chain, thereby decreasing the value of a . As the torsional angle increases, the density of the lattice decreases (Fig. 4.6).

Experimentally, it is difficult to find a consensus on the temperature behavior of the lattice parameters. Prosa *et al.* [34] in their diffraction studies of oriented P3AT solution cast films found a increasing with temperature but b remaining constant. Łużny and Proń [35], on the other hand, from the temperature dependence of the diffractograms of their powder and film samples, agree that with rising temperature, a increased, but found that, unaccountably, b decreased. Generally speaking, increasing temperature increases the torsion in the polymer main chain.

For the one-chain cell, it can be seen that the cell parameter b (starting from a value one half of b in the two-chain cell) increases much more slowly with φ_5 than is the case for the two-chain cell. The result of the torsion is to reduce the crystal density from 1.1 at $\varphi_5=0^\circ$ to 0.7 at $\varphi_5=50^\circ$. It seems that the one-chain cell structure has better packing than two-chain cell structure. In corresponding investigations on the two-chain structure the density at $\varphi_5=50^\circ$ was 0.4, implying very poor packing of the polymer chains.

The lattice density decreases as the torsional angle φ_5 increased. This finding is helpful in explaining why P3AT has higher conductivity at higher pressure because high pressure can make the lattice denser and decrease the possible torsion in the polymer chain, making it more planar and giving better π -conjugation. The effects of pressure on torsional angles will be investigated in Chapter 5.

4.6.2 Lattice Energy Profile of Two-chain Staggered Structure

Fig. 4.8 is the energy profile of a staggered (two-chain) lattice structure when a torsion φ_5 is applied to the inter-ring C-C bonds according to the torsional periodicities defined in Section 4.4. It shows that in each torsional schemes A, B and C, the lattice energy increases with φ_5 from its minimum value in the planar polythiophene backbone at $\varphi_5=0^\circ$. Each energy curve dips to form a local minimum at 50° - 60° .

Measured values of the torsion angle are uncertain. A torsion of 45° is derived from the spectral shift in the UV spectrum of poly[3-(octyloxy)-4-methylthiophene] [36]. A 40° twist was estimated in PDOBT [30] and 30° from an infra red and Raman study of vibrational effects in hexyl and octyl P3ATs [37]. Łuzny and Proń [35] found that a computer matching of their diffraction data obtained from poly(3-decylthiophene) led to an angle of 40° between the rings. The differences between the torsional angles calculated here and those measured by experiment may originate in the length of the alkyl chains, the types of thiophene ring linkage and the temperature. In this simulation, the temperature is effectively 0 K. Another reason may be that the relaxation process in the calculation could not completely relax the alkyl chains from their all *trans* conformations. In fact, alkyl chains can undergo torsion so that *gauche* and *cis* conformations probably exist [5].

The occurrence of the angle 0° between the thiophene rings occurring in each of our adopted torsional schemes A, B, C implies a planar bithiophene unit, and the occurrence of two adjacent 0° angles in sequence C implies a planar trithiophene unit. Interestingly, from combined UV/photoelectron spectroscopic and quantum chemical

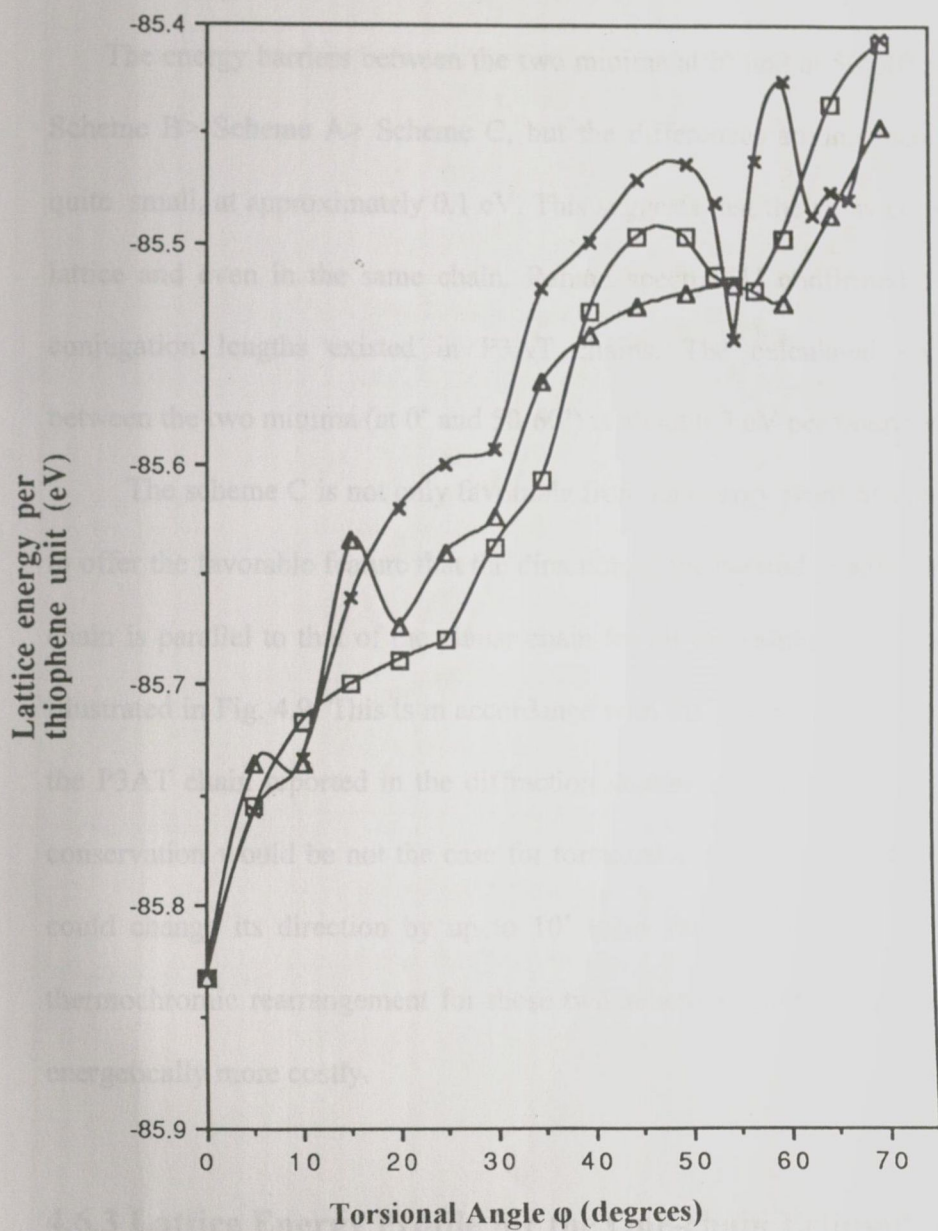


Fig. 4. 8 The lattice energy per thiophene unit for the two-chain staggered structure in which the chains have been subjected to torsion schemes A(\square), B(\times) and C(\triangle).

analyses, Salaneck and coworkers [38] find 'soft conformation modes' which they identify with polythiophene chains containing planar bithiophene units showing mutual torsional angles of 45° with adjacent rings and planar trithiophene making 60° with their neighbors.

The energy barriers between the two minima at 0° and at $50\text{-}60^\circ$ are in the order: Scheme B > Scheme A > Scheme C, but the differences among these sequences are quite small, at approximately 0.1 eV. This suggests that they may coexist in the same lattice and even in the same chain. Raman spectra [1] confirmed that different π -conjugation lengths existed in P3AT chains. The calculated energy difference between the two minima (at 0° and $50\text{-}60^\circ$) is about 0.3 eV per thiophene ring unit.

The scheme C is not only favorable from an energy point of view, it also seems to offer the favorable feature that the direction of the twisted $[+\varphi, 0, 0, -\varphi, 0; +\varphi, 0, 0, -\varphi, 0]$ chain is parallel to that of the planar chain for all the values of torsional angle φ_5 as illustrated in Fig. 4.9. This is in accordance with the preservation of the orientation of the P3AT chain reported in the diffraction studies of Tashiro *et al.* [10]. This axial conservation would be not the case for torsional schemes A and B, when each chain could change its direction by up to 10° (also shown in Fig. 4.9). As a result the thermochromic rearrangement for these two schemes would be expected to be more energetically more costly.

4.6.3 Lattice Energy Profile for the One-chain Eclipsed Structure

Fig. 4.10 shows the energy profiles of the eclipsed lattices when the A, B and C torsional schemes are imposed on the main chains, respectively. The figures also

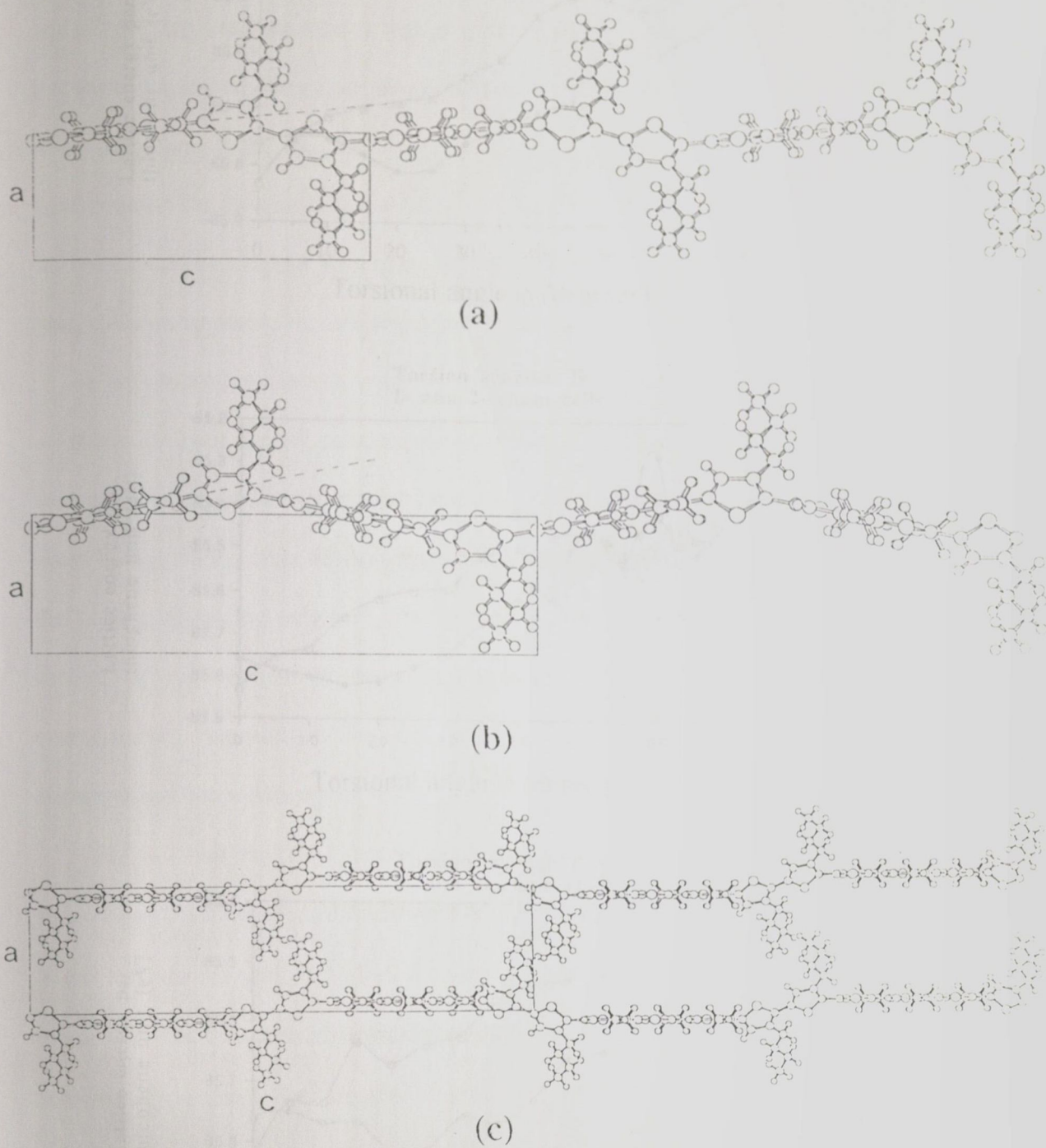


Fig. 4.9 Effect of torsional periodicity on the polymer main chain structure. (a) Torsional scheme A applied, (b) Torsional scheme B applied, (c) Torsional scheme C applied. An adjacent chain is included in (c). In torsional schemes A and B each chain can change its direction by up to 10° .

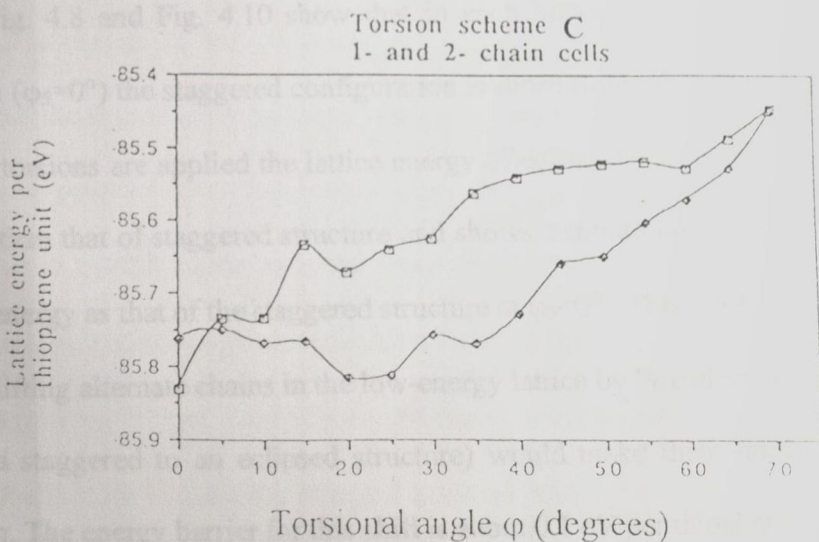
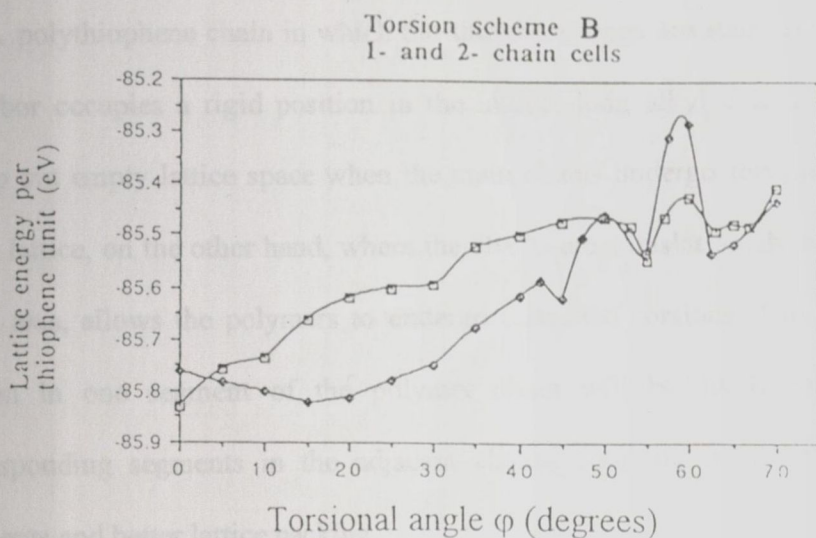
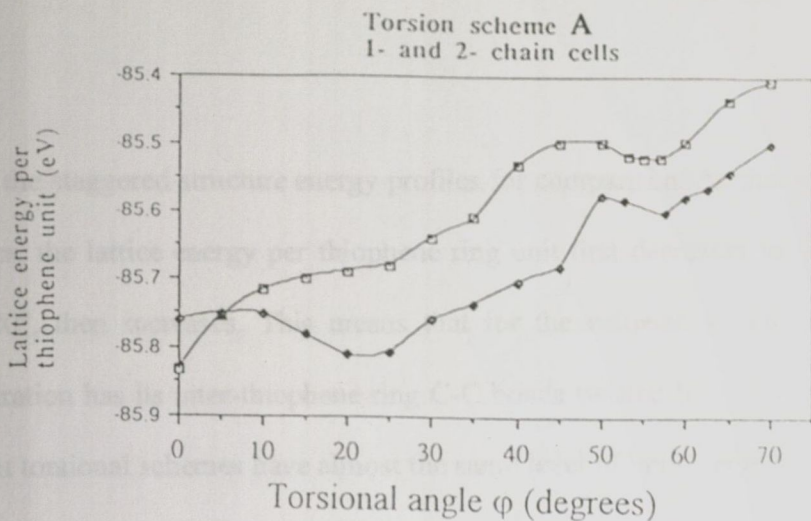


Fig. 4.10 A comparison of the lattice energy profile of the one-chain eclipsed structure (•) with that of the two-chain staggered structure (□) for torsional schemes A, B and C.

contain the staggered structure energy profiles for comparison. As the torsional angle increases, the lattice energy per thiophene ring unit first decreases to a minimum at about 20° , then increases. This means that for the eclipsed structure the favored configuration has its inter-thiophene ring C-C bonds twisted by about 20° . The three different torsional schemes have almost the same level of lattice energy per thiophene unit, so thermodynamically they could coexist in the same lattice.

A polythiophene chain in which the thiophene rings are staggered relative to its neighbor occupies a rigid position in the lattice: long alkyl chains would have to sweep out empty lattice space when the main chains undergo torsions. An eclipsed-chain lattice, on the other hand, where the chains are translationally equivalent along the **b** axis, allows the polymers to undergo concerted torsions. This is because any torsion in one segment of the polymer chain will be likely to be copied in corresponding segments in the adjacent chains, resulting in a dovetailing of the segments and better lattice packing.

Fig. 4.8 and Fig. 4.10 show that in each torsional scheme when there is no torsion ($\varphi_5=0^\circ$) the staggered configuration is more stable than the eclipsed structure. When torsions are applied the lattice energy of eclipsed structure decreases until it is lower than that of staggered structure and shows a minimum at about 20° , which has same energy as that of the staggered structure at $\varphi_5=0^\circ$. This confirms the expectation that shifting alternate chains in the low-energy lattice by $\frac{1}{2} c$ along **c** (converting them from a staggered to an eclipsed structure) would make them undergo spontaneous torsion. The energy barrier for this shift is about 0.1 eV per thiophene unit.

Like the energy profiles of the staggered structure the eclipsed-ring profiles also show minima in the $\varphi_5=50-60^\circ$ region for the torsional schemes A and B, though not for C. The energy difference between the minima at 20° and at ca. 55° is about 0.3 eV.

4.6.4 Information for the Thermo-chromic Distortion

The calculations reported here allow two principal kinds of distortion to be described for P3AT lattices:

1. The chains are in a structure in which stacked rings along **b** are staggered as in Fig. 4.2, leading to a high energy minimum at $\varphi_5 \approx 55^\circ$. Although there are estimated torsions near this value, the doubling of the cell **b** axis at this torsion (Fig. 4.5), with no reduction of *a*, produces a crystal density less than 0.5 that of the lowest-energy lattice. The torsion has therefore swept out an excessive amount of lattice space. But here the torsion of alkyl chains, which might reduce the decrease of the lattice density, has not been considered explicitly.
2. Each chain stacked along **b** is translationally invariant, so that the rings are eclipsed. Concerted chain torsions occur, leading to a local minimum at $\varphi_5 \approx 20^\circ$. Although this value is smaller to the experimental estimates, it involves a far less drastic change in cell parameters (Fig. 4.5) over the φ_5 range concerned; as a result the crystal density is just over 0.75 that of the planar structure.

Three possible transitions may happen. The first is from $\varphi_5 = 0^\circ$ in the staggered structure to $\varphi_5 \approx 20^\circ$ in the eclipsed structure. The energy barrier is about 0.1 eV per thiophene unit. Another two possibilities involve changes from $\varphi_5 = 0^\circ$ of the staggered structure or $\varphi_5 \approx 20^\circ$ of the eclipsed structure to $\varphi_5 \approx 55^\circ$ of the staggered or eclipsed structure. In both of them the energy barrier is about 0.3 eV per thiophene unit.

4.6.5 Electronic Bandgap Change with Torsional Angle φ_5 in Different Torsional Sequences

Fig. 4.11 is the electronic bandgap change with torsional angle of polymer main chain in the three different torsional schemes calculated from extended Hückel theory. As expected, the electronic band gap increases as the torsional angle is enhanced in all the three torsional schemes. But the electronic bandgap increases more quickly in the torsional scheme A ($+\varphi, 0, -\varphi, 0$) than it does in the other two, B ($+\varphi, -\varphi, 0, +\varphi, -\varphi, 0$) and C ($+\varphi, 0, 0, -\varphi, 0, +\varphi, 0, 0, -\varphi, 0$), with the scheme C having the lowest increase. The electronic bandgap differences for the three transitions proposed in Section 4.6.4 are listed in Table 4.1. The electronic spectra and UV-vis spectra [1-2] showed that the electronic bandgap change during the thermochromic transition is about 0.5 eV, and the *ab initio* calculations [39] suggested that it is in the order of 0.7 eV. It seems the torsional angle change from 0° or 20° to about 55° is more favourable than the transition from 0° to 20° .

Table 4.1 The electronic bandgap differences calculated by EHT when the polymer main chain imposed some torsional angles in the three different torsional schemes, in units of eV.

	Scheme A	Scheme B	Scheme C
$0^\circ \leftrightarrow 55^\circ$	0.7275	0.3968	0.3636
$20^\circ \leftrightarrow 55^\circ$	0.675	0.3486	0.3232
$0^\circ \leftrightarrow 20^\circ$	0.0525	0.0472	0.0404

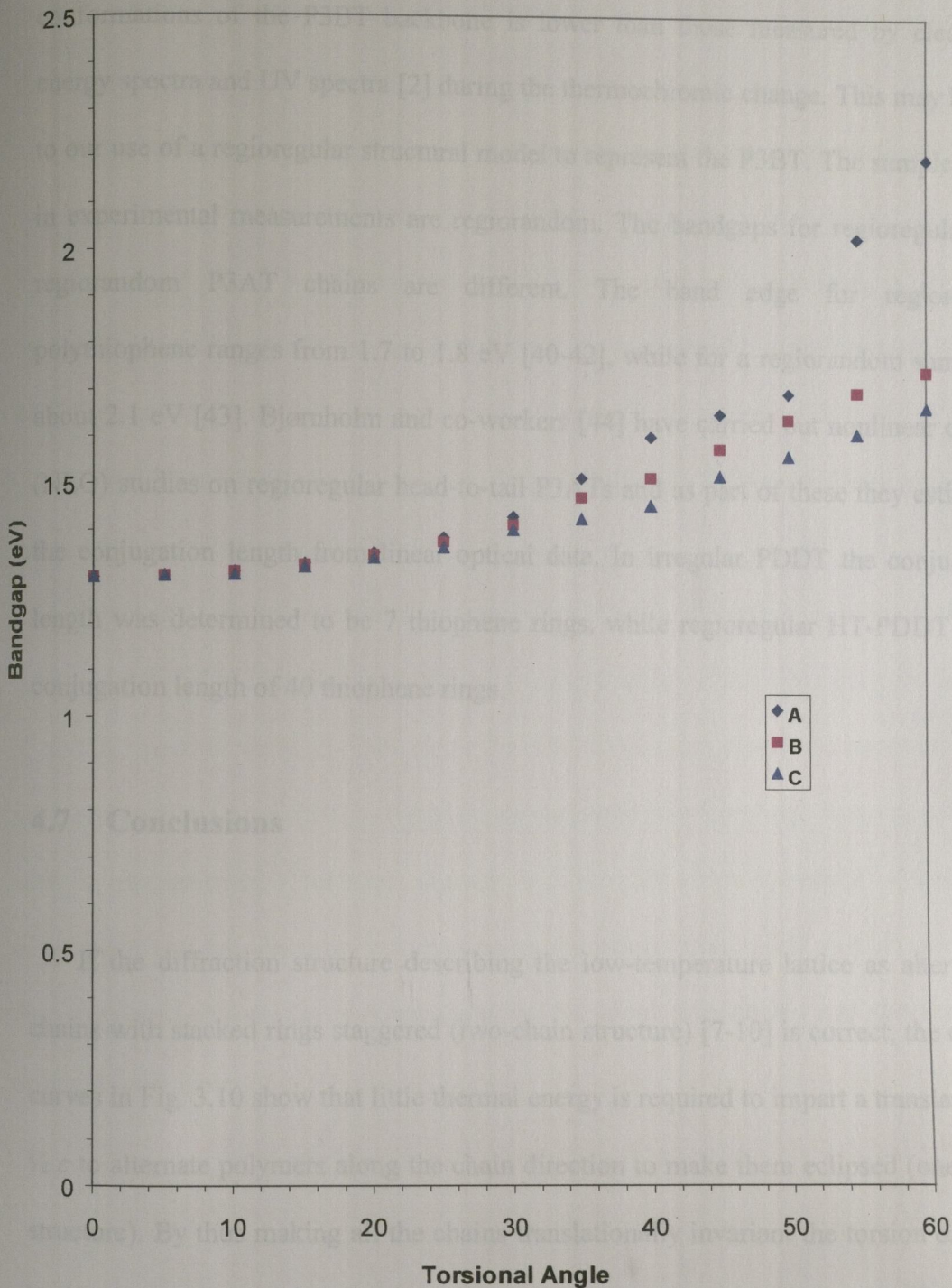


Fig. 4.11 The bandgap of P3BT calculated by EHT as a function of torsional angle φ_5 (in units of degree) at three different torsional schemes. A represents torsional scheme A $(+\varphi, 0, -\varphi, 0)$, B – torsional scheme B $(+\varphi, -\varphi, 0, +\varphi, -\varphi, 0)$ and C $(+\varphi, 0, 0, -\varphi, 0, +\varphi, 0, 0, -\varphi, 0)$.

From our EHT calculations, the change in bandgap between the stable conformations of the P3BT backbone is lower than those measured by electronic energy spectra and UV spectra [2] during the thermochromic change. This may be due to our use of a regioregular structural model to represent the P3BT. The samples used in experimental measurements are regiorandom. The bandgaps for regioregular and regiorandom P3AT chains are different. The band edge for regioregular polythiophene ranges from 1.7 to 1.8 eV [40-42], while for a regiorandom sample is about 2.1 eV [43]. Bjørnholm and co-workers [44] have carried out nonlinear optical (NLO) studies on regioregular head-to-tail P3ATs and as part of these they estimated the conjugation length from linear optical data. In irregular PDDT the conjugation length was determined to be 7 thiophene rings, while regioregular HT-PDDT has a conjugation length of 40 thiophene rings.

4.7 Conclusions

If the diffraction structure describing the low-temperature lattice as alternating chains with stacked rings staggered (two-chain structure) [7-10] is correct, the energy curves in Fig. 3.10 show that little thermal energy is required to impart a translation of $\frac{1}{2}c$ to alternate polymers along the chain direction to make them eclipsed (one-chain structure). By thus making all the chains translationally invariant the torsion of chain backbone would be facilitated to give a value of ca. 20° . It may be significant that such an eclipsed structure follows also from the investigations of diffraction workers [11-13].

Of the three torsional schemes investigated one of them (scheme C), which generates planar bithiophene and trithiophene units, preserves the original direction of the polymer chains in the lattice.

This simulation suggests that several stable main chain torsional configurations may coexist in a lattice structure. The polymer main chains have higher energy (torsional angle ca. 55°) conformations with different conjugation lengths, which are thermally accessible. It also suggests that there are two possible transitions ($\varphi_5=0$ or $\varphi_5=20^\circ$ to $\varphi_5\approx 55^\circ$) with the electronic bandgap enhanced in the range of 0.3 to 0.7 eV (Calculated from ETH), which may give some information for the mechanism of the thermochromic change of P3ATs.

However, up to now, we have not considered the conformation changes (such as torsion) in the alkyl side chains, which was confirmed by earlier simulation work [5-6] and by experiments [1-2]. The role of the alkyl chains was seen to be necessary for the thermochromism of P3ATs, because unsubstituted polythiophene does not exhibit such a phenomenon. The next chapter will describe how molecular dynamics simulations can provide more information on the nature of the alkyl side chains and the coupling between the conformations of the alkyl side chains and that of the polymer main chains.

[10] Tachiro K, Kuboyashi M, Morita S, Kawai T, and Yoshino K. *Synth. Met.*, 1995, 69:397

[11] Smalølsen E J, Mårdalen J, Carlsen P H, Legumina P, Travers J-P, and Rensouche E. *Synth. Met.*, 1993, 55-57:365

[12] Mårdalen J, Smalølsen E J, Gauntun O R, and Carlsen P H. *Solid State Commun.*, 1991, 80:687

[13] Mårdalen J, Smalølsen E J, Gauntun O R, and Carlsen P H. *Synth. Met.*, 1992, 45:263

Bibliography:

- [1] Iwasaki K, Fujimoto H, and Matsuzaki S. *Synth. Met.*, 1994, **63**:101
- [2] Tashiro K, Ono K, Minagawa Y, Kobayashi M, Kawai T, and Yoshino K. *J. Polym. Sci.: Part B: Polym. Phys.*, 1991, **29**:1223
- [3] Yoshino K, Nakajima S, Park D H, and Sujimoto R. *Japan. J. Appl. Phys.*, 1988, **27**:L716
- [4] Yoshino K, Nakajima S, Onoda M, and Sujimoto R. *Synth. Met.*, 1989, **28**:C349
- [5] Corish J, Morton-Blake D A, Feeley D E, B ni re F and Marchetti M. *J. Chem. Phys. B*, 1997, **101**:10075
- [6] Corish J, Morton-Blake D A, B ni re F, Lantoine M and Marchetti M. *Materials Science Forum 17*, 1997, **239-241**:185
- [7] Kawai T, Nakazono M, Sugimoto R, Yoshino K. *Jpn. J. Appl. Phys.*, 1992, **61**:3400
- [8] Tashiro K, Ono K, Minagawa Y, Kobayashi M, Kawai T, and Yoshino K. *J. Polym. Sci., Part B: Polym. Phys.*, 1991, **29**:1223
- [9] Kawai T, Nakazono M, and Yoshino K. *J. Mater. Chem.*, 1992, **2**:903
- [10] Tashiro K, Kobayashi M, Morita S, Kawai T, and Yoshino K. *Synth. Met.*, 1995, **69**:397
- [11] Samuelsen E J, M rdalen J, Carlsen P H, Leguennec P, Travers J-P, and Ressouche E. *Synth Met.*, 1993, **55-57**:365
- [12] M rdalen J, Samuelsen E J, Gautun O R, and Carlsen P H. *Solid State Commun.*, 1991, **80**:687
- [13] M rdalen J, Samuelsen E J, Gautun O R, and Carlsen P H. *Synth. Met.*, 1992, **48**:263

- [14] Takeuchi H, Furukawa Y, and Harada J. *J. Chem. Phys.*, 1986, 84:2882
- [15] Bauer G and Mikosh H. *J. Mol. Struct.*, 1986, 142:21
- [16] Moore W J. "*Physical Chemistry*", Longman, London, 1972
- [17] Petrucci R H and Wismar R K. "*General Chemistry with Qualitative Analysis*", 2nd Ed., Macmillan, London, 1987
- [18] Bailar J C, Moeller T, Kleinberg J, Guss C O, Castellion M E, and Metz C. "*Chemistry*", Harcourt Brace Jovanovich, San Diego, CA, 1989
- [19] Mintmire J W, White C T, and Elert M L. *Synth. Met.*, 1988, 25:109
- [20] Leslie M. *Physica*, 1985, 131 B:145
- [21] Isaacs N. "*Physical Organic Chemistry*", Harlow Longman Scientific and Technical, 1987
- [22] Williams D E. *J. Chem. Phys.*, 1967, 47:4680
- [23] Hopfinger A J. "*Conformational Properties of Macromolecules*", Academic Press, New York, 1973
- [24] Feeley D, and Morton-Blake D A. *J. Mole. Struct. (Theochem)*, 1995, **331**:127
- [25] Corish J, Morton-Blake D A, Veluri K, and Bénérière F. *J. Mole. Struct. (Theochem)*, 1993, **283**:121
- [26] Corish J, Morton-Blake D A, and Veluri K. *Molecular Simulation*, 1995, **14**:381
- [27] Veluri K, Corish J, Morton-Blake D A, and Bénérière F. *J. Mole. Struct. (Theochem)*, 1995, **334**:109
- [28] Corish J, Morton-Blake D A, Veluri K, and Bénérière F. *Radiation Effects and Defects in Solids*, 1995, **134**:171
- [29] Veluri K. *Ph.D. Thesis*, University of Dublin, Trinity College, 1994
- [30] Fell H J, Samuelsen E J, Mårdalen J, Bakken E, and Carlsen P H J. *Synth. Met.*, 1995, **69**:301

- [31] Xie H, Corish J, Morton-Blake D A, and Aasmundtveit K. *Radiation Effects & Deffects in Solids*, 1999, **151**:261
- [32] Xie H, Corish J, Ali G, Morton-Blake D A, and Aasmundtveit K. *Synth. Met.*, 1999, **101**:318
- [33] Xie H, Corish J, Morton-Blake D A, and Aasmundtveit K. *Synth. Met.*, 2000, **113**:65
- [34] Prosa T J, Winokur M J, Moulton J, Smith P, and Heeger A J. *Macromolecules*, 1992, **25**:4364
- [35] Łuzny W and Proń A. *Synth. Met.*, 1996, **79**:37
- [36] Roux C, and Leclerc M. *Macromolecules*, 1992, **22**:2141
- [37] Zerbi G, Chierichetti B, and Ingnas O. *J. Chem. Phys.*, 1991, **94**:4646
- [38] Salaneck W R, Ingnas O, Themans B, Nielsson J O, Sjogren B, Osterholm H, Brédas J L, and Svensson S. *J. Chem. Phys.*, 1988, **89**:4631
- [39] Brédas J L, and Heeger A J. *Macromolecules*, 1990, **23**:1150
- [40] McCullough R D, and Lowe R D. *J. Chem. Soc., Chem. Commun.*, 1992, 70
- [41] McCullough R D, Tristram-Nagle S, Williams S P, Lowe R D, and Jayaraman M. *J. Am. Chem. Soc.*, 1993, **115**:4910
- [42] Chen T-A, Wu X, and Rieke R D. *J. Am. Chem. Soc.*, 1995, **117**:233
- [43] Brédas J L, Themans B, Fripiat J G, and André J M. *Phys. Rev. B. Conds. Mat.*, 1984, **29**:6761
- [44] Bjørnholm T, Greve D R, Geisler T, Petersen J C, Jayaraman M, and McCullough R D. *Adv. Mater.*, 1996, **8**:920

Chapter 5

MD SIMULATION OF THERMALLY INDUCED CONFORMATION CHANGES AND THEROCHROMIC MECHANISM OF POLY(3-ALKYLTHIOPHENE)S

5.1 Introduction

Molecular Dynamics (MD) simulation is one of the most important molecular simulation methods. The technique provides a way to calculate the effects of molecular motions due to thermal or other agitation. MD has been used in the study of polymers and has provided detailed information on a wide range of topics. For example, the diffusion of small penetrants in polymers [1-3], the conformational statistics of an amorphous polymer chain [4,5], glass transitions [6,7], the relationship between microstructure and macroproperties, such as flexibility, mechanical properties and the miscibility of polymer blends [8,9] have all been studied by MD techniques.

Regiorandom poly(3-alkylthiophene)s are partially crystalline and regioregular HT-P3ATs are highly crystalline. Molecular Dynamics simulations have been reported for polymer crystals such as poly(ethylene oxide) (PEO) [10,11], polyethylene [12,13], and poly(p-phenyleneterephthalamide) (PPTA) [14]. Because MD allows thermal agitation, it can provide atomic-level information of the dynamical processes in P3ATs and thermally induced conformation changes both in the polymer main chains and in the alkyl side chains at the same time. The application

of MD should therefore be very helpful in understanding the thermochromism of P3ATs.

5.2 Computational Structure

The two-chain Kawai structure of crystalline P3AT was selected for this simulation because it gave good results in the previously described static lattice atomistic simulation. An orthorhombic unit with two chains (one in $b=0$, another in $\frac{1}{2}b$, with zero setting angle) was used. Again the butyl group was chosen as the alkyl side chain. The lattice parameters a and b used to describe the unit cell were 13.50Å and 7.30Å, which are mean values of those measured by experiments [15-19] and those optimized by GULP.

Simulations were carried out using a primary MD box consisting of 8 crystallographic unit cells ($2 \times 2 \times 2$ supercell), as shown in Fig. 5.1, containing of 608 atoms in 8 chains. The volume of the supercell is 6117.68 Å³. Periodic boundary conditions were applied in all three dimensions to avoid lattice 'surfaces'. The influence of chain ends was eliminated by creating effectively infinite chains by the use of a link cell, in which the last carbon atom in a chain is bonded to the nearest periodic image of the first carbon atom of the same chain.

The x-ray diffraction refined geometric positions of atoms were chosen as a convenient starting configuration for the atoms in the MD box. Within the restrictions placed on the system by the boundary conditions discussed above, the system was free to adopt any configuration permitted by the force field described in Chapter 3. In principle, therefore the initial positions should not influence the average equilibrated structure.

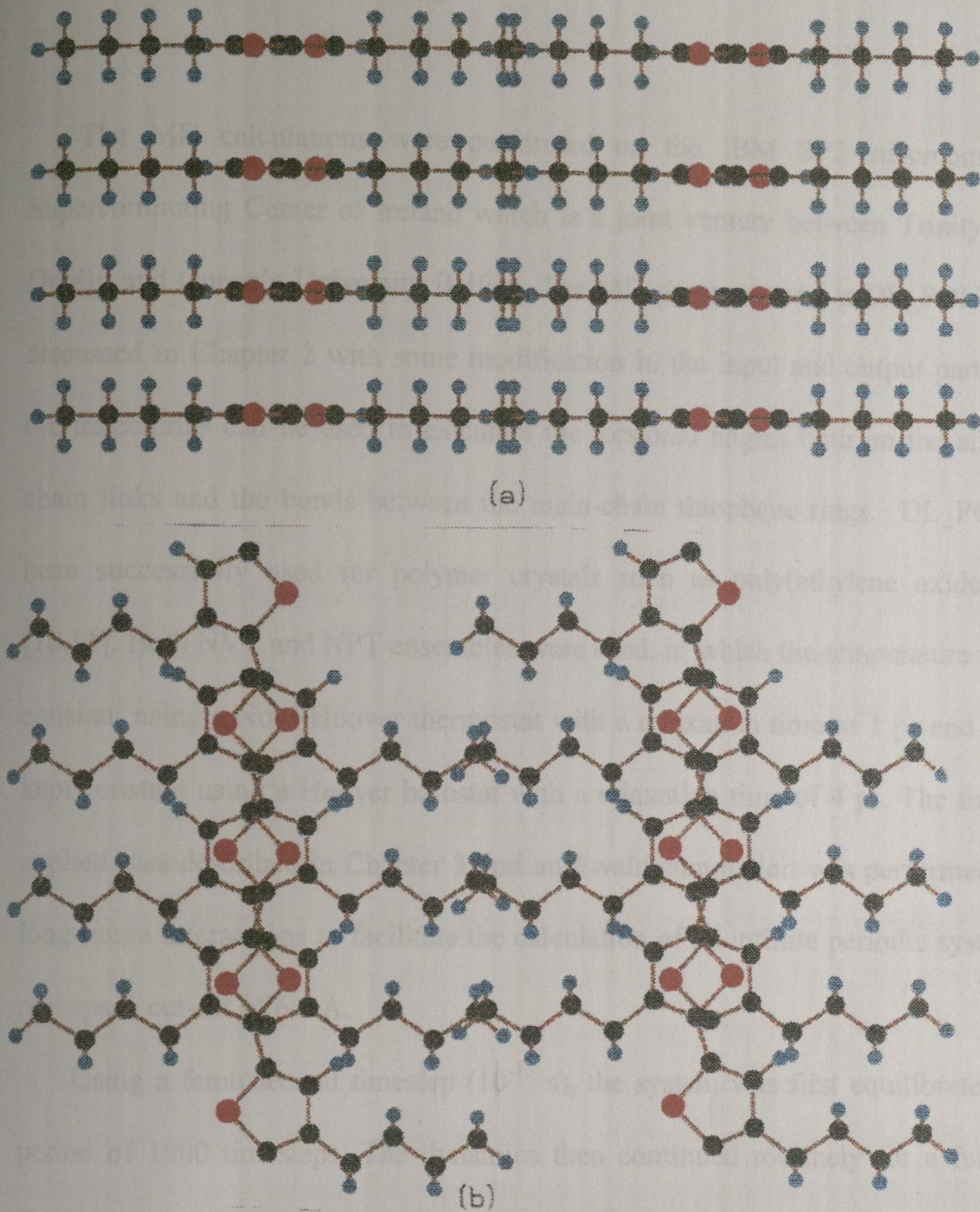


Fig. 5.1 The $2 \times 2 \times 2$ supercell structure of P3BT with $a=27 \text{ \AA}$, $b=14.6 \text{ \AA}$ and $c=15.52 \text{ \AA}$. (a) viewed along **c** axis; (b) viewed along **b** axis. The atoms in P3BT are represented by different colors in the diagram, red – S atom, gray – C atom and blue – H atom.

5.3 Method of Calculations

The MD calculations were performed on the IBM SP2 supercomputer at Supercomputing Center of Ireland which is a joint venture between Trinity College Dublin and Queen's University Belfast. The MD program used is DL_POLY_2.0 as discussed in Chapter 2 with some modification in the input and output parts so that the trajectories can be used to calculate the torsional angles both on the alkyl side-chain links and the bonds between the main-chain thiophene rings. DL_POLY has been successfully used for polymer crystals such as poly(ethylene oxide) (PEO) [10,11]. Both NVT and NPT ensembles were used, in which the temperature was kept constant using a Nosé-Hoover thermostat with a relaxation time of 1 ps and pressure kept constant using a Hoover barostat with a relaxation time of 4 ps. The force field applied was described in Chapter 3 and an Ewald summation was performed for the long-range interactions to facilitate the calculation of an infinite periodic system with real space cut-off of 6.0 Å.

Using a femtosecond timestep (10^{-15} s), the system was first equilibrated over a period of 1000 timesteps. The dynamics then continued routinely for a further 10^5 timesteps in order to obtain trajectory data that might detect migrations. The evolution of torsional angles on both the polymer main chains and the alkyl side chains were monitored every 10 timesteps over a 100 ps interval and configurations were stored every 1 ps interval for subsequent analysis.

A proper account of the thermal motions described by the alkyl chains and their relaxations could be provided by molecular dynamics simulations. An elucidation of the *librational* activities of the various P3AT segments is within the powers of MD, and this can provide a useful insight into the thermal behavior of the polymer

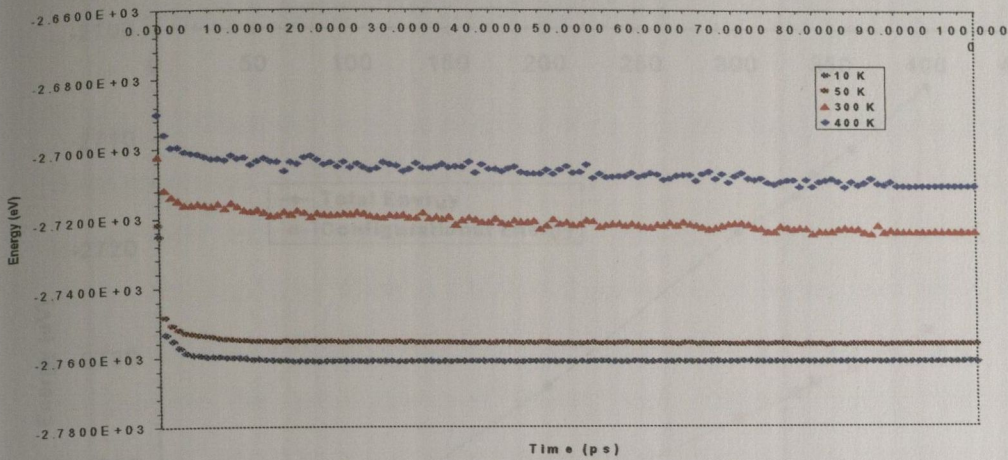
backbone and alkyl side chains through analysis of the polymer conformations at different temperatures. The changes of conformation are monitored by torsional angles (in units of degree), distribution of torsional angles (DTA), radial distribution functions (RDF) and conformation snapshots.

5.4 Results and Discussion

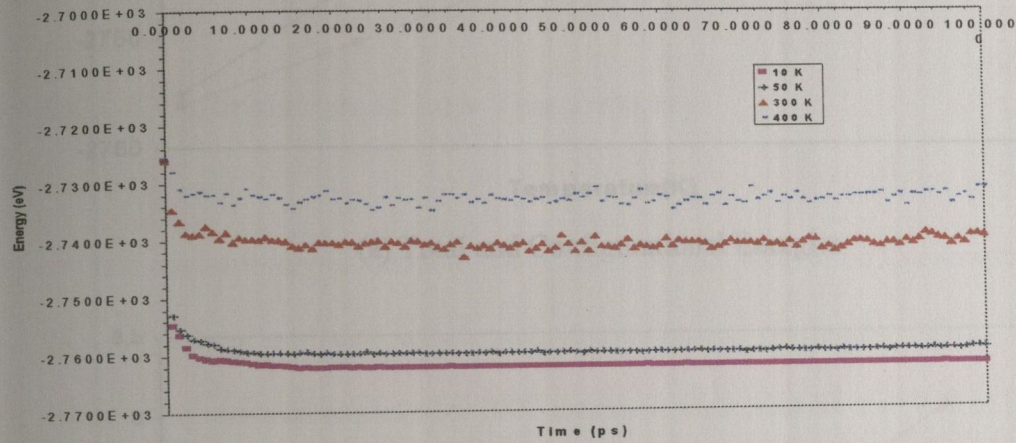
5.4.1 Energy Change with Simulation Time

Because of the interest in the configuration change and torsion in the system, special interest is paid to the total energy, configurational energy and torsional energy of the system change with time as the calculation proceeds in NVT ensemble.

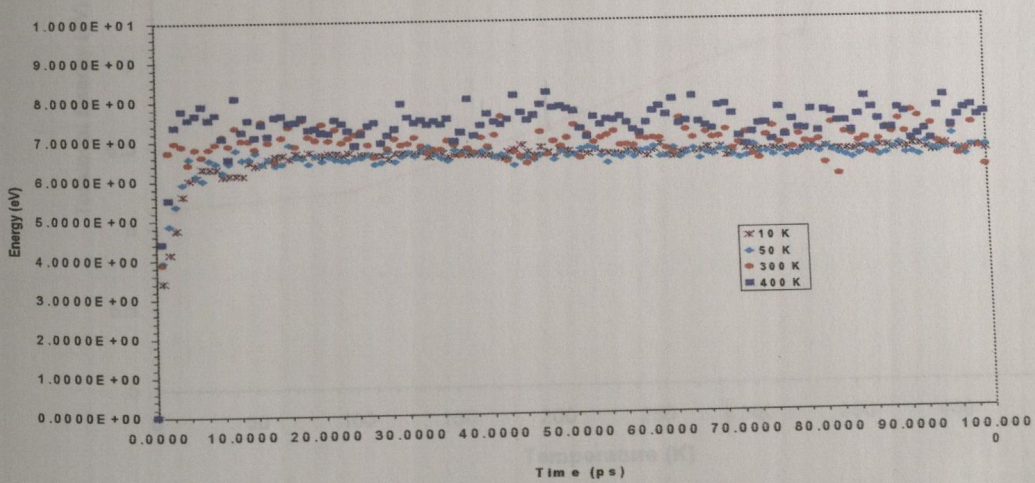
Fig. 5.2 shows the plots of total energy, configurational energy and torsional energy change with time as the calculation proceeds. The total energy decreases with calculation time (Fig. 5.2a), which is caused by the decay of the potential energy. Generally speaking, the kinetic energy is almost invariable with calculation time because we used an NVT ensemble. At the beginning (before 10ps), the total energy decreases very quickly. After that it decreases more gradually with time with increasing relaxation. At lower temperatures, the system relaxes completely after 20ps. These are also reflected in the change of the trajectories. After 20 ps, the conformations recorded are the same as the calculation time proceeds. At higher temperatures (300 K and 400 K), the total energy fluctuates more than that at lower temperatures (10 K and 50 K). The change of configurational energy with time is similar to that of total energy (Fig.5.2b). The torsional energy increases sharply with calculation time in the early stages and then fluctuates with time around the equilibrium position (Fig.5.2c). The variation of energies is apparently enlarged with increasing temperature. These results indicate that after 100 ps relaxation the trajectories are good enough to analyze the torsional angles on both the main chains and the alkyl side chains and the thermally induced conformation changes.



(a) Total Energy

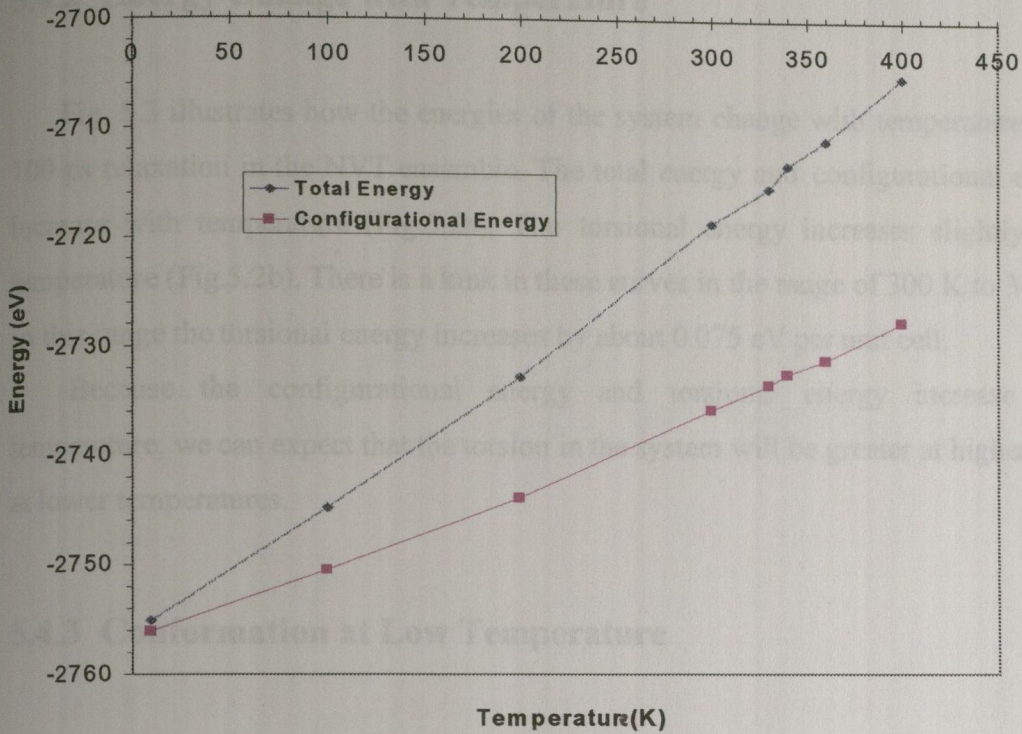


(b) Configurational Energy

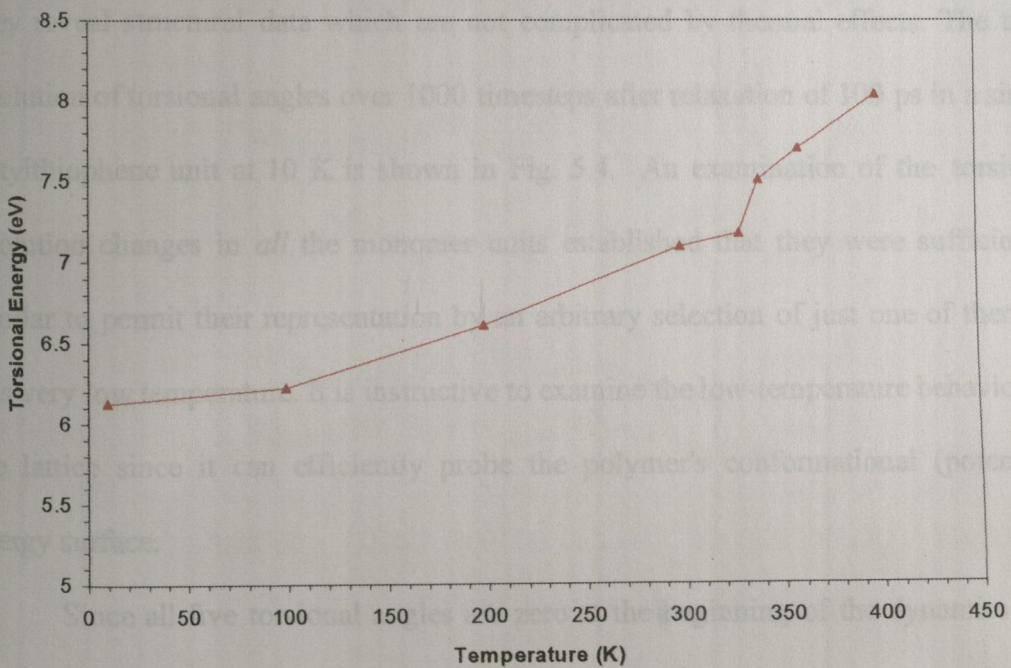


(c) Torsional Energy

Fig. 5.2 The plots of energies of P3BT system as the calculation proceeds in NVT ensemble at a selection of temperatures as illustrated in the diagrams. (a) Total energy, (b) Configurational Energy, (c) Torsional energy.



(a) Total and Configurational Energies



(b) Torsional Energy

Fig. 5.3 The energies of P3BT system after 100 ps relaxation in NVT ensemble as a function of temperature. (a) Total and configurational energies, (b) Torsional energy.

5.4.2 Energy Change with Temperature

Fig. 5.3 illustrates how the energies of the system change with temperature after 100 ps relaxation in the NVT ensemble. The total energy and configurational energy increase with temperature (Fig.5.2a). The torsional energy increases slightly with temperature (Fig.5.2b). There is a kink in these curves in the range of 300 K to 360 K. In this range the torsional energy increases by about 0.075 eV per unit cell.

Because the configurational energy and torsional energy increase with temperature, we can expect that the torsion in the system will be greater at higher than at lower temperatures.

5.4.3 Conformation at Low Temperature

It is useful firstly to examine the behavior of the torsions at low temperature, as they reveal structural data which are not complicated by thermal effects. The time evolution of torsional angles over 1000 timesteps after relaxation of 100 ps in a single butylthiophene unit at 10 K is shown in Fig. 5.4. An examination of the torsional evolution changes in *all* the monomer units established that they were sufficiently similar to permit their representation by an arbitrary selection of just one of them at this very low temperature. It is instructive to examine the low-temperature behavior of the lattice since it can efficiently probe the polymer's conformational (potential) energy surface.

Since all five torsional angles are zero at the beginning of the dynamics (see Fig. 5.1), Fig. 5.4 shows that during the preceding 10^5 timesteps the thermal energy establishes a distinct conformational pattern. Link 1 (see Fig. 4.1) shows that the alkyl chain tilts by about 20° from a conformation in which it is coplanar with the main chain. The values of φ_2 and φ_3 show that the *trans* linkage is closely retained by

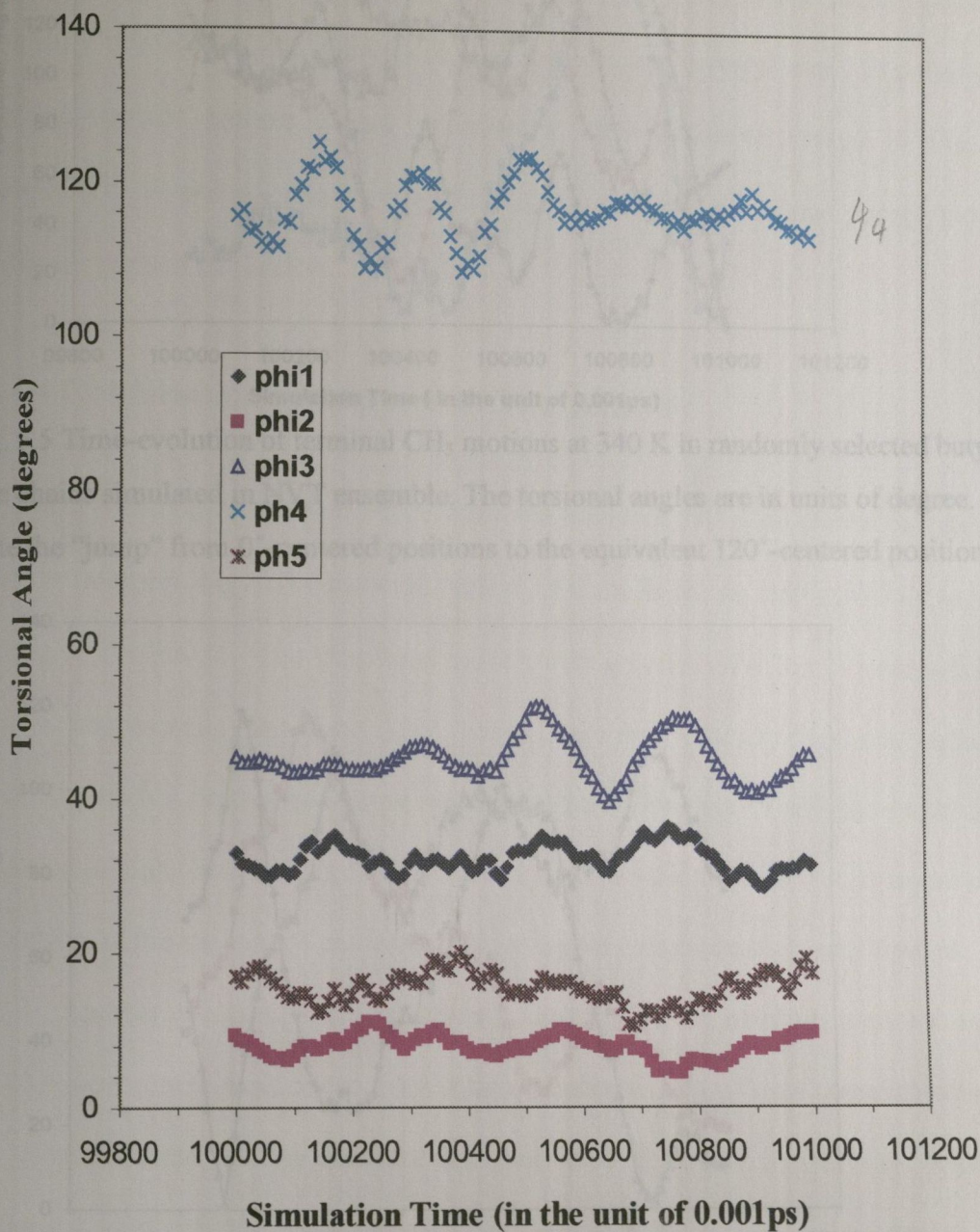


Fig. 5.4 Time-evolution of torsional angles in a thiophene monomer unit at 10 K simulated in NVT ensemble.

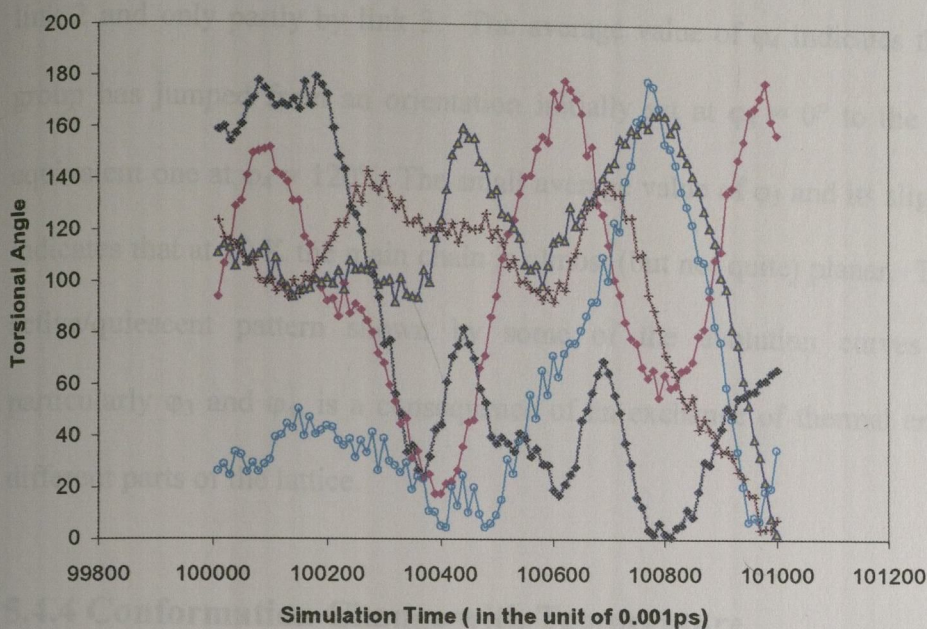


Fig. 5.5 Time-evolution of terminal CH₃ motions at 340 K in randomly selected butyl side chains simulated in NVT ensemble. The torsional angles are in units of degree. Note the “jump” from 0°-centered positions to the equivalent 120°-centered positions.

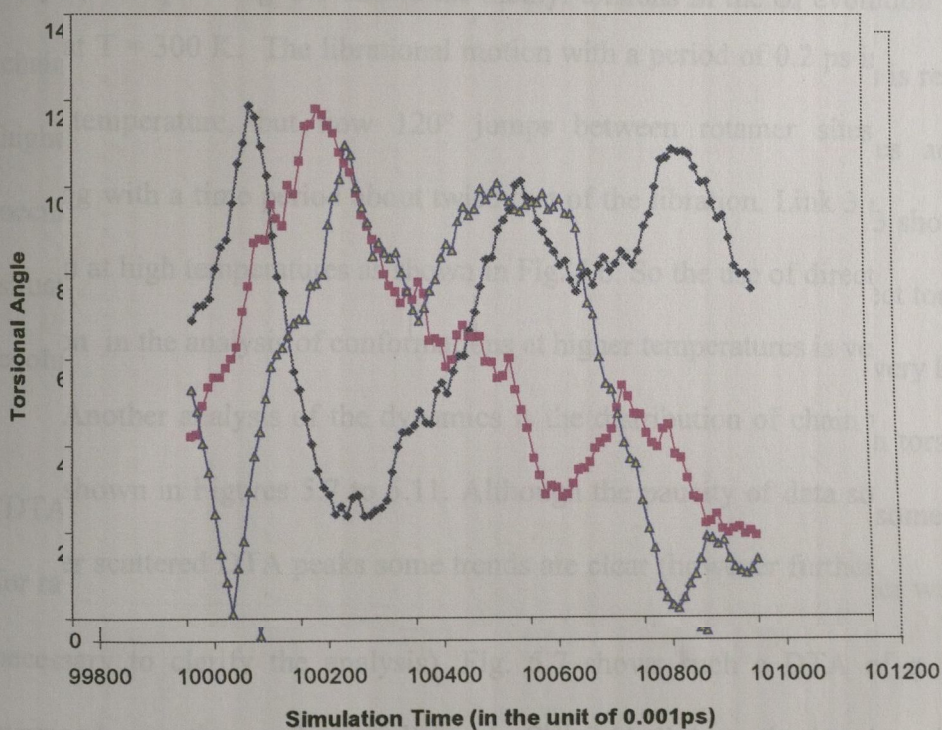


Fig. 5.6 Time-evolution of torsional angle ϕ_3 at 340 K in randomly selected butyl side chains simulated in NVT ensemble. The torsional angles are in units of degree. Note that ϕ_3 can jump from *trans* to *gauche* at this temperature.

link 2 and only partly by link 3. The average value of φ_4 indicates that the methyl group has jumped from an orientation initially set at $\varphi_4 = 0^\circ$ to the symmetrically equivalent one at $\varphi_4 = 120^\circ$. The small average value of φ_5 and its slight oscillations indicates that at 10 K the main chain is almost (but not quite) planar. The alternating active/quiescent pattern shown by some of the evolution curves in Fig. 5.4, particularly φ_3 and φ_4 , is a consequence of an exchange of thermal energy between different parts of the lattice.

5.4.4 Conformation Change with Temperature

On warming up to room temperature the torsional evolution curves become less easy to interpret. Fig. 5.5 shows the methyl torsions in the φ_4 evolution in five butyl chains at $T = 300$ K. The librational motion with a period of 0.2 ps is retained at the higher temperature, but now 120° jumps between rotamer sites are common, occurring with a time period about twice that of the libration. Link 3 shows the same situation at high temperatures as shown in Fig. 5.6. So the use of direct torsional angle evolution in the analysis of conformations at higher temperatures is very limited.

Another analysis of the dynamics is the distribution of chain torsional angles (DTA) shown in Figures 5.7 to 5.11. Although the paucity of data sometimes makes for rather scattered DTA peaks some trends are clear (however further work would be necessary to clarify the analysis). Fig. 5.7 shows such a DTA of φ_1 for torsions averaged over time and over all bonds $C^{(3)}-C_4H_9$ linking the butyl to the thiophene ring, at various temperatures. At 10 K (only) the DTA plot shows a rough peak near $\varphi_1 = 20^\circ$. If genuine, such a peak would agree with the torsional angle evolution trace in Fig. 5.4 where the implied tilting of the butyl group from the plane of the main

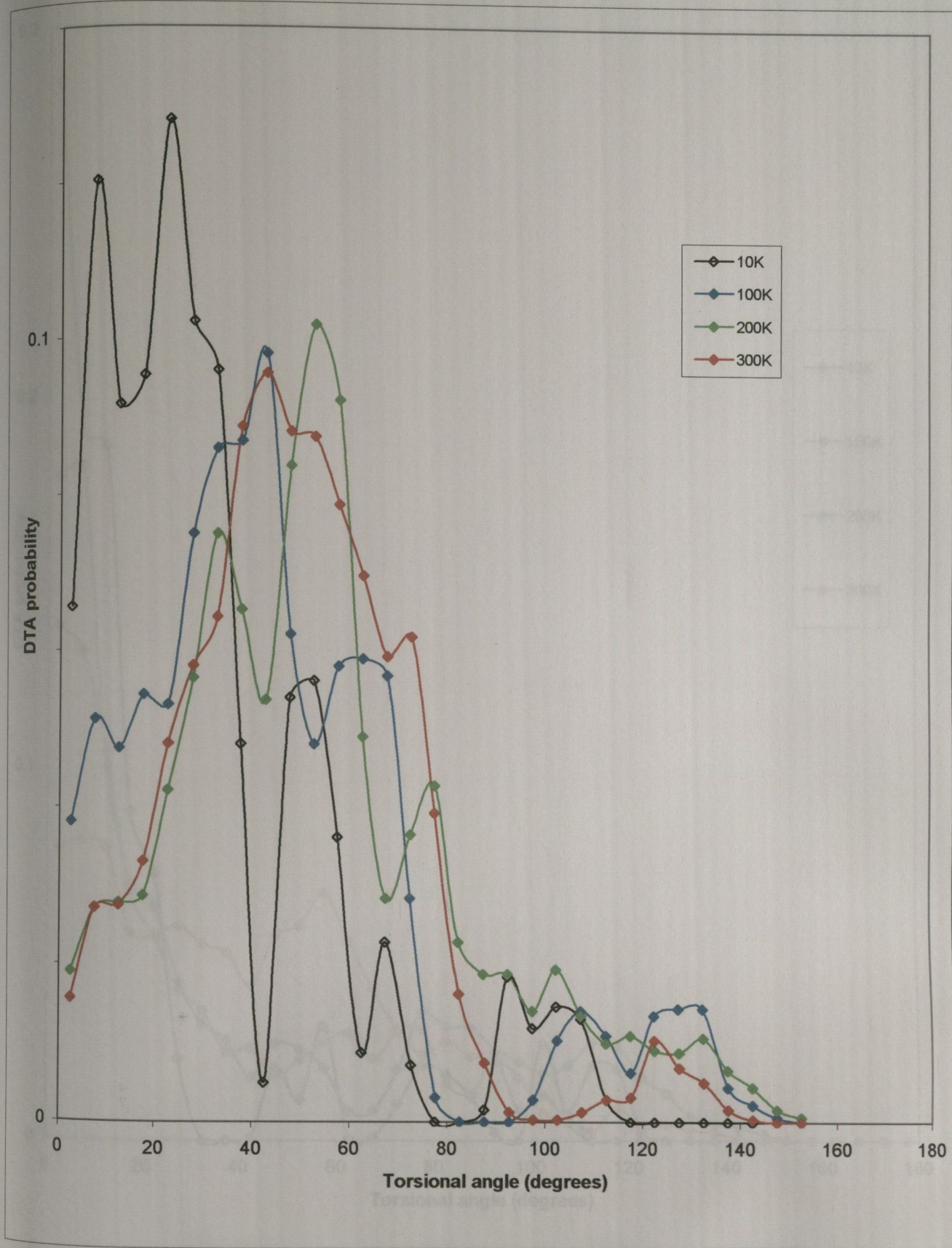


Fig. 5.7 DTA for ϕ_1 at different temperatures in the NVT ensemble

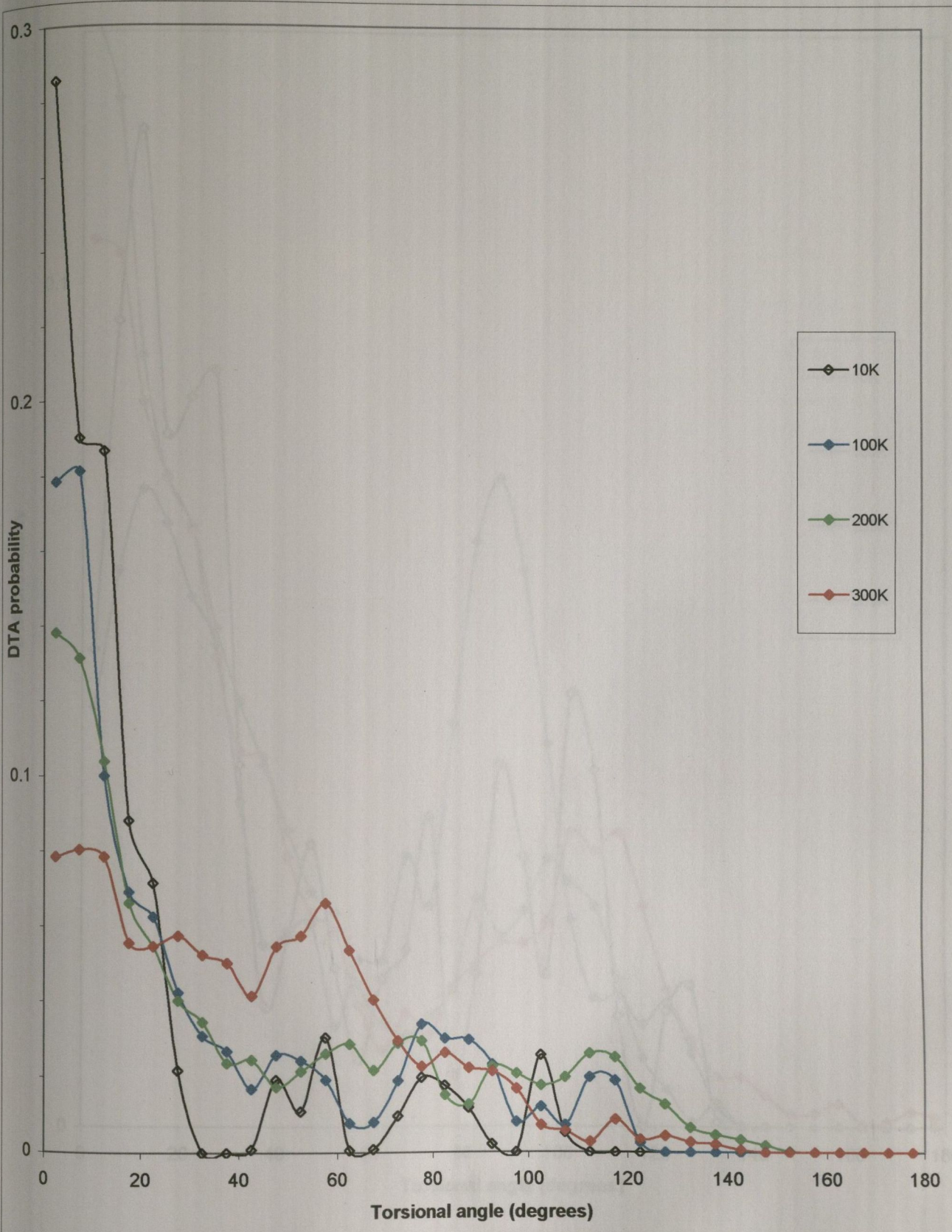


Fig. 5.8 DTA for φ_2 at different temperatures in the NVT ensemble

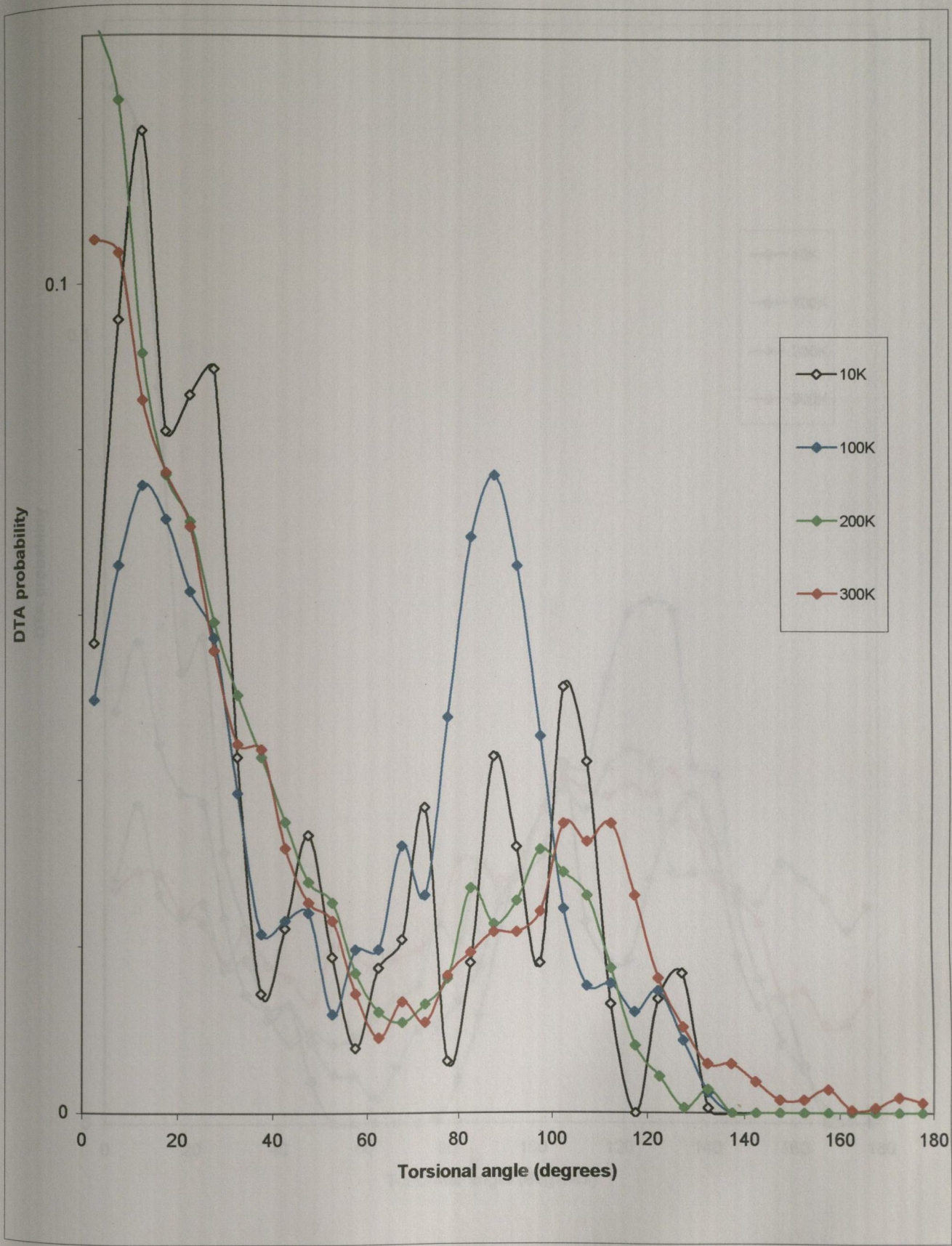


Fig. 5.9 DTA for φ_3 at different temperatures in the NVT ensemble

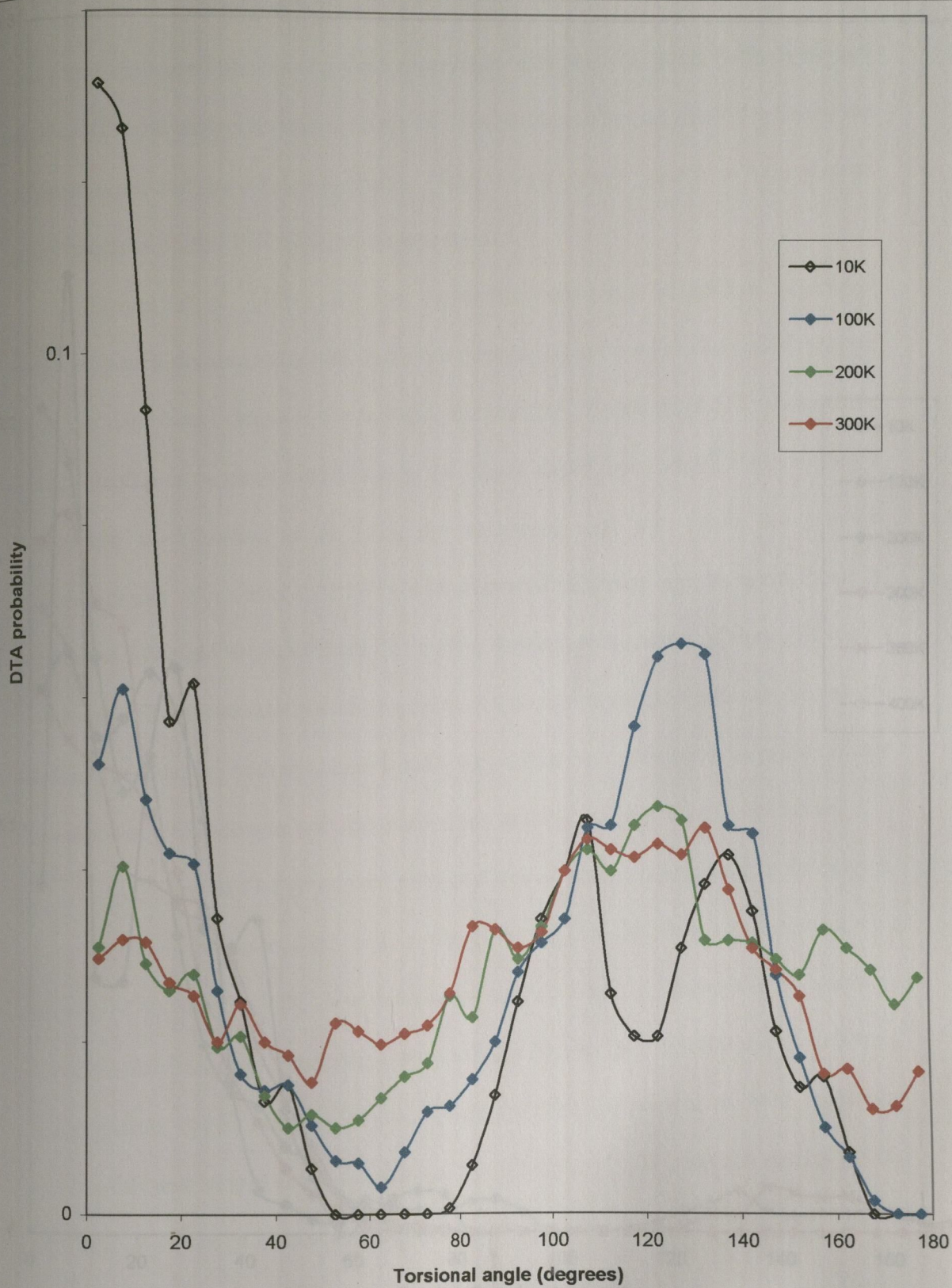


Fig. 5.10 DTA for φ_4 at different temperatures in the NVT ensemble

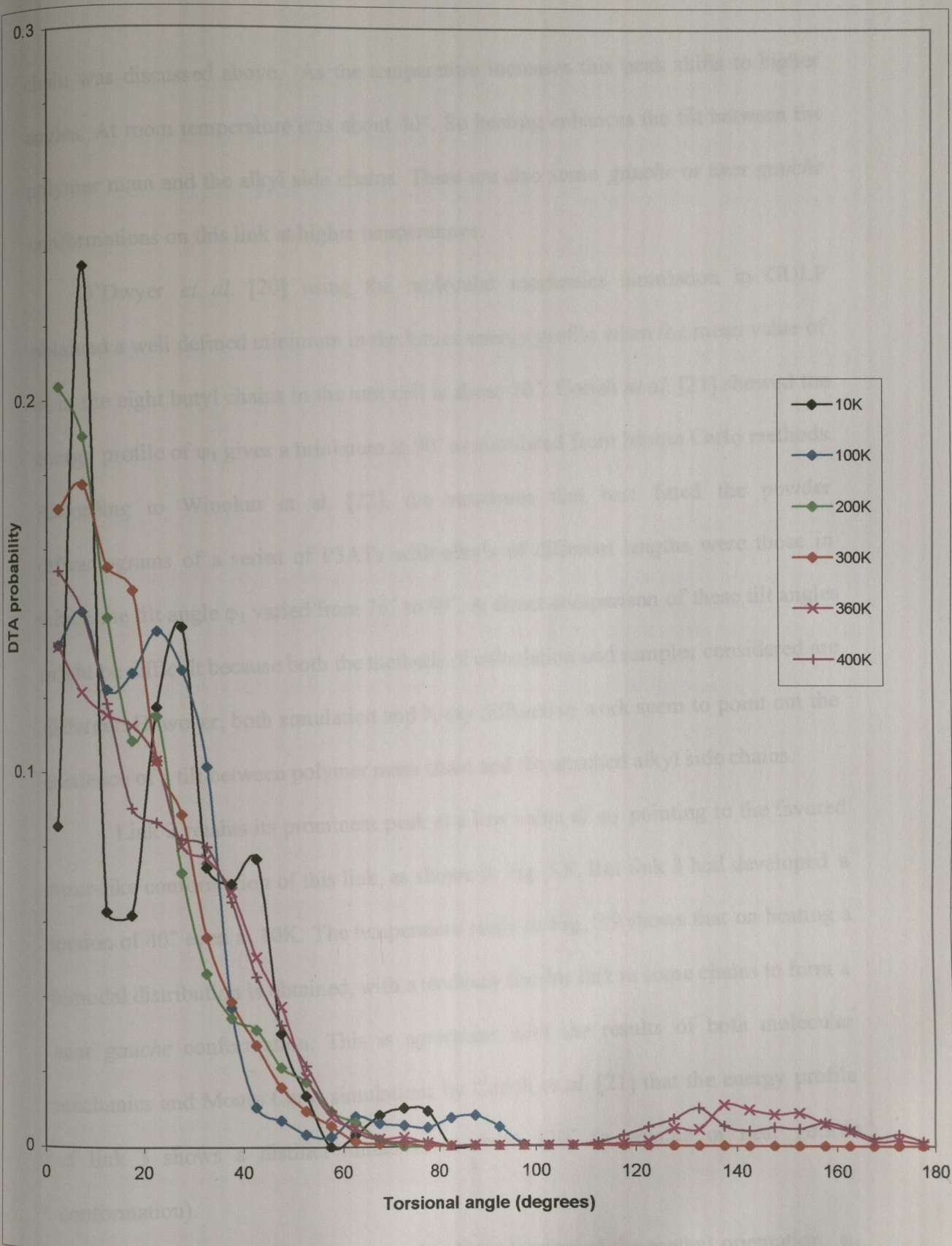


Fig. 5.11 DTA for ϕ_5 at different temperatures in the NVT ensemble. Note that all the plotted points in the range $90^\circ < \phi_5 < 180^\circ$ for temperatures up to 300K superimpose near DTA = 0. Only those for $T = 360$ and $T = 400$ K depart from these small values.

chain was discussed above. As the temperature increases this peak shifts to higher angles. At room temperature it is about 40° . So heating enhances the tilt between the polymer main and the alkyl side chains. There are also some *gauche* or near *gauche* conformations on this link at higher temperatures.

O'Dwyer *et al.* [20] using the molecular mechanics simulation in GULP obtained a well defined minimum in the lattice energy profile when the mean value of ϕ_1 in the eight butyl chains in the unit cell is about 70° . Corish *et al.* [21] showed the energy profile of ϕ_1 gives a minimum at 90° as simulated from Monte Carlo methods. According to Winokur *et al.* [22], the structures that best fitted the powder diffractograms of a series of P3ATs with alkyls of different lengths were those in which the tilt angle ϕ_1 varied from 76° to 89° . A direct comparison of these tilt angles might be difficult because both the methods of calculation and samples considered are different. However, both simulation and X-ray diffraction work seem to point out the existence of a tilt between polymer main chain and the attached alkyl side chains.

Link 2 retains its prominent peak at a low value of ϕ_2 pointing to the favored *trans*-like conformation of this link, as shown in Fig. 5.8. But link 3 had developed a torsion of 40° even at 10K. The temperature study in Fig. 5.9 shows that on heating a bimodal distribution is obtained, with a tendency for this link in some chains to form a near *gauche* conformation. This is agreement with the results of both molecular mechanics and Monte Carlo simulations by Corish *et al.* [21] that the energy profile of link 3 shows a distinct minimum at about 120° (a *gauche* or near *gauche* conformation).

Fig. 5.10 shows a similar torsional-distribution of the methyl orientation, ϕ_4 . The reason for the developing bimodality of DTA with increasing temperature is clear. After 10^5 timesteps at 10 K most of the CH_3 groups are still in the $\phi = 0^\circ$

orientation in which they were set; when the temperature is raised to 100 K the configurational entropy drives them in the direction of equal distributions at 0° and 120° . As temperature continues to increase, the *cis* conformation also appears. It means that the methyl group can make complete rotations easily at high temperature. Higher temperatures also broaden the DTA peaks. Again it agrees with the MM and MC simulations of Corish *et al.* [21] that the methyl group presents a 120° periodicity with lower energy barrier (approximately 0.2 eV).

Fig. 5.11 is the DTA of torsions ϕ_5 between two adjacent thiophene rings. The prominent maxima at 0° at the various temperatures in Fig. 5.11 indicate that most of the polythiophene main chains have an average conformation which is almost (but not quite) planar. It should be noted that *only* at temperatures up to room temperature the DTA data show very small occurrences of torsions ϕ_5 near or higher than 90° — all the points for $T < 340$ K show negligible probability in this torsion range.

In summary, the alkyl side chains (except the methyl end group) are at conformations that are near *trans* but show small changes from all-*trans* at very low temperatures. As the temperature increases, although they remain largely *trans*, more *gauche*-like conformations appear with increasing temperature (although statistics from a considerably larger sample would be required to support these rather tentative conclusions). The methyl group is very active. Even at 10K it shows some higher energy conformations. The methyl group can make complete rotations at high temperatures. For the polymer main chains, most thiophene rings are in *anti* or near *anti* conformations but above 340K (67°C), there are small but probably significant contributions of torsional angles greater than 90° .

According to the above analysis, two more conclusions can be made. The first is that the polymer main and most alkyl side chains that are attached to it are not in the

same plane. A tilt exists between them and this increases with temperature. The second is that the links on the alkyl side chains can be divided into two groups, active links such as link 4 (the methyl group) and relatively stable links such as the inner links (link 1 and link 2).

The thermally induced conformational changes can also be confirmed by radial distribution functions (RDF). Figures 5.12 and 5.13 are the RDF of C-C at different temperatures. Fig. 5.12 is for the C-C in the alkyl side chains and Fig. 5.13 for the C-C on the polymer main chains. The peak ($r=3.916\text{\AA}$) in Fig. 5.12 corresponds to the distance between C_1 to C_4 in the alkyl side chains when all C-C links are in the *trans* conformations. The intensity of this peak decreases as the temperature increases. If one of the links undergoes torsion, the distance between C_1 to C_4 decreases. A shift of the most intense peak from a C-C distance of 3.3 to 3.5 \AA shows that *gauche* or near-*gauche* conformations develop from *trans* conformations. However, the survival of the main peak at 3.196 \AA to above room temperature testifies to the stability of the fully extended (all-*trans*) conformation of the side chains. The diminution in the intensity of the peaks in Fig. 5.13 on heating shows that the *anti* conformations decrease with increasing temperature. There are only two main peaks in the RDF of H-H as shown in Fig. 5.14 which correspond to the distances between $H_1\dots H_1$ (or $H_2\dots H_2$) and $H_1\dots H_2$ in the side chain segments $H_1H_2C-CH_1H_2$, respectively. This shows that most of the links in the alkyl side chains remain in the *trans* conformations even above room temperature although the peaks are blunted by thermal torsions.

The conformational changes with temperature are also shown in the "snapshots" of the chain conformations at different temperatures. Fig. 5.15 is a comparison of conformations at 10, 300 and 340 K after 100 ps relaxation. More torsions can be seen

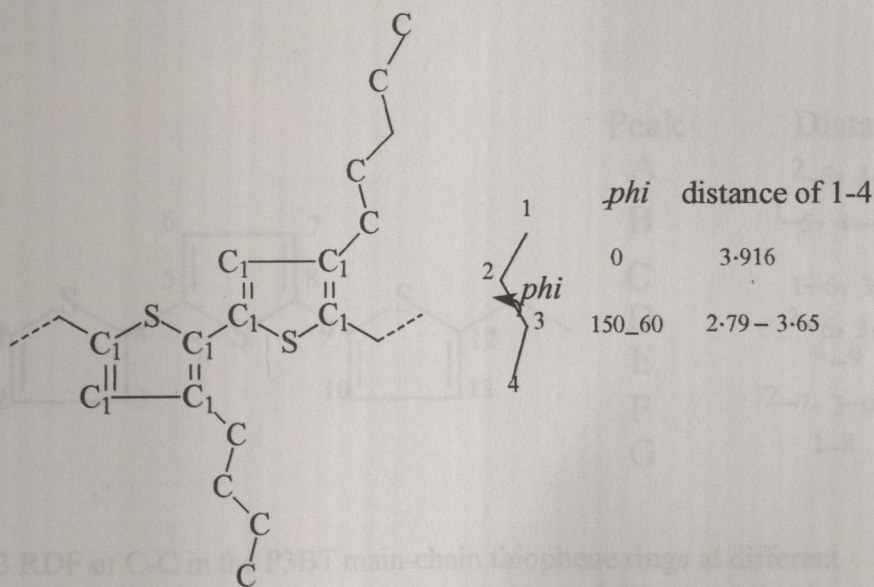
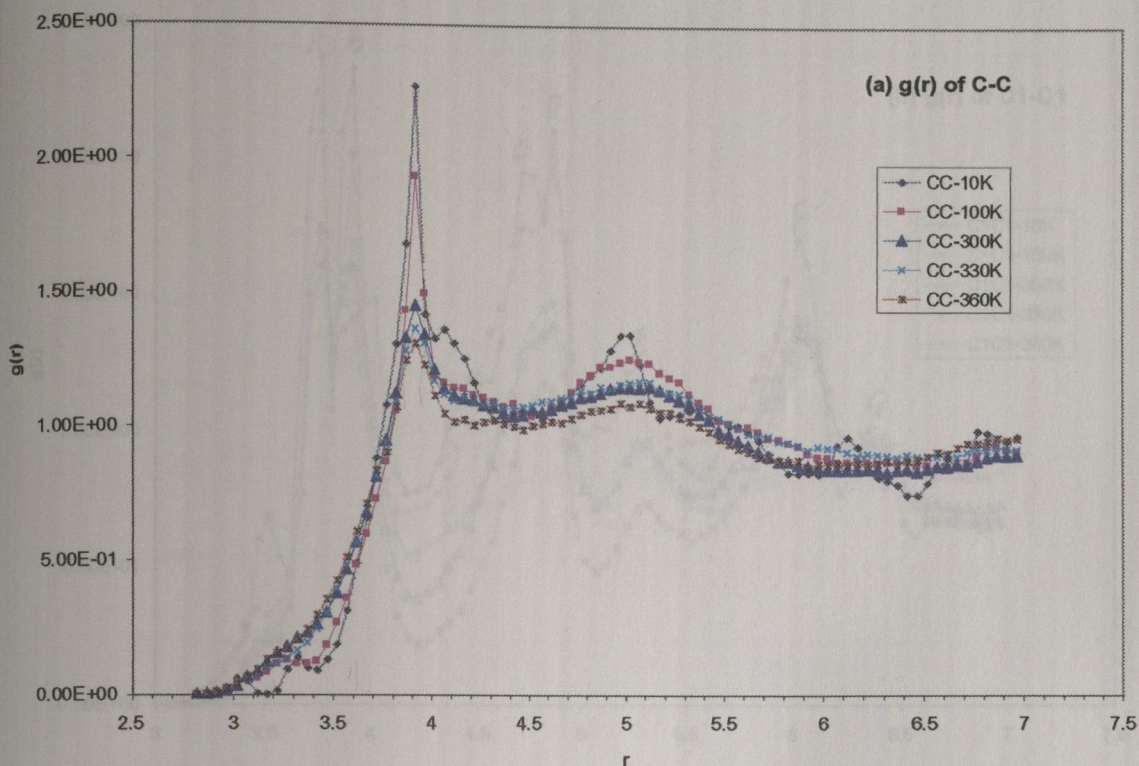
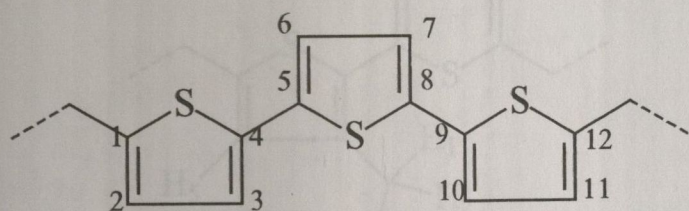
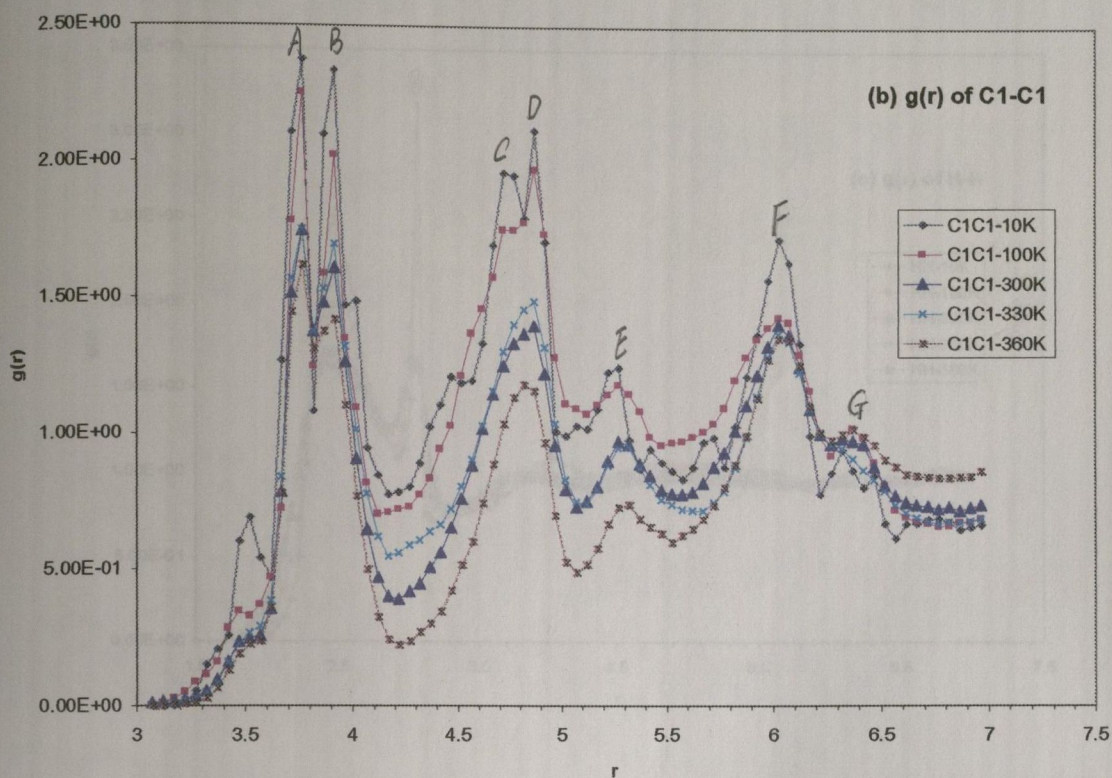
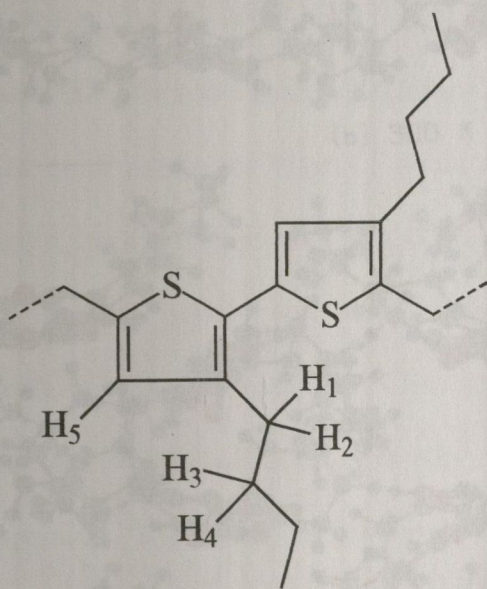
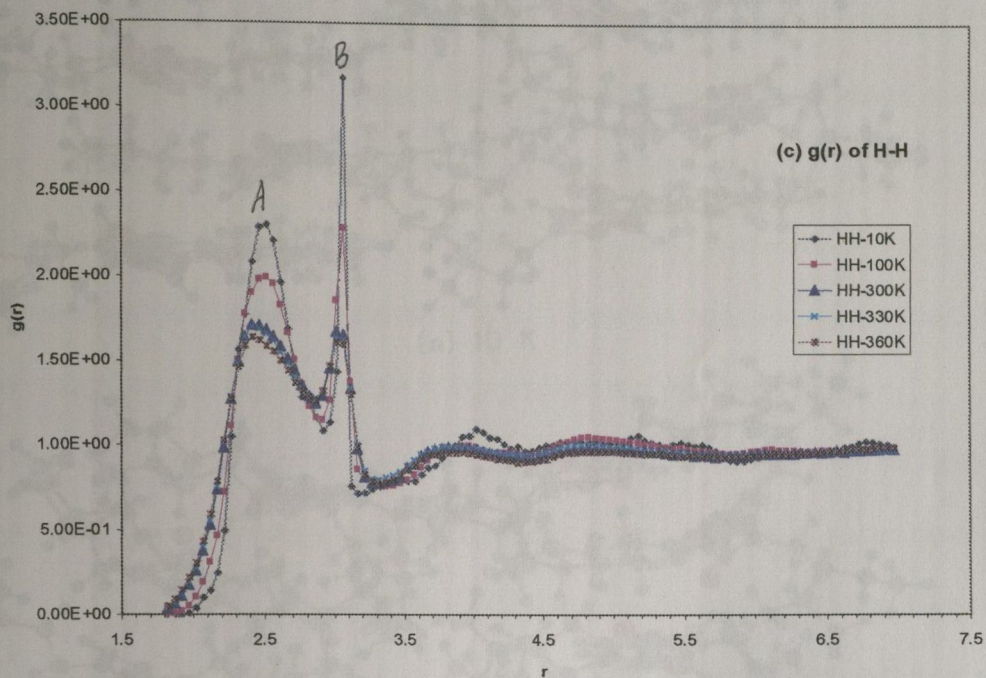


Fig. 5.12 RDF of C-C in the alkyl side chains at different temperatures. When all the links in the alkyl side chain are in *trans* (0°), the distance (r) (in units of Å) between alkyl carbon number 1 and 4 is 3.916 Å. The appearance of *gauche* in the alkyl chain will reduce the distance.



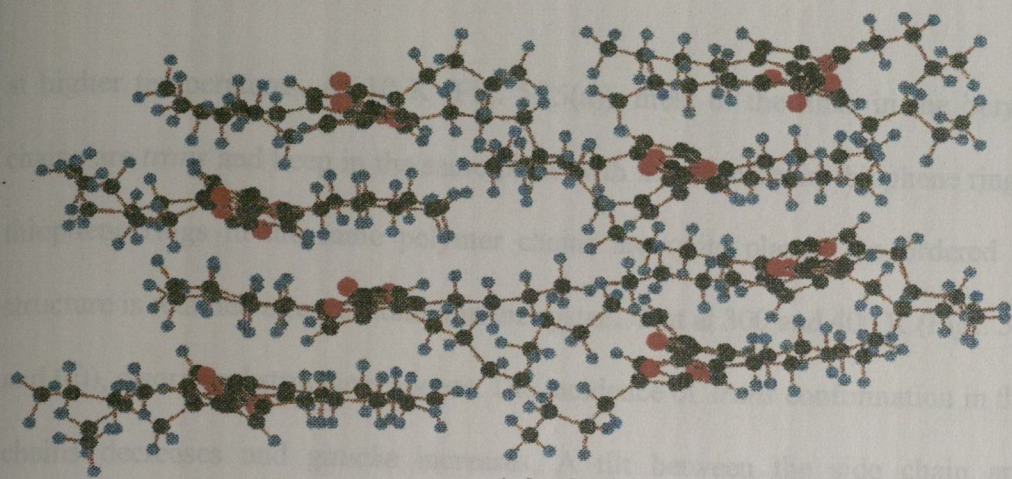
Peak	Distance
A	2-5, 4-7
B	1-5, 4-8, 3-6
C	1-6, 3-8
D	2-6, 3-7
E	4-9
F	2-7, 3-9, 4-10
G	1-8

Fig. 5.13 RDF of C-C in the P3BT main-chain thiophene rings at different temperatures. The peak A corresponds to the distance (in units of Å) between carbon number 2 and 5, or 4 and 7; B (1-5, or 4-8, or 3-6); C (1-6, or 3-8); D (2-6, or 3-7); E (4-9); F (2-7, or 3-9, or 4-10); G (1-8).

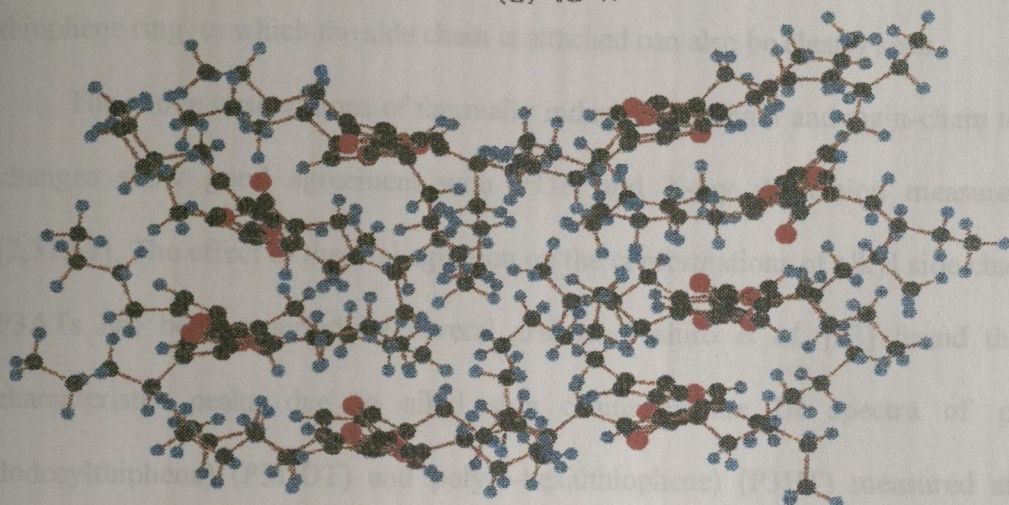


Peak	Distance
A	1-3, 2-4
	3-5, 4-5
B	2-3, 1-4

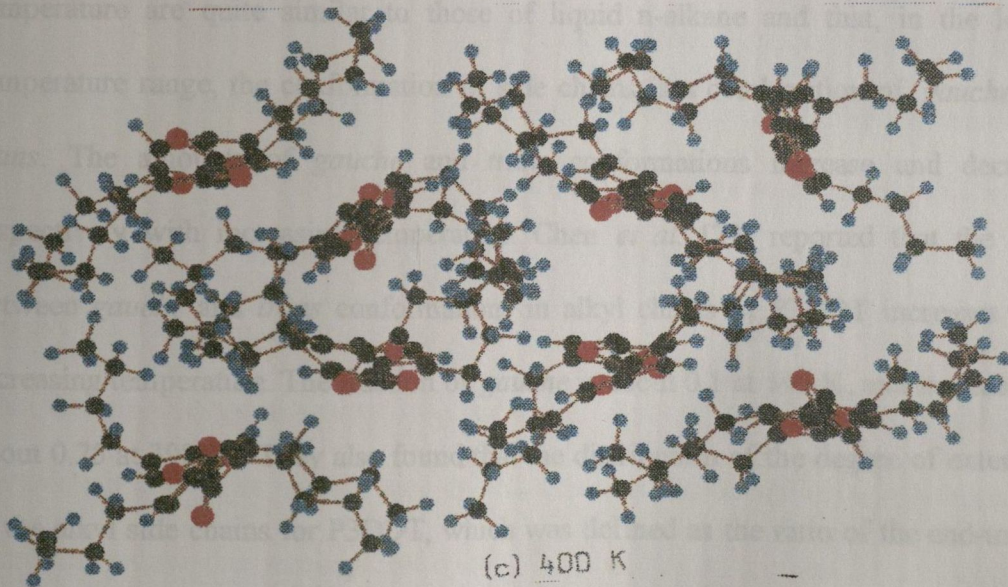
Fig. 5.14 RDF of H-H in P3BT at different temperatures. The peak A corresponds to the distance (in units of Å) between hydrogen number 1 and 3, or 2 and 4, or 3 and 5, or 4 and 5; B (2-3, or 1-4).



(a) 10 K



(b) 300 K



(c) 400 K

Fig. 5.15 A comparison of conformations of P3BT after 100 ps relaxation at 10, 300 and 400 K. (a) 10 K, (b) 300 K and (c) 400 K. The atoms in P3BT are represented by different colors, red – S atom, gray – C atom and blue – H atom.

at higher temperatures. At 10 K (Fig. 5.15(a)), most of the links in the butyl side chains are *trans* and keep in the same plane with the main chain thiophene rings. The thiophene rings in the same polymer chains are quite planar. An ordered planar structure is retained after relaxation in the system. But at 300 and 400 K (Figs. 5.15(b) and (c)), disordered structures appear. The incidence of *trans* conformation in the side chains decreases and *gauche* increases. A tilt between the side chain and the thiophene ring to which the side chain is attached can also be clearly seen.

The above observations of thermally induced side-chain and main-chain torsion changes show good agreement with FTIR and X-ray diffraction measurements [2,37,61]. The effect of thermal agitation on the conformations of alkyl side chains of P3ATs has been reported by several groups. Tashiro *et al.* [23] found that the characteristic peaks due to alkyl side chains in the IR spectra of poly(3-dodecylthiophene) (P3DDT) and poly(3-hexalthiophene) (P3HT) measured at high temperature are quite similar to those of liquid n-alkane and that, in the lower temperature range, the conformation of side chains is a combination of *gauche* and *trans*. The amounts of *gauche* and *trans* conformations increase and decrease respectively with increasing temperature. Chen *et al.* [24] reported that the ratio between *gauche* and *trans* conformations in alkyl chains of P3DDT increases with increasing temperature. The fraction of *gauche* is about 0.1 at 143 K, and increases to about 0.25 at 398 K. They also found that the distribution of the degree of extension of the alkyl side chains for P3DDT, which was defined as the ratio of the end-to-end distance of the side chain to that of the fully extended side chain, shifts slightly from 0.9 at 143 K to 0.8 at 398 K. The degree of extension is distributed in the range from 0.8 to 1.0 at 143 K, indicating that the alkyl side chain is not fully extended but has some degree of coil; the distribution is broadened to the range 0.65-1.0 as the

temperature rises to 398 K. Using IR spectroscopy, Zerbi *et al.*[25] found that the population of non-*trans* conformation within the alkyl side chains increases with temperature.

Tashiro *et al.* [23] measured the temperature dependence of the X-ray diffraction pattern of P3DDT. Their results showed that at room temperature an intense peak (002) was observed at $2\theta=23^\circ$. As the temperature increases, the peak intensity decreased markedly and a new peak was observed at 24° . These observations and the contraction of the chain length by about 5% confirmed the skeletal deformation of polymer main chain through torsional rotations around the bonds between the thiophene rings under thermal agitation.

Fig. 5.16 The average torsional angle $\langle\varphi_5\rangle$ (in units of degree) as a function of

5.4.5 Thermochromic Changes

It is suggested that thermochromism originates in the change of the gap between the valence and conduction π bands. The change of the bandgap results from the enhanced torsional angles in the polymer main chains as discussed in Chapter 4. So it is necessary to investigate the change of φ_5 with thermal agitation. Fig. 5.16 shows the temperature variation of $\langle\varphi_5\rangle$ (average of φ_5), which is the angle between the thiophene rings averaged over time and over all the inter-ring bonds in the simulation cell. The upward step at 330 K indicates that while $\langle\varphi_5\rangle$ is appreciably constant below this temperature there is a 10° shift to a value at which it again remains reasonably constant at 340 K and above. We suppose that this shift corresponds to a thermochromic change. This shift happens in the same temperature range as does the kink of torsional energy described in Subsection 5.3.2.

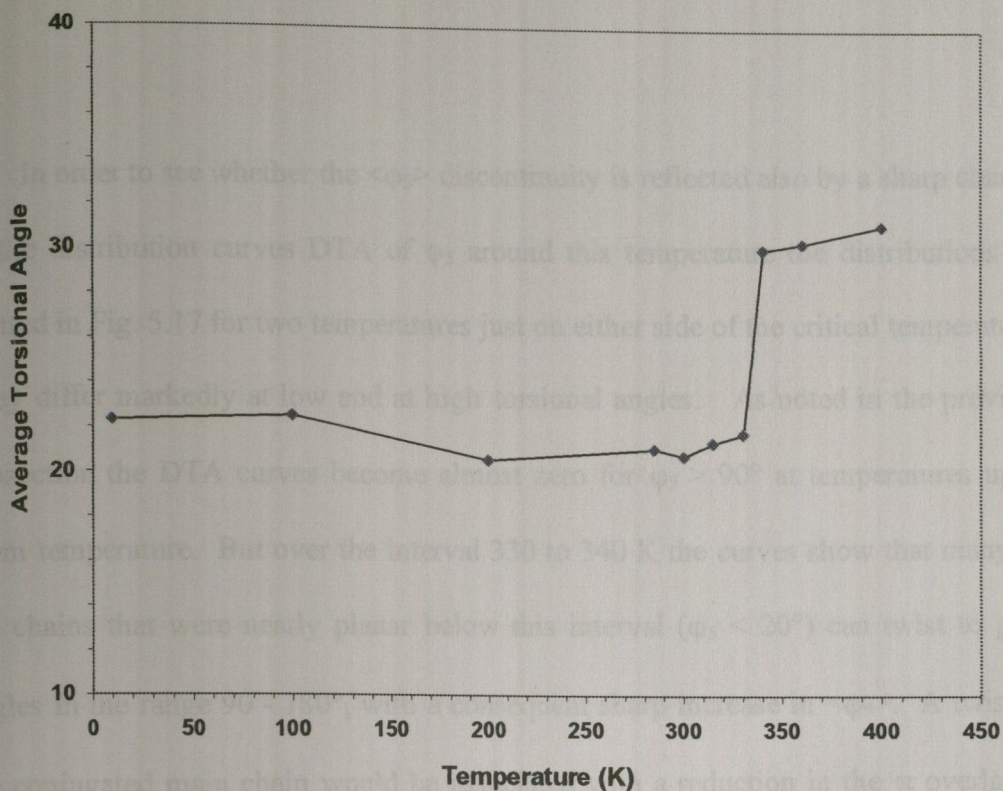


Fig. 5.16 The average torsional angle $\langle \phi_5 \rangle$ (in units of degree) as a function of temperature.

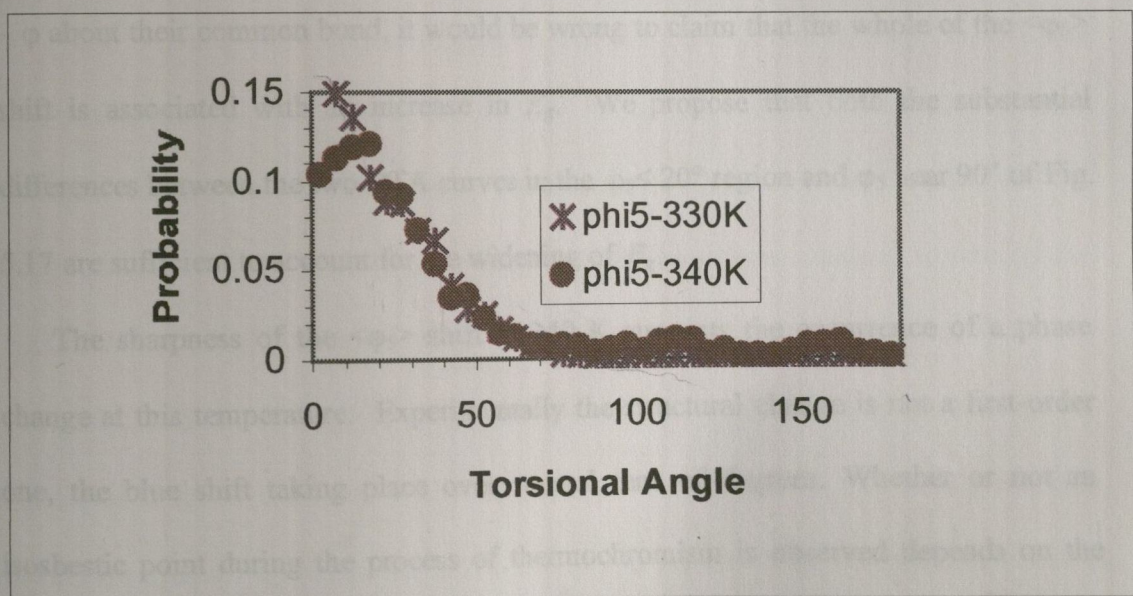


Fig. 5.17 A comparison of DTA of ϕ_5 (in units of degree) at 300 K and at 340 K.

In order to see whether the $\langle\varphi_5\rangle$ discontinuity is reflected also by a sharp change in the distribution curves DTA of φ_5 around this temperature the distributions are plotted in Fig. 5.17 for two temperatures just on either side of the critical temperature. They differ markedly at low and at high torsional angles. As noted in the previous subsection the DTA curves become almost zero for $\varphi_5 > 90^\circ$ at temperatures up to room temperature. But over the interval 330 to 340 K the curves show that many of the chains that were nearly planar below this interval ($\varphi_5 < 20^\circ$) can twist to give angles in the range $90 - 180^\circ$, with a consequent sharp increase in $\langle\varphi_5\rangle$. A twist in the conjugated main chain would be associated with a reduction in the π overlap of adjacent thiophene rings and hence with a dilation of the gap energy, E_g , between the π valence and conduction bands. Since a π overlap integral between the $2p_x$ atomic orbitals of adjacent carbon atoms is the same if one of them is rotated by φ as by $180^\circ - \varphi$ about their common bond, it would be wrong to claim that the whole of the $\langle\varphi_5\rangle$ shift is associated with an increase in E_g . We propose that both the substantial differences between the two DTA curves in the $\varphi_5 < 20^\circ$ region and φ_5 near 90° of Fig. 5.17 are sufficient to account for the widening of E_g .

The sharpness of the $\langle\varphi_5\rangle$ shift at 340 K suggests the occurrence of a phase change at this temperature. Experimentally the structural change is not a first-order one, the blue shift taking place over several tens of degrees. Whether or not an isosbestic point during the process of thermochromism is observed depends on the sample used [26-28]. The explanation for the different behavior of the material on an experimental macroscopic scale probably involves the presence of amorphous and polymorphic crystalline components. Another reason is that most real samples used in the experiments are regiorandom P3ATs while the model used in the calculations is

regioregular HT-P3AT. As mentioned before, regiorandom P3ATs are partially crystalline and contain structural defects in the polymer chains, whereas regioregular HT-P3AT is self-assembled and highly crystalline.

The $\langle\varphi_5\rangle$ shift between 330 and 340 K correlates with the conformational changes in the alkyl side chains. A comparison of the distribution of torsional angles in the alkyl side chains at these two temperatures (Fig. 5.18) shows significantly greater variations in φ_1 and φ_2 than in φ_3 and φ_4 . Fig. 5.19 shows that $\langle\varphi_1\rangle$ and $\langle\varphi_2\rangle$ also make an abrupt change from 330 K to 340 K correlating with the $\langle\varphi_5\rangle$ shift.

5.4.6 Effect of Conformations in Alkyl Side Chains on the Shift

in $\langle\varphi_5\rangle$

The previous section has suggested that the shift of the average main-chain torsional angle $\langle\varphi_5\rangle$ between 330 K and 340 K correlates with the thermally induced changes in the alkyl side chain conformations. In order to investigate the dependencies of $\langle\varphi_5\rangle$, each of the side chain links have been clamped in turn by the application of a high torsional potential to inhibit the torsional motion of this link.

Fig. 5.20 shows $\langle\varphi_5\rangle$ as a function of temperature when one of the links in the alkyl side chains is clamped. When the torsions of inner links 1 or 2 were prevented, the abrupt shift of $\langle\varphi_5\rangle$ between 330 °C and 340 °C did not occur. However, the shift is still seen to take place when the torsion of link 3 was prevented. This suggests that the conformations of alkyl side chains are very important to the change of conformation in the polymer main chain. The torsion of inner links (link 1 and link 2) appear to play

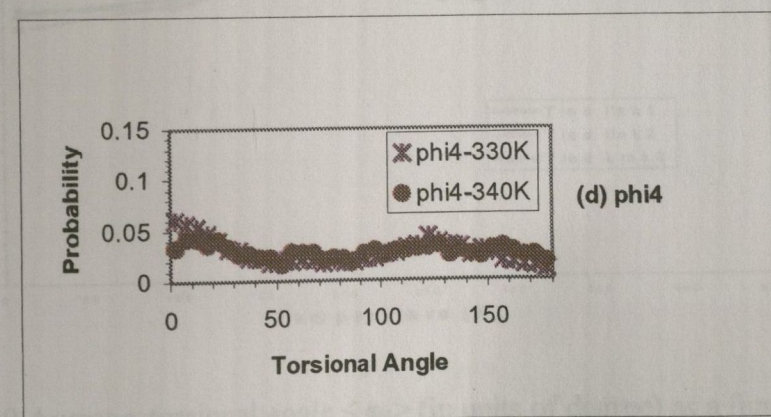
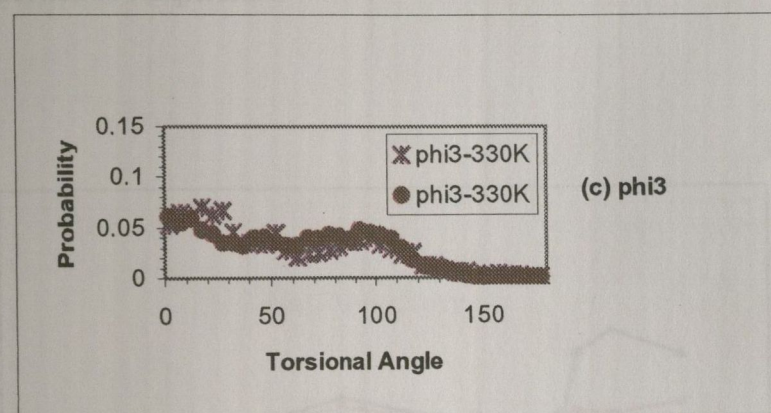
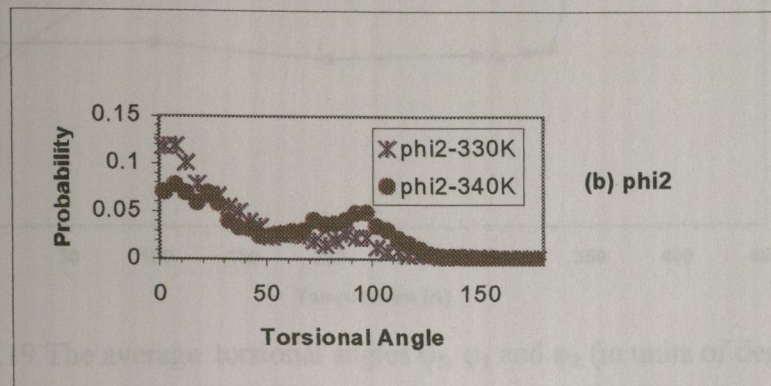
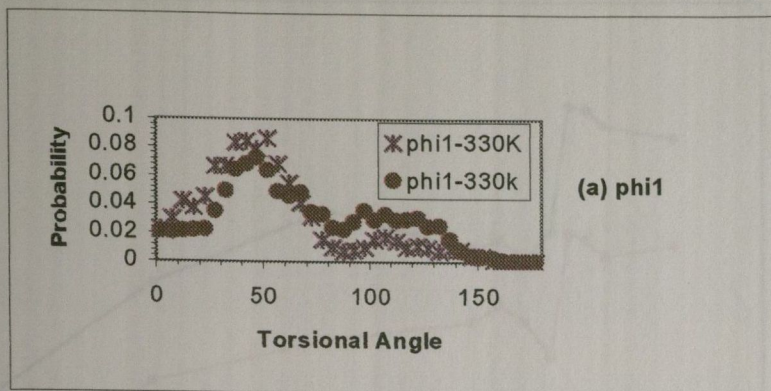


Fig. 5.18 A comparison of DTA at 330 and 340 K for the torsional angles (in units of degree) in the P3BT alkyl side chains. (a) ϕ_1 , (b) ϕ_2 , (c) ϕ_3 , (d) ϕ_4 .

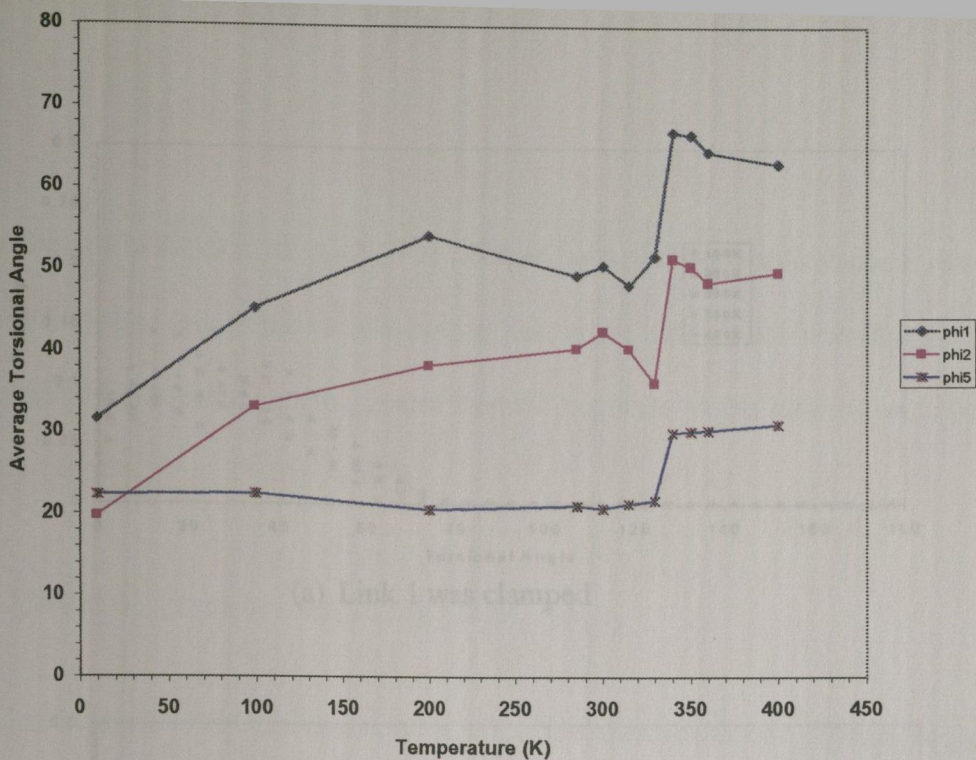


Fig. 5.19 The average torsional angles ϕ_5 , ϕ_1 and ϕ_2 (in units of degree) as a function of temperature.

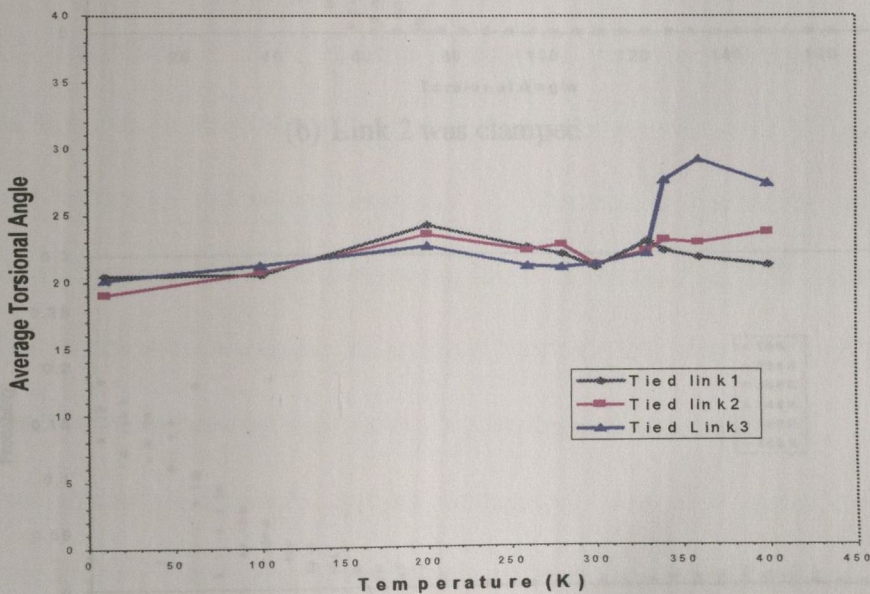
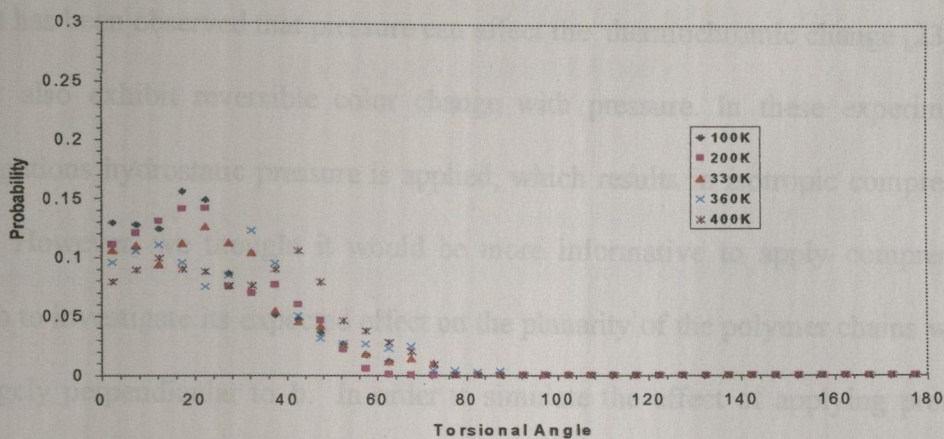


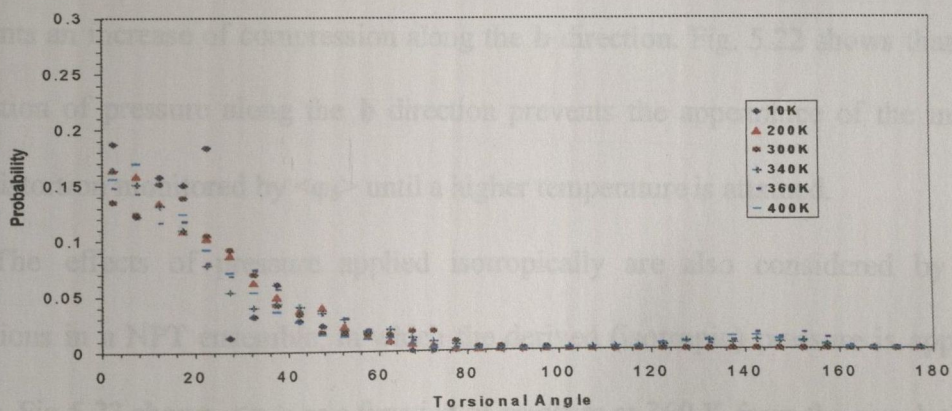
Fig. 5.20 Average torsional angle $\langle \phi_5 \rangle$ (in units of degree) as a function of temperature when one of the links in the alky side chains was clamped.



(a) Link 1 was clamped



(b) Link 2 was clamped



(c) Link 3 was clamped

Fig. 5.21 DTA of φ_5 (in units of degree) at various temperatures as one of the links in the side chains was clamped. (a) Clamped link 1, (b) Clamped link 2, (c) Clamped link 3.

a particular role in the shift of $\langle\varphi_5\rangle$. The DTA of φ_5 at various temperatures is shown in Fig. 5.21 when one of the carbon-carbon link in the side chains was clamped. It shows that no big torsional angle (greater than 90°) appears as the stable inner links 1 and 2 are clamped (Figs. 5.21(a) and (b)).

5.4.7 Effect of Pressure on the Shift of $\langle\varphi_5\rangle$

It has been observed that pressure can affect the thermochromic change [23] and P3ATs also exhibit reversible color change with pressure. In these experimental investigations hydrostatic pressure is applied, which results in isotropic compression forces. However, we thought it would be more informative to apply compression along **b** to investigate its expected effect on the planarity of the polymer chains which are largely perpendicular to **b**. In order to simulate the effect of applying pressure along one direction (**b** axis), the MD simulation was performed on a NVT ensemble at three fixed values of the lattice parameter *b*. Decreasing the lattice parameter *b* represents an increase of compression along the **b** direction. Fig. 5.22 shows that the application of pressure along the **b** direction prevents the appearance of the main-chain distortion monitored by $\langle\varphi_5\rangle$ until a higher temperature is attained.

The effects of pressure applied isotropically are also considered by the simulations in a NPT ensemble, in which the derived (isotropic) pressure is applied directly. Fig. 5.23 shows $\langle\varphi_5\rangle$ as a function of pressure at 360 K from the simulations in NPT ensemble. Under these conditions of low pressure and high temperature, $\langle\varphi_5\rangle$ is above 30° . But it decreases as the pressure increases and finally remains at 20° that should be presented at low temperature at normal pressure. So higher pressure reduces the torsional angles on the polymer main chains. The change of the average torsional

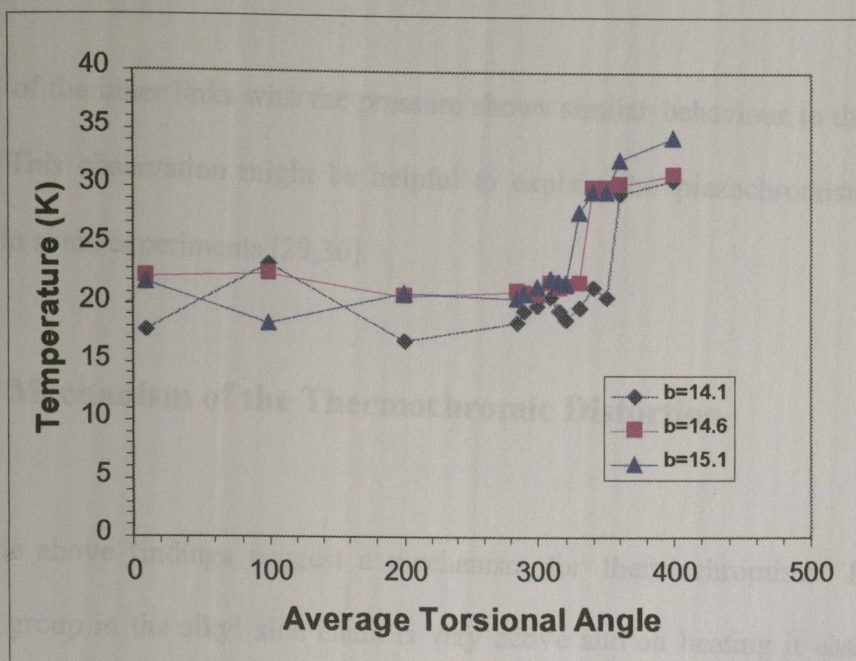


Fig. 5.22 Average torsional angle $\langle\varphi_5\rangle$ (in units of degree) as a function of temperature at three different values of the lattice parameter b in NVT ensemble.

(a) $b=14.1$ Å, (b) $b=14.6$ Å, (c) $b=15.1$ Å.

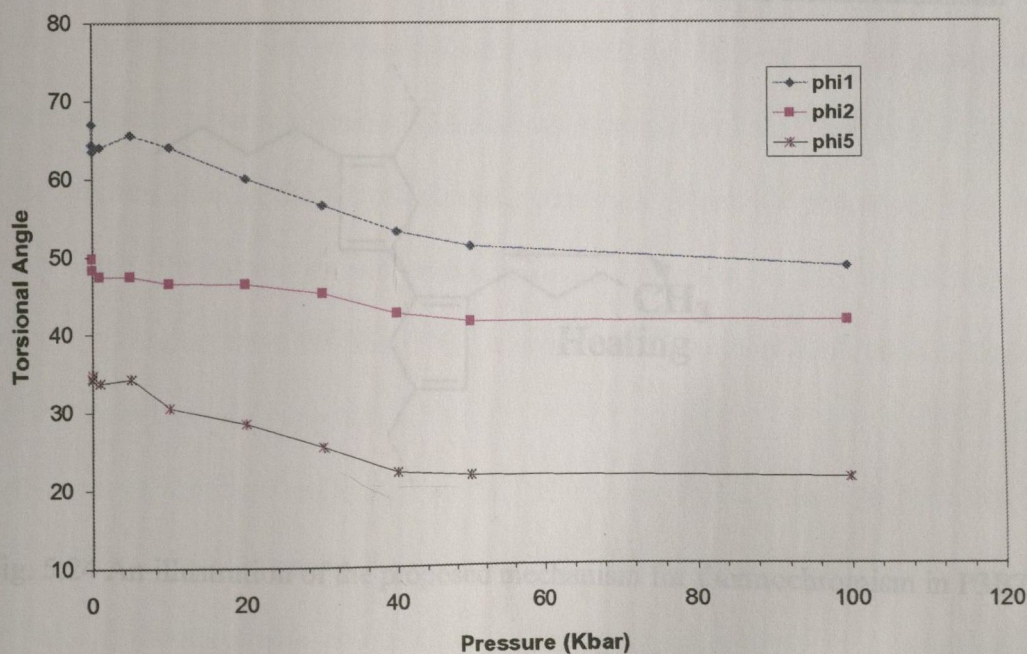


Fig. 5.23 Average torsional angle $\langle\varphi_5\rangle$ (in units of degree) as a function of pressure at 360 K calculated in NPT ensemble, $\langle\varphi_1\rangle$ and $\langle\varphi_2\rangle$ are also included.

angles of the inner links with the pressure shows similar behaviour to that shown by $\langle\varphi_5\rangle$. This observation might be helpful to explain the piezochromism of P3ATs found in some experiments [29,30].

5.4.8 Mechanism of the Thermo-chromic Distortion

The above findings suggest a mechanism for thermochromism. The flexible methyl group in the alkyl side chain is very active and on heating it easily initiates rotation and induces the inner links on the same alkyl side chain to undergo torsion as shown in Fig. 5.24. As the temperature rises to a point when the torsions in the relatively stable inner links (link 1 and link 2) gain sufficient thermal energy, they induce and support a shift in the average torsional angle $\langle\varphi_5\rangle$ in the rigid polymer main chain, which changes the electronic structure and results in thermochromism.

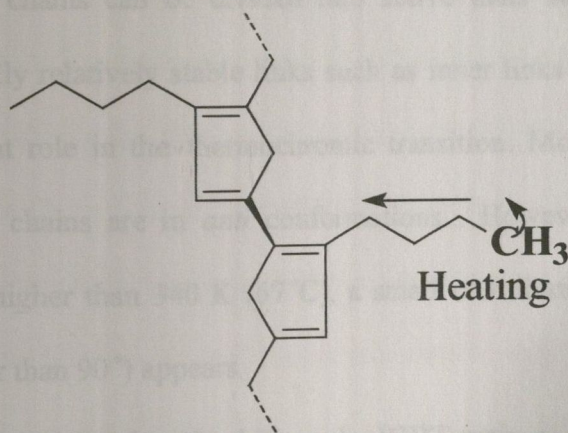


Fig. 5.24 An illustration of the proposed mechanism for thermochromism in P3BT.

This mechanism also explains why polythiophene itself as well as P3ATs with alkyl carbon number less than three are not thermochromic. The former does not have alkyl

side chains, while the latter do not have relatively stable inner links and the active alkyl torsions in these polymers can not support the average torsional angle shift in the rigid polymer main chain.

5.5 Conclusions

The all *trans* conformations of alkyl side chains and π -electronic conjugation help to stabilize a planar structure of P3AT main chains. Although the alkyl chains mainly exist in *trans* or near *trans* conformations up to room temperature, they show some changes from all-*trans* even at very low temperature. As the temperature is increased, the probability of *gauche* and other non-*trans* conformations increases. The methyl group can make complete rotations at high temperatures. A tilt between alkyl side chains and polymer main chain exists and is enhanced by heating. The links in the alkyl side chains can be divided into active links such as methyl group and conformationally relatively stable links such as inner links (link 1 and link 2). They play a different role in the thermochromic transition. Most thiophene rings in the polymer main chains are in *anti* conformations. However, as the temperature is increased to higher than 340 K (67°C), a small contribution of high torsion angles (near or greater than 90°) appears.

An average torsional angle shift on the P3BT main chains from 330 K to 340 K occurs, which is supported by the torsion shift of conformationally relative stable inner links in the alkyl side chains. From an energy point of view, it is tempting to think that the alkyl side chains act as thermal 'conductors' to transit conformational energy initiated by the methyl group.

These MD findings are consistent with previous experimental measurements and suggest a role of the alkyl side chains in the process of thermochromism. FTIR [23,26] spectra showed that on heating an increasing proportion of *gauche* conformations in the alkyl side chains of P3ATs reduces the conjugation length of the polymer main chains and causes the thermochromic transition. The steric hindrance between the neighboring side chains with *gauche* conformations is thought to destroy the planar structure of the main chains. Our MD results can also be interpreted from this steric view. It is difficult to use FTIR to follow the torsional changes in the polymer main chains with temperature because no typical frequency relative to this torsion is available.

Raman [26] spectra confirmed that different conjugation length may occur in P3AT main chains and X-ray [23] diffraction showed that the torsional angles between thiophene rings in the main chains increased with temperature. However, no detailed investigations of the torsional angles have been reported up to now.

Although an isosbestic point was found using electronic absorption spectra and UV-vis spectra during the thermochromic process [27,28], most experimental results suggest that the thermochromic transition is continuous. This contradicts our abrupt shift in the average torsional angle in the polymer main chains, which may be due to the structural model that we used. In our simulation, we only considered the highly crystalline regioregular HT-P3BT. But actual samples of P3AT used in experiments are semicrystalline, in which crystalline, quasi-ordered and amorphous phases equilibrate with each other. The crystalline phase is mainly composed of an ordered structure, while the amorphous phase is composed of both ordered and disordered structures. Below the melting temperature both the crystalline and amorphous phases could show the thermochromic phenomenon, but the energy needed might be

different. Yang *et al.* [27,28] also suggested that the regularity of the polymers could play an important role in the behavior of thermochromic transition from an experimental view.

The thermochromic transition temperature range of P3ATs is found to increase with decreasing length of the alkyl side [31]. The range for poly(3-dodecylthiophene) is from 303 K to 353 K. No exact thermochromic transition temperature range has been reported for P3BT. The temperature found in our work for the thermochromic change may be in a reasonable range, but probably tends to be a little low. Simulations of P3ATs with different alkyl side chains should be carried out in the future.

Finally, our results from MM and MD simulations are consistent. They both indicate that the stable thermally accessible conformations with higher torsional angles in the polymer main chains are required for thermochromism to exist. In MM simulations three different torsional periodicities with certain conjugation length in the polymer main chains were considered. A thermally accessible stable conformation is found both in the two-chain model (55°) and in the one-chain model (20° or 55°) in all the periodicities that were considered. The changes between these stable conformations provided good information on thermochromic phenomenon. However, the effects of conformations in the alkyl side chains were not explicitly investigated although they play an important role in thermochromism as shown in our MD investigations. All the torsional probabilities between the thiophene rings in the polymer main chains are taken account of in the MD simulations, which can also follow the dynamic interactions between the alkyl side chains and the polymer main chains. The thermally induced conformation changes in both the alkyl side chains and in the polymer main chains provide a direct path to investigate the thermochromic

behavior of P3ATs. With the help of thermally induced conformational changes in the alkyl side chains, a step-like increase in the mean value of the torsional angle between the thiophene rings occurred at high temperature, which reduces the planarity of the polymer chains. Further the energy change from one stable conformation to another shows good agreement with the electronic bandgap increase during the thermochromic transition determined by experiments.

- [5] Kee R L, *J Chem Phys*, 1994, 100:1610
- [6] Han J, Gee R B, and Boyd R H, *Macromolecules*, 1994, 27:748
- [7] Smith G D, Yoon D Z, Zhu W, and Ediger M D, *Macromolecules*, 1994, 27:5543
- [8] Deutsch H B, and Binder K, *Macromolecules*, 1992, 25:6241
- [9] Kikuchi H, Tokumitsu H, and Seki E, *Macromolecules*, 1998, 31:7526
- [10] Aaboe A, and Thomas J, *Comp. and Theo. Polym. Sci.*, 1993, 7:87
- [11] Neyertz S, Brown D, and Thomas J O, *J Chem Phys*, 1994, 101:10064
- [12] Ryckaert and Klein M L, *J Chem Phys*, 1986, 85:1403
- [13] Karawasa N, Desgauris S, and Goddard III W A, *J Phys Chem*, 1991, 95:2260
- [14] Rutledge G C, and Suter D W, *Macromolecules*, 1991, 24:1921
- [15] Kawai T, Nakazono M, Sugimoto R, and Yoshino K, *Int J Appl Phys*, 1992, 61:3400
- [16] Tashiro K, Ono K, Minagawa Y, Kobayashi M, Kawai T, and Yoshino K, *J Polym Sci, Part B: Polym Phys*, 1991, 29:1235
- [17] Kawai T, Nakazono M, and Yoshino K, *J Mater Chem*, 1992, 2:903
- [18] Tashiro K, Kobayashi M, Morita S, Kawai T, and Yoshino K, *Synth Met*, 1995, 69:397
- [19] Gustafsson G, Inganäs O, Österholm B, and Lögdlund J, *Polymer*, 1991, 32:1574
- [20] O'Dwyer S O, and Murray-Blake D A, to be published

Bibliography:

- [1] Takeuchi H. *J. Chem. Phys.*, 1990, **93**:2062
- [2] Takeuchi H. *J. Chem. Phys.*, 1990, **93**:4490
- [3] Takeuchi H, and Okazaki K. *J. Chem. Phys.*, 1990, **92**:5643
- [4] Neuburger N, Bahar I, and Mattice W L. *Macromolecules*, 1992, **25**:2447
- [5] Roe R J. *J. Chem. Phys.*, 1994, **100**:1610
- [6] Han J, Gee R H, and Boyd R H. *Macromolecules*, 1994, **27**:7748
- [7] Smith G D, Yoon D Z, Zhu W, and Ediger M D. *Macromolecules*, 1994, **27**:5563
- [8] Deutsch H P, and Binder K. *Macromolecules*, 1992, **25**:6241
- [9] Kikuchi H, Tokumitsu H, and Seki K. *Macromolecules*, 1993, **26**:7326
- [10] Aabloo A, and Thomas J. *Comp. and Theo. Polym. Sci.*, 1997, **7**:47
- [11] Neyertz S, Brown D, and Thomas J O. *J. Chem. Phys.*, 1994, **101**:10064
- [12] Ryckaert and Klein M L. *J. Chem. Phys.*, 1986, **85**:1613
- [13] Karawasa N, Dasgupta S, and Goddard III W A. *J. Phys. Chem.*, 1991, **95**:2260
- [14] Rutledge G C, and Suter U W. *Macromolecules*, 1991, **24**:1921
- [15] Kawai T, Nakazono M, Sugimoto R, and Yoshino K. *Jpn. J. Appl. Phys.*, 1992, **61**:3400
- [16] Tashiro K, Ono K, Minagawa Y, Kobayashi M, Kawai T, and Yoshino K. *J. Polym. Sci., Part B: Polym. Phys.*, 1991, **29**:1223
- [17] Kawai T, Nakazono M, and Yoshino K. *J. Mater. Chem.*, 1992, **2**:903
- [18] Tashiro K, Kobayashi M, Morita S, Kawai T, and Yoshino K. *Synth. Met.*, 1995, **69**:397
- [19] Gustafsson G, Ingänas O, Österholm H, and Laasko J. *Polymer*, 1991, **32**:1574
- [20] O'Dwyer S O, and Morton-Blake D A. *to be published*

- [21] Corish J, Morton-Blake D A, Feeley D E, B ni re F and Marchetti M. *J. Chem. Phys. B*, 1997, **101**:10075
- [22] Prosa T J, Winokur M J, Moulton J, Smith P, and Heeger A J. *Macromolecules*, 1992, **25**:4364
- [23] Tashiro K, Ono K, Minagawa Y, Kobayashi M, Kawai T, and Yoshino K. *J. Polym. Sci.: Part B: Polym. Phys.*, 1991, **29**:1223
- [24] Chen S A, and Lee S J. *Synth. Met.*, 1995, **72**:253
- [25] Zerbi G, Chierichetti B, and Ingnas O. *J. Chem. Phys.*, 1991, **94**:4646
- [26] Iwasaki K, Fujimoto H, and Matsuzaki S. *Synth. Met.*, 1994, **63**:101
- [27] Yang C, Orfino F P, and Holderoft S. *Macromolecules*, 1996, **29**:6511
- [28] Li J, and Pang Y. *Macromolecules*, 1997, **30**:7487
- [29] Yoshino K, Nakao K, Onoda M and Sugimoto R. 1988, *Solid State Commun.*, **68**:513
- [30] Isotaro H, Ahlskog M, and Stubb H. *Synth. Met.*, 1992, **48**:313
- [31] Ingn s O, Gustafsson G, Salaneck W R,  sterholm J-E, and Laakso J. *Synth. Met.*, 1989, **28**:377

Chapter 6

MOLECULAR SIMULATION OF DIFFUSION OF DOPANTS (Cl⁻ and BF₄⁻) IN P3AT LATTICES

6.1 Introduction

Part III

MOLECULAR SIMULATION OF TRANSPORT BEHAVIOUR OF DOPANTS (Cl⁻ AND BF₄⁻) IN POLY(3-ALKYLTHIOPHENE) LATTICES

Although polaron and bipolaron are believed to be the primary carriers of charge transport in conducting polymer systems such as P3AT, it is difficult to directly investigate the charge transport behavior in the polymer. Fortunately, some oxidized or reduced species (dopants or counterions) are incorporated during the doping process. In the real case, people usually study the transport behavior of dopants (or counterions) instead of a direct investigation of the charge transport behaviour. To develop materials with desired electronic properties, it is vital to understand the transport of dopants in the device cycle which controls the distribution of the dopants in the material and influences the electrostatic behaviour of the device.

No direct experimental method has been found that will reveal the location and migration path of the dopant ions in the oxidized state of the conducting polymer. Using MM simulation techniques, Veluri [1] predicted the most likely structures

Chapter 6

MD SIMULATION OF DIFFUSION OF DOPANTS

(Cl⁻ and BF₄⁻) IN P3AT LATTICES

6.1 Introduction

π -conjugated conducting polymers show characteristic doping effects such as a drastic increase in conductivity, an apparent change in color and changes in other electronic and optical properties. These characteristic properties have been interpreted in terms of the formation of solitons, polarons and bipolarons as discussed in Chapter 1. Although polarons and bipolarons are believed to be the primary source of charge carriers in non-degenerate ground state conjugated polymers such as P3ATs, it is difficult to directly investigate the charge transport behavior in the polymers. Fortunately, some oxidant or reductant species (dopants or counterions) are incorporated during the doping process. In the real case, people usually study the transport behavior of dopants (or counterions) instead of a direct investigation of the charge transport behaviour. To develop materials with desired electronic properties, it is vital to understand the transport of dopants in the redox cycle which controls the distribution of the dopants in the material and influences the electronic behaviour of the device.

No direct experimental method has been found that will reveal the location and migration path of the dopant ions in the oxidised state of the conducting polymers. Using MM simulation techniques, Veluri [1] predicted the most likely structures for

BF_4^- , ClO_4^- , and Cl^- doped polypyrrole and polythiophene and in particular the most probable sites that were occupied by the dopants in those structures. Using defect lattice simulation method, the same author also calculated the energy barriers of the migration of the dopant ions along the paths that were proposed.

Although the diffusion coefficients of dopants in conducting polymers can be measured by experimental methods, such as Galvanostatic pulse method [2-3], the measurements are affected by a large number of factors. Despite extensive literature searches we have been unable to find any report on the diffusion of dopants in P3ATs. MD simulation can provide information on the mean square displacements of dopants at different times and it can therefore be further used to calculate the diffusion coefficients and activation energies for the diffusion process. In doing this it is well to remember that it may be providing a simple model of the complex situation that is encountered in the migration process in the real materials.

In this and next Chapters we report on the use of MD and MM calculations to investigate the transport behavior of dopants in P3AT lattices. In this chapter, the most likely lattice structures of P3BT doped by Cl^- or BF_4^- with the dopants in their most probable sites are first predicted by a combination of MM and MD simulation methods. Then the MD simulation is employed to investigate the diffusion behavior of dopants based on the structural models proposed. In the next Chapter, the MM simulation is used to search for the most likely migration path of dopants. The effects of concentration and the sizes of dopants are also considered in the investigations of transport behaviour of the dopants.

6.2 The Charge Model for the Main Chain in Doped P3ATs

P3ATs are π -conjugated polymers with non-degenerate ground state structures. As discussed in Chapter 1, during the doping process (oxidation) of non-degenerate ground state polymers, a polaron is first formed in the polymer chains with a free radical and a positive charge. Upon further oxidation, a bipolaron with two positive charges is produced at higher doping levels. The polaron or bipolaron is believed to extend over about 4 pyrrole or thiophene rings [4-5]. In Veluri's MM simulation of polythiophene and polypyrrole [1], the same number of positive charges corresponding to the negative charges carried by the dopants was distributed almost equally on its atoms of the pyrrole or thiophene rings.

It is important to define a charge model in the polymer chains created by doping before simulating the transport behavior of dopants in P3AT lattices. This is because it affects the Coulombic potentials between the dopant ions and the polymers. The above three charge models (polaron, bipolaron and the charges evenly distributed) are considered and compared in this work. As discussed in Chapter 1 the charge model in the polymer chain depends on the concentration of the dopants. Normally the doping concentration is defined as the mole ratio between the dopant and monomer. Here we define it in another way for convenience. If there is one dopant per alkylthiophene unit in the bulk, we would describe such a P3AT lattice as 100% "doped". So a 50% doping level is one dopant per two alkylthiophene units and 25% one dopant per four alkylthiophene unites. The polaron charge and bipolaron charge models as shown in Fig. 6.1 are used in our simulation of P3BT with doping level 25% and 50%, respectively. Another charge model choice is when the same number of positive charges corresponding to the negative charges carried by the dopants are evenly

distributed among the five atoms constituting the thiophene rings in P3BT main chains. This is analogous to the charge model used in Veluri's MM investigation [1] of migration of dopants in polythiophene and polypyrrole lattices. The differences that result from the use of these models will be discussed in Section 6.4.3.

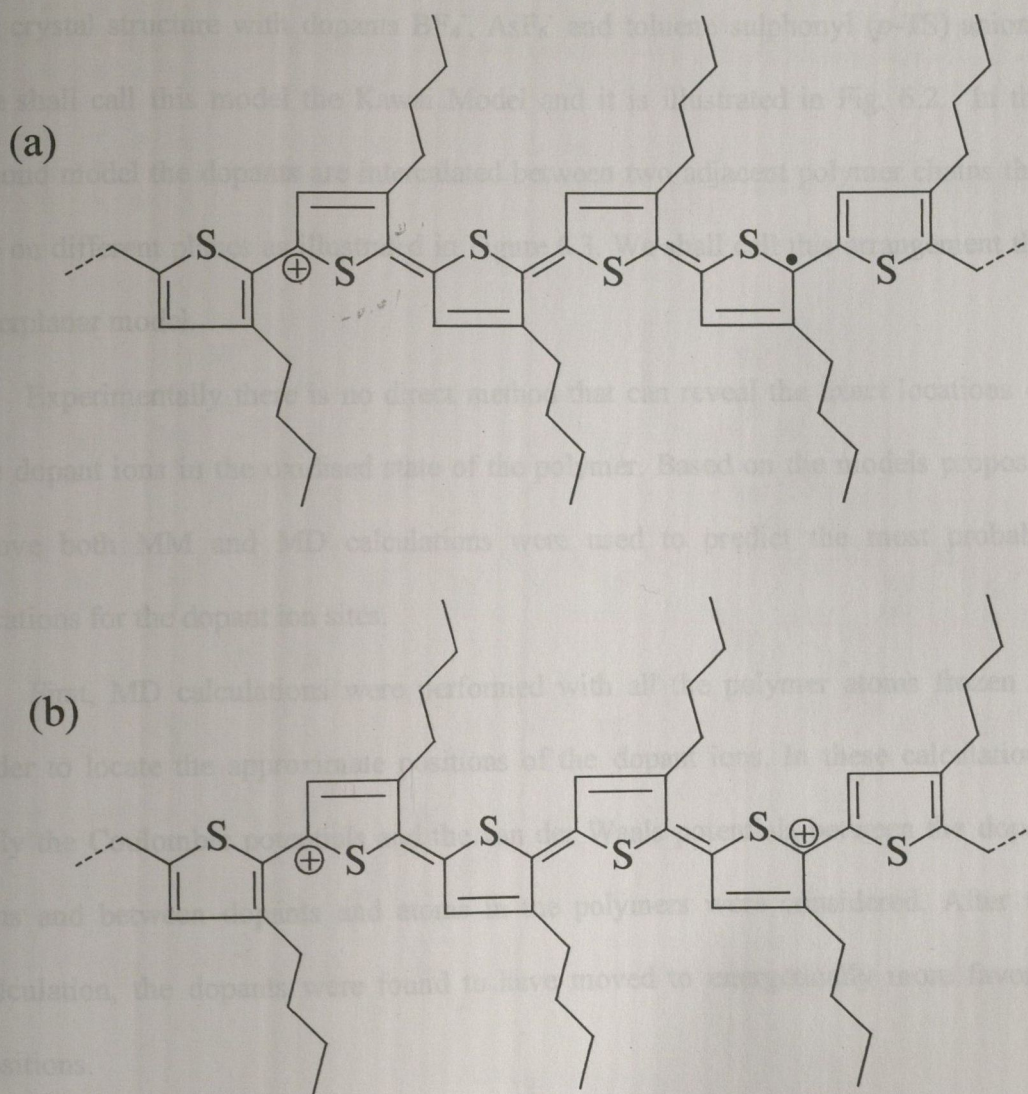


Figure 6.1 The charge distribution associated with (a) a polaron (b) a bipolaron on a P3BT chain, which extends over four thiophene rings.

6.3 Dopant Position and Lattice Structure

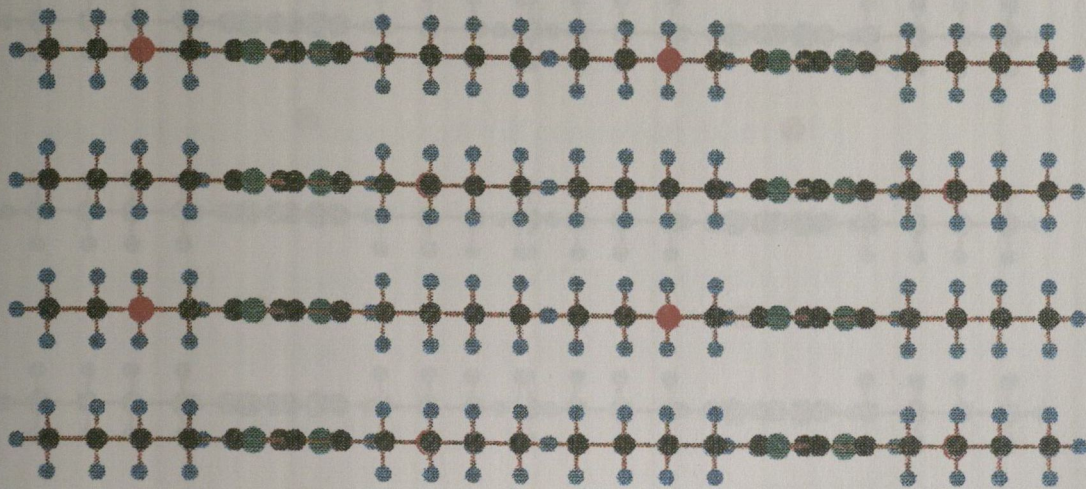
Two possible locations of the dopants are proposed in this simulation. The first is that in which the dopants occupy the sites between adjacent polymer chains that are in the same plane as proposed by Kawai *et al.* [6] from their X-ray diffraction study of the crystal structure with dopants BF_4^- , AsF_6^- and toluene sulphonyl (*p*-TS) anions. We shall call this model the Kawai Model and it is illustrated in Fig. 6.2. In the second model the dopants are intercalated between two adjacent polymer chains that are on different planes as illustrated in Figure 6.3. We shall call this arrangement the interplanar model.

Experimentally there is no direct method that can reveal the exact locations of the dopant ions in the oxidised state of the polymer. Based on the models proposed above both MM and MD calculations were used to predict the most probable locations for the dopant ion sites.

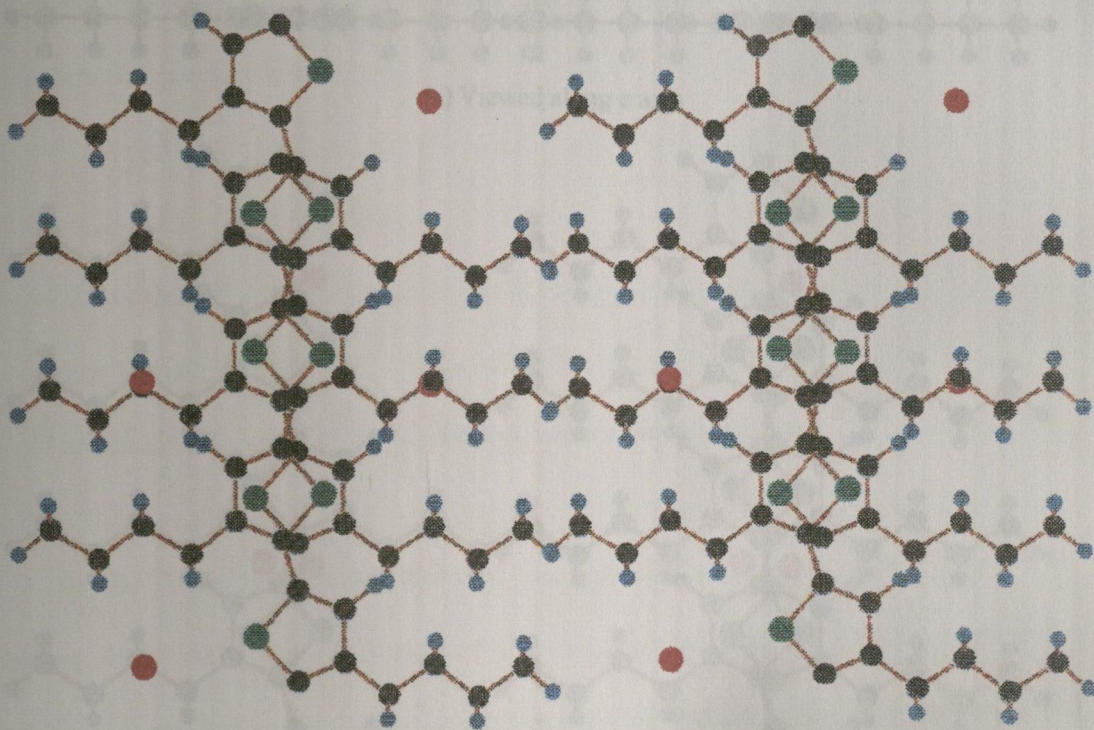
First, MD calculations were performed with all the polymer atoms frozen in order to locate the approximate positions of the dopant ions. In these calculations, only the Coulombic potentials and the van der Waals potentials between the dopant ions and between dopants and atoms in the polymers were considered. After the calculation, the dopants were found to have moved to energetically more favored positions.

Then the energy minimization methods in the GULP code were employed to further optimize these dopant positions by changing its position along *x*, *y*, and *z* directions to lower the energy of the assembly.

In the simulations, an orthorhombic lattice cell was used in accordance with the lattice structure as determined by diffraction [6]. The lattice parameters *a* and *b* were

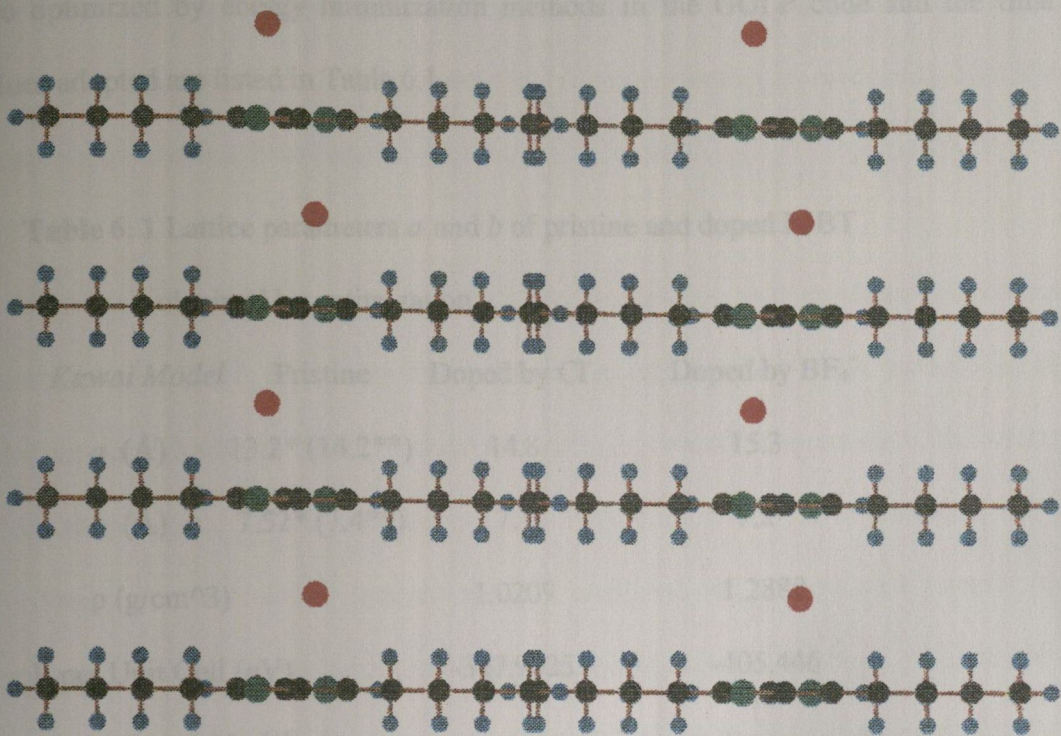


(a) Viewed along c axis

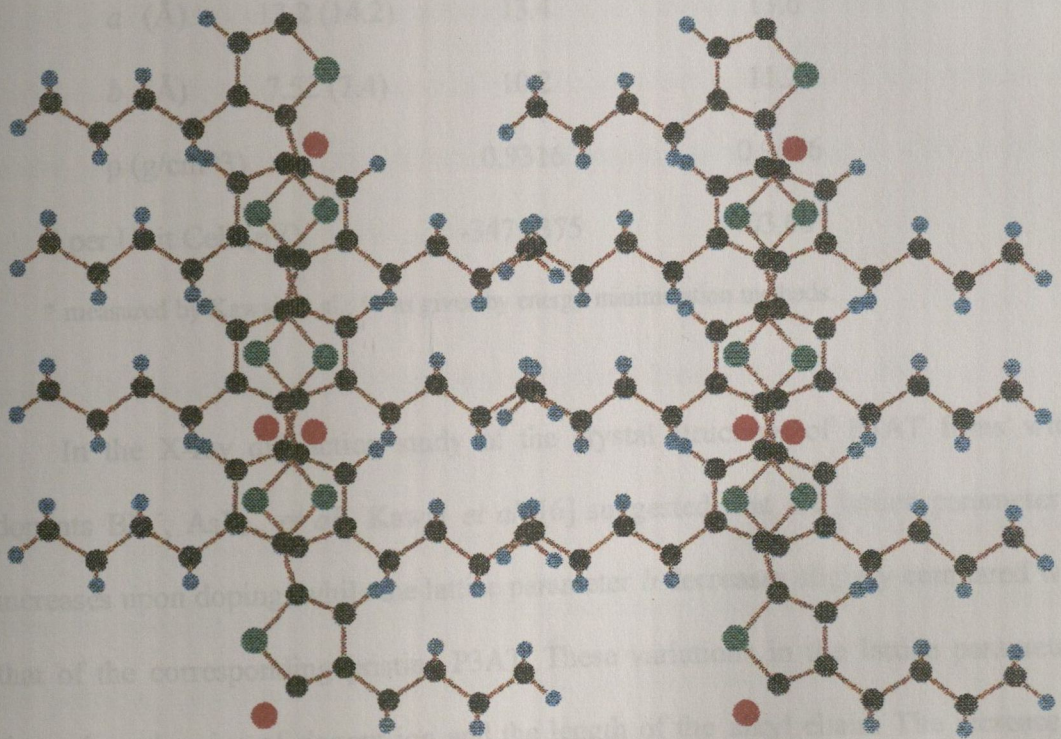


(b) Viewed along b axis

Fig. 6.2 The Kawai structural model for Cl^- doped P3BT. (a) viewed along c axis, (b) viewed along b axis. The atoms in the system are represented by different colors: green – S, gray – C, blue – H and red – dopant ion Cl^- .



(a) Viewed along c axis



(b) Viewed along b axis

Fig. 6.3 The interplanar structural model for Cl⁻ doped P3BT. (a) viewed along c axis, (b) viewed along b axis. The atoms in the system are represented by different colors: green – S, gray – C, blue – H and red – dopant ion Cl⁻.

also optimized by energy minimization methods in the GULP code and the final values adopted are listed in Table 6.1.

Table 6. 1 Lattice parameters a and b of pristine and doped P3BT

obtained by optimization.

<i>Kawai Model</i>	Pristine	Doped by Cl^-	Doped by BF_4^-
a (Å)	13.2* (14.2**)	14.8	15.3
b (Å)	7.52* (7.4**)	7.1	7.2
ρ (g/cm ³)		1.0209	1.2888
E per Unit Cell (eV)		-347.9825	-405.446
<i>Interplanar Model</i>			
a (Å)	13.2 (14.2)	13.4	13.6
b (Å)	7.52 (7.4)	10.2	11.2
ρ (g/cm ³)		0.9316	0.9656
E per Unit Cell (eV)		-347.3375	-403.687

* measured by Kawai, et al.; ** as given by energy minimization methods.

In the X-ray diffraction study of the crystal structural of P3AT films with dopants BF_4^- , AsF_6^- , *et al.*, Kawai *et al.* [6] suggested that the lattice parameter a increases upon doping, while the lattice parameter b decreases slightly compared with that of the corresponding pristine P3AT. These variations in the lattice parameters depend on the size of dopant ion and the length of the alkyl chain. The increase in dopant size would be expected to increase the lattice parameter a but not to change the lattice parameter b greatly. Their measured lattice parameters a and b of P3BT with BF_4^- dopant are 15.1 Å and 7.1 Å, respectively, which show good agreement

with those calculated following the optimization in the energy minimization routine. Kawai *et al.* [6] attributed the decrease of b upon doping to an increase in the attractive interaction between the dopants and the neighboring conjugated electron systems.

For the interplanar model, which is similar to the structure of doped polythiophene [7], we have been unable to find an experimental result with which to compare our calculations. In this model the lattice parameter b increases with the size of dopant, while the lattice parameter a shows little change with the dopant size.

From our calculated lattice energy considerations, the Kawai model is thermodynamically more stable than the interplanar model for both Cl^- and BF_4^- dopants. This is probably due to the better lattice packing in the Kawai model. In this model lattice, the dopant ions are located in a hexahedral (cuboidal) vacant spaces composed of alkyl side chains and polymer main chains, whereas in the interplanar model lattice the dopant ions are intercalated between two adjacent stacked polymer main chains that are in different planes.

6.4 MD Simulation of P3BT Lattice with Dopant Cl^- or BF_4^-

The functions and specified parameters of the atomistic potentials used have been discussed in detail in Chapter 3. The lattice models and the charge distribution in the polymer chains employed were the same as those described in Sections 6.3 and 6.2 of this Chapter. The simulations were carried out on a NVT ensemble for 1000 ps. This long calculation time is good for the investigation of the diffusion of dopant ions in the polymer lattice. In order to allow the calculation of the transport properties of interest, simulations at three temperatures at least are necessary. These have been

done for each of the two lattice models described above and at two different dopant levels. Cl^- and BF_4^- were chosen as dopants because they represent the simplest single-atom dopant and the simplest multiple-atom dopant, respectively. This choice also allows a comparison of the effects of the sizes of dopant ions. The concentrations (doping levels) and temperatures were chosen so that the highest level of mobile species was present in the simulations in order to improve the statistics for the analysis of the system. A 25% doping level was found to be typical in experiments and 50% doping level is possible in the high doping area in real samples. These doping levels ensure that the conducting polymers present typical conductivity. The temperatures of the simulations were chosen firstly, give a reasonable temperature range, 10 K low temperature, 300 K room temperature, 450 K high temperature, and secondly, to ensure that the temperatures of all the simulations were less than the melting point of the polymers so that the polymer lattice structure was maintained. Simulations at other temperatures were also carried out in order to estimate the activation energy of diffusion.

The simulations were performed at atmospheric pressure. The procedure and program codes are the same as those described in Chapter 4. The results are shown in the following sections and include both MSD (mean square displacement) curves of dopants and RDF (radial distribution function) plots for chosen atoms of the dopant and the polymer. The MSD curves are used to evaluate the absolute diffusion coefficients and also the activation energy of diffusion. The trajectories of the MD calculations are also analyzed in order to understand the movement of dopants and the effect of the doping on polymer dynamical conformations.

6.4.1 Cl⁻ doped P3BT Lattice

As mentioned in Chapter 1 it has been established that π -conjugated conducting polymers undergo a semiconductor to metal transition at a critical dopant concentration at mole ratio of 0.1 to 0.12 between dopant and polymer. The number of structural units comprising the polymer could vary from chain to chain in real samples. Here we define the doping level of the Cl⁻ and BF₄⁻ dopants in P3BT as a percentage doping level using the occupancy of dopant sites with respect to the thiophene rings as described in Section 6.2. Experimentally 100% doping level has never been reported in conducting polymers. However, doping levels in the range of 25-50% occur with, the actual value depending on the experimental conditions of the polymer synthesis and the nature of the dopant [8-9]. In these simulations we consider the influence of concentration of dopants to the transport behavior at 25% and 50% doping levels.

6.4.1.1 P3BT Doped at 25% level with Cl⁻

Because no reliable lattice structural model is available for the Cl⁻ doped P3BT lattice, we use two different trial structural models (Kawai and interplanar) as discussed above. In each model, two different distributions of the positive charge are applied in the polymer chains to balance the negative charge of doped Cl⁻ ions and to ensure a zero total charge in the simulation system. These charge distributions have been discussed in Section 6.2.

The MSD plots for the Cl⁻ ion at three temperatures are shown in Figure 6.4 to 6.7 for the different models. As can be seen most plots are adequate to allow the slope

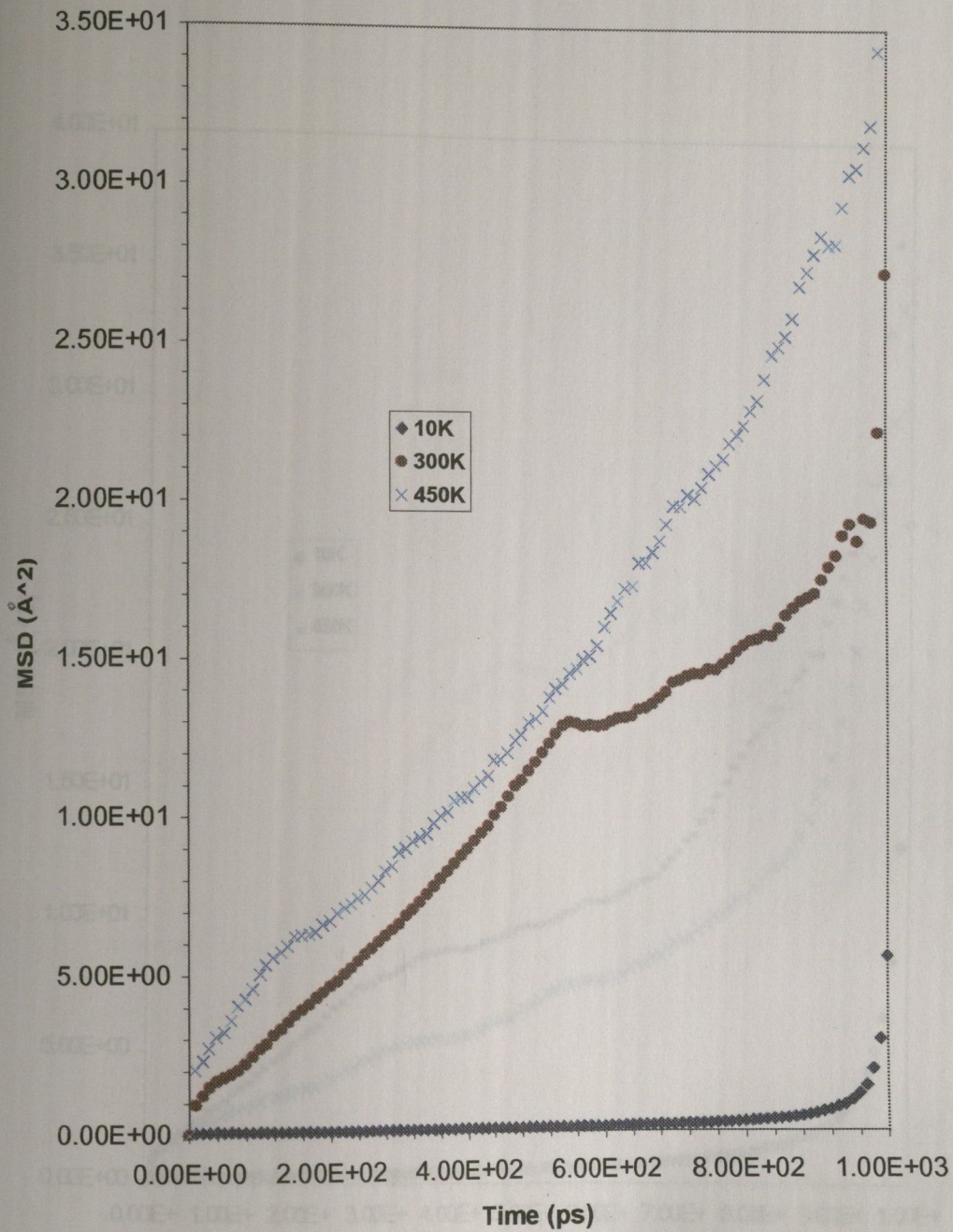


Fig. 6.4 MSD of Cl⁻ in 25% Cl⁻ doped P3BT lattice at 10, 300 and 450 K (the Kawai structural model and the charges evenly distributed in the in the polymer main chains).

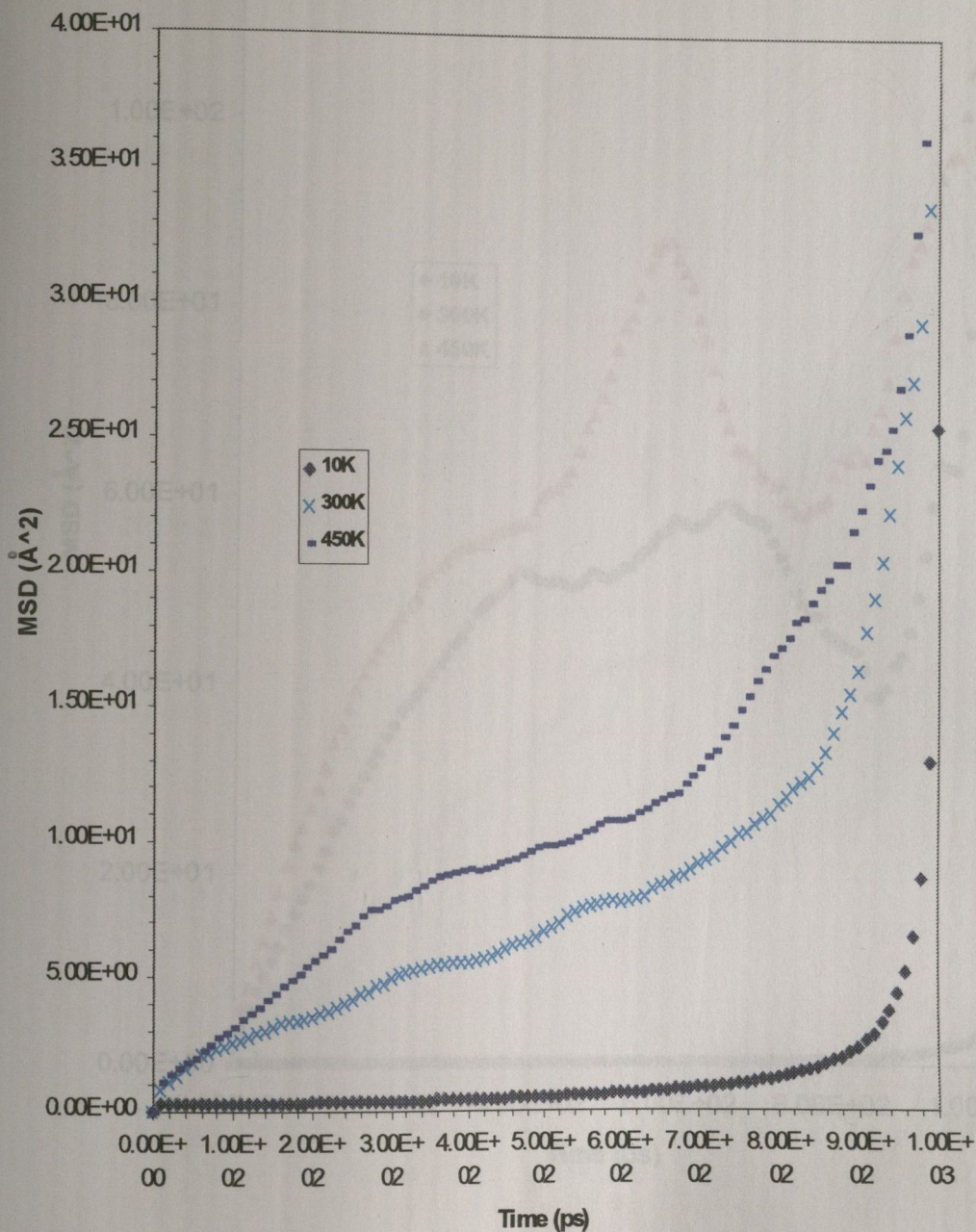


Fig. 6.5 MSD of Cl⁻ in 25% Cl⁻ doped P3BT lattice at 10, 300 and 450 K (the

Kawai structural model and polaron charge model in the polymer main chains).

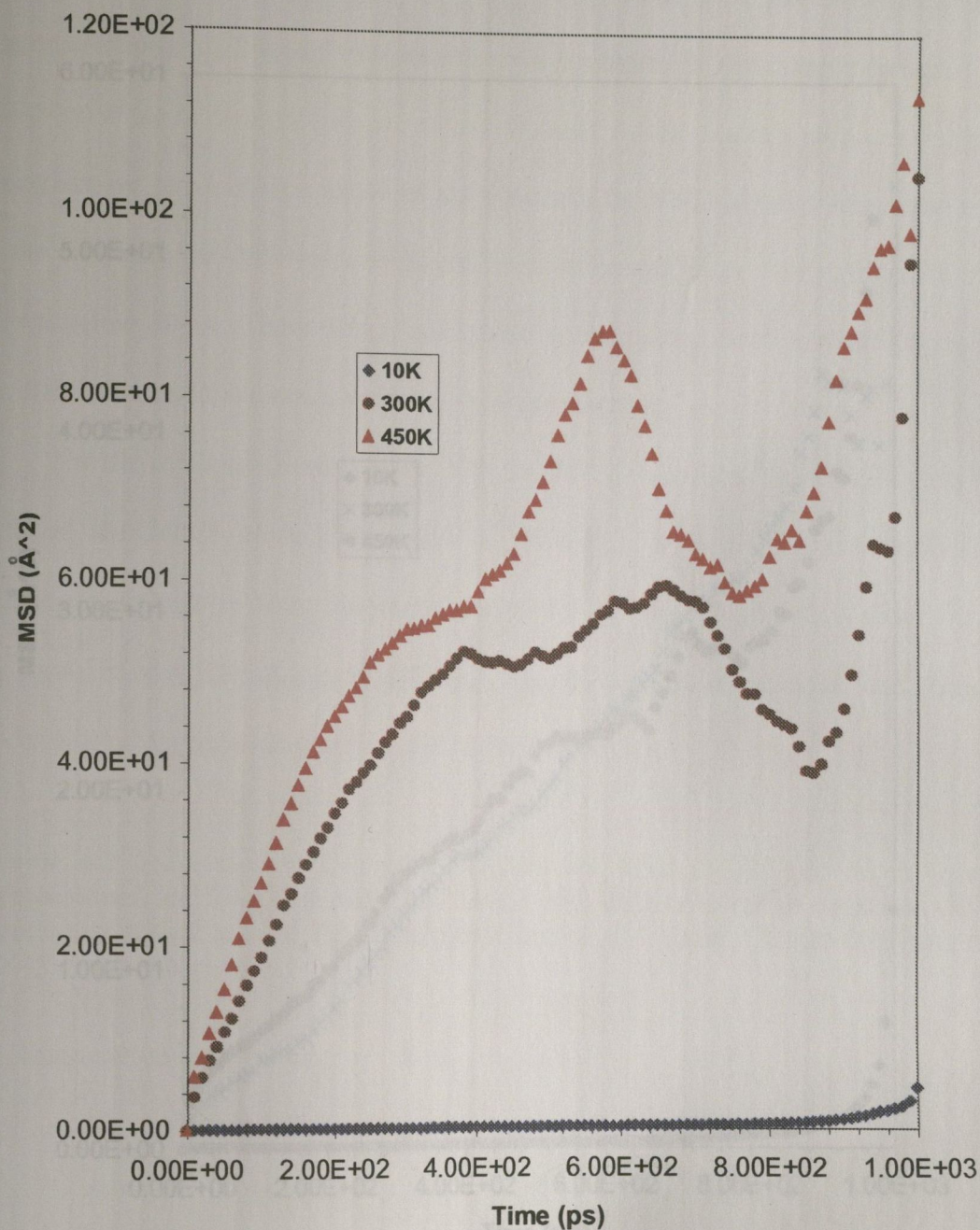


Fig. 6.6 MSD of Cl⁻ in 25% Cl⁻ doped P3BT lattice at 10, 300 and 450 K (the interplanar structural model and the charges evenly distributed in the polymer main chains).

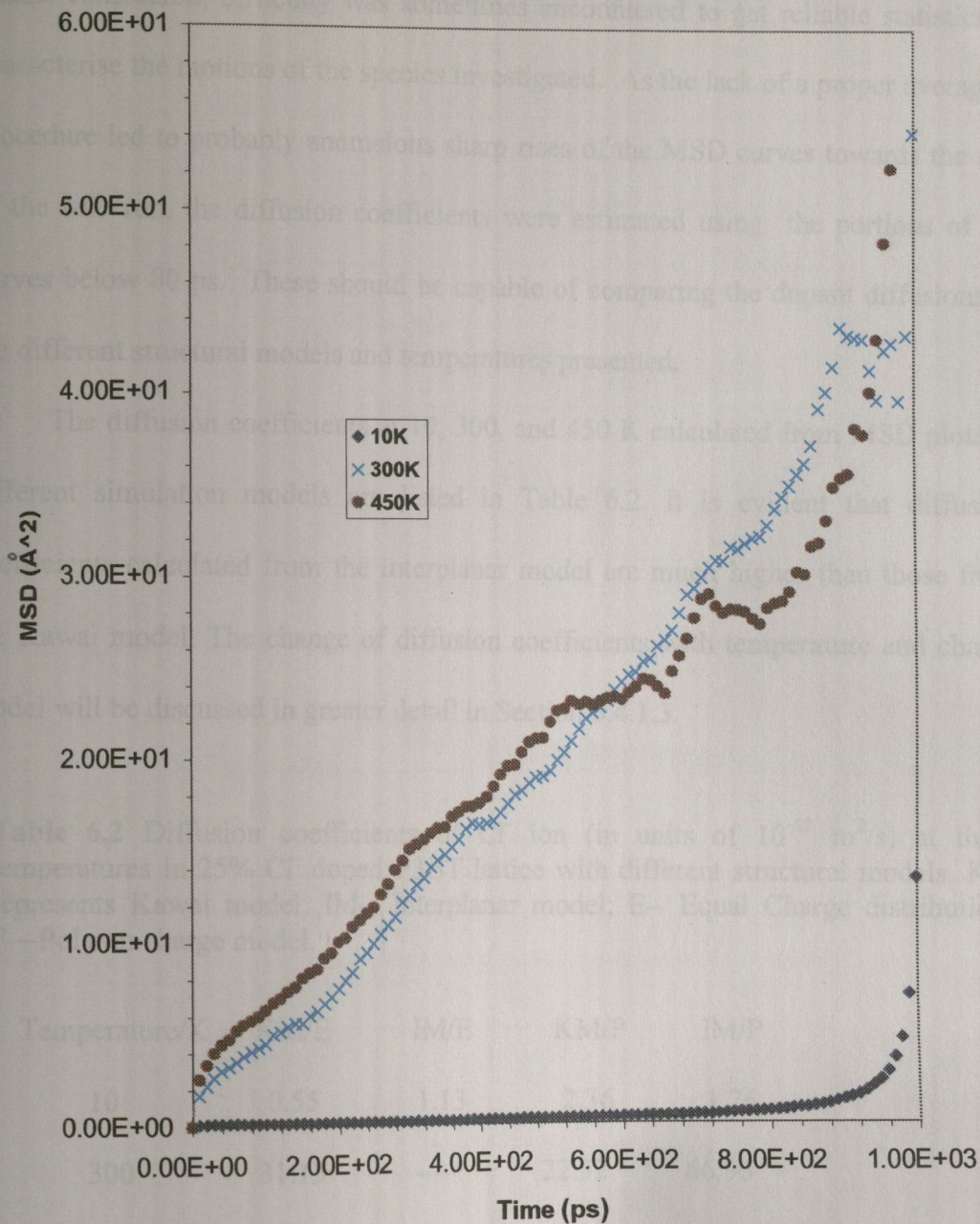


Fig. 6.7 MSD of Cl⁻ in 25% Cl⁻ doped P3BT lattice at 10, 300 and 450 K (the interplanar structural model and polaron charge model in the polymer main chains).

of the central region to be evaluated so that the value of the diffusion coefficient of the Cl^- ion can be determined. Probably due to too small a number of dopants and chains considered, difficulty was sometimes encountered to get reliable statistics to characterise the motions of the species investigated. As the lack of a proper averaging procedure led to probably anomalous sharp rises of the MSD curves towards the *end* of the MD run, the diffusion coefficients were estimated using the portions of the curves below 80 ps. These should be capable of comparing the dopant diffusions in the different structural models and temperatures presented.

The diffusion coefficients at 10, 300, and 450 K calculated from MSD plots in different simulation models are listed in Table 6.2. It is evident that diffusion coefficients calculated from the interplanar model are much higher than those from the Kawai model. The change of diffusion coefficients with temperature and charge model will be discussed in greater detail in Section 6.4.1.3.

Table 6.2 Diffusion coefficients of Cl^- ion (in units of $10^{-12} \text{ m}^2/\text{s}$) at three temperatures in 25% Cl^- doped P3BT lattice with different structural models. KM represents Kawai model; IM-- Interplanar model; E-- Equal Charge distribution; P—Polaron charge model.

Temperature/K	KM/E	IM/E	KM/P	IM/P
10	0.55	1.13	2.36	1.26
300	31.15	----*	22.52	66.96
450	44.63	----	34.82	68.62

* No diffusion coefficient is calculated due to inadequate statistics for these conditions.

The diffusion coefficient, D , increases with temperature. However, a plot of $\log D$ vs. reciprocal Kelvin temperature does not increase linearly as would be expected for diffusion of small molecules or ions in a lattice. It will be shown later

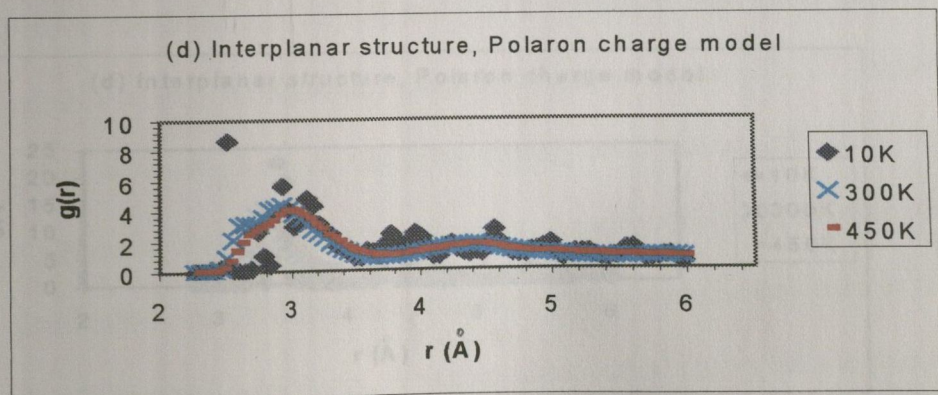
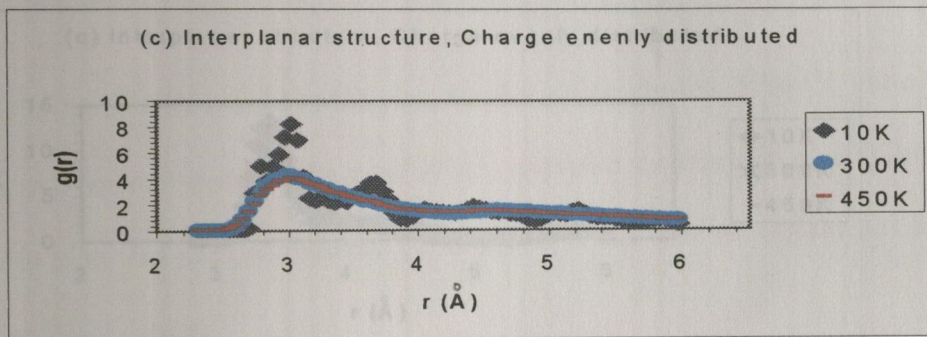
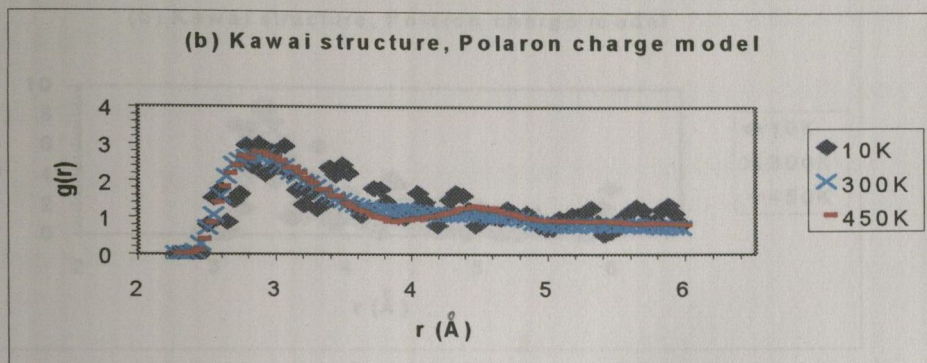
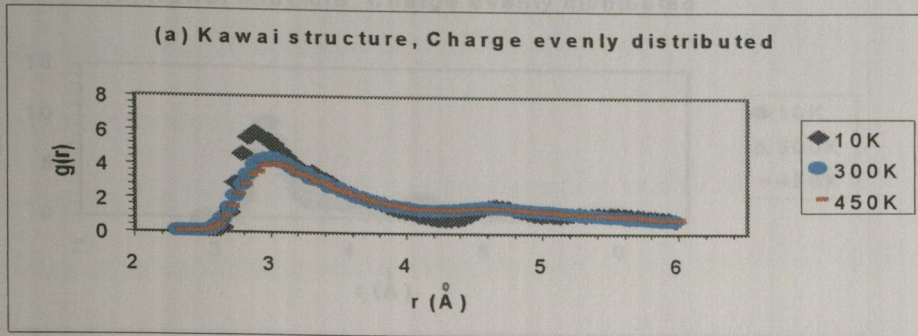


Fig. 6.8. RDF of C-Cl in 25% Cl⁻ doped P3BT lattice with different models.

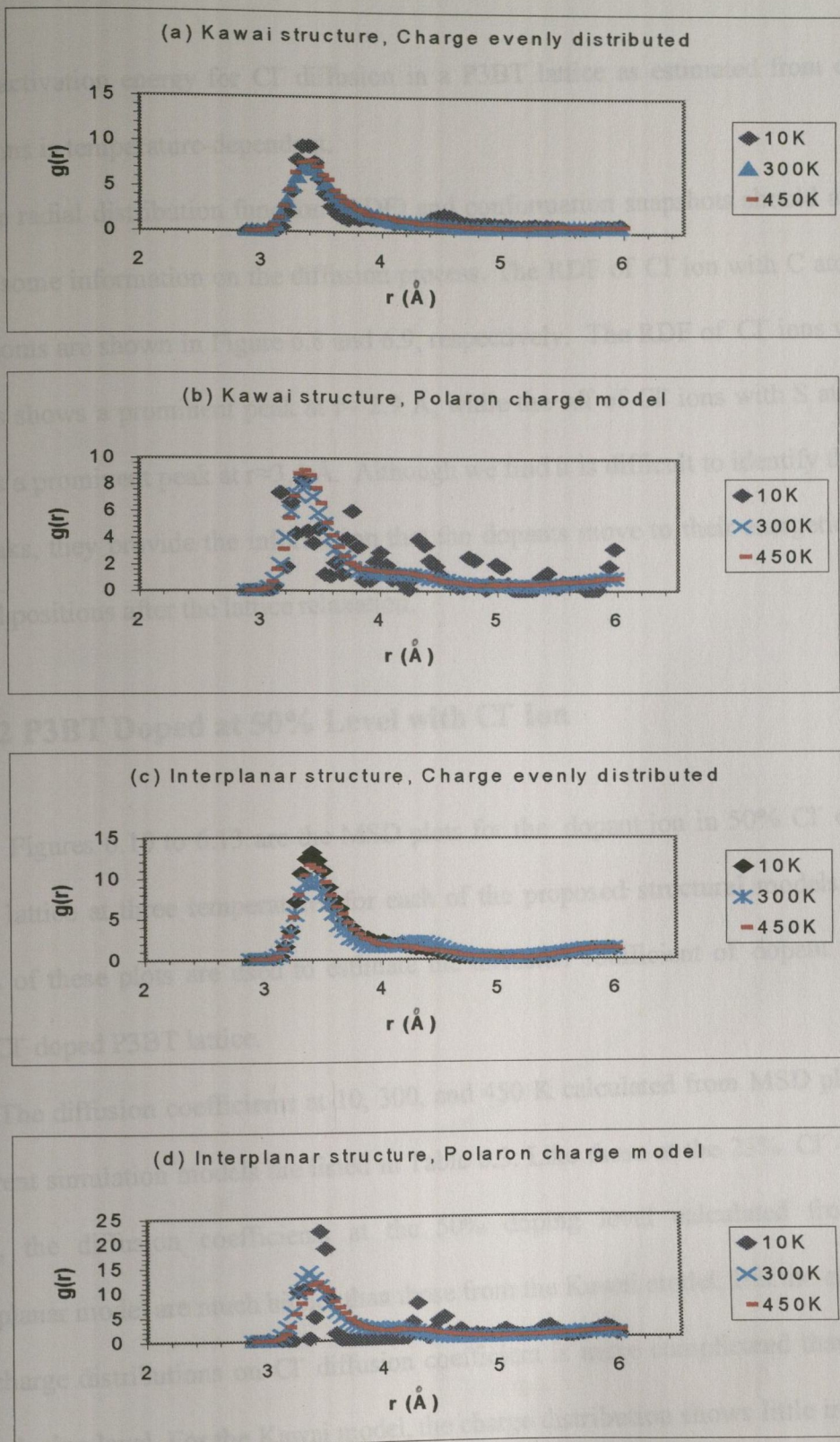


Fig. 6.9. RDF of S-Cl in 25% Cl⁻ doped P3BT lattice with different models.

that the activation energy for Cl^- diffusion in a P3BT lattice as estimated from our simulations is temperature-dependent.

The radial distribution function (RDF) and conformation snapshots should also provide some information on the diffusion process. The RDF of Cl^- ion with C atoms and S atoms are shown in Figure 6.8 and 6.9, respectively. The RDF of Cl^- ions with C atoms shows a prominent peak at $r \approx 2.9 \text{ \AA}$, while the rdf of Cl^- ions with S atoms presents a prominent peak at $r \approx 3.4 \text{ \AA}$. Although we find it is difficult to identify these two peaks, they provide the information that the dopants move to their energetically favored positions after the lattice relaxation.

6.4.1.2 P3BT Doped at 50% Level with Cl^- Ion

Figures 6.10 to 6.13 are the MSD plots for the dopant ion in 50% Cl^- doped P3BT lattice at three temperatures for each of the proposed structural models. The slopes of these plots are used to estimate the diffusion coefficient of dopant ion in 50% Cl^- doped P3BT lattice.

The diffusion coefficients at 10, 300, and 450 K calculated from MSD plots in different simulation models are listed in Table 6.3. Like those at the 25% Cl^- doping level, the diffusion coefficients at the 50% doping level calculated from the interplanar model are much higher than those from the Kawai model. But the effect of the charge distributions on Cl^- diffusion coefficient is more complicated than at the 25% doping level. For the Kawai model, the charge distribution shows little influence on the Cl^- diffusion coefficient. For the interplanar model, at 300 K the diffusion coefficient of Cl^- is four times higher in the lattice with evenly charge distribution than that with bipolaron charge model; but at 450 K the diffusion coefficient of Cl^- is

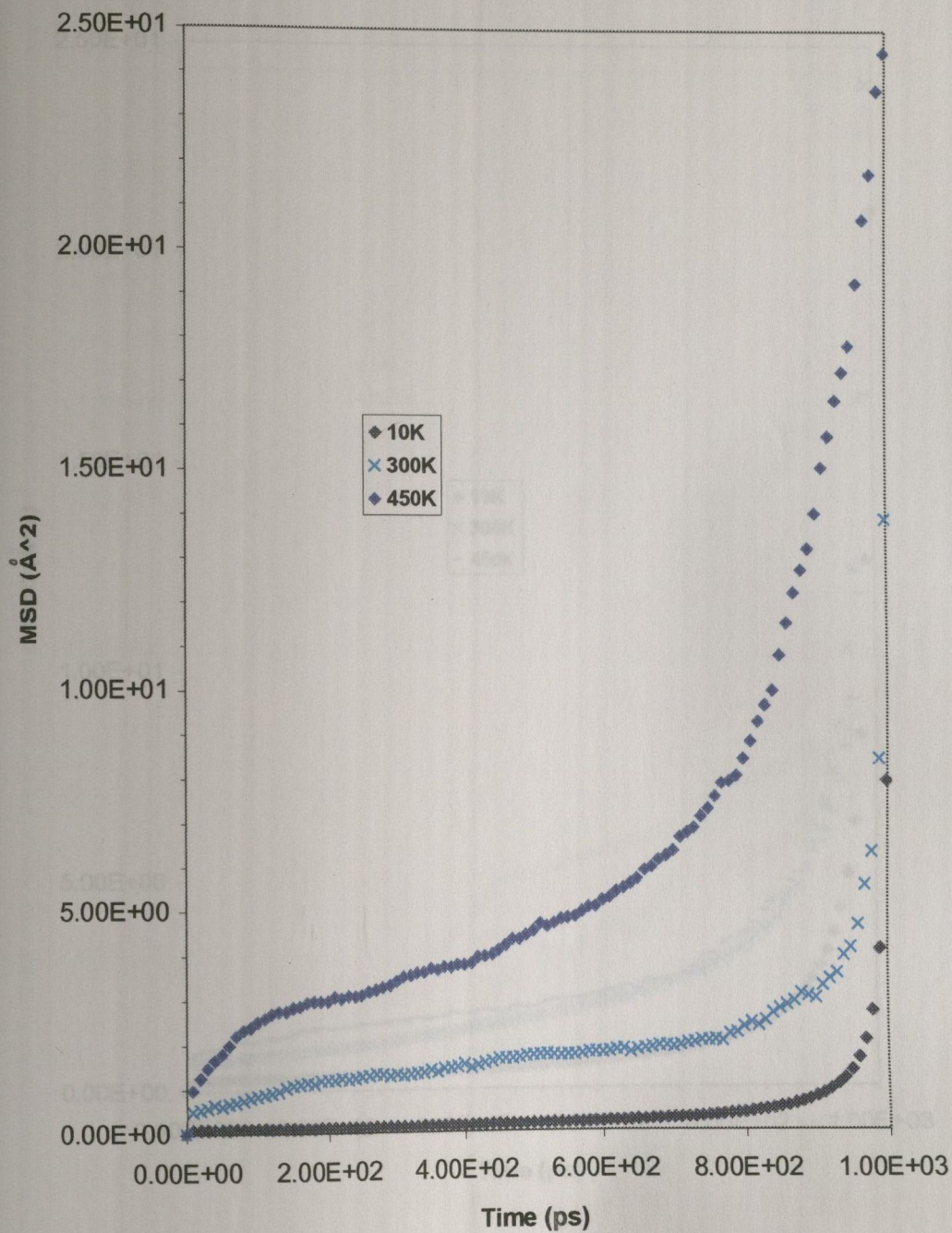


Fig. 6.10 MSD of Cl⁻ in 50% Cl⁻ doped P3BT lattice at 10, 300, 450 K (the Kawai structural model and the charges evenly distributed in the polymer main chains).

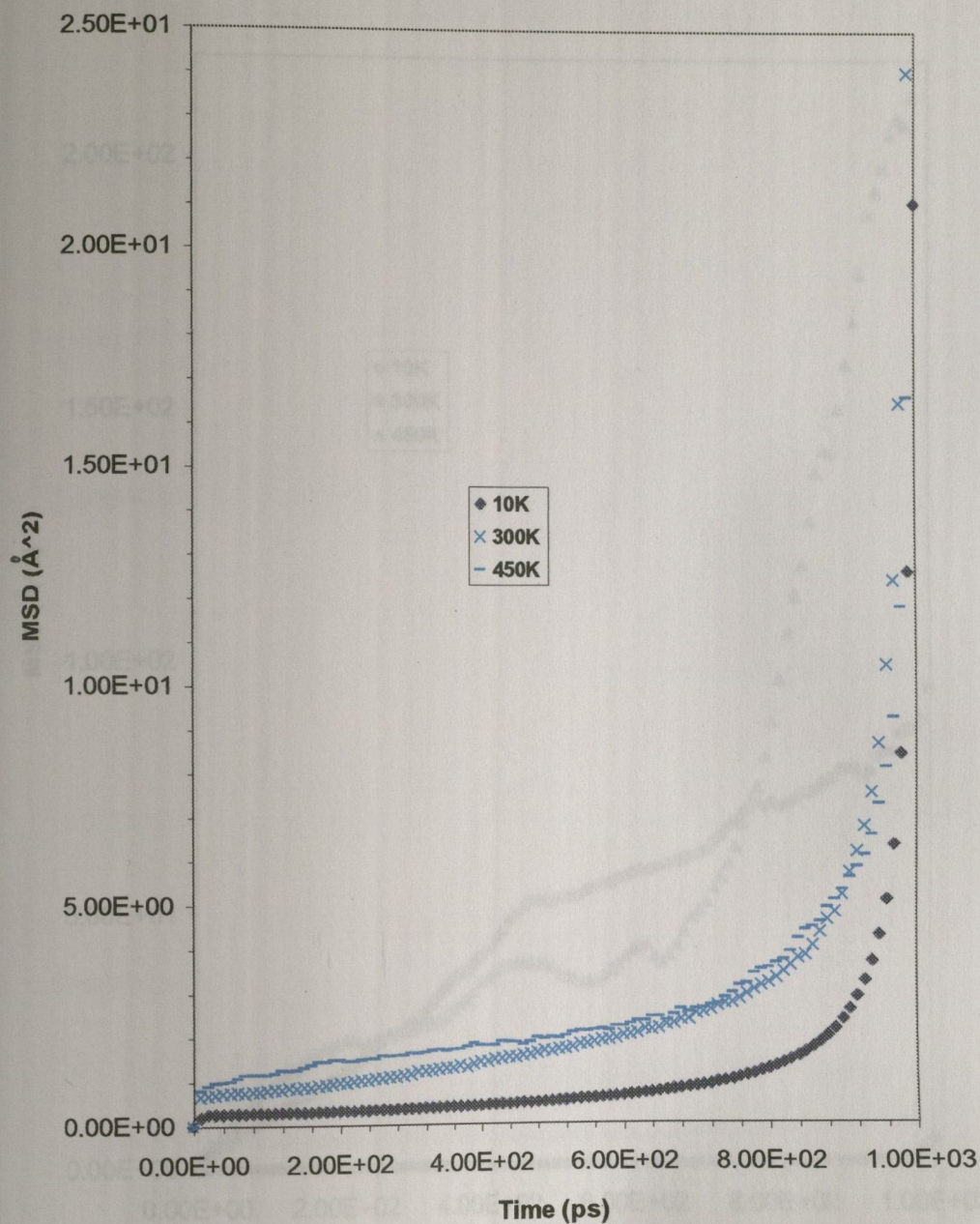


Fig. 6.11 MSD of Cl⁻ in 50% Cl⁻ doped P3BT lattice at 10, 300 and 450 K (the Kawai structural model and bipolaron charge model in the polymer main chains).

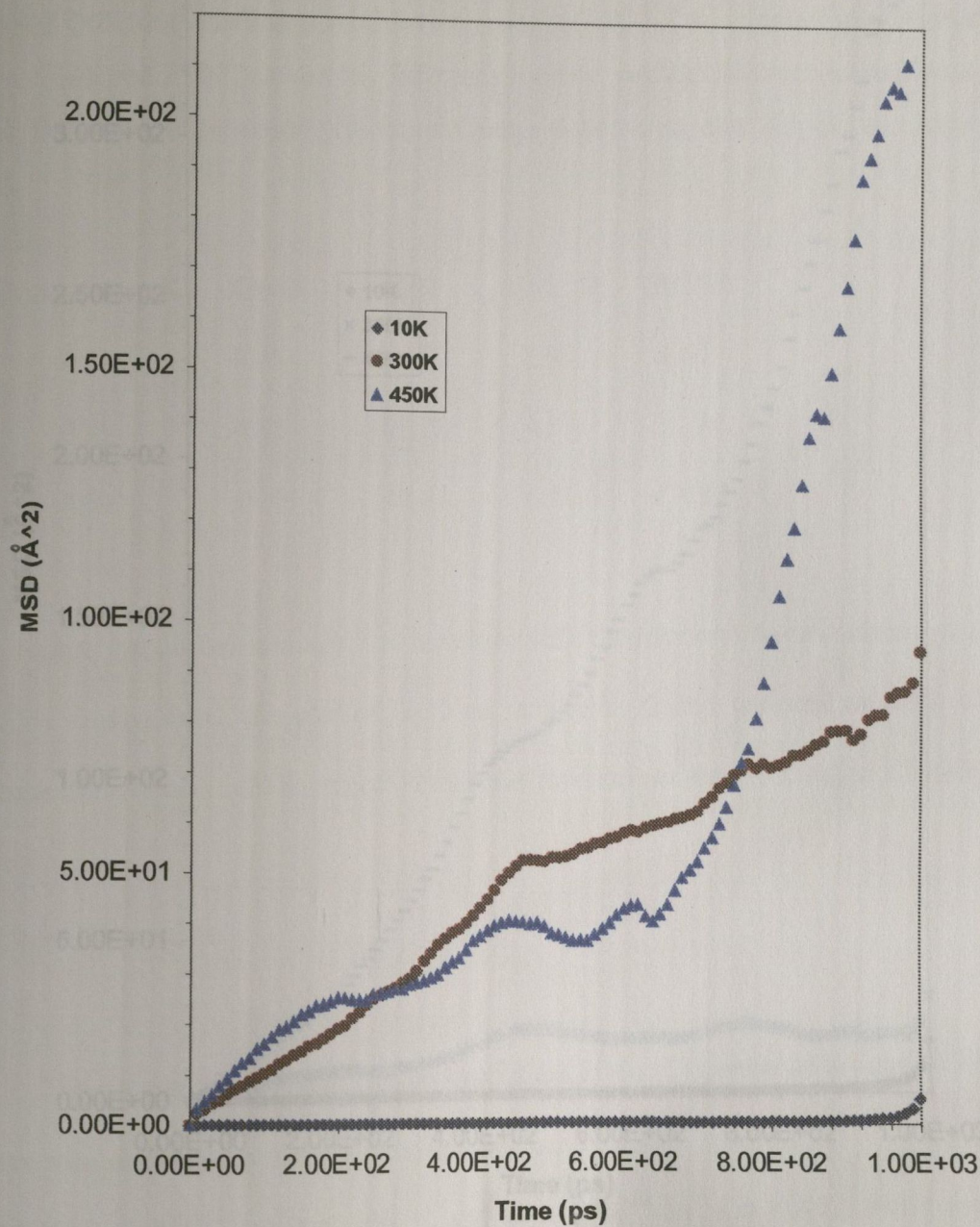


Fig. 6.12 MSD of Cl⁻ in 50% Cl⁻ doped P3BT lattice at 10, 300 and 450 K (the interplanar structural model and the charges evenly distributed in the polymer main chains).

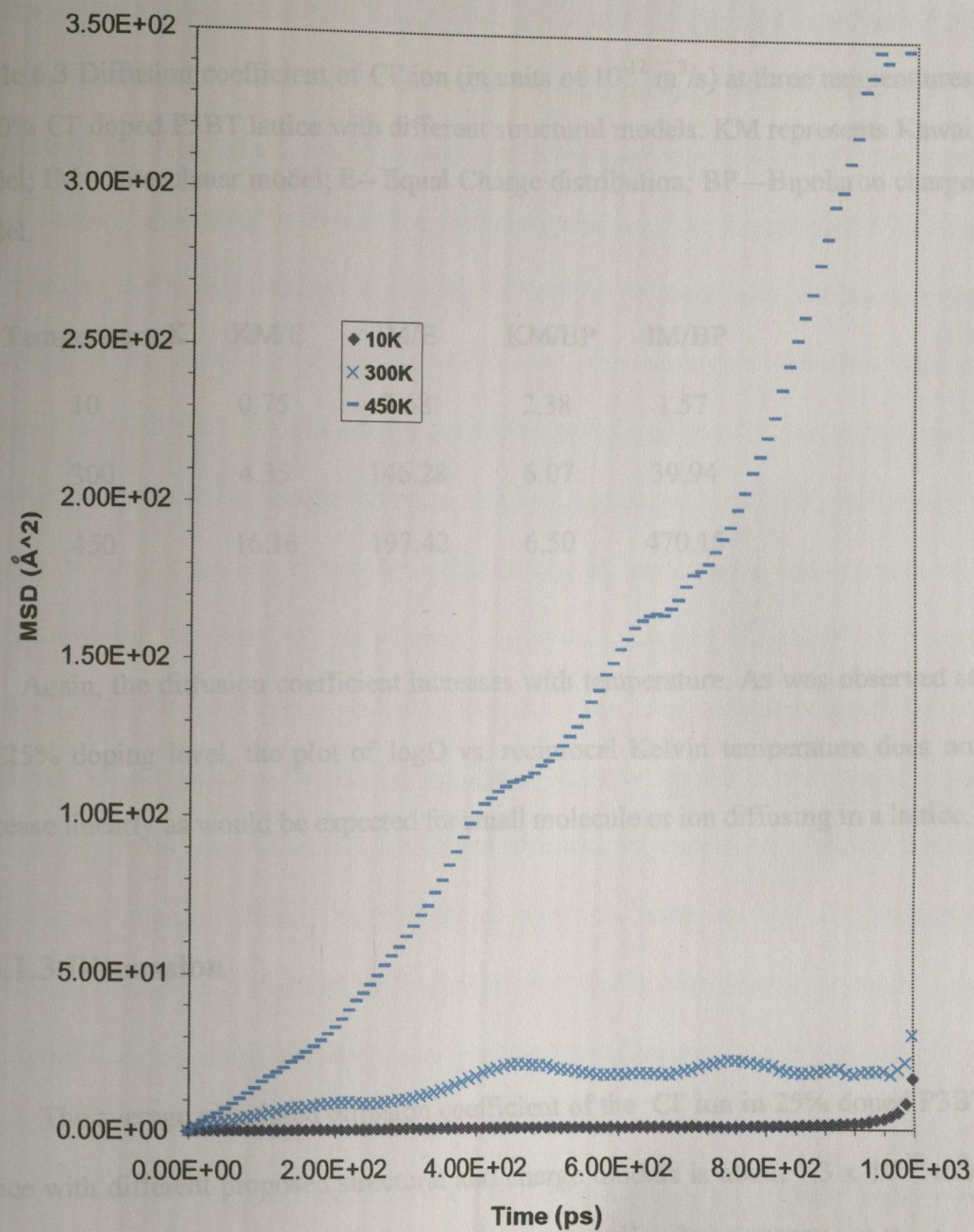


Fig. 6.13 MSD of Cl⁻ in 50% Cl⁻ doped P3BT lattice at 10, 300 and 450 K (the interplanar structural model and bipolaron charge model in the polymer main chains).

two times lower in the lattice with even charge distribution than it was in that with bipolaron charge model.

Table 6.3 Diffusion coefficient of Cl⁻ ion (in units of 10⁻¹² m²/s) at three temperatures in 50% Cl⁻ doped P3BT lattice with different structural models. KM represents Kawai model; IM-- Interplanar model; E-- Equal Charge distribution; BP—Bipolaron charge model.

Temperature/K	KM/E	IM/E	KM/BP	IM/BP
10	0.75	0.68	2.38	1.57
300	4.35	146.28	6.07	39.94
450	16.16	197.42	6.50	470.15

Again, the diffusion coefficient increases with temperature. As was observed at the 25% doping level, the plot of logD vs. reciprocal Kelvin temperature does not increase linearly as would be expected for small molecule or ion diffusing in a lattice.

6.4.1.3 Discussion

The average calculated diffusion coefficient of the Cl⁻ ion in 25% doped P3BT lattice with different proposed structural and charge models is about 1.3 x 10⁻¹² m²/s at 10 K, 51.6 x 10⁻¹² m²/s at 300 K, and 66.5 x 10⁻¹² m²/s at 450K; while those calculated for 50% doped P3BT lattice are 1.3 x 10⁻¹² m²/s at 10 K, 49.1 x 10⁻¹² m²/s at 300 K, and 172.4 x 10⁻¹² m²/s at 450 K. No measurements of the diffusion coefficient of Cl⁻ in P3ATs system have been reported. However, Tezuka, *et al.* [10] reported that the diffusion coefficient of ClO₄⁻ ion in polythiophene film was about 3

$\times 10^{-14} \text{ m}^2/\text{s}$ at room temperature. Mohammad [11] has studied the diffusion of dopants into and out of electrochemically prepared polythiophene films in electrochemical cells containing BF_4^- , ClO_4^- , AsF_6^- and SbF_6^- ions. He suggested that the dopant diffusion rates are in the range of $10^{-18} \text{ m}^2/\text{s}$ to $10^{-14} \text{ m}^2/\text{s}$ at 273 K. Compared to these values, our diffusion coefficients are much higher (at least 100 times larger). This may be due to the following reasons. The first is that P3BT (as represented in the calculations) is a highly crystalline polymer with a self-assembled structure as discussed in Chapter 1, which may provide higher diffusion rates of dopants in P3BT than that in partially crystalline polythiophene. The second reason is that the process of the dopant diffusion in a real sample of conducting polymers is seen to be very complex. It may be influenced by a simultaneous involvement of a charge-transfer reaction of the dopant with the polymer, reaction of dopant (counterion) with the polymer chain and interchain reactions such as crosslinking and swelling of the polymer by the doping agent. Another reason is that since a real sample of polythiophene contains both crystalline and amorphous regions, the dopants in different regions should have different diffusion rates so that the measured diffusion coefficient is decided by the lowest one. In our simulation, we neglect the amorphous region and the other possible complex influences in the real sample of conducting polymers.

In Morrison's [12] MD study of lithium triflate diffusion in polymer electrolyte, polyethylene oxide (PEO), he calculated from MSD plots that the diffusion coefficients of both Li^+ and triflate anion are in the range of $1\text{-}100 \times 10^{-12} \text{ m}^2/\text{s}$. They are in the same scale as our results. PEO is semicrystalline and the structural model used in Morrison's simulations is amorphous. We are not interested in comparing them on a basis of molecular structures but we know PEO is a good electrode material

in Li^+ batteries [12]. So from the magnitudes of the diffusion coefficients of its dopant ions, regioregular HT-P3BT might be expected to constitute a potential electrode material.

If the diffusion rates calculated here are even approximately correct for crystalline P3ATs, then doped P3ATs should be good materials for battery applications, where the rates of charge and discharge are determined by diffusion and values around $10^{-12} \text{ m}^2/\text{s}$ are ideal. These applications are possible, since regioregular HT-P3ATs also show much higher conductivity than does polythiophene.

At low temperatures (10 K), the diffusion coefficients calculated from all the proposed models are in the region of $1 \times 10^{-12} \text{ m}^2/\text{s}$. The doping level also appears to have little influence on the dopant diffusion rates at low temperature. But the diffusion rates increase with temperature. At room temperature (300 K) and at the higher temperature (450 K), the diffusion rates calculated from interplanar model are 3 to 10 times higher than those from the Kawai model. This is because in the Kawai model, the Cl^- dopants are located in the hexahedral vacant sites enclosed by two polymer main chains and three alkyl side chains in the same plane and two other alkyl side chains in the adjacent planes as shown in Figure 6.2. If the dopant migrates, it has to cross over one of the side or main chains that enclose it. But in the interplanar model, the dopants are located between two polymer main chains (Figure 6.3). They can migrate along the polymer main chain direction without any obstruction. At these temperatures, the diffusion coefficients increase with doping level for the interplanar model, however, they decrease with increasing doping level for the Kawai model. The charge model in the polymers shows limited influence on the diffusion coefficients, especially for the Kawai structural model.

The Cl^- ions appear to be capable of a high mobility in the P3BT polymer lattice. Not only are the calculated diffusion coefficients of Cl^- in the P3BT lattice much higher than those reported for the dopants in polythiophene but the activation energies of Cl^- diffusion calculated from our simulations are much lower than the values reported for the dopants in polythiophene or other conducting polymers. Figure 6.14 shows the plot of $\log D$ as a function of reciprocal Kelvin temperature at 50% doping level in P3BT lattice for the Kawai model. This is not a linear relationship. Below 250 K, the activation energy, E_a , given by its slope is 2.7 kJ mol^{-1} . Above this temperature the value of E_a is $11.82 \text{ kJ mol}^{-1}$. The value of E_a for Cl^- diffusion in P3BT lattice calculated for the other models and doping levels that we used is more or less about 10 kJ mol^{-1} . The reported activation energies for dopants diffusion in polythiophene or polypyrrole are approximately 100 kJ mol^{-1} [11,13]. These calculated results again suggest that the dopants should be highly mobile in the P3BT lattice and that regioregular HT-P3AT should show high ionic conductivity.

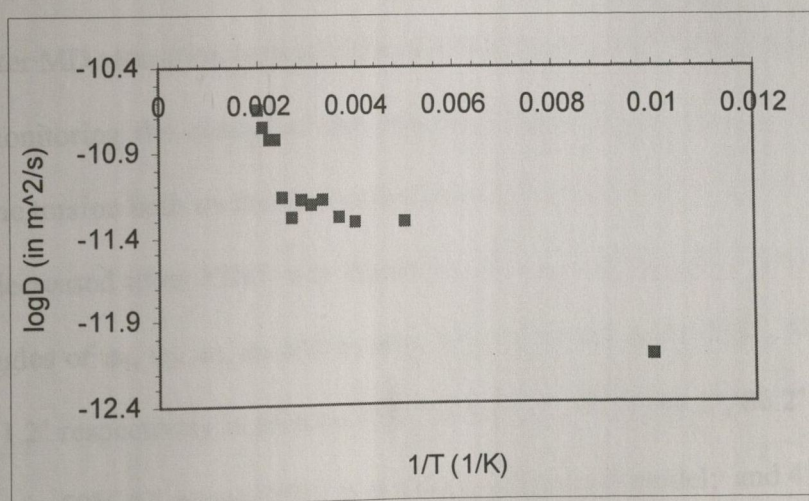


Fig. 6.14 LogD of Cl^- as a function of reciprocal Kelvin temperature at 50% doping level in the Kawai structural model with even charge distribution.

From the snapshots of conformation, we also found that the doping increases the structural order of P3BT especially at 50% doping level. Figures 5.15 to 5.16 compare the conformation of pristine P3BT and 50% Cl⁻ doped P3BT after relaxation with the Kawai or interplanar structural models at 300 and 400 K, respectively. At high temperature, the conformation of P3BT in both the Kawai and interplanar models is much more ordered after doping than is that of the pristine form. This may be due to the electrostatic interaction between the dopants and the polymers.

When dopants are placed in the Kawai model, the polymer main chains are stacked along the **b** axis and show alternating shifts along the \pm **a** axes in the conformations at both temperatures. This does not happen for the interplanar model. Whether or not it actually occurs in practice we just do not know, but it suggests that the dopant Cl⁻ ions like to be associated with both the alkyl side chains (as in the Kawai model) and with the main-chain thiophene rings (as in the interplanar model). The dopants keep the polymer main chains stacked linearly along the **b** axis in the interplanar structural model. This kind of linear stack of the polymers was found to disappear after MD relaxation both at 300 and 400 K in the case of pristine P3BT.

By monitoring the change of the torsional angles φ_1 , φ_2 , φ_3 , φ_4 and φ_5 , we found that the torsion both on the alkyl side chains and between main-chain thiophene rings was decreased after P3BT was doped by Cl⁻. At 400 K, the mean values of torsional angles of φ_1 , φ_2 , φ_3 , φ_4 and φ_5 after MD relaxation were 63.2°, 49.9°, 56.5°, 89.7° and 31.2° respectively in pristine P3BT, but 48.9°, 42.5°, 44.2°, 86.2° and 23.7°, respectively, in 50% Cl⁻ doped P3BT in the Kawai structural model; and 47.1°, 38.7°, 45.6°, 89.4° and 23.4°, respectively, in 50% Cl⁻ doped P3BT in the interplanar structural model.

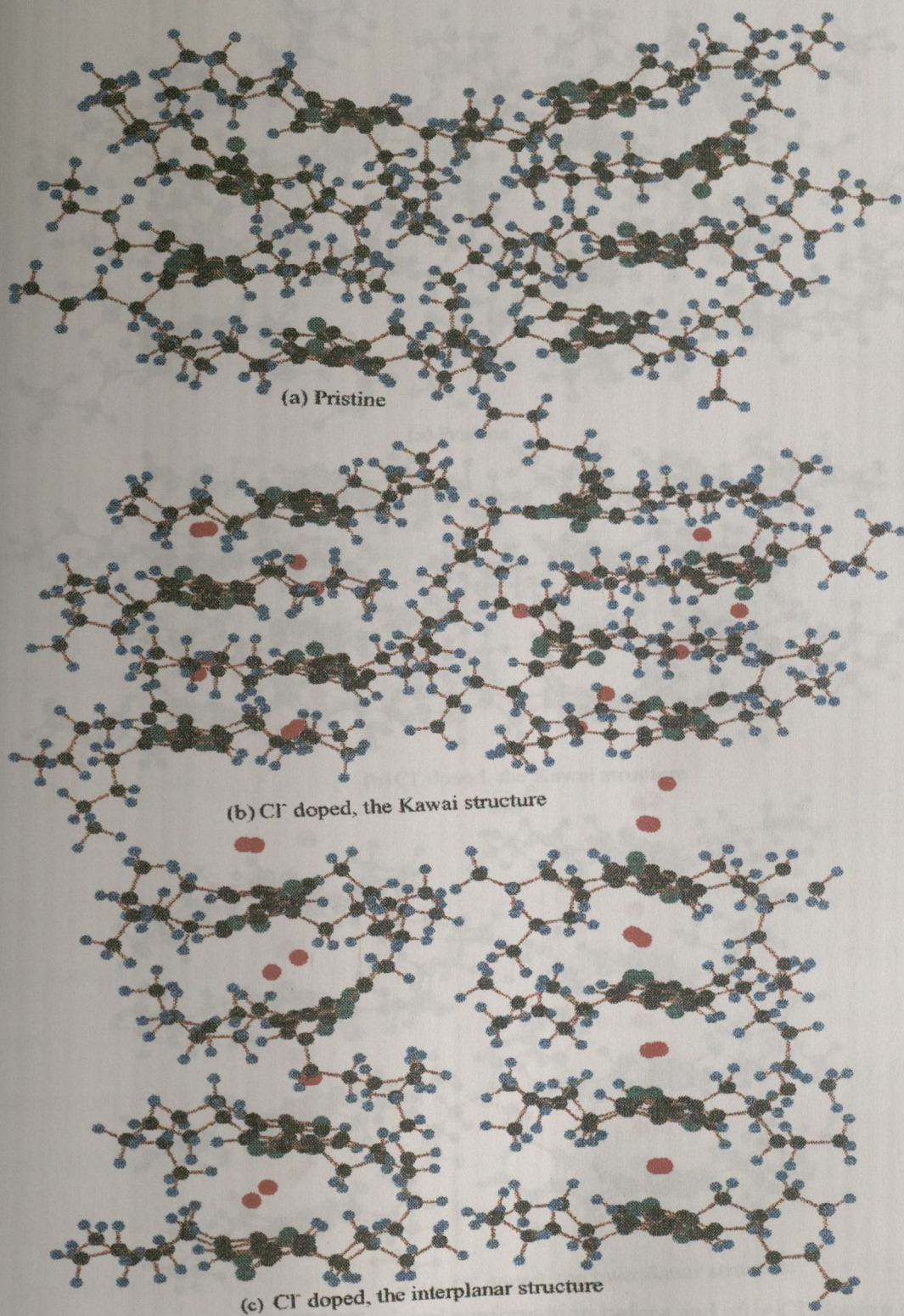


Fig. 6.15 A comparison of P3BT relaxed conformation before and after Cl⁻ doping at 50% doping level at 300 K. (a) Pristine, (b) Cl⁻ doped, the Kawai structure, (c) Cl⁻ doped, the interplanar structure. The atoms in the system are represented by different colors: green – S, gray – C, blue – H and red – dopant ion Cl⁻.

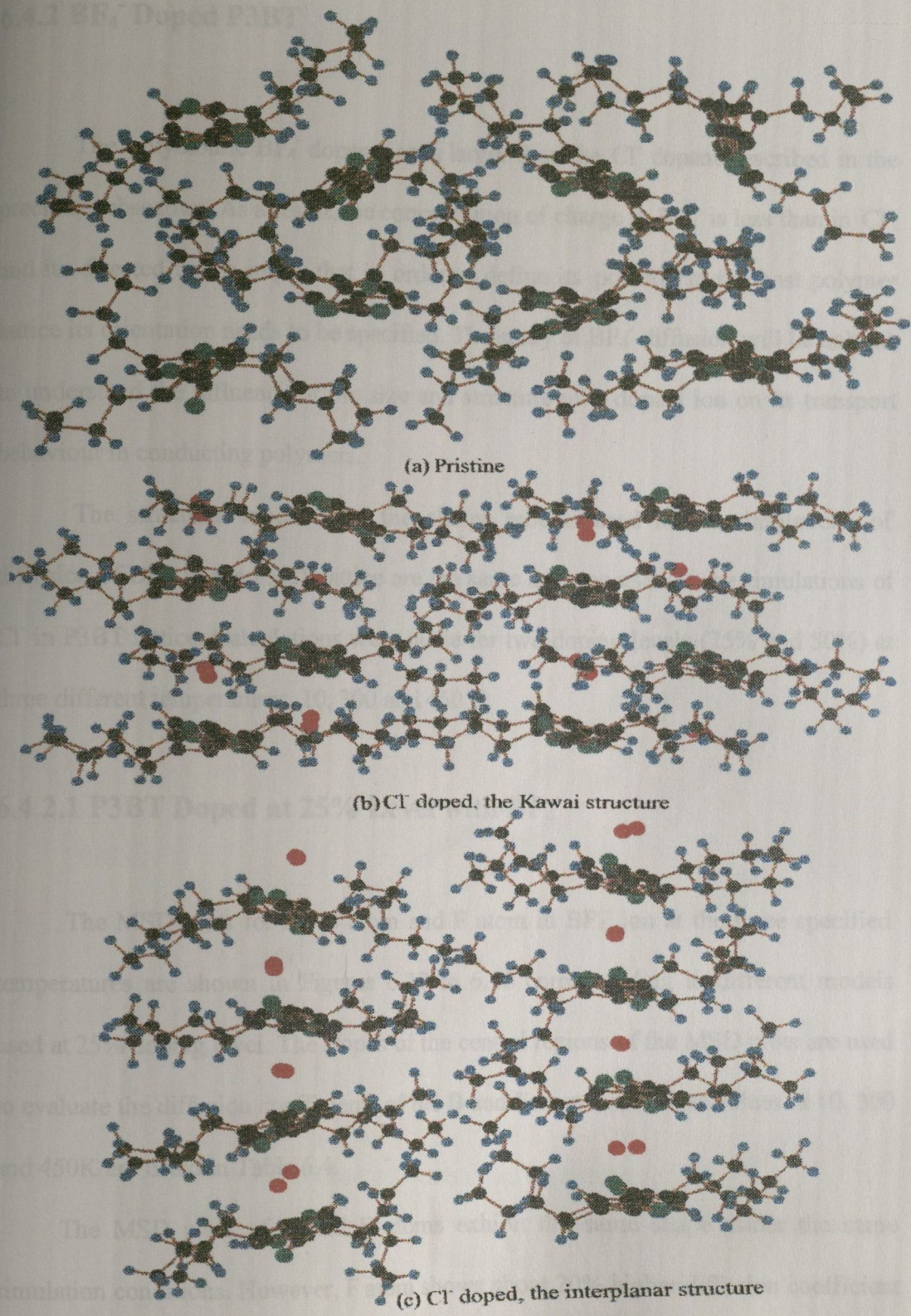


Fig. 6.16 A comparison of P3BT relaxed conformation before and after Cl⁻ doping at 50% doping level at 400 K. (a) Pristine, (b) Cl⁻ doped, the Kawai structure, (c) Cl⁻ doped, the interplanar structure. The atoms in the system are represented by different colors: green – S, gray – C, blue – H and red – dopant ion Cl⁻.

6.4.2 BF_4^- Doped P3BT

The polyatomic BF_4^- dopant ion is larger than the Cl^- dopant described in the previous subsection. As a result, the concentration of charge in BF_4^- is less than in Cl^- , and its directed bonds imply that in order to define its position in the host polymer lattice its orientation needs to be specified. The study of BF_4^- diffusion will be helpful to understand the influence of the size and structure of a dopant ion on its transport behaviour in conducting polymers.

The structural models and the charge models used in the simulations of diffusion of BF_4^- in the P3BT lattice are the same as those used in the simulations of Cl^- in P3BT lattice. Calculations were made for two doping levels (25% and 50%) at three different temperatures, 10, 300 and 450 K.

6.4.2.1 P3BT Doped at 25% Level with BF_4^-

The MSD plots for the B atom and F atom in BF_4^- ion at the three specified temperatures are shown in Figures 6.17 to 6.20 corresponding to different models used at 25% doping level. The slopes of the central regions of the MSD plots are used to evaluate the diffusion coefficients of the B and F atoms, and these values at 10, 300 and 450K are listed in Table 6.4.

The MSD plots of B and F atoms exhibit the same shape under the same simulation conditions. However, F atom shows about 20% higher diffusion coefficient than B atom although they are in the same BF_4^- dopant ions. This results from the additional rotational freedom associated with the F atom. It is therefore better to use

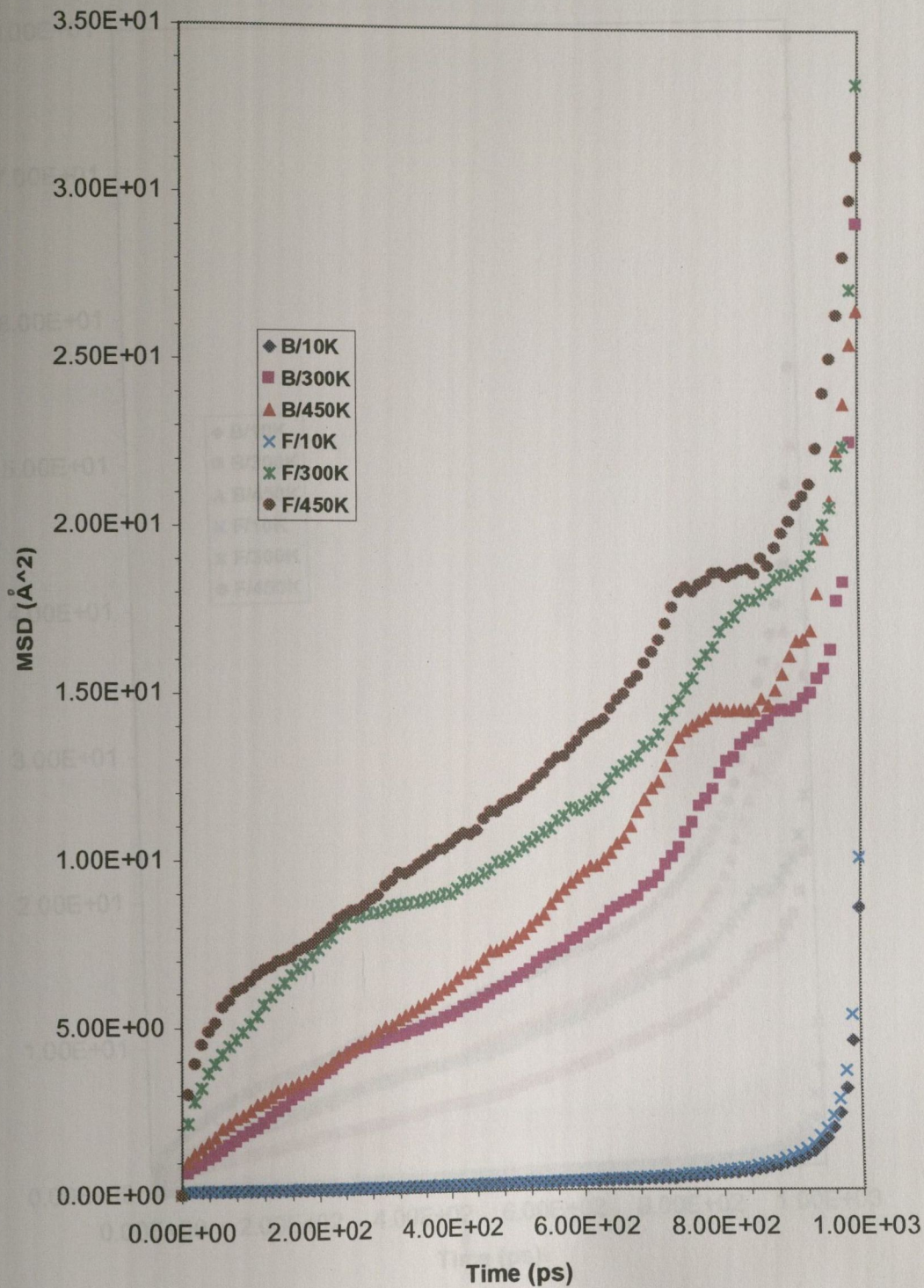


Fig. 6.17 MSD of B and F in 25% BF_4^- doped P3BT lattice at 10, 300 and 450 K (the Kawai structural model and the charges evenly distributed in the polymer main chains).

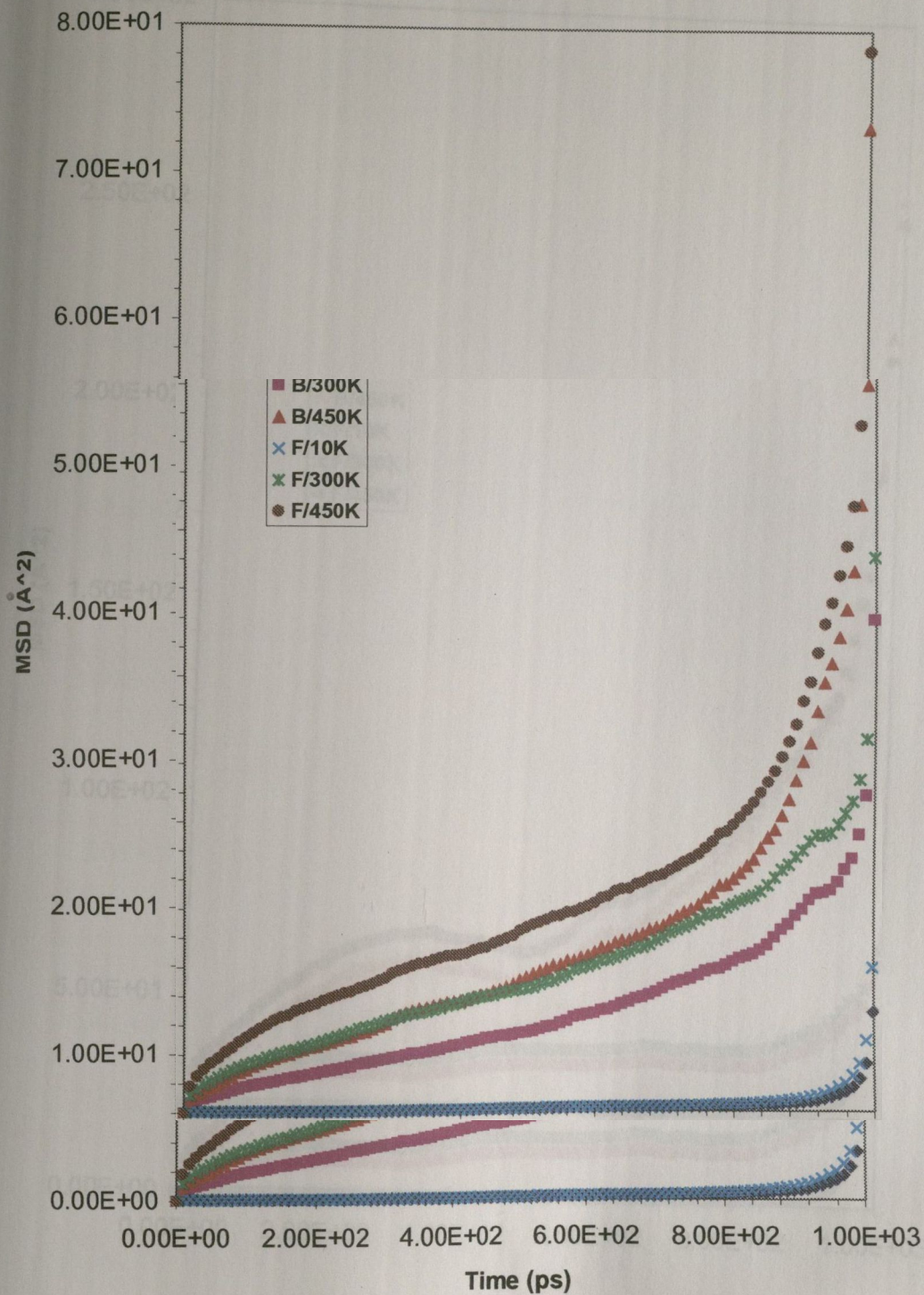


Fig. 6.18 MSD of B and F in 25% BF_4^- doped P3BT lattice at 10, 300 and 450 K (The Kawai structural model and polaron charge model in the polymer main chains).

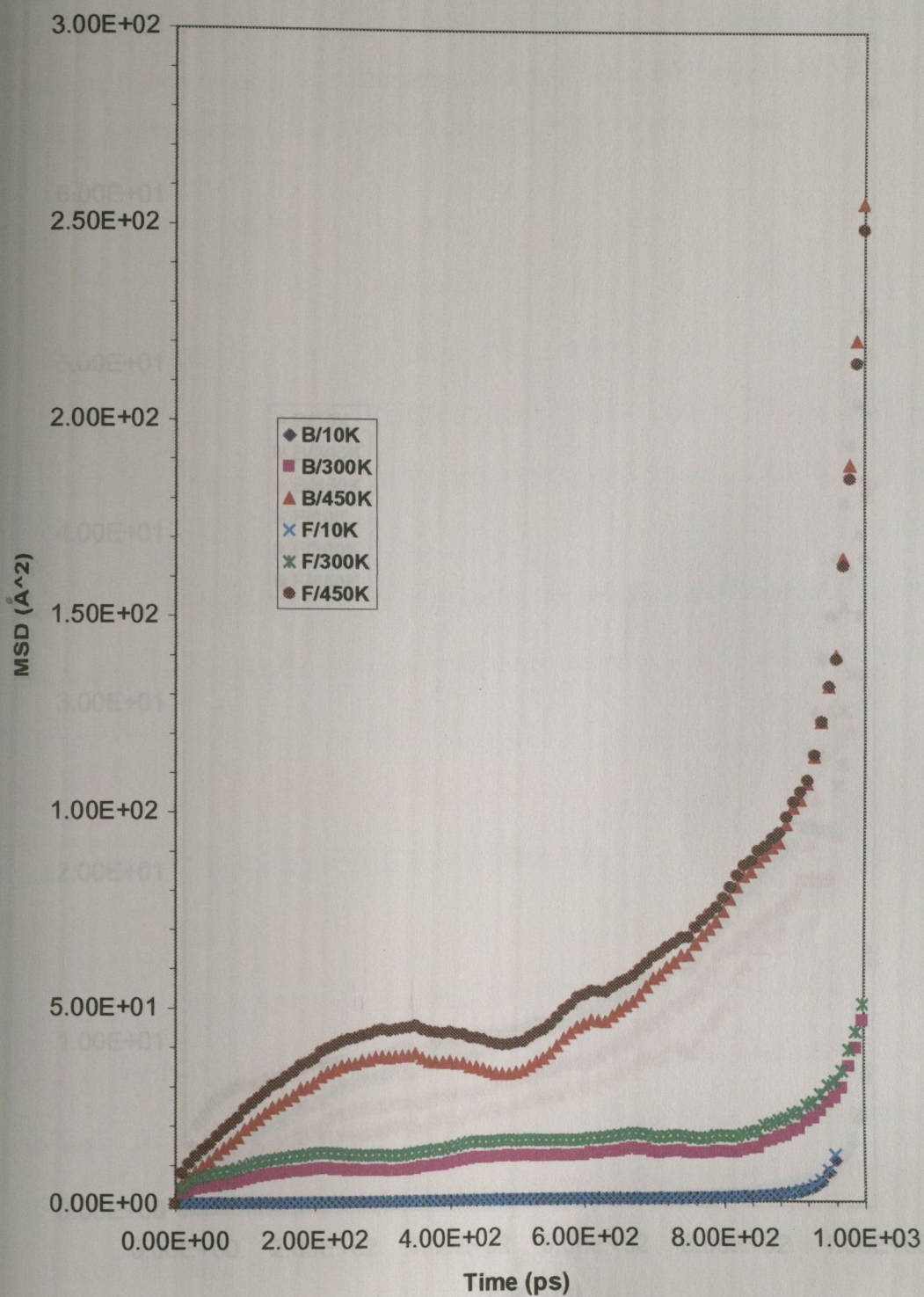


Fig. 6.19 MSD of B and F in 25% BF_4^- doped P3BT lattice at 10, 300 and 450K (the interplanar structural model and the charges evenly distributed in the polymer main chains).

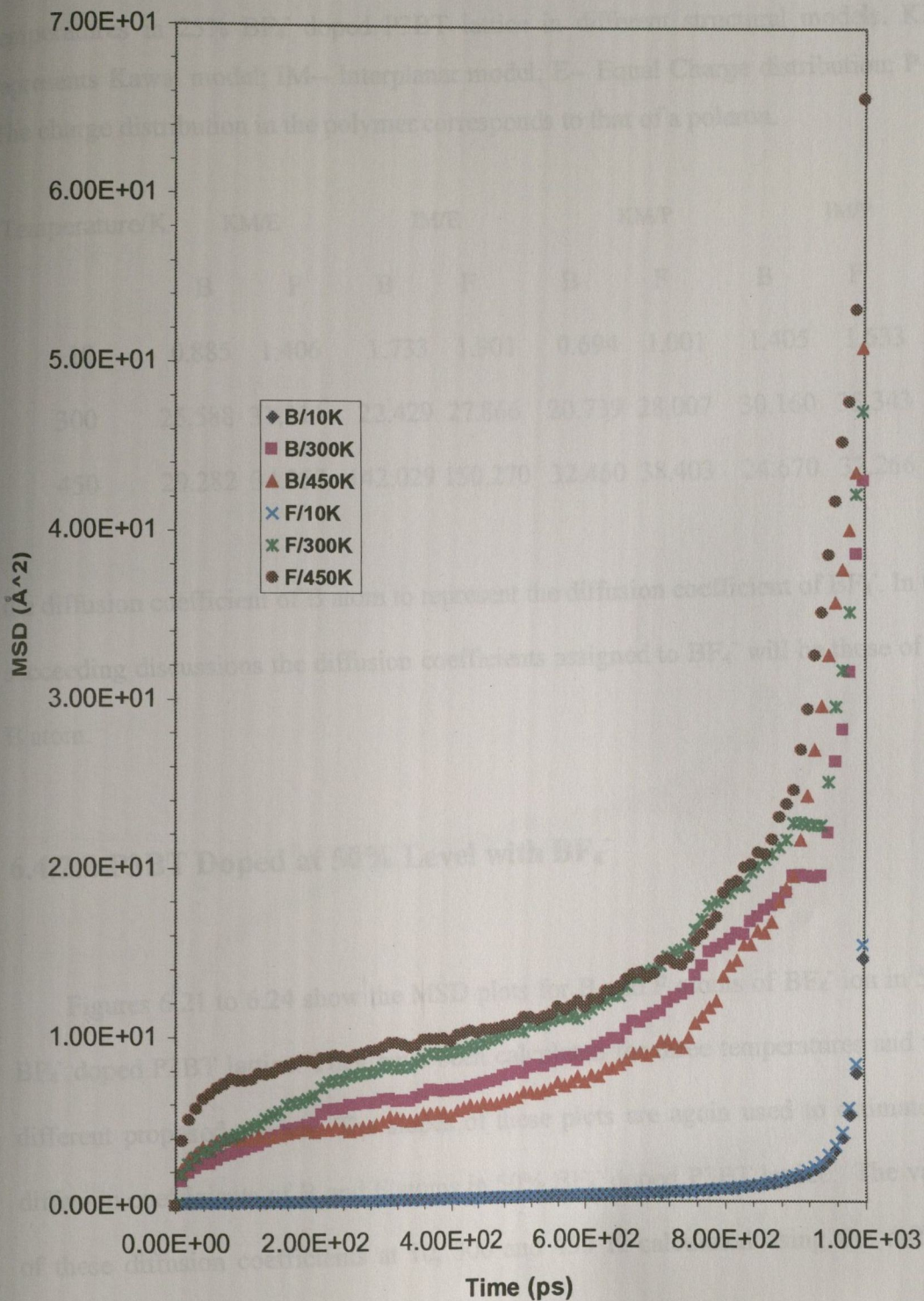


Fig. 6.20 MSD of B and F in 25% BF_4^- doped P3BT lattice at 10, 300 and 450 K (the interplanar structural model and polaron charge model in the polymer main chains).

Table 6.4 Diffusion coefficients (in units of $10^{-12} \text{ m}^2\text{s}^{-1}$) of B and F atoms at three temperatures in 25% BF_4^- doped P3BT lattice in different structural models. KM represents Kawai model; IM-- Interplanar model; E-- Equal Charge distribution; P— The charge distribution in the polymer corresponds to that of a polaron.

Temperature/K	KM/E		IM/E		KM/P		IM/P	
	B	F	B	F	B	F	B	F
10	0.885	1.406	1.733	1.901	0.694	1.001	1.405	1.533
300	25.588	31.811	22.429	27.866	20.739	28.007	30.160	35.343
450	29.282	34.353	142.029	150.270	32.460	38.403	24.670	32.266

the diffusion coefficient of B atom to represent the diffusion coefficient of BF_4^- . In the succeeding discussions the diffusion coefficients assigned to BF_4^- will be those of the B atom.

6.4.2.2 P3BT Doped at 50% Level with BF_4^-

Figures 6.21 to 6.24 show the MSD plots for B and F atoms of BF_4^- ion in 50% BF_4^- doped P3BT lattice. They have been calculated for three temperatures and with different proposed models. The slopes of these plots are again used to estimate the diffusion coefficients of B and F atoms in 50% BF_4^- doped P3BT lattice. The values of these diffusion coefficients at 10, 300 and 450 K calculated using the different simulation models are listed in Table 6.5.

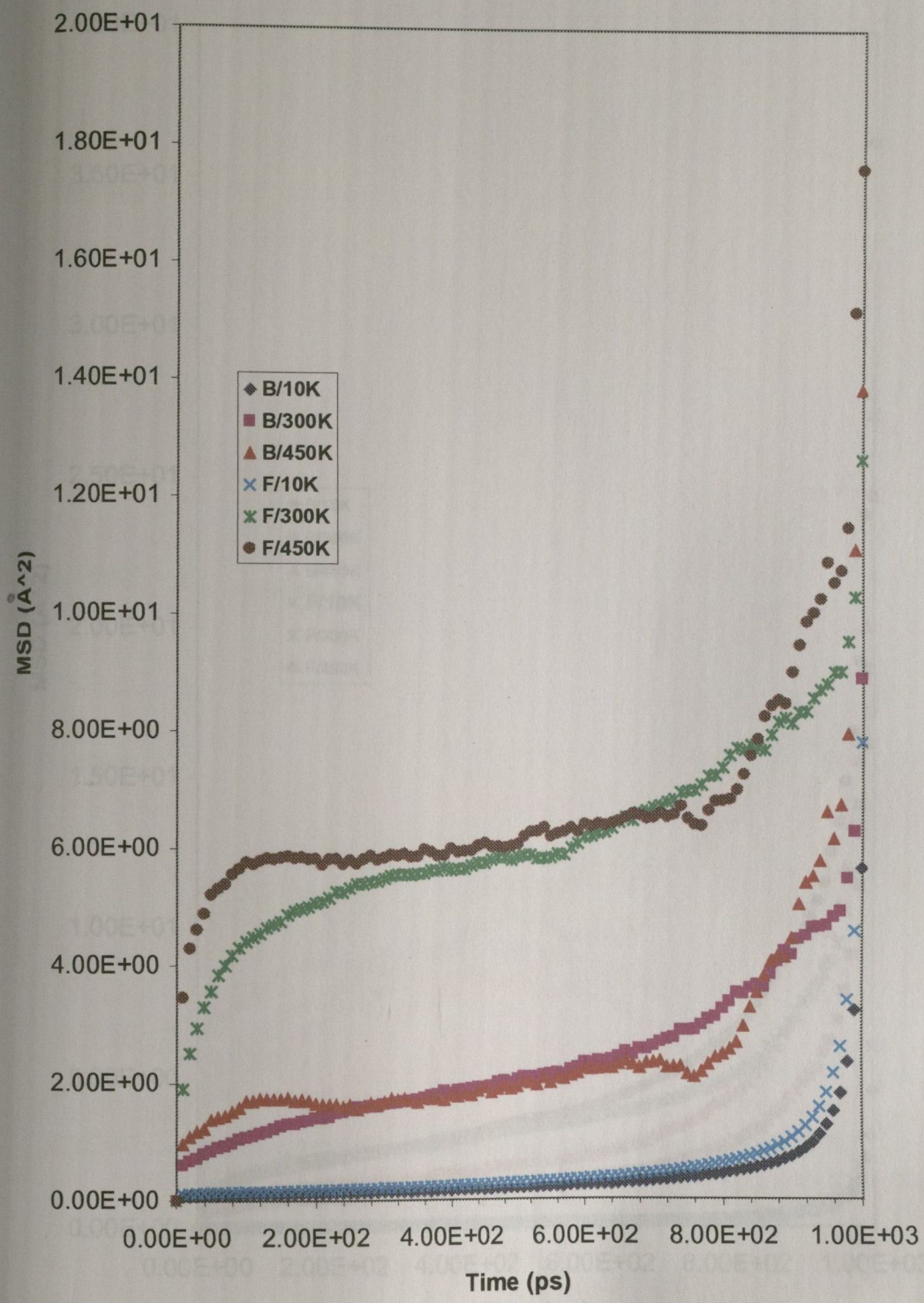


Fig. 6.21 MSD of B and F in 50% BF_4^- doped P3BT lattice at 10, 300 and 450 K (the Kawai structural model and the charges evenly distributed in the polymer main chains).

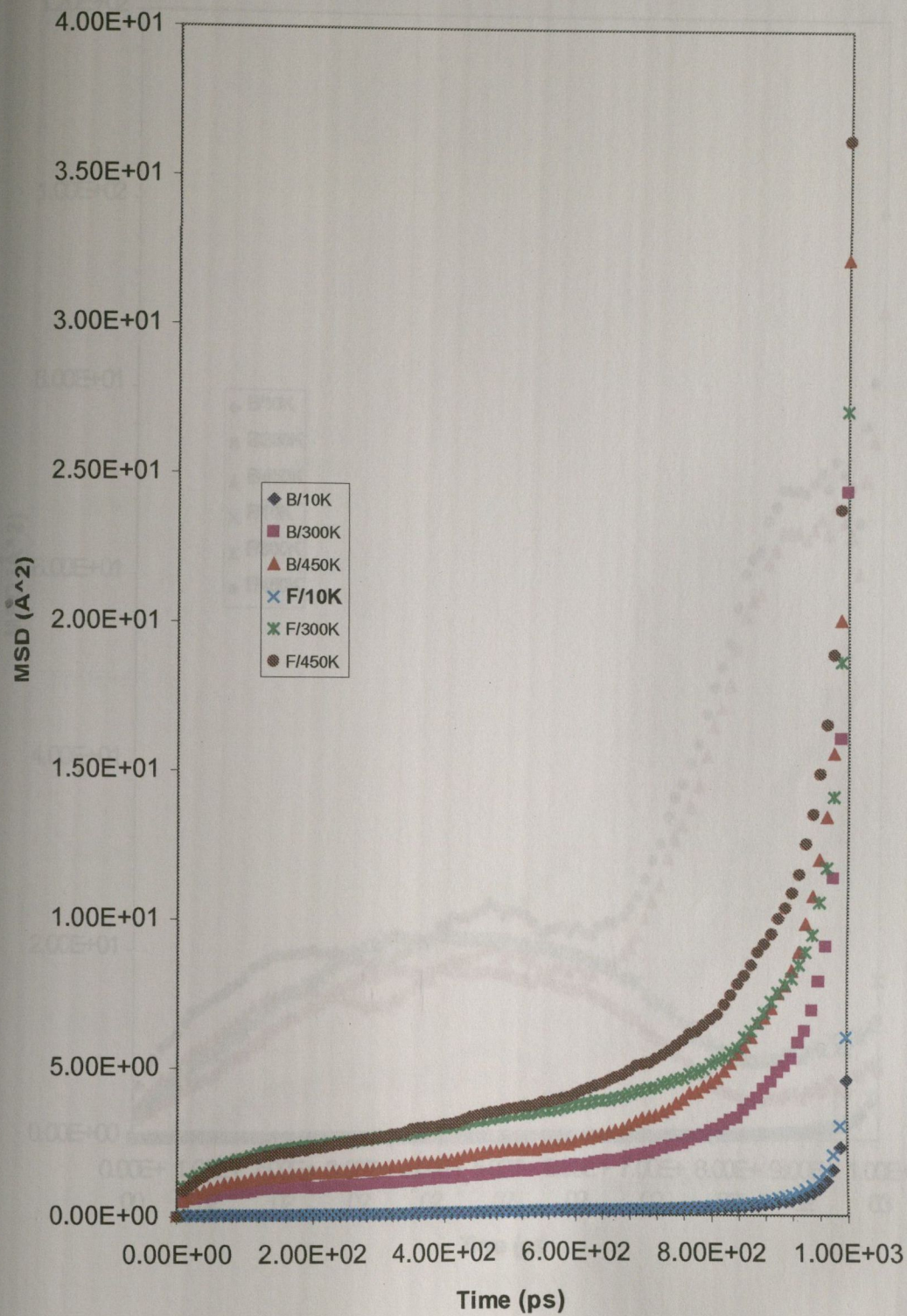


Fig. 6.23 MSD of B and F in 50% BF_4^- doped P3BT lattice at 10, 300 and 450 K (the

Kawai structural model and bipolaron charge model in the polymer main chains).

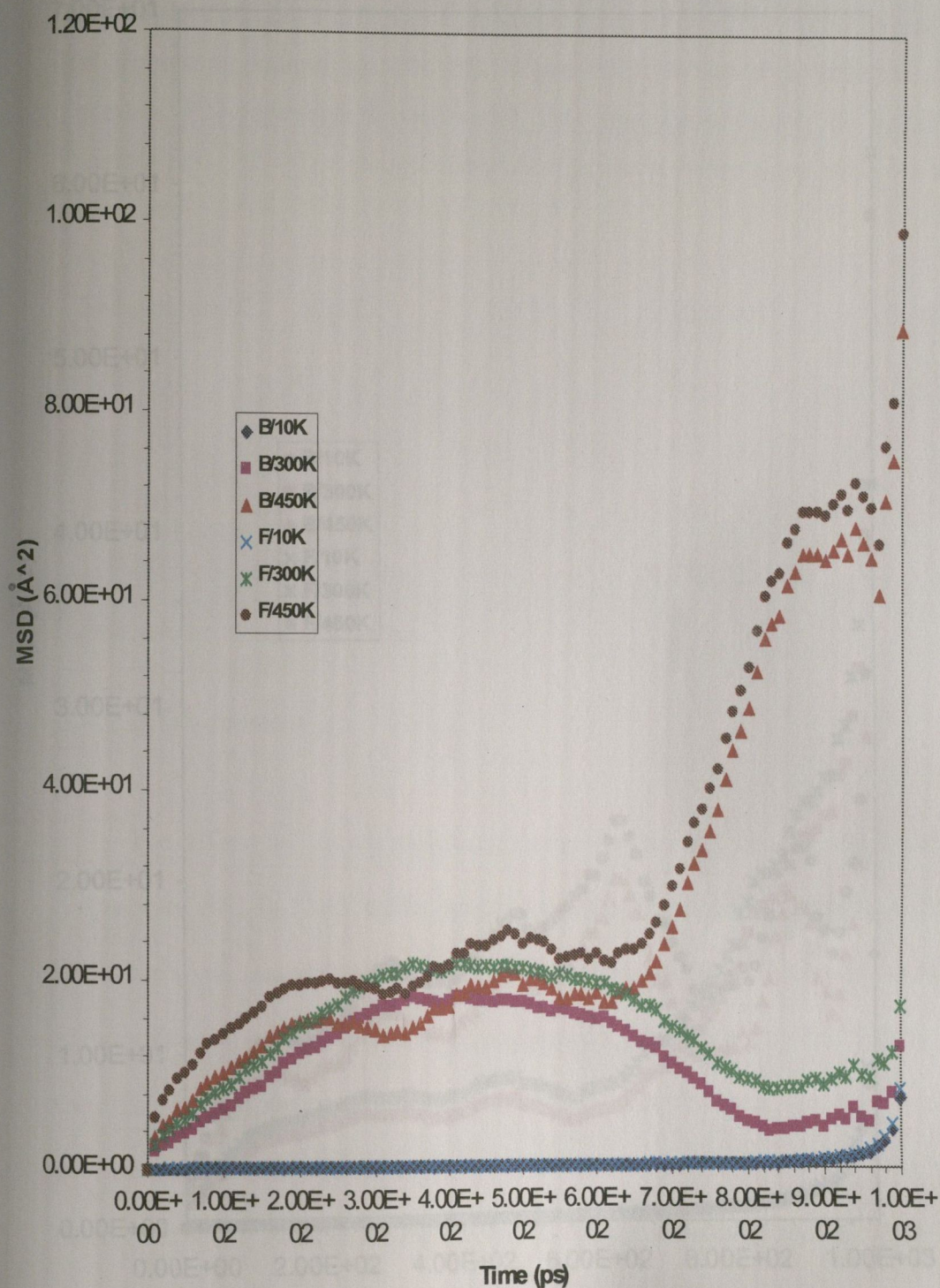


Fig. 6.23 MSD of B and F in 50% BF_4^- doped P3BT lattice at 10, 300 and 450 K (the interplanar structural model and the charges evenly distributed in the polymer main chains).

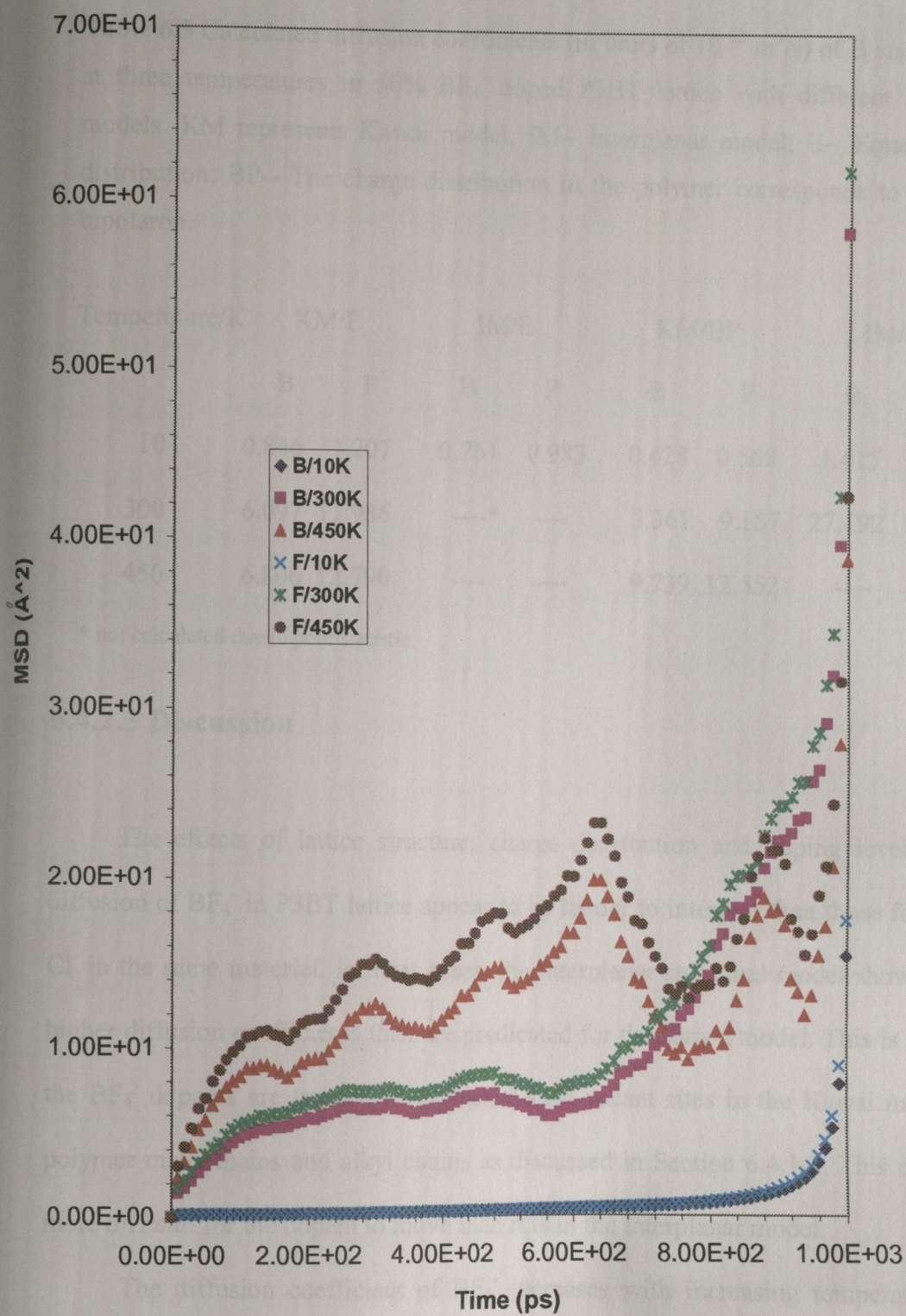


Fig. 6.24 MSD of B and F in 50% BF_4^- doped P3BT lattice at 10, 300 and 450 K (the interplanar structural model and bipolaron charge model in the polymer main chains).

Table 6.5 Calculated diffusion coefficients (in units of 10^{-12} m²/s) of B and F atoms at three temperatures in 50% BF₄⁻ doped P3BT lattice with different structural models. KM represents Kawai model; IM-- Interplanar model; E-- Equal Charge distribution; BP-- The charge distribution in the polymer corresponds to that of a bipolaron.

Temperature/K	KM/E		IM/E		KM/BP		IM/BP	
	B	F	B	F	B	F	B	F
10	0.846	1.207	0.761	0.983	0.428	0.568	1.415	1.614
300	6.097	11.986	----*	----	5.361	9.157	27.192	30.140
450	6.806	12.790	----	----	9.739	12.552	----	----

* not calculated due to poor statistic

6.4.2.3 Discussion

The effects of lattice structure, charge distribution and doping level on the diffusion of BF₄⁻ in P3BT lattice appear to be harder to interpret than those found for Cl⁻ in the same material. In most cases, the interplanar structural model shows much higher diffusion coefficients than are predicated for the Kawai model. This is because the BF₄⁻ dopants are trapped in the hexahedral vacant sites in the Kawai model by polymer main chains and alkyl chains as discussed in Section 6.4.1.3. This makes it more difficult for the dopant to move than it is in the interplanar model.

The diffusion coefficient of BF₄⁻ increases with increasing temperature. At 25% doping level, the diffusion coefficient of BF₄⁻ averaged from different proposed models is 1.2×10^{-12} m²/s at 10 K, 24.7×10^{-12} m²/s at 300K, and 57.1×10^{-12} m²/s at 450 K; while at 50% doping level the corresponding values are: 0.9×10^{-12} m²/s at 10 K, 29.6×10^{-12} m²/s at 300 K, and 38.4×10^{-12} m²/s at 450 K.

Although the diffusion coefficient of BF_4^- is lower than that of Cl^- , the values of both dopants are of similar order of magnitude and are much higher than the diffusion coefficients of BF_4^- reported from experimental measurements in other conducting polymers such as polythiophene and polypyrrole. Mohammad [11] estimated that the diffusion coefficient for the BF_4^- diffusion in polythiophene- BF_4^- or polypyrrole- BF_4^- systems was less than $1 \times 10^{-14} \text{ m}^2/\text{s}$ at 273 K. But he noted that BF_4^- showed a much enhanced diffusion coefficient at temperatures above 273 K. He also suggested that the sample thickness, morphology and doping level would affect the behaviour of diffusion. The reasons for the diffusion coefficient from our simulations being 100 times higher than those reported from experiments have been discussed in Section 6.4.1.3. The models we used in the calculations are ideally crystalline and the P3BT in the lattice is regioregular head-to-tail.

A complete discussion of this subject would consider factors such as (1) the overall charge on the ion, (2) the size of the ion, (3) the concentration of the ion (the 'doping level'), (4) the nature of the host matrix and (5) the morphology of the system. As the diffusion considered occurs in the same host polymer matrix (P3BT) we shall not take explicit account of the nature of the polymer. However if a comparison were to be made for diffusion in different hosts, then many of the factors described below, partial atomic charges and structures of main chain and side chains if any, would play an important rôle.

As far as the diffusing ion is concerned, the greater the overall charge on the ion the greater the magnitude of the Madelung energy and hence the greater the Coulombic stabilisation of the ion in its site in the host matrix. In other words, diffusion will be slower for an ion bearing a high overall charge than one with a small charge. On the other hand if we are considering the migration of the ion in an

externally applied electric field, (conduction) then the higher the charge on the ion the greater would be its response to the field.

In the present case, however, all the diffusing ions (Cl^- and BF_4^-) considered have the same overall charge (-1). The charge density on the diffusing ion increases with the size of dopant ion. The resulting high atomic charge density will result in strong Coulombic stabilisation of the ion in a region of the host matrix where the predominant charge is opposite to that of the ion, thus inhibiting diffusion. Conversely a larger ion would be subject to a weaker Coulombic effect, thereby facilitating its diffusion.

The other obvious effect of the size of the diffusant ion is steric [11,14]. In an amorphous (glassy) region of the polymer host, a small ion can diffuse more easily than a bulky ion through the same channel. However in a crystalline region where (as is the case for the work described here) the ions are thought of as constituting a *crystal sublattice* rather than 'dopants' in the sense used for inorganic semiconductors, a lattice with large diffusant ions should have larger lattice a and/or b parameters than for small ions (as discussed in an earlier chapter.) As a result, 'the diffusion channels' will be greater than in the latter, so that ion transport is not necessarily impeded by the effect of greater ion size.

The lower calculated diffusion coefficient for BF_4^- than for Cl^- is most likely because the steric effect is greater than the Coulombic effect due to the larger size of the former. Although the lattice parameters a and b are larger in BF_4^- doped P3BT than in Cl^- doped P3BT (as shown in Table 6.1), the diffusion channel could be not uniform in BF_4^- doped P3BT lattice and the narrow places in the channel slow down the diffusion of BF_4^- . Another reason may be that the orientations of BF_4^- may also affect its diffusion.

Generally diffusion coefficients are reported to increase with an increase in the diffusant concentration in a typical insulating polymer matrix [15-18]. This is not the case with our simulation results on doped conjugated conducting polymers because unlike insulating polymers positive charge centers are created on conjugated polymer chains upon doping.

The effect of the doping level (ion concentration) does not permit a simple discussion. Let us first consider a *low* concentration of ions in a crystalline region of the material. If the lattice parameters a and b are appropriate to those of the 'doped' lattice, then a low concentration would imply the presence of sites where there are no ions, so that the a and b parameters would be excessively large for those regions. The response of the lattice is then to contract as it would around a lattice vacancy, as was shown in lattice defect simulations of doped polyacetylene, polyparaphenylene and polythiophene [19,20]. (An excessive amount of empty regions causes the rupture of the lattice, transforming the region into an amorphous one [19,20].) Such a deformation inhibits ion transport. Increasing the doping level stabilises the lattice, as shown by the comparison of the MD snapshots of the pristine and doped P3AT lattices) and facilitates at least a limited degree of ion diffusion. The effect of increased diffusion at higher doping levels is known experimentally. At *high* doping levels, the mutual Coulombic repulsions associated with a large concentration of guest ions in the polymer matrix has the effect of hindering transport.

Finally, any attempt to compare calculated values with measured diffusion data must take account of the morphology of the doped material, and here the use of atomistic methods (at least in the way described in this work) is limited. It is known that small dopant ions diffuse more rapidly through the voids in polyacetylene (i.e., between the grains or fibres) than *within* the grains. In a material containing various

grain sizes it is difficult to predict the effect on the diffusion: transport through the grains (either the crystalline or amorphous regions) might then constitute a limiting step of the diffusion process. It would be interesting in future work to apply MD to simulate ion transport across a grain boundary.

6.5 Conclusion

Experimental information on the structure of doped P3AT lattices is very limited especially for the locations of dopant in the lattice. In the calculations described here the two most likely structures (Kawai and interplanar) of doped P3BT lattice were examined using a combination of MD and MM simulations. The lattice parameters of the Kawai structure show good agreement with the only available X-ray measurements [6] of the lattice structure of doped P3BT that we have found. These two structures with polaron, bipolaron and even charge distributions were used as trial models for the study of transport behavior of dopants in the P3BT lattice.

The diffusion of two dopants, Cl^- and BF_4^- , in P3BT lattice at 25% and 50% doping levels was studied by MD simulations over the full range of temperature. For each of the structural models, the calculated diffusion coefficients of dopants were found to be more than 100 times higher and the activation energy 10 times lower than those measured for the unsubstituted polyheterocyclic conducting polymers—polythiophene and polypyrrole. This suggests that dopants in P3BT should have higher mobility, which is agreement with the requirement for the regioregular HT-P3ATs possessing high conductivity. The diffusion coefficient of dopants in P3BT lattice calculated from our simulation is of the order of 1 to $100 \times 10^{-12} \text{ m}^2/\text{s}$. If this is true for doped P3AT lattice, then these should be excellent potential materials for

battery applications, where the rates of charge and discharge are determined by such diffusion processes and values in the range of 10^{-12} m²/s are considered to be ideal.

The study of diffusion from MD simulation shows that the diffusion coefficients of dopants in the P3BT lattice are affected by temperature, dopant concentration and size. The diffusion coefficients of Cl⁻ and BF₄⁻ dopants increase with temperature but decrease with dopant size. The effect of dopant concentration on diffusion coefficients is not like the case of small molecule diffusion in an insulating polymer matrix in which the diffusion increases with diffusant concentration [15-17]. In the system described here the calculations suggest that the rate of diffusion depends on the dopant type and structural model used. Our simulations also indicate that dopants in a lattice described by the interplanar structural model should possess higher mobility than would be found in the lattice described by the Kawai structure.

However, the structural models used in these simulations are of ideal crystals. The polymers in the lattice are supposed to be regioregular head-to-tail (HT). Although regioregular HT-P3ATs have been synthesized [18, 21-23] and are reported to be highly crystalline [23-25], portions of P3AT chains could be regiorandom, and in any case the polymer material is composed of both crystalline and amorphous phases. So the diffusion coefficients of dopants calculated here could be higher than those in the real P3AT materials. But this prediction can not as yet be tested as no experimentally determined rates of diffusion of dopants in P3ATs could be found in the literature.

Bibliography:

- [1] Veluri K. *Ph.D. Thesis*, University of Dublin, 1994
- [2] Scott J C, Pfluger P, Krounbi M T, and Street G. *Phys. Rev.*, 1983, **B28**:2140
- [3] Houze E, and Nechtschein M. *Phys. Rev.*, 1996, **B5**:14309
- [4] Brédas J L, Themans B, Fripiat J G, and André J M. *Phys. Rev. Conds. Mat.*, 1984, **B29**:6761
- [5] Salmon M, Diaz A F, Logan A J, Krounbi M, and Bargon J. *Mol. Cryst. Liq. Cryst.*, 1983, **83**:1297
- [6] Kawai T, Nakazono M and Yoshino K. *J. Mater. Chem.*, 1992, **2**(9):903
- [7] Mitchel F J, Davis G R, Cywinski R, and Hannon A C. *Polym. Commun.*, 1989, **30**:98
- [8] Kanazawa K K, Diaz A F, Gill W D, Grant P M, Street G P, Gardini G P, and Kwak J F. *Synth. Met.*, 1979, **1**:329
- [9] Tourillon G and Garnier F. *J. Electroanao. Chem.*, 1982, **135**:173
- [10] Tezuka Y, Aoki K, and Ishii A. *Electrochimica Acta*, 1999, **44**(12):1871
- [11] Mohammad F. *Synth. Met.*, 1999, **99**:149
- [12] Morrison G. *Ph.D. Thesis*, The University of Kent at Canterbury, 1997
- [13] Mirebeau P. *J. Phys. C*, 1983, **3**(6):44
- [14] Brédas J L, Chance R R, Baughman R H, and Silbey R, *J. Chem. Phys.*, 1982, **76**:3673
- [15] Takeuchi H. *J. Chem. Phys.*, 1990, **93**:2602
- [16] Takeuchi H. *J. Chem. Phys.*, 1990, **93**:4490
- [17] Takeuchi H, and Okazaki K. *J. Chem. Phys.*, 1990, **92**:5643

- [18] McCullough R D, Tristram-Nagle S., Williams S P, Lowe R D, and Jayaraman M. *J. Am. Chem. Soc.*, 1993, **55**:1198
- [19] Corish J, Hanratty V C A, Morton-Blake D A, and B ni re F. *Rad. Eff. Defects Solids*, 1991, **119**:499
- [20] Corish J, Hanratty V C A, Morton-Blake D A, and B ni re F. *Mol. Simulation*, 1992, **9**:65
- [21] McCullough R D, Williams S P, Tristram-Nagle S., Jayaraman M, Ewbank P C, and Miller L. *Synth. Met.*, 1995, **69**:279
- [22] Chen T.-A., and Rieke R D. *Synth. Met.*, 1993, **60**:175
- [23] Chen T.-A., Wu X., and Rieke R D. *J. Am. Chem. Soc.*, 1995, **117**:233
- [24] McCullough R D. *Adv. Mater.*, 1998, **10**:93
- [25] Leclerc M and Fa d K. *Adv. Mater.*, 1997, **9**:1087

Chapter 7

MM Simulation of the Migration of Dopants (Cl^- and BF_4^-) in P3BT Lattices

7.1 Introduction

The molecular mechanics methodology using the CASCADE [1] code has been successful in predicting the migration of dopants Cl^- , BF_4^- and ClO_4^- in polythiophene and polypyrrole by defect lattice methods [2]. The same methods had also been used in the study of the migration of charged dopants in graphite [3,4], polyacetylene [5,6] and polyparaphenylene [6]. In those studies routes for the migration of dopant ions, via a classical vacancy mechanism between two dopant sites, were first proposed using the dopant sites which had been determined from energy minimization methods on the 'perfect lattice'. Then the dopant was moved along the route by fixing its position at different points, allowing the remainder of the crystal to relax and calculating the defect energies. The energy barriers of migration of dopants in the lattice were estimated from the energy profile associated with the trajectory having the least adiabatic energy. However, it only considered one dopant (interstitial) migrating via a vacancy mechanism i.e., between two specified vacant sites. The possible influence from the migration of another dopant next to the vacancy was ignored. The filling of the new vacancy created by the migration of the interstitial was also neglected.

When an electric field is applied in an electrochemical cell containing doped conducting polymer electrodes all the dopant ions in the polymer matrix would be expected to migrate along the direction of the electric field e.g., dopant Cl^- would

move in the direction of the anode. To understand such kind of mobility, a simulation of all dopant ions migrating along one direction in the polymer lattice would be very helpful.

Our simulation of the mechanism of the thermochromism of poly(3-alkylthiophenes) by the perfect lattice simulation method using MM in Chapter 4 has provided a new insight on this process. Combined with MD simulation, the most likely lattice structures of P3BT doped with Cl^- and BF_4^- were also predicted in Section 3 of Chapter 6. These results provide the motivation to apply similar methods to predict the migration of dopant ions along the route with lowest energy barrier as indicated by our simulations.

In the current Chapter, the best migration routes are first suggested for the dopants in the P3BT lattice with the two different proposed structural models (the Kawai and interplanar) as described in Chapter 6 by simulating the dopant migrating in a wide variety of directions considered to be feasible. Then the MM simulations of migration of dopants at two different doping levels (25% and 50%) are performed by fixing the dopants in different positions on the proposed routes. The results of these investigations furnish migrational energy profiles and trajectories which allow the energy barriers associated with the motion of the ions to be estimated.

7.2 Calculation Methods

The MM simulations are performed by the perfect lattice method using GULP as described in Chapter 2. The potentials and parameters used have been derived in detail in Chapter 3. The charge created by oxidation (electron transfer from the polymer to the dopant) is evenly distributed over the atoms of the thiophene rings as

discussed in Section 2 of Chapter 6. In the simulations, the dopants are first moved in a wide range of directions to determine the migration route with the lowest energy barriers for migration. When this has been established the ions are fixed at certain positions along the migration route selected. When their positions are fixed, the minimization is carried out allowing all other atoms in the structure to relax to give the lowest energy of the system.

7.3 Results and Discussion

7.3.1 Migration Route of Dopant Cl in P3BT Lattice

In Section 3 of chapter 6, we investigated two possible structural models of the P3BT lattice: the Kawai and interplanar models. In the interplanar model, the dopants are located between two polymer chains that belong to two different planes. After analysis of the trajectories in the MD simulations, we suggest that the most likely migration path for dopants in this structural model is along the *c* axis as shown in Figure 7.1. This was confirmed by MM simulations in which the dopants were moved in various directions. For the Kawai structural model, the dopants are located in a hexahedral vacant sites which are enclosed by two polymer main chains and three alkyl side chains in the same plane and another two alkyl side chains above and below them. Irrespective of the directions in which dopants migrate, they must cross over either an alkyl side chain or a polymer main chain. The simulations show the trajectories along the *c* axis and over an alkyl side chain as shown in Figure 7.2 to be the most energetically favorable route.

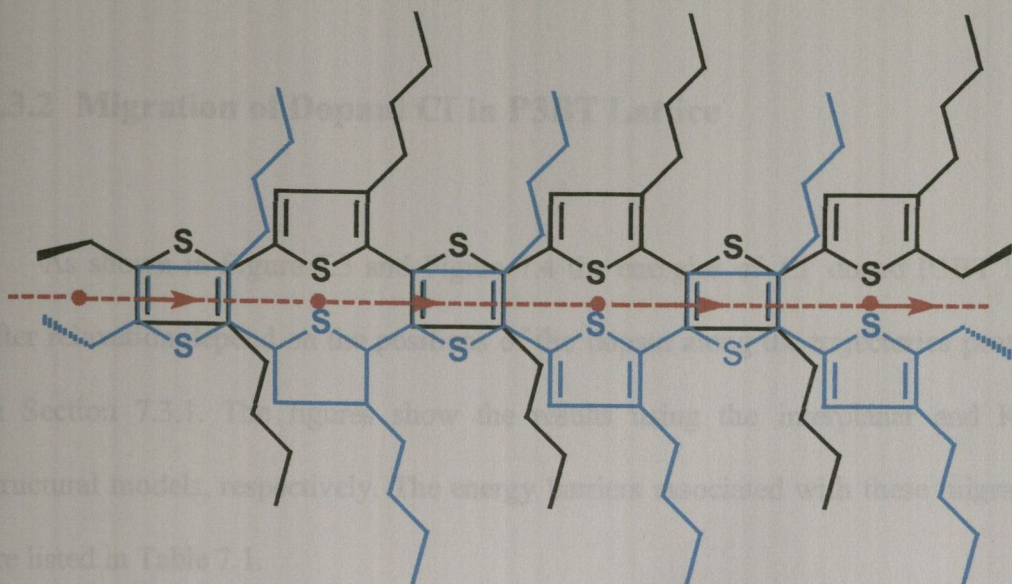


Figure 7.1 The most likely migration path of dopant in interplanar structural Model.

The dopants are located in half way between the two planes that are shown in black and blue colours.

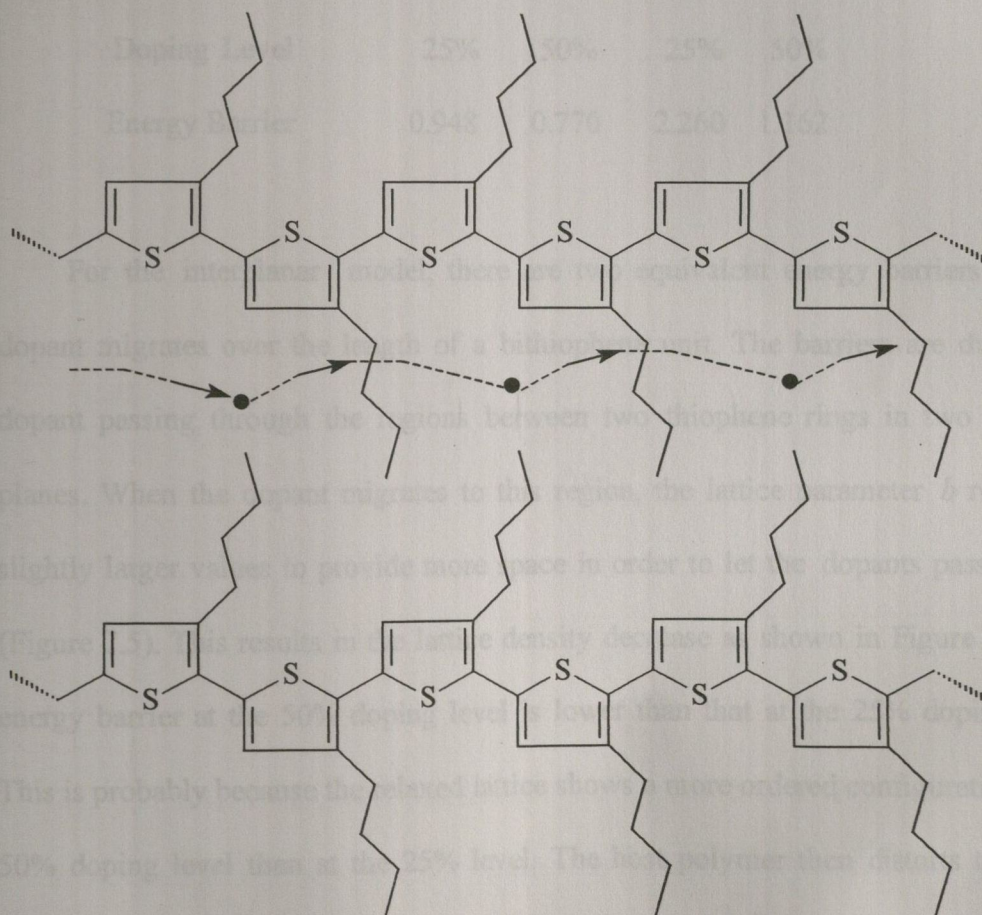


Figure 7.2. The most likely migration path of dopant in Kawai structural model. The two polymer chains and the dopants are in the same plane.

7.3.2 Migration of Dopant Cl⁻ in P3BT Lattice

As shown in Figure 7.3 and Figure 7.4 the energies of Cl⁻ doped P3BT lattice after relaxation depend on the positions of the dopant along the trajectories proposed in Section 7.3.1. The figures show the results using the interplanar and Kawai structural models, respectively. The energy barriers associated with these migrations are listed in Table 7.1.

Table 7.1 The energy barriers in eV for migration of dopant Cl⁻ in P3BT lattice.

Structural Model	Interplanar		Kawai	
Doping Level	25%	50%	25%	50%
Energy Barrier	0.948	0.770	2.260	1.162

For the interplanar model, there are two equivalent energy barriers when a dopant migrates over the length of a bithiophene unit. The barriers are due to the dopant passing through the regions between two thiophene rings in two different planes. When the dopant migrates to this region, the lattice parameter b relaxes to slightly larger values to provide more space in order to let the dopants pass through (Figure 7.5). This results in the lattice density decrease as shown in Figure 7.6. The energy barrier at the 50% doping level is lower than that at the 25% doping level. This is probably because the relaxed lattice shows a more ordered configuration at the 50% doping level than at the 25% level. The host polymer then distorts to inhibit migration of the dopant. When the dopants pass through the region between two thiophene rings (i.e., where the two thiophene rings on the two polymer chains above

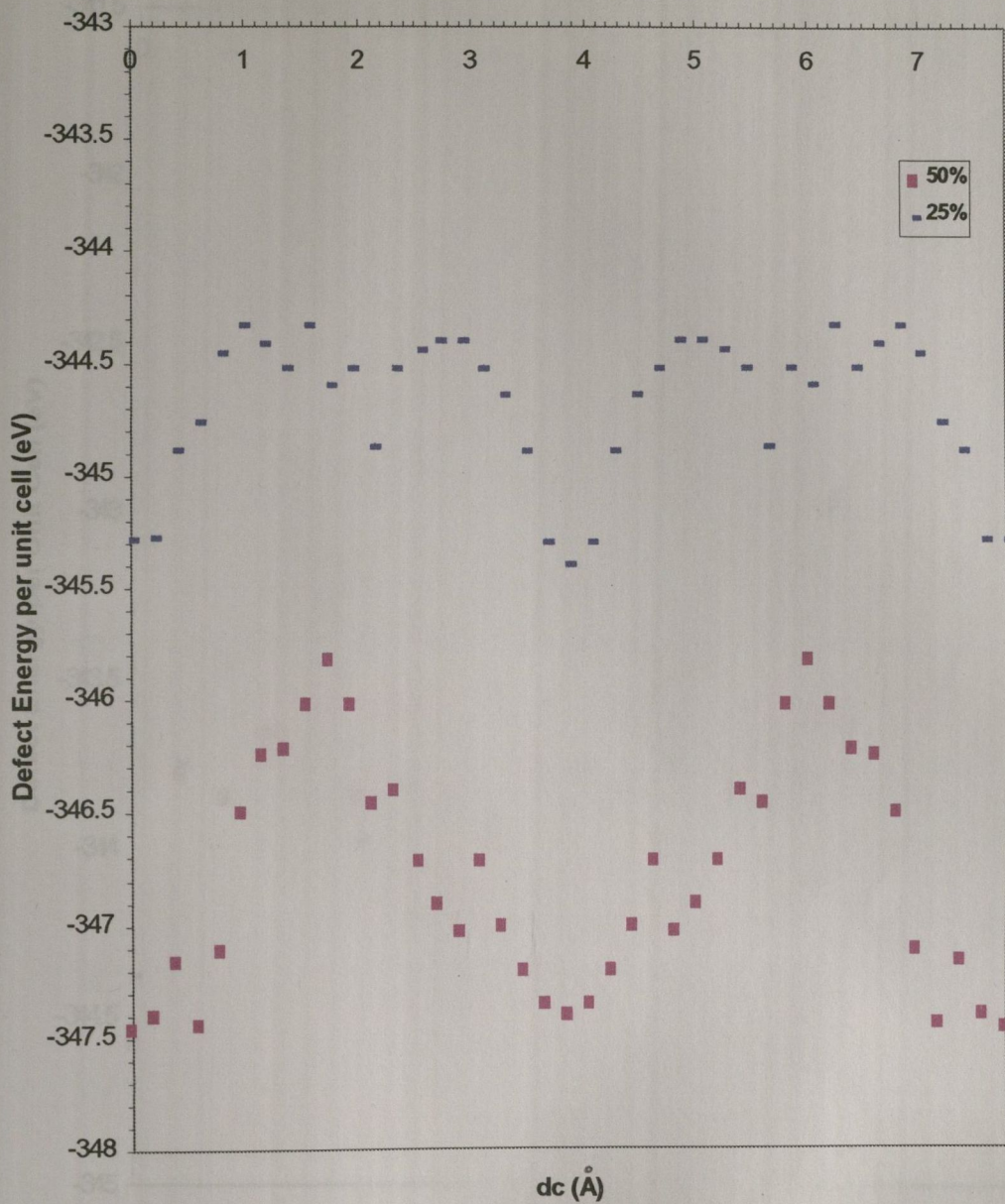


Fig. 7.3 Lattice energy after relaxation when dopant Cl^- at doping levels indicated in the diagram migrates in P3BT lattice with the interplanar structural model along the path as proposed in Figure 7.1. dc is the distance that dopants migrated along the c axis.

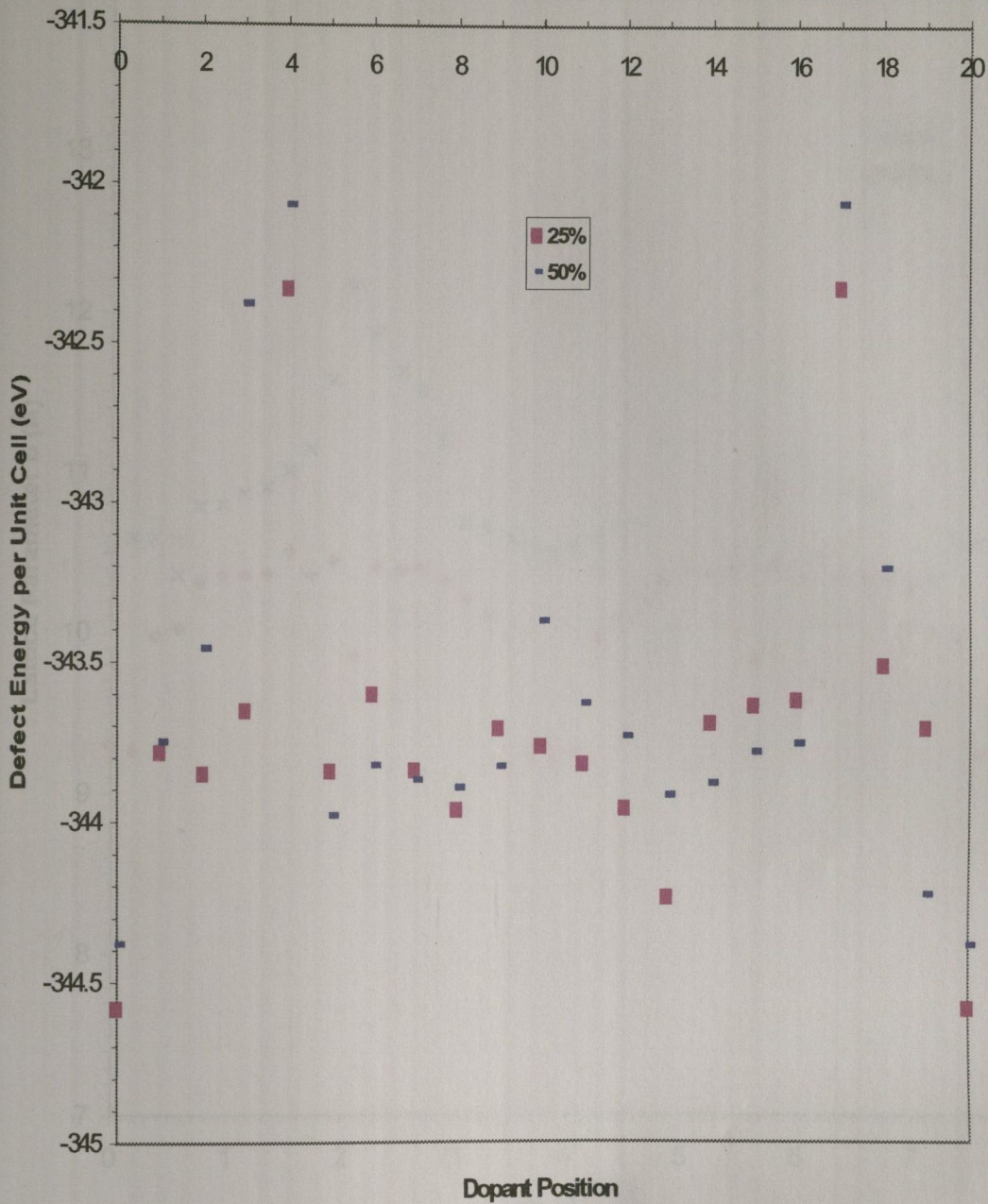


Fig. 7.4 Lattice energy after relaxation when dopant Cl^- at the doping levels indicated in the diagram migrates in P3BT lattice with the Kawai structural model along the path as proposed in Figure 7.2. Twenty points in the path were selected as the dopant position with the distance between two nearest points is the same.

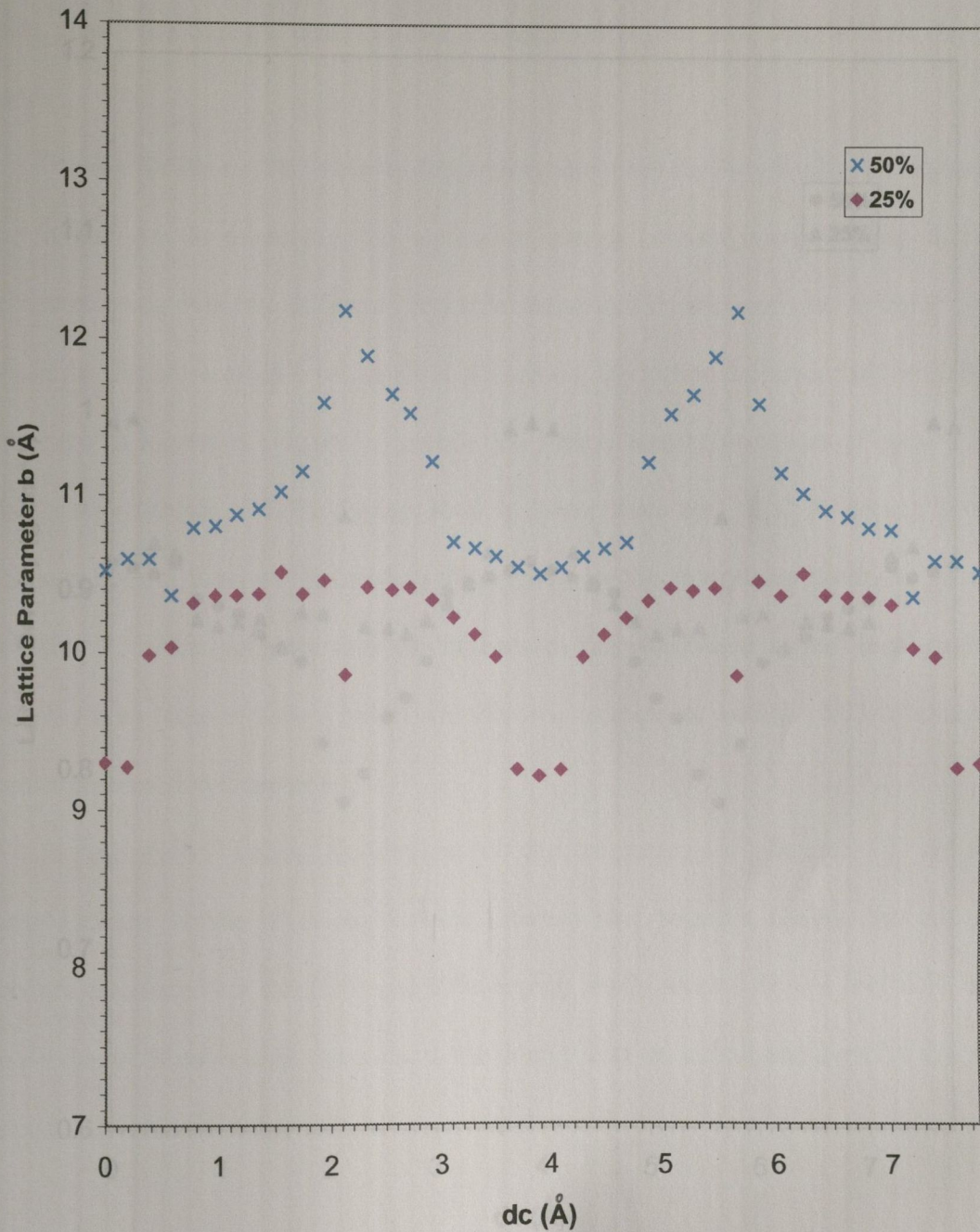


Fig. 7.5 Change in the lattice parameter b when dopant Cl^- at the doping levels indicated in the diagram migrates in P3BT lattice with the interplanar structural model along the path as proposed in Figure 7.1. dc is the distance that dopants migrated along the c axis.

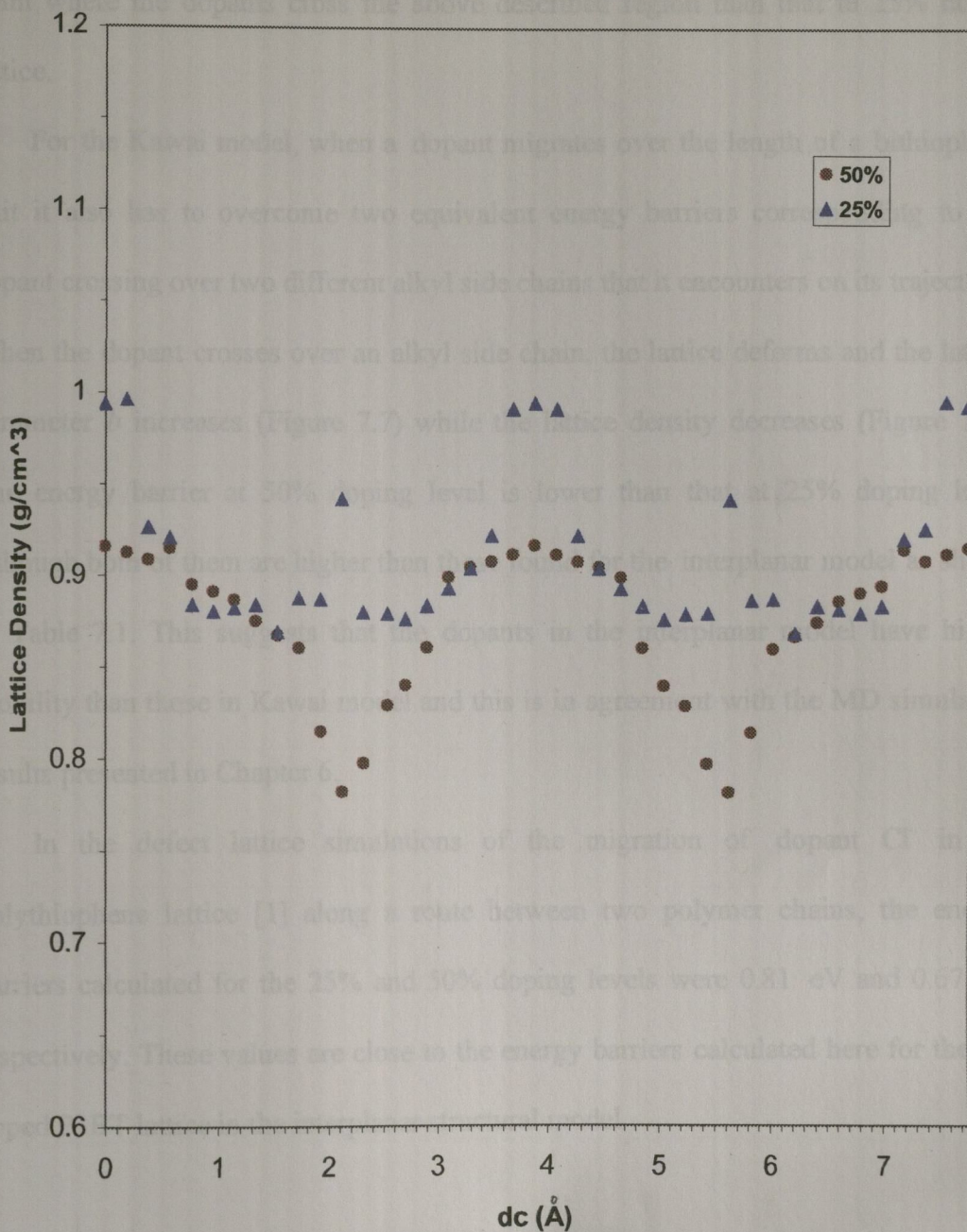


Fig. 7.6 Change in the lattice density when dopant Cl^- at the doping levels

indicated in the diagram migrates in P3BT lattice with the interplanar structural model along the path as proposed in Figure 7.1. dc is the distance that dopants migrated along the c axis.

and below the dopant sandwich the dopant), the relaxation causes some deformation in the lattice. This deformation was found to be smaller in the 50% doped lattice at the point where the dopants cross the above described region than that in 25% doped lattice.

For the Kawai model, when a dopant migrates over the length of a bithiophene unit it also has to overcome two equivalent energy barriers corresponding to the dopant crossing over two different alkyl side chains that it encounters on its trajectory. When the dopant crosses over an alkyl side chain, the lattice deforms and the lattice parameter b increases (Figure 7.7) while the lattice density decreases (Figure 7.8). The energy barrier at 50% doping level is lower than that at 25% doping level although both of them are higher than those found for the interplanar model as shown in Table 7.1. This suggests that the dopants in the interplanar model have higher mobility than those in Kawai model and this is in agreement with the MD simulation results presented in Chapter 6.

In the defect lattice simulations of the migration of dopant Cl^- in the polythiophene lattice [1] along a route between two polymer chains, the energy barriers calculated for the 25% and 50% doping levels were 0.81 eV and 0.67 eV, respectively. These values are close to the energy barriers calculated here for the Cl^- doped P3BT lattice in the interplanar structural model.

7.3.3 Migration of Dopant BF_4^- in P3BT Lattice

The same procedures as those described in Section 7.2 for Cl^- doped P3BT have used to attempt to simulate the movement the BF_4^- dopant through the P3BT lattice. However, in this case insufficient stable lattice configurations were found to permit

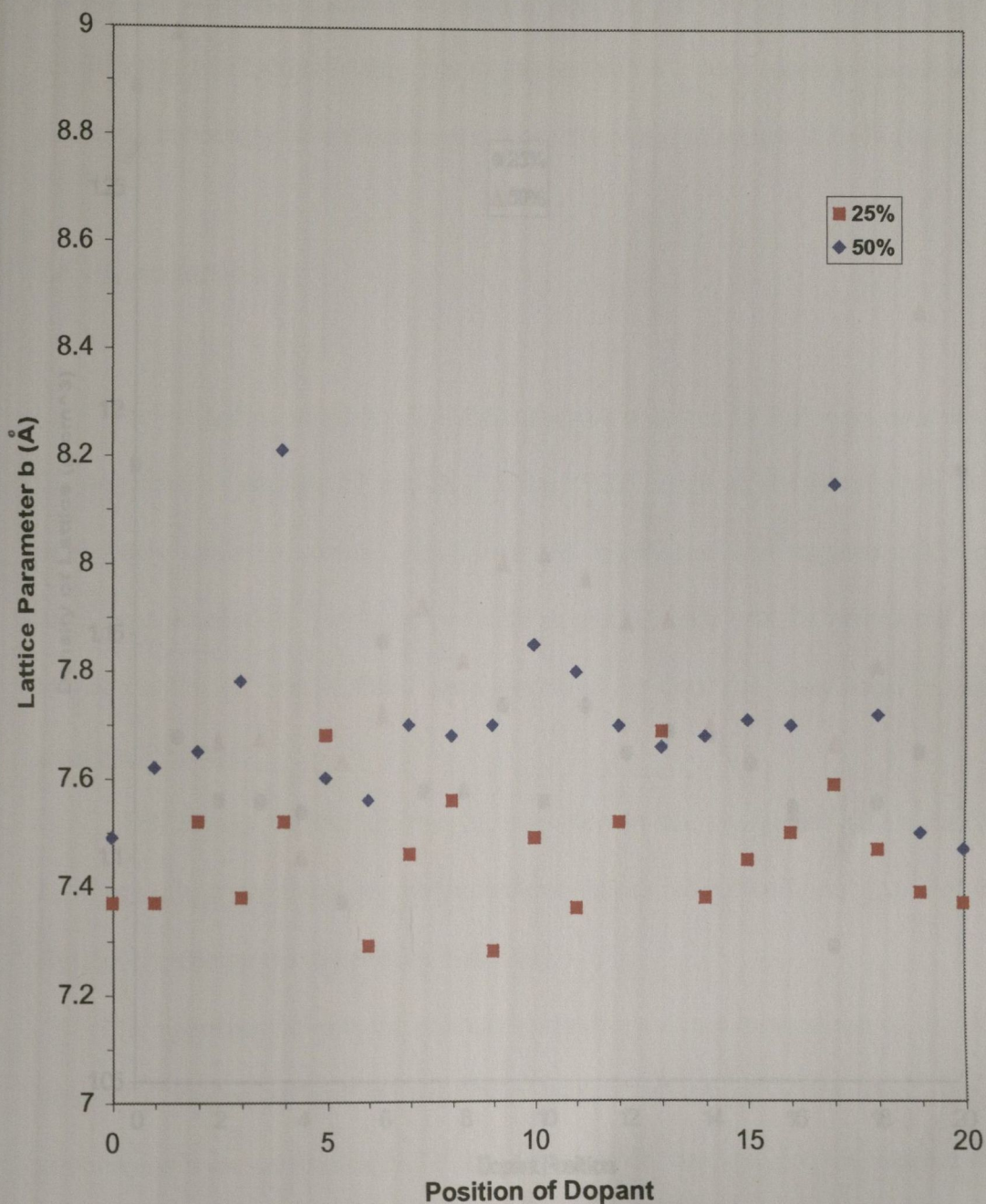


Fig. 7.7 Change in the lattice parameter b when dopant Cl^- at the doping levels indicated in the diagram migrates in P3BT lattice with the Kawai structural model along the path as proposed in Figure 7.2. Twenty points in the path were selected as the dopant position with the distance between two nearest points is the same.

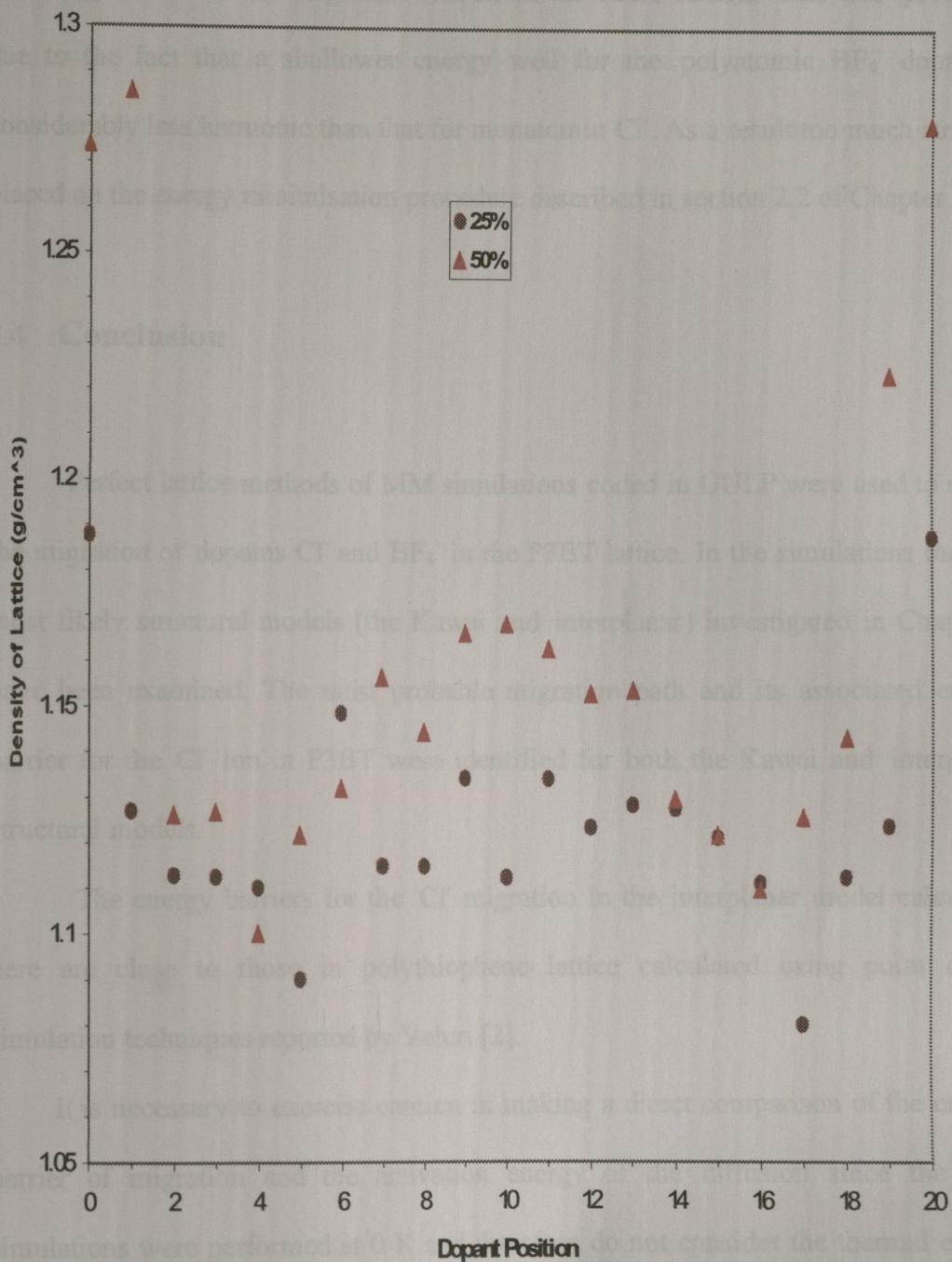


Fig. 7.8 Change in the lattice density when dopant Cl⁻ at the doping levels indicated in the diagram in P3BT lattice with the Kawai structural model along the path as proposed in Figure 7.2. Twenty points in the path were selected as the dopant position with the distance between two nearest points is the same.

the postulation of a dopant trajectory. For this reason it was not possible to calculate an energy barrier for the migration of BF_4^- in the P3BT lattice. This was probably due to the fact that a shallower energy well for the polyatomic BF_4^- dopant is considerably less harmonic than that for monatomic Cl^- . As a result too much strain is placed on the energy minimisation procedure described in section 2.2 of Chapter 2.

7.4 Conclusion

Perfect lattice methods of MM simulations coded in GULP were used to study the migration of dopants Cl^- and BF_4^- in the P3BT lattice. In the simulations the two most likely structural models (the Kawai and interplanar) investigated in Chapter 6 have been examined. The most probable migration path and its associated energy barrier for the Cl^- ion in P3BT were identified for both the Kawai and interplanar structural models.

The energy barriers for the Cl^- migration in the interplanar model calculated here are close to those in polythiophene lattice calculated using point defect simulation techniques reported by Veluri [2].

It is necessary to exercise caution in making a direct comparison of the energy barrier of migration and the activation energy of the diffusion since the MM simulations were performed at 0 K and therefore do not consider the thermal effects as in MD simulations. But the migration path for Cl^- in the lattice with interplanar structural model optimized from MM simulations is in agreement with the analysis of the trajectory of dopant diffusion in MD simulations.

The study of diffusion from MD and migration from MM contributes an understanding of the transport behavior of dopants in P3AT lattice. Both of them

indicate that dopants in a lattice described by the interplanar structural model should possess higher mobility than would be found in the lattice described by the Kawai structure. This prediction can only be verified by further experimental investigations such as the structural measurements by X-ray diffraction and experimental measurements of the diffusion/migration of dopants in P3ATs.

[3] Morton-Blake D.A., Conish J., and Beniere F. *Phys. Rev.* 1988, B37:4180

[4] Conish J., Jugo F., Morton-Blake D.A., Leslie M., and Beniere F. *Phys. Rev.* 1991, B44:10870

[5] Conish J., Hazraty V.C.A., Morton-Blake D.A., and Beniere F. *Rep. Eff. Defects Solids*, 1991, 119-499

[6] Conish J., Hazraty V.C.A., Morton-Blake D.A., and Beniere F. *Mol. Simulation*, 1992, 9:65

Bibliography:

- [1] Leslie M. "*Daresbury Laboratory Report*", (DL/SCI/TMB36T), 1984
- [2] Veluri K. *Ph.D. Thesis*, University of Dublin, 1994
- [3] Morton-Blake D A, Corish J, and B ni re F. *Phys. Rev.*, 1988, **B37**:4180
- [4] Corish J, Jugie F, Morton-Blake D A, Leslie M, and B ni re F. *Phys. Rev.*, 1990, **B41**:10870
- [5] Corish J, Hanratty V C A, Morton-Blake D A, and B ni re F. *Rad. Eff. Defects Solids*, 1991, **119**:499
- [6] Corish J, Hanratty V C A, Morton-Blake D A, and B ni re F. *Mol. Simulation*, 1992, **9**:65

Chapter 8

CONCLUSIONS AND FUTURE WORK

The work presented in this thesis has comprised two distinct areas: molecular simulation of thermochromic phenomena in P3ATs and of the location and transport behaviour of dopant species in P3AT lattices. Regioregular HT-P3BT was selected for the work because butyl is the shortest alkyl to confer thermochromism on a P3AT polymer. In addition, regioregular HT-P3ATs are highly crystalline and also show high conductivity. Both MM and MD simulation methods have been used in the investigations. Thermochromism in these materials is an interesting phenomenon that involves thermally induced conformation transitions. To understand the mechanism of thermochromism, MM was used to search for stable high-energy conformations that would be thermally accessible. MD was then used to investigate the thermally induced conformation changes on both the P3BT main chain and alkyl side chains. The transport behavior of the single-atom dopant Cl^- ion and the multiple-atom dopant BF_4^- ion in P3BT lattices was then simulated using a combination of MD and MM simulation techniques.

A new force field has been developed for pristine and Cl^- or BF_4^- doped P3BT lattices. It involves bond stretch, bond angle, torsional, van der Waals and Coulombic potentials. The fitted parameters for the functions of these potentials were taken from literature. The force field was tested and provided good results in both energy minimization and molecular dynamics techniques. For example, the optimized lattice

parameters a and b of both doped and non-doped P3BT lattices were found to be reasonably consistent with those measured from X-ray diffraction experiments.

In the search for stable conformations of P3BT with different torsional angles between main-chain thiophene rings, three torsional periodicities (4-ring $[\varphi, 0, -\varphi, 0]$, 6-ring $[\varphi, -\varphi, 0, \varphi, -\varphi, 0]$, and 10-ring $[\varphi, 0, 0, -\varphi, 0, \varphi, 0, 0, -\varphi, 0]$) and two possible lattice structures (two-chain staggered lattice and one-chain eclipsed lattice) were thoroughly investigated. Regardless of any torsional schemes, for the two-chain staggered structure, the global energy minimum is at $\varphi=0$, while for the one-chain eclipsed structure, the global energy minimum is at $\varphi=20^\circ$. The energy barrier between these two global minima is about 0.1 eV. This small thermal energy suggests that it is possible for the two-chain staggered structure to change into the one-chain eclipsed structure by effecting a translation of $\frac{1}{2} c$ to alternate polymer chains along the chain direction. This favors the formation of an out-of-plane distortion. An energy minimum at main-chain torsional angle $\varphi \approx 50^\circ$ was also observed. This appears to agree well with experimentally determined found torsions of poly(dialkylbithiophene)s, i.e., in the region of $40-60^\circ$ [1-2]. The energy barrier (0.3 eV) and the bandgap increase (0.35-0.7 eV) support the idea that the conformational change between the global minima ($\varphi=0$ for two chain structure and $\varphi=20^\circ$ for the one-chain structure) and the minimum at $\varphi \approx 50^\circ$ might correspond to the thermochromic transition although this would not be favored by consideration of the lattice density. In this MM simulation, changes in the alkyl side-chain conformations were not examined although they did occur during the energy minimization. In fact, as was demonstrated by the results of the MD calculations reported in this thesis, the conformations of side chains are very important in the mechanism of the thermochromic phenomenon. The present MD simulation work has shown how the

alkyl side-chain conformations are affected by the temperature and how they in turn influence the main chain torsions. But the precise role of the alkyl side-chain conformations in the mechanism of the thermochromism should form the subject of future investigations.

The dynamical behavior of both P3BT main-chain and side-chain conformations was monitored by MD simulation over a full range of temperatures. By monitoring the torsional angles in the polymer main chain and in the alkyl side chains, a step-like increase in the average torsional angle, $\langle\phi_5\rangle$, between the main-chain thiophene rings was found from 330 K to 340 K, which suggests the occurrence of an abrupt reduction in the planarity of conjugated main chain leading to thermochromism. It was shown that the abrupt jump of $\langle\phi_5\rangle$ from 20° to 30° is probably associated with the accumulation of torsional energy in the alkyl side chains. At low temperatures, the butyl group is largely in the fully extended low-energy *trans* conformations. As the temperature is increased, *gauche* and other higher energy conformations appear and their populations then increase with the temperature. These thermally induced conformation changes are also confirmed by the radial distribution functions of C-C and H-H and show good agreement with the FTIR and X-ray diffraction results reported by several groups [3-6]. The work reported here has allowed a mechanism for the thermochromic phenomenon to be proposed based on the MD observations that the torsional energy accumulated in the alkyl side chains upon heating could transfer to the polymer main chains and cause these to show an abrupt twisting. This mechanism is also supported by the MM results of the simulations which show the possibility of transitions between stable conformations with different main-chain torsional angles (such as changes in ϕ_5 from 20° to 50° as mentioned above).

The side-chain conformations play a particular role in the thermochromic transition. If link 1 or link 2 in the butyl group is clamped so that it can not move then the MD simulations show no thermochromic changes for P3BT. They also predict that higher pressure would delay the onset of the thermochromic change to a higher temperature range. But these inferences concerning the transmission of energy from the alkyl side chains to the polymer main chain are qualitative and it would be desirable to conduct further investigations on this subject. Neither has the effect of the length of the alkyl side chain on the temperature of thermochromic change been simulated in this work and should perhaps also form the subject of future investigations.

Little information is available on the lattice structure of doped P3ATs. Experimentally it is difficult to reveal the sites of the dopant ions in the oxidised states of conductive polymers. The MM and MD calculations allowed us to identify two likely sites for the dopants Cl^- and BF_4^- in P3BT lattices, one in each of the Kawai and interplanar models. These sites were then used for the investigation of diffusion and migration of dopants in P3BT lattices.

The MD investigations gave the calculated values for the absolute diffusion coefficients of Cl^- and BF_4^- in regioregular HT-P3BT lattices that were much higher than those of dopants in the similar π -conjugated conducting polymers such as polythiophene and polypyrrole. The diffusion coefficients calculated here were found to increase with temperature. At room temperature they are in the range of $1-100 \times 10^{-12} \text{ m}^2 \text{ s}^{-1}$, which indicated that doped P3ATs might be good materials for battery applications.

Finally, MM simulations were used to reveal the migration pathways of Cl^- and BF_4^- dopants in the P3BT lattices. The calculated energy barriers for the dopants in the interplanar model were found to be lower than in the Kawai model.

Both of the diffusion coefficients calculated from MD and migration energy barriers calculated using MM indicate that dopants in a lattice described by the interplanar structural model would possess higher mobilities than those in the lattice described by the Kawai structure. This prediction can only be verified by further experimental investigations such as the structural measurements by X-ray diffraction and by measurements on diffusion/migration of dopants in P3ATs and that only if both the dopant sites in the interplanar and Kawai models actually occur.

The Kawai model was first suggested by Kawai *et al.* [7] based on their X-ray diffraction measurements of electrochemically doped P3AT films. No report has been found for the interplanar model for doped P3ATs, but it is also reasonable because diffraction studies [8] on the structures of AsF_6^- doped polyparaphenylene showed that the dopant takes the position between the adjacent polymer chains. Our energy minimization optimization for the 50% Cl^- doped P3BT lattice structure found that the Kawai structure was slightly more stable than the interplanar structure, but the energy difference was only 0.645 eV per unit cell. If the diffusion coefficients of dopants in P3BT are measured and then compared with the results presented here it might be possible to distinguish between the two structural models.

Bibliography:

- [1] Fell H J, Samuelsen E J, Mårdalen J, Bakken E, and Carlsen P H J. *Synth. Met.*, 1995, **69**:301
- [2] Isotaro H, Ahlskog M, and Stubb H. *Synth. Met.*, 1992, **48**:313
- [3] Iwasaki K, Fujimoto H, and Matsuzaki S. *Synth. Met.*, 1994, **63**:101
- [4] Tashiro, Ono K, Minagawa Y, Kobayashi M, Kawai T, and Yoshino K. *J. Polym. Sci.: Part B: Polym. Phys.*, 1991, **29**:1223
- [5] Zerbi G, Chierichetti B, and Ingnas O. *J. Chem. Phys.*, 1991, **94**:4646
- [6] Prosa T J, Winokur M J, Moulton J, Smith P, and Heeger A J. *Macromolecules*, 1992, **25**:5364
- [7] Kawai T, Nakazono M and Yoshino K. *J. Mater. Chem.*, 1992, **2**(9):903
- [8] Stamm M and Hocker J. *J. Phys. Paris*, 1983, **44**:667